THE UNIVERSITY *of* EDINBURGH

Characterisation and Prediction of Crystallisation Fouling in Reverse Osmosis and Nanofiltration Membrane Processes

Emad Alhseinat

A thesis submitted for the degree of Doctor of Philosophy

The University of Edinburgh

School of Engineering

January 22, 2013

Abstract

Membrane technologies are considered a promising solution for water scarcity in arid regions. However, fouling is a major challenge facing the application of membrane technologies. Fouling limits the economic viability and reduces the overall efficiency of membrane processes. Therefore, fouling mitigation is a crucial factor in spreading the use of membrane technologies for new applications. The first step in fouling mitigation is to predict the propensity of fouling. Unfortunately, there are immense limitations in current industrial practises for fouling propensity prediction. These limitations come from using outdated and inapplicable approaches, in which crucial assumptions are made. For example, in the case of crystallisation fouling or "scaling" one of the major simplifications is the use of pure scaling salt data to predict the propensity of scaling when, in reality, co-precipitation is present. This research work aims to introduce a new approach to systematic assessment of the fouling problem under real and complex conditions and to enhance understanding of the importance of including interactive effects and co-precipitation in the prediction of scaling propensity.

In this research work a novel procedure accounting for the local variation of thermodynamic properties along a long membrane channel is proposed. A new approach considering ion interaction and process hydrodynamics for the prediction of the scaling propensity is then introduced. This new approach provides for the first time a completely theoretical assessment for pure salt scaling propensity along a full scale filtration channel without the use of any empirical constants. A new procedure for including the effect of co-precipitation on scaling propensity prediction is developed. The effect of process pressure on solubility products is included theoretically for the first time to enhance the accuracy of scaling propensity prediction during the full scale RO process. This research work helps to produce more reliable and accurate prediction of the onset of scaling which will help strategies to mitigate scaling and increase the overall efficiency of RO/NF processes. The new approach can be applied in practical situations and could be developed to a user-friendly programme able to give an accurate prediction of the fouling propensity in full scale processes allowing the optimisation of membrane processes accordingly.

Moreover, comprehensive experimental work has been carried out during this PhD research work to enhance understanding of crystallisation fouling and co-precipitation. The effect of salinity and dissolved organics (DO) in $CaSO_4$ and $SrSO_4$ precipitation and co-precipitation are studied and discussed. Quantitative and qualitative thermodynamic and kinetic analyses combined with structural analyses of deposits are carried out to investigate the effect of salinity, DO presence and co-precipitation on $SrSO_4$ and $CaSO_4$ precipitation. The observations in this experimental study are very important for a deeper understanding of the effect of scaling salts' coexistence, salinity and DO presence on the behaviour of the scaling salts. This is crucial to reaching a reliable prediction of the scaling propensity within RO/NF processes.

Finally, the new developed approaches in this thesis have been validated using set of hydrodynamic tests. This set of tests has been carried out using a newly installed laboratory membrane rig. Moreover, a new technique to simulate full scale membrane processes is proposed using a laboratory membrane rig combined with the programs previously developed in this thesis. This new technique can be used to study the effect of process hydrodynamics on scaling and process performance of full scale membrane processes using a laboratory membrane rig. The outcomes of this research work can be used to investigate the optimal operating conditions and to guide design criteria for different RO/NF practical scenarios.

Declaration of originality

I hereby declare that the research recorded in this thesis and the thesis itself was composed and originated entirely by myself in the School of Engineering at the University of Edinburgh. I declare also that the work in this thesis has not been submitted for any other degree or professional qualification except as specified.

Emad Alhseinat

Acknowledgements

First and foremost, I would like to thank Allah, for giving me the patience and helping me finishing this thesis.

I would like to show my appreciation to Prof. Roya Sheikholeslami for her supervision during the first two years of this PhD. She spent a lot of her personal time reviewing my work and papers. I would like to take this opportunity to acknowledge my second supervisor Prof Jose Torero for his support, especially during the first year of this PhD. I would like to express my deep thanks and appreciation to Dr. Donald Glass for supervising me in my third year and providing me with all the support I needed to complete this PhD. I would like to thank Dr. Adam Cowlard for his help in Matlab and Dr. Aristides Kiprakis for his help in the rig control. Also, I am thankful for all my professors at the Jordan University of Science and Technology, Prof Mousa Abu Arabi, Prof Abdelrahman Tamimi, Dr Awni Al-Otoom and others for their support during my undergraduate and master studies.

I would like to thank the School of Engineering and the University of Edinburgh for providing me with financial and logistical support. My special thanks goes to Katharine Moore for her support and providing the funding I needed for attending international conferences. Also, I wish to give special thanks to the technical staff, Bryan, Douglas, Steven and others who helps me commissioning and starting up the lab.

Last but not least; I would like to deeply thank my friends Yousef, Abdullah, Rami Ime, Doug, Pai and the rest of my friends who make it easy to me to keep working by providing me with regular pleasant breaks from hectic work of PhD. My wife Hala, my sons Yousef, and the new arrival Keenan, deserve special thanks. I am deeply thankful for the love, excellent support, patience and encouragement that they provided me during my study. My family in Jordan, my lovely Dad and Mom, Yousef and Ibtisam, my sister Bayian and my brothers Mohammed, Ahamd, Sami, Sohib, and Esam, all of them have participated in my successes and they will continue do so.

Table of contents

List of figures

List of tables

Nomenclature

A_ϕ	Interaction parameter Pitzer model (-)
$B, B^{'}, B^{\phi}$	Interaction parameter Pitzer model (-)
B_s	Salt permeability constant, m/s
c_0	Initial feed salt concentration, mg/l
$c(x)$	Localized feed salt concentration, mg/l
$c_w(x)$	Localized salt concentration on membrane surface, mg/l
C, C^{ϕ}	Interaction parameter Pitzer model (-)
C_s	Salt's solubility
D	Diffusion coefficient, m^2/s
d_h	The hydraulic diameter, m
f^{ϕ}	Interaction parameter Pitzer model (-)
G	Standard Gibbs free energy
H	Height of membrane channel, m
I	Ionic strength, mol/Kg
K_m	The mass transfer coefficient, m/s
k_{spacer}	Coefficient to account for transmembrane pressure drop due to existence of spacers in membrane channel
Ksp	Thermodynamic solubility product
L	The length of the membrane channel, m
L^*	The length of entry region, m
m_D	The rate of deposition per unit area
m_f	The mass of deposit per unit area
m_R	The rate of removal per unit area
Mw	Molecular weight of the solute
n	Number of segments
N	The number of ions in solution that can result from one salt molecule
r	Salt rejection of membrane
P	Process pressure, bar
P_0	Reference pressure, 1 bar
p_f	The static pressure in the feed, Pa
p_p	The static pressure in the permeate, Pa

Q_F	Feed water flowrate
Q_P	Product flowrate
R	Process recovery
R_g	The universal gas constant
R_m	Membrane resistance, Pa s/m
T	Temperature, K
t	Time, s
u_0	Initial feed flow velocity, m/s
$u(x)$	Localized cross flow velocity, m/s
V	Volume of the dissolution reaction
$\overline{V}$	Molal volume of dissolution reaction
v	Permeate velocity, m/s
$v(x)$	Localized permeate flux, m/s
x	Location along membrane channel, m
y	The coordinate perpendicular to membrane surface
z_i	Ionic charge of component i (-)
Z	Modified ionic strength, mol/Kg

Greek letters

α	Osmotic coefficient, Pa l/mg
α_1 ,α_2	Interaction parameter Pitzer model (-)
δ	The thickness of boundary layer
Δ	Denote the difference between two values
$\Delta c(x)$	Localized difference between feed salt concentration and permeate salt concentration
$\Delta c_w(x)$	Localized difference between feed salt concentration on membrane surface and permeate salt concentration
$\Delta_r C_p^o$	Standard heat capacity change of precipitation reaction
$\Delta\pi(x)$	Localized osmotic pressure across the membrane, Pa
$\Delta_f G^{\Phi}$	Standard Gibbs free energy change of formation
$\Delta_{reac} G^{\Phi}$	Standard molar Gibbs free energy change of reaction
ΔH_{reac}	Enthalpy change of reaction
$\Delta_r H^o$	Standard enthalpy change of the precipitation reaction

ΔK_r^o	Standard compressibility change of the precipitation reaction
$\Delta \overline{K_r^o}$	Standard molal compressibility change of the precipitation reaction
Δp	The trans-membrane static pressure, Pa
$\Delta p(x)$	Localized trans-membrane static pressure, Pa
Δp_0	Initial transmembrane pressure, Pa
Δp_{fric}	Frictional losses due to friction by the membrane surfaces and spacers, Pa
$\Delta_r S^o$	Standard entropy change of precipitation reaction
ΔV_r^0	Standard volume change of precipitation reaction
$\Delta \overline{V_r^o}$	Standard molal volume change of precipitation reaction
γ	Activity coefficient
ρ	Density, Kg/m^3
σ	The interfacial tension between the crystal and the aqueous solution , $J.m^{-2}$
η	Water viscosity , Pa.s
Φ, Φ', Φ^{ϕ}	Interaction parameter Pitzer model (-)
$\Phi_{osmotic}$	Pitzer osmotic coefficient
λ_{ij}	The second virial coefficient
μ_{ijk}	Third virial coefficient
Ψ	Interaction parameter Pitzer model (-)
ξ	Dummy integration variable

Subscripts

0	Reference or initial value
i	Segment number or component index
j	Component index
n	*n*th component
w	Denote the variable at membrane wall

Superscripts

Φ	Reference temperature value
0	Reference value
f	Formation
r	Reaction

Abbreviations

aq	Aqueous phase
Cf	Co-precipitation Correction Factor
CF	Concentration Factor
CP	Concentration Polarisation Factor
DO	Dissolved Organic
ED	Electrodialysis
EDR	Electrodialysis Reversal
exp	Experimental value
IAP	Ion Activity Product
LPF	Local Permeate Flux
MF	Microfiltration
NF	Nanofiltration
RO	Reverse Osmosis
SPI	Scaling Potential Index
s	*Solid phase*
theo	Theoretical value
UF	Utrafiltration

Characterisation and Prediction of Crystallisation Fouling in Reverse Osmosis and Nanofiltration Membrane Processes

Chapter 1

General Introduction

1. General introduction

Water scarcity is one of the major problems that restrict economic development all over the world. Actually, as an angle on the development triangle Human resources, Energy and Water; availability of freshwater resources affects the economic development of all countries. In fact, the availability of freshwater resources is crucial to those countries that look for economic development. Regrettably, fresh water resources shortage may lead to devastating wars, especially in arid reigns such as the Middle East and Africa that could affect the entire world. As a result, universal welfare is threatened under water shortage stress conditions. Despite the fact that 70% of the earth's crust is covered with water; 98% of this water is saline water and only 2% is fresh water. And taking into account that 90% of this 2% fresh water is frozen in glaciers; fresh water can be categorized as an ''endangered'' commodity and it should be considered priceless [1]. Thus, a massive effort should be invested in research for finding new water treatment and desalination technology and to decrease the overall cost of the available technologies.

1.1 Summary of background and motivation

Water desalination is considered a promising technology that could satisfy the requirement for fresh water. Membrane processes are considered as one of the most important technologies for water desalination due to its lower cost compared to other desalination processes such as thermal distillation [2]. However, the operation of membrane processes is plagued by fouling. In particular, fouling increases operational costs by lowering the lifetime of membranes and raising their energy consumption. Moreover, fouling adds extra cost to the capital expenses since the process needs further pre-treatment units to minimize its effect. For these reasons fouling is considered a fundamental limitation to economic viability of membrane water treatment and desalination [3]. Needless to say, the additional energy, materials (membranes and equipment) and chemicals required to combat fouling add to the carbon footprint which make the process environmentally unfriendly.

The first step in fouling mitigation is to determine the fouling propensity of a feed water. Research studies usually consider a single foulant or a single fouling mechanism and they do not take into account interactive and hydrodynamic effects. As such, they are generally inapplicable to industrial conditions where in reality interactive effects and multiple mechanisms are present and must be considered during any comprehensive assessment of fouling, as discussed in detail by Sheikholeslami in her monograph about fouling in membranes and thermal units [4].

Moreover, the current practices for assessing fouling propensity are based on empirical relationships and are not suitable for membrane processes [5]. For example, the empirical indices used for assessment of the potential of precipitation fouling, (commonly referred to as scaling), were mostly developed in the 1950's and 1960's and not for membrane processes. Even the commonly used indices for calcium carbonate fouling, such as Langelier Saturation Index (LSI) [6], Stiff-Davis Stability Index (S&DSI) [7], Ryznar Stability Index [8], and Puckorius Scaling Index [9] are mostly empirically based; and the LSI and S & DSI, which are based on the theoretical concept of saturation, include significant simplifications and empirical relationships in their derivation and do not reflect the high salinities, the interactive effects and the operational conditions within the membrane module [4, 5]. Therefore, the application of theses indices for membrane desalination is limited.

Furthermore, most of the fouling models that should describe fouling in membrane processes are developed for homogenous membrane systems, which assume uniform flow properties and fouling rate over the whole of the membrane surface. This assumption renders the existing models unrealistic in describing full-scale RO/NF process that have a long membrane channel, along which system variables and parameters change substantially [10, 11]. Therefore, there is need for a new, reliable approach which is designed specifically for full scale RO/NF membrane processes. This new approach should predict the fouling propensity in a full-scale RO/NF processes by incorporating the varying local water composition, flux, and flow properties into a new model for assessing the scaling propensity. Also this approach

should help to understand the effect of co-precipitation and to incorporate its effect where it is needed.

1.2 Research objective and scope

The main key goal of this thesis is to establish a reliable approach to predict the onset of fouling during full scale RO/NF processes. This new approach should be capable of theoretically predicting the fouling propensity along a long membrane channel. It should consider the science of fouling, the feed water chemistry and thermodynamics, and combine these with the principles of osmosis, mass transport across the membrane and conservation of mass to assess the local scaling potential of the sparingly soluble salt of concern within the RO/NF module and on the membrane surface. It should result in a simulated model for scientifically and theoretically predicting the onset of crystallization fouling within an RO/NF module. The suggested model is expected to be a very powerful tool that could help in the specific design of RO/NF process as well as in simulations of the operating variables for optimization of RO/NF systems.

To achieve this main goal a new approach for assessing the thermodynamic activity coefficients and osmotic coefficient for saline water in full scale RO/NF processes will be developed. This approach enables us to study from fundamental principles, locally on the membrane surface, the effects of hydrodynamics, salinity, temperature and concentration of the sparingly soluble salts on the fouling potential along the feed module next to the membrane surface. Moreover, in view of the fact that different ions have different specific passages, this approach would incorporate the effect of relative solution composition along a membrane module; this is very significant for a nanofiltration (NF) module which has different passages for monovalent and divalent ions. This approach will overcome the challenge of determining and incorporating the locally varying concentration of foulants (and factors affecting them) and the effect of concentration polarization to predict the local fouling propensity along the membrane channel. The only available theoretical index, the Scaling Potential Index (SPI) [5, 12] will be modified and incorporated so that reliable prediction of pure salt precipitation can be achieved without any need

for empirical parameters and/or constants. A semi theoretical approach will be suggested to overcome the effect of scaling salts co-precipitation. The effect of process pressure on the solubility product will be incorporated theoretically to predict the onset of scaling in a full scale RO/NF processes. Thus, the consequence of ignoring the effect of process pressure on solubility product and scaling propensity prediction will be highlighted and discussed. Therefore, a fundamental and more realistic description of fouling propensity and onset of fouling next to membrane along feed channel will be developed and explained. Moreover, the effects of initial applied pressure, initial cross flow velocity, initial feed water salinity, clean membrane resistance and feed water temperature on fouling propensity and onset of fouling along the channel will be investigated and discussed.

Moreover, to understand better the effect of co-precipitation, a series of experimental studies which aims to study comprehensively the effect of salinity and dissolved organics (DO) on $CaSO_4$ and $SrSO_4$ precipitation and co-precipitation has been carried out during this PhD work. The developed model has been verified experimentally using a laboratory membrane rig. This experimental work will enhance the understanding of crystallisation fouling and the effect of co-precipitation and will give an example of the experimental programme that could be followed to achieve more reliable scaling propensity prediction in case of co-precipitation.

1.3 Organisation of the thesis

The rest of thesis is subdivided into 7 chapters briefly outlined below.

Chapter 2: *Background and Literature Review*.

A review of the literature covering RO/NF membrane process, membrane fouling, as well as fundamental theories and principles of crystallisation fouling, co-precipitation interactions and scaling potential indices are presented here. The scope covered addresses only the background information that is necessary for subsequent appreciation of the material in this thesis.

Chapter 3: *Reliable thermodynamic description of RO/NF concentrates along full scale module using the Pitzer Model.*

In this chapter a reliable thermodynamic description of the behaviour of RO/NF concentrates in their passage along a full scale module will be described using the Pitzer model. The primary novelty of the developed approach is its ability to predict the local thermodynamic behaviour (activity coefficient and osmotic coefficients) at different axial position in a long membrane filtration channel. The Matlab programs that have been developed to achieve this reliable description will be described and verified in this chapter. The chapter has been divided into seven sections. The first section gives a general introduction in which the motivation for creating this approach has been highlighted and discussed; also the importance and general logic of the proposed approach has been discussed. The second section of the chapter is divided into two subsections in which a brief discussion of the activity models is provided. The next three sections (3.3,3.4, and 3.5) discuss the developed Matlab programs for activity coefficient and osmotic coefficient calculation, the modelling of the species concentration changes along a full scale RO/NF module, and the developed Matlab program that account for the change of activity coefficients, osmotic coefficients and species concentrations along a full scale RO/NF filtration channel. Section 3.6 discuses the confidence of the simulation and section 3.7 gives a brief summary of the chapter.

Chapter 4: *A New Reliable Approach for Assessing the Fouling Propensity along a Full-Scale RO/NF Process channels.*

This Chapter aims to develop a new approach for assessing scaling (crystallization/precipitation fouling) propensity through the previously proposed and tested approach in chapter 3. This approach incorporates the variation of the local foulant properties along the membrane filtration channel into fundamental transport and conservation equations to achieve a unified and scientific assessment of the scaling potential. Thus, a high accuracy simulation of the local fouling propensity along a full-scale RO/NF module is obtained. This work has overcome the challenge of determining and incorporating the locally varying concentrations of foulants (and factors affecting them) and the effect of concentration polarization to predict the local fouling propensity along the membrane channel. The chapter has been divided into four sections. Section 4.1 highlights the importance of developing this new

approach and then describes the contents of the chapter. Section 4.2 subdivided to three subsections. In section 4.2.1 the only available theoretical index, the Scaling Potential Index (SPI) [5, 12] has been discussed and modified so that reliable prediction of pure salt precipitation can be achieved without any need for empirical parameters and/or constants. In section 4.2.2 a semi-theoretical approach has been suggested to overcome the effect of scaling salt co-precipitation. In section 4.2.3 the effect of process pressure on the solubility product has been incorporated theoretically to predict the onset of scaling in a full scale RO/NF processes. The consequences of ignoring the effect of process pressure on solubility product and scaling propensity prediction are highlighted and discussed. Thus, a fundamental and more realistic description of the variation of fouling propensity and the onset of fouling next to the membrane along the feed channel is developed and explained.

In section 4.3, Matlab simulations have been conducted to investigate the onset of local scaling propensity along full-scale RO process under various conditions. The effects of initial applied pressure, initial cross flow velocity, initial feed water salinity, clean membrane resistance and feed water temperature on fouling propensity and onset of fouling along the channel are investigated and discussed in this section. Finally this chapter has been summarised in section 4.4.

The next three chapters in this thesis introduce the experimental work that has been carried out to enhance the understanding of crystallisation fouling.

Chapter 5: *Material and Methodology for the Experimental Work*
The experimental work in this thesis has been designed to carry out a comprehensive study of crystallisation fouling within a RO process. The experimental work consists of two sections; the batch section and the hydrodynamic section. This chapter describes the material and the methodology that have been used during the batch and hydrodynamic experimental work of this thesis.

Chapter 6: *Batch experimental work (A Comprehensive Study of the Precipitation and Co-Precipitation of $CaSO_4$ and $SrSO_4$ with and without the presence of Dissolved Organics at Different Salinity Levels).*

This chapter aims to study comprehensively the effect of salinity and dissolved organics (DO) on $CaSO_4$ and $SrSO_4$ precipitation and co-precipitation. A series of isothermal batch tests at 30^oC have been carried out with and without the presence of dissolved organics (DO) for salinity values ranging between 0.35-1.5 M of NaCl, 0.0475 M $CaSO_4$ concentration and two values of $SrSO_4$ concentration (0.005 M and 0.02 M). This chapter also gives an example and describes the experimental procedure that could be followed to evaluate the Co-precipitation Correction Factor which is proposed and discussed in section 4.2.2. The observations in this experimental study are very important for a deeper understanding of the effect of scaling salts' coexistence, salinity and DO presence on the behaviour of the scaling salts. This is crucial to reaching a reliable prediction of the scaling propensity within RO/NF processes.

.

Chapter 7: *Hydrodynamic experimental work (Validation of the Proposed Approach Using Laboratory membrane rig).*

In this chapter a series of experiments is designed and carried out to test the proposed approach in a laboratory membrane rig. Also in this chapter a new technique to simulate full scale membrane process is proposed. This new technique can be used to assist the effect of process hydrodynamic and operating conditions on scaling and process performance.

Chapter 8 – *Thesis Conclusions and Future Work*

The main achievements of this PhD work are summarised in this chapter. Recommendations for future studies and possible expansion of research scope are elaborated.

Chapter 2

Background and Literature Review

2. Background and literature review

This chapter aims to introduce the required background and knowledge that will be needed in subsequent chapters. The first section gives a general overview of the history and theory behind the Reverse Osmosis (RO) and Nanofiltration (NF) processes. The second section discusses the fundamentals of RO/NF technology. The third section discusses the fouling phenomenon and its effect on RO and NF processes. The fourth section discusses crystallisation fouling. The fifth section highlights the necessity of distinguishing between the full scale industrial process and the simple process models. Also in this section current industrial practice for fouling prediction will be discussed. The deficiencies in current practice for assessing fouling propensity will also be highlighted in this section. This chapter highlights the importance of having reliable fouling propensity predictions.

2.1 General overview

Membrane processes in water treatment and desalination can be classified to three major groups: Microfiltration (MF)/ Utrafiltration (UF) processes, reverse osmosis (RO)/ nanofiltration processes (NF), and electrodialysis (ED)/ electrodialysis reversal (EDR). These groups of membrane processes can be distinguished from each other by the type of membrane, the mechanism of retention, the process driving force and the primary application [13]. Microfiltration (MF)/utrafiltration (UF) processes depend on size exclusion and follow a sieving mechanism. These two processes do not remove any dissolved constituents in contrast to NF and RO processes. MF, UF, NF, and RO are pressure-driven membrane processes while ED is electrically driven membrane process. Figure 2.1 shows the different types of membrane processes and their removal abilities for respective targets based on their sizes. The mechanisms and the associated driving forces for these membrane processes are summarised in Table 2.1.

RO and NF are primarily targeted toward the removal of dissolved species via semipermeable membranes. The first RO membranes were developed at the

University of California in the early 1960s by Loeb and Sourirajan. These membranes were produced to generate drinking water from seawater. NF membranes were developed later in the late 1970s as a modification of RO membranes [13]. NF membranes were developed to reduce the RO membranes' rejection characteristics for small charged ions such as sodium and chloride. NF membranes have different retentions for monovalent and divalent ions while RO membranes have higher rejection for all ions. Thus, the applications of NF membranes are directed to the processes in which the total dissolved solid (TDS) is not the major concern, such as softening and water treatment of surface water. RO processes are more directed toward the desalination of high salinity water.

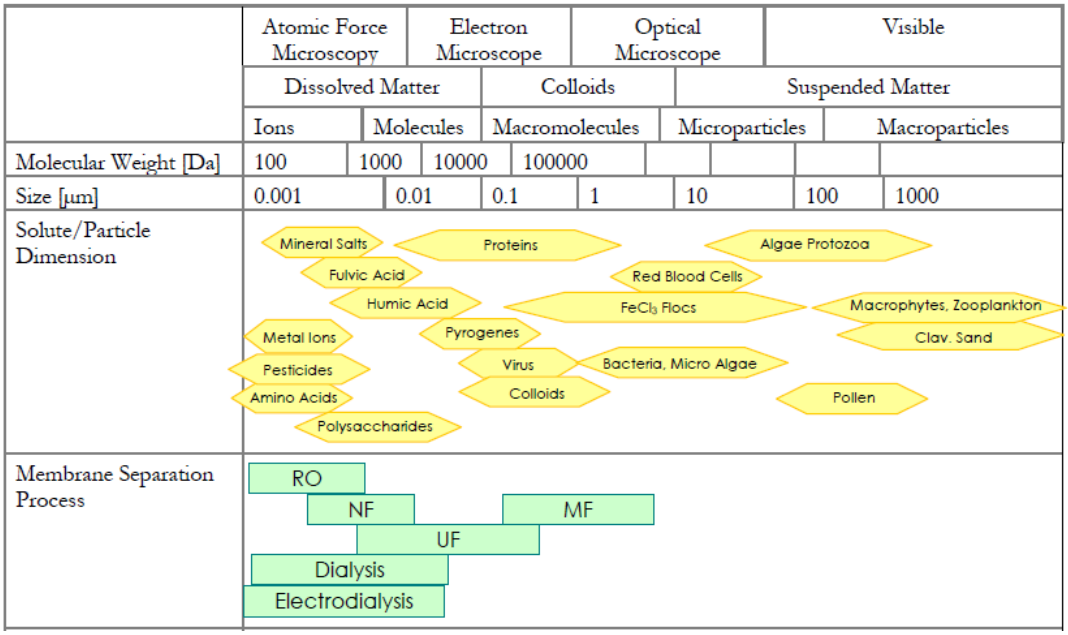

Figure 2.1: *Membrane processes and their respective target dimensions [14].*

In RO membranes, the rejection mechanism is a function of the relative chemical affinity of the solute to the membrane material. The rejection mechanism in NF membranes combines both physical sieving and the chemistries of solute and membrane, though the rejection mechanisms are still poorly understood [14]. Detailed discussion of the rejection mechanism is beyond the scope of this thesis and the reader is referred to the following references for more in-depth discussion [14, 15].

There are two primary materials used to manufacture RO and NF membranes, cellulose acetate and its derivatives and the various polyamides used in thin-film composite membrane construction [13]. Lee et al., [16] have recently published a comprehensive review of RO membrane materials. In their review they comprehensively review the historical development of commercially successful RO membrane materials and they also address the emergence of nano-technology in membrane materials science, which offers attractive alternatives to polymeric materials. These nano-structured membranes include zeolite membranes, thin film nano-composite membranes, carbon nano-tube membranes and biomimetic membranes. They conclude that the advances in membrane permoselectivity in the past decade have been relatively slow, and that membrane fouling remains the most severe problem. More recently, Kang and Cao [17] have published papers reviewing the development of antifouling reverse osmosis membranes for water treatment. They emphasise the conclusion of Rana and Matsuure [18] that all membranes are subject to fouling and no membranes are free from fouling under any circumstances. Thus, they conclude that the selection and use of RO membranes should be based on foulant characteristics in the feed solution and other variables such as module design optimisation, proper pre-treatment and effective membrane cleaning. Membrane fouling and its science will be discussed in more detail later in this chapter as the main aim of this thesis is to introduce a new approach for reliable fouling propensity prediction that can be applied for any types of RO/ NF membranes.

Table 2.1: *Summary of the mechanism of membrane processes, membrane type and pore size, and driving forces [4].*

Membrane Process	Mechanism	Membrane		Driving force
		Type	Pore	
MF	Sieving	Porous	0.1-10 μm	Pressure
UF	Sieving	Porous	5-100 nm	Pressure
NF	Sieving	Porous	1-10 nm	Pressure
RO	Sorption-diffusion	Dense skin	Non-porous	Pressure
ED/EDR	Charge and size	Ion exch.	Non-porous	Electrical

To integrate the membrane into real processes the membrane must be supported and packaged, as the membrane by itself is fragile [13]. There are several membrane module configurations being used in the industry for RO/NF processes. Table 2.2

shows a comparative guide to the performance of different types of membrane modules. The spiral wound module is widely use in desalination; as shown in table 2.2 spiral wound modules offer a good balance in terms of permeability, packing density, fouling and ease of operation [19]. The membrane module construction greatly affects flow hydrodynamics and fouling behaviour [4]. The effect of full scale membrane configurations on fouling prediction will be discussed in more detail later in this thesis.

Table 2.2: *A comparative guide to performance of different membrane modules [4].*

	Plate and frame	Spiral wound	Tubular		
			Concentric	Capillary	Hollow fiber
Cost/area	High	Low	High	High	Low
Replacement cost	Low	Mod./Low	High	Mod.	Mod.
Flux	Exc./good	Good	Good	Fair/poor	Fair/poor
Packing density	Good/fair	Good	Poor	Low	Exc.
Energy usage	Medium	Medium	High	High	Low
Fouling/cleaning	Good/fair	Good/fair	Exc.	Fair/poor	Poor

2.2 Reverse osmosis (RO) and nanofiltration (NF)

2.2.1 Fundamental of RO/NF

RO and NF employ semipermeable membranes to primarily target the removal of dissolved species using a diffusion-controlled separation process [13]. RO and NF are pressure-driven membrane processes. In these processes, pressures higher than the natural osmotic pressure of the feed water must be applied on the feed side of the membrane to force the water through the membrane. The solutions passed through the membrane are collectively called permeate and the solutions that cannot pass through the membrane are called concentrate [4]. Figure 2.2 shows the relationship between osmosis and reverse osmosis.

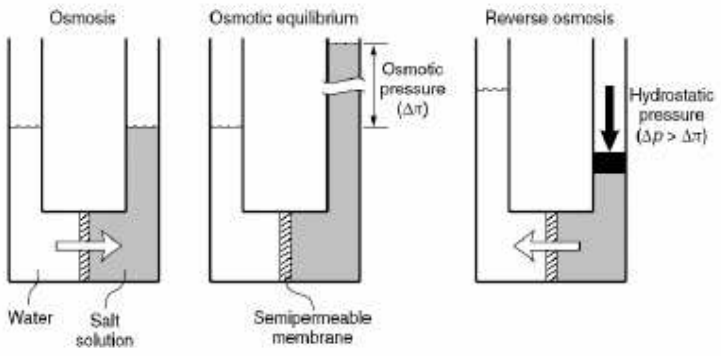

Figure 2.2: *A schematic illustration of the relationship between osmosis and reverse osmosis [15].*

Permeate flux is defined as the amount of permeate that passes throgh a unit area of membrane per unit time. The permeate flux is related to the pressure driving force by Eq.2.1.

$$v = \frac{\Delta p - \Delta \pi}{R_m} \qquad (2.1)$$

where v (m/s) is the permeate flux, Δp(bar) is the trans-membrane static pressure difference, Δπ (bar) is the difference in osmotic pressure between the feed and permeate side, and R_m (s.bar/m) is the membrane resistance to the permeate flow.

Δπ is calculated by Eq 2.2; α relates the osmotic pressure to concentration through application of the van't Hoff formula shown in Eq. 2.3; N is the number of ions in solution that can result from one salt molecule (N is 2 for NaCl); R_g is the universal gas constant; T is the absolute temperature; Mw is the molecular weight of the solute; and $\varphi_{osmotic}$ is the osmotic coefficient.

$$\Delta \pi = \alpha \Delta c \qquad (2.2)$$

Δc is the difference between the salts concentration at the membrane surface, c_w, and the salt concentration on the permeate side, c_p.

$$\alpha = \frac{N \varphi_{osmotic} R_g T}{Mw} \qquad (2.3)$$

The salt flux across the membrane is given by Equation 2.4 [20]:

$$v_s = c_p.v = B_s(c_w - c_p) \qquad (2.4)$$

where B_s is the salt permeability constant.

The observed salt rejection fraction r_o, which expresses membrane performance based on solute bulk concertation, c_b, is given by Eq. 2.5 [20]:

$$r_o = \frac{c_b - c_p}{c_b} \qquad (2.5)$$

while the real rejection fraction, r, depends on the actual solute concentration prevailing on the membrane surface and is given by Eq. 2.6 [20]:

$$r = \frac{c_w - c_p}{c_w} \qquad (2.6)$$

The ratio of the permeate flowrate to the feed water flowrate is referred as the recovery rate (R) and is given by Eq. 2.7:

$$R = \frac{Q_p}{Q_F} \qquad (2.7)$$

where Q_F and Q_P are the feed water flowrate and product flowrate respectively.

The observed concentration factor CF_o, which can be use to represent the observed degree of concentration of the brine, can be defined by the ratio of the bulk concentrate conentration, c_b, to the feed conentration, c_f, and is related to the recovery rate by Eq. 2 .8:

$$CF_o = \frac{c_b}{c_f} = \frac{1}{1-R} \qquad (2.8)$$

And a real concentration factor CF can be defined by the ratio of membrane surface concetration, c_w, to the feed conentration, c_f.

The dissolved species concentration at the membrane surface, c_w, is higher than the concentration of these species in the bulk c_b. This is due to the rejection of the dissolved species by the membrane which leads to accumulation of these substances in front of the membrane [19]. This phenomenon is called concentration polarisation

(CP). The next section discusses the concentration polarisation phenomenon in more detail.

2.2.2 Concentration polarisation

In RO/NF membrane processes due to the high solvent permeation and lower permeation of other species, a thin layer of these species accumulates adjacent to the membrane surface [21]. This phenomenon as mentioned above is called concentration polarization (CP). CP has several disadvantages in the performance of the separation processes. The increase of ionic concentrations near the membrane surface leads to increase of the osmotic pressure and thus reduces the permeate flux as can be seen from Eq. 2.1. Moreover, this high concentration of the salts near the membrane surface will increase the permeation of salts through the membrane and thus increase the concentration of these salts in the permeate side which can be shown by Eq. 2.4. Another important disadvantage as a result of high salts concentration near the membrane surface is that some of these salts exceed their solubility limit and precipitate on the membrane surface, which increases the overall resistance and thus decreases the process efficiency. Therefore, understanding the CP phenomenon and expecting its development is essential for design and operation of RO/NF processes.

Immense efforts have been made to understand the CP phenomenon due its effect on overall performance and economic viability of membrane separation processes. The Boundary Layer Film Model [22] is one of the most common approaches describing the CP within a membrane module. The velocity profile of a fluid within a membrane channel is shown in Fig. 2.3 [15]. The velocity at the membrane surface is zero due to the no slip condition. Thus the flow near the membrane surface is always laminar. The velocity reaches the maximum in the middle of the channel and there the flow can often be considered turbulent.

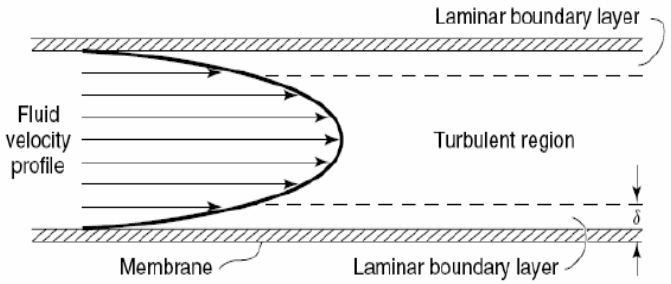

Figure 2.3: *The velocity profile through a channel of a membrane module [15].*

Concentration gradients due to concentration polarization are assumed to be restricted to the boundary layer. Fig. 2.4 illustrates the salt concentration gradient formed on a RO membrane channel [22].

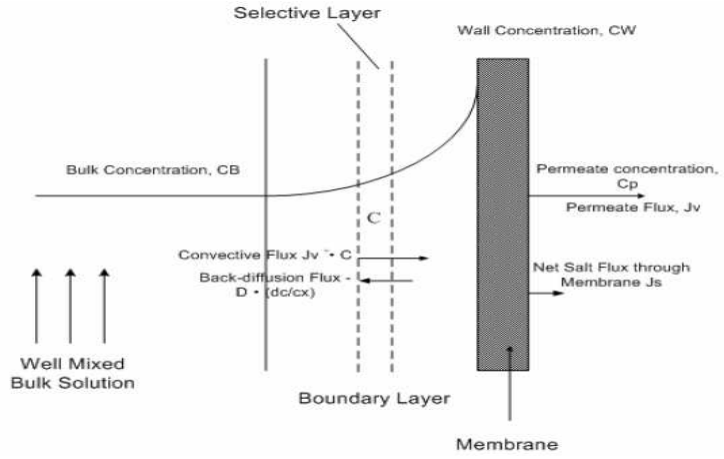

Figure 2.4: *The concentration gradient on the filtration membrane channel [22].*

As a result of the concentration gradient which results from the difference between the solute concentration at the membrane surface, $c_{w,}$ and the bulk solute concentration, c_b , solute back diffusion will take place. At steady state, the transport of the solute within the boundary layer can be described using the following mass balance equation [23]:

$$\begin{pmatrix} Net\ \ salt\ \ flux \\ through\ \ the\ membrane \end{pmatrix} = \begin{pmatrix} convective\ \ salt\ \ flux \\ towards\ \ the\ membrane \end{pmatrix} - \begin{pmatrix} diffusive\ \ salt\ \ flux \\ away\ \ from\ the\ membrane \end{pmatrix}$$

This mass balance can be expressed mathematically as [23] by Eq.2.9:

$$v_s = vc_p = vc - D\frac{\partial c}{\partial y} \qquad (2.9)$$

Solving Eq. 2.9 using the following boundary conditions:

At the solution-film interface: $y = 0$; $c = c_b$.

At the membrane wall surface: $y = \delta$; $c = c_w$ where δ is the thickness of boundary layer and y is the coordinate perpendicular to the membrane surface, gives Eq. 2.10.

$$\frac{c_w - c_p}{c_b - c_p} = \exp\left(\frac{v}{D/\delta}\right) = \exp\left(\frac{v}{K_m}\right) \qquad (2.10)$$

D is the diffusion coefficient of salt of solute; K_m is defined as the mass transfer coefficient and represents the ratio of diffusion coefficient to film thickness.

For low permeate concentration Eq.2.10 can be reduced to Eq. 2.11:

$$\frac{c_w}{c_b} = CP = \exp\left(\frac{v}{D/\delta}\right) = \exp\left(\frac{v}{K_m}\right) \qquad (2.11)$$

CP is the ratio of the concentration on the wall to the concentration in the bulk and is defined as the concentration polarization modulus [15].

As can be drawn from Eqs 2.10 and 2.11, the factors that may decide the degree of concentration polarization are the boundary layer thickness δ, the diffusion coefficient of the solute D , the ratio of c_p to c_w and the permeate flux v. Thus the concentration polarization can be minimized by increasing the feed fluid velocity so that the boundary layer thickness can be reduced. The concentration polarization modulus CP increases exponentially with either an increase of the permeate flux, v, or a decrease in the mass transfer coefficient, K_m; thus the CP will be high at high permeation rates and low flow velocities.

The CP can be determined experimentally by measuring the permeate flux, v, and the mass transfer coefficient, K_m. The permeate flux v can be measured easily. Measuring the mass transfer coefficient K_m is the primary challenge for determining the CP. Sutzkover et al, [20] have proposed a simple approach for determining the mass transfer coefficient and the concentration polarization modulus in a RO system. Their technique is based on evaluation of the permeate flux decline induced by the

addition of a salt solution to an initially salt-free water feed. According to this approach the mass transfer coefficient is given by Eq. 2.12:

$$K_m = \frac{v_{salt}}{\ln\left\{\frac{\Delta p}{\pi_b - \pi_p}\left[1 - \frac{v_{salt}}{v_{H_2O}}\right]\right\}} \qquad (2.12)$$

Thus, the value of K_m can be evaluated from the osmotic pressures π_b and π_p of the saline feed and of the permeate respectively and by measuring the permeate flux of pure water, v_{H_2O}, and the permeate flux of saline solution, v_{salt}. Sutzkover et al [20] have discussed other experimental methods for determining the mass transfer coefficient and the concentration polarization. The reader is referred to their paper [20] for further details.

The generalised correlations for the calculation of mass transfer coefficients in conventional flow through ducts can provide a reasonable estimate of the mass transfer in membrane concentration polarization layers [20]. Gekas and Hallstrom [24] critically reviewed the mass transfer correlations used to describe the transport in membrane operations. Eq.2.13 gives the generalised correlation that relates the Sherwood number (Sh = $K_m d_h/D$), to the Reynolds (Re = $\rho.u.d_h/\eta$), and Schmidt (Sc = $\eta/(\rho.D)$), numbers.

$$\mathrm{Sh} = a'' \mathrm{Re}^{b'} \mathrm{Sc}^{c''} \qquad (2.13)$$

where a'', b' and c'' are adjustable parameters that can be determined experimentally, K_m is the mass transfer coefficient, d_h is the hydraulic diameter, D is the diffusion coefficient, ρ is the density, u is cross flow velocity, and η is viscosity.

According to [25] the relations mostly used in membrane literature are:
Laminar flow conditions, where L is the length of the membrane channel and the length of entry region is $L^* = 0.029 d_h$ .Re
$L < L^*$ (Grober); $\mathrm{Sh} = 0.664\ \mathrm{Re}^{0.5}\mathrm{Sc}^{0.33}(d_h/L)^{0.33}$
$L > L^*$(Graetz-Leveque); $\mathrm{Sh} = 1.86\mathrm{Re}^{0.33}\mathrm{Sc}^{0.33}(d_h/L)^{0.33}$

Turbulent flow conditions (Re > 2000-4000)

Sc<1 (Chilton-Colburn or Dittus-Boelter); $Sh = 0.023\ Re^{0.8}Sc^{0.33}$

$1 \le Sc \le 1000$ (Dessler); $Sh = 0.23\ Re^{0.875}Sc^{0.25}$

Sc>1000 (Harriott-Hamilton); $Sh = 0.0096\ Re^{0.91}Sc^{0.35}$

Dresner [26] studied the concentration polarisation in laminar flow between parallel plats in reverse osmosis. Dresner [26] assumed a completely rejection of the solute by the membrane and a constant permeate flux and a fully developed velocity profile along the whole filtration channel. According to Dresner, CP can be calculated at the entrance of the filtration channel using the dimensionless permeation group, $\zeta = \frac{v^3 d_h L}{3uD^2}$; v is the permeate flux, by the following equations.

for $\zeta \le 0.02$; $CP = 1+1.536\zeta^{0.33}$

for $\zeta \ge 0.02$; $CP = 1+ \zeta +5\ [1-\exp(-(\zeta/3)^{0.5})]$

for the downstream region

$$CP = 1 + \frac{v^3 d_h L}{3uD^2}$$

For turbulent flow Dresner used Chilton-Colburn analogy to derive the following formula.

$CP = 25(v/u)\ Re^{0.25}Sc^{0.67}$

The mass transfer literature correlations depend on equipment geometry, feed flow rate, and solute system. Therefore, confidence in the evaluation of CP requires the determination of the mass transfer coefficient for the specific membrane configuration and feed water [20].

2.2.3 Full scale RO/NF processes

The fundamental transport theories and models are sufficient to describe the behaviour of a small piece of RO/NF membrane [27]. However, direct application of these models to describe the performance of long membrane filtration channels as employed in full scale RO/NF systems has been criticised by several authors [10, 28-30], because in full scale systems the process parameters vary substantially along the

long membrane channel and cannot be adequately described with basic membrane transport theories [10, 27-31].

Several attempts have been conducted to model full scale RO/NF processes. These models can be classified in two main categories. The first category considers the entire system as a "black box" and deals only with average values. The black box models are simple and do not need extensive resources of personnel and computing facilities. However, these models overestimate product water recovery and quality [32]. The other category is more accurate since it accounts for the local variation of parameters within the membrane channel [32]. In this thesis a model that is based on a series of differential mass and momentum balances will be developed and applied to account for the variation of process parameters along long membrane filtration channel. A more mathematical and detailed description of this model will be provided in chapter 3 of this thesis.

2.3 Fouling

Water treatment and reclamation has gained enormous attention as a consequence of potable water shortages all over the world, especially in arid regions such as the Gulf and indeed in most Middle Eastern countries. The problem of fouling is considered a fundamental limitation of the application of membrane processes for water reclamation and treatment. However, to predict and mitigate fouling one first needs to consider and understand fouling science.

2.3.1 Fouling science and fundamentals

Fouling is defined as the accumulation of unwanted materials at an interface or a transfer surface "at the membrane surface in the case of RO and other membrane processes". Fouling phenomena have been a subject of interest since the early 1970's from prominent scientists in the field such as Epstein [33], Watkinson [34] and Taborek [35, 36]. Taborek [35] highlighted their complexity and referred to fouling as a "science" or "art". In 1981, Epstein with his pioneering 5x5 matrix of fouling "types" and "stages" paper [33] was the first to put a scientific basis to the description of fouling. In 1999, Sheikholeslami, after years of having worked on

different types of fouling both on membranes and in thermal units, published her review paper [37] introducing a new variant of fouling to Epstein's categories. Later, Sheikholeslami greatly expanded Epstein's pioneering work and scientifically classified fouling by a 6×6 matrix of fouling types and stages as described elsewhere in detail, in her monograph on the science of fouling in membrane and thermal units [4].

2.3.1.1 Fouling types

Epstein [33] classified the fouling into five major groups as described below:

1) Crystallisation/Precipitation fouling: This type of fouling occurs when the solubility limit of a soluble salt is exceeded and the salt starts to precipitate onto the membrane surface. This type of fouling will be discussed in more detail later in this thesis.

2) Particulate fouling: This type of fouling take place when suspended solids in the process feed start to accumulate onto the membrane surface.

3) Biological fouling: This type of fouling happens as result of the attachment and metabolism of biological matter on the membrane surface.

4) Corrosion fouling: This type of fouling is more prevalent in thermal processes such as heat exchangers. In this type of fouling a reaction take place on the transfer surface and thus the surface characteristics are modified even if the deposit is fully removed. Sheikholeslami [4] has broadened this type of fouling to include both ionic and non-ionic reactions with the surface, encompassing metallic surfaces as well as non-metallic surfaces, and called it surface reaction fouling. Silica polymerization on the membrane surface can be given as an example of surface reaction fouling in a membrane process [38].

5) Chemical reaction fouling: In this type of fouling the foulant is formed as a result of chemical reactions within the system. However, the transfer surface itself should not participate in the reaction.

Sheikholeslami in her monograph [4] extend Epstein's description and added composite fouling as a new type of fouling. For further discussion of fouling types, the reader is referred to [4, 33].

2.3.1.2 Fouling stages

For all the above types of fouling, the successive events that commonly occur in most situations are as follow [33]:

1. Initiation: This refers to the time period before the fouling is being observed.

2. Transport: In cross-flow RO/NF membrane processes the fouling species will be transported to the membrane surface via convection, diffusion and drag due to permeation [39]. Figure 2.5 illustrates the transport of solute in a cross-flow RO system.

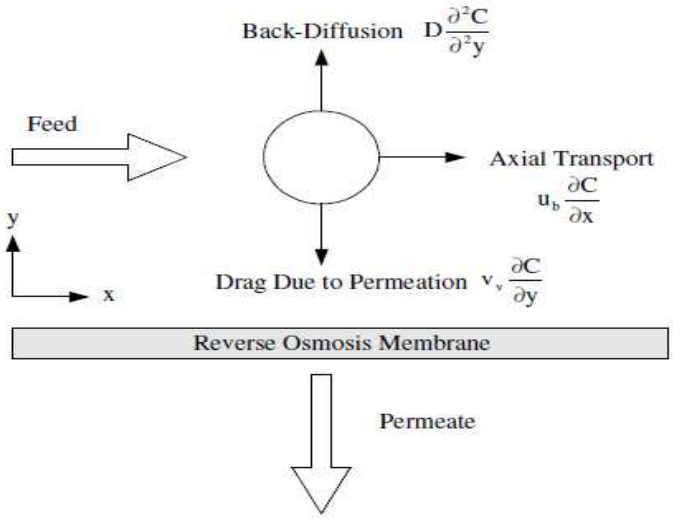

Figure 2.5: *Transport of solute in a cross-flow RO system [39].*

3. Attachment is the adherence of solid particles to the surface. For crystallisation fouling, attachment refers to the surface integration of cations and anions into the crystalline structure [39]. This will be discussed further in section 2.5.1 under crystal growth.

4. Ageing: This stage involves changes in the physical, chemical, or biological structure of fouling layers. The ageing begins straight after the deposition process has started [4, 39].

5. Removal: Removal can occur during the cleaning of the foulant and is then known as dissolution, or it can occur during normal operation as a result of fluid shear or turbulent bursts [4].

2.3.1.3 Fouling- a general model

The net rate of deposit growth can be mathematically described as the difference between the rate of deposition and rate of removal [40]. Thus the net rate of deposition growth can be described in Equations such as 2.14:

$$\frac{dm_f}{dt} = m_D - m_R \qquad (2.14)$$

where m_f is the mass of deposit per unit area; m_D and m_R are the rate of deposition and removal per unit area, respectively. The fouling curve of any system can be obtained by plotting the mass of solid deposited per unit area m_f versus time t. Figure 2.6 below shows the different scenarios for the fouling curve.

1) Linear rate behaviour: This trend occurs when the deposition rate is much larger than the removal rate or when there is no removal process. This behaviour is observed for very hard deposits which have a great degree of adhesion.
2) Asymptotic behaviour: This trend is observed as the removal rate becomes equal to the deposition rate and hence the net rate of deposition approaches zero. Here the mass per unit area of the fouling deposit approaches an asymptotic value and the thickness of the deposit remains almost constant.
3) Falling rate behaviour: This approach indicates a decrease in the net deposition rate, though the rate of removal is still less than the rate of deposition. However, the net rate of deposition decreases with time.
4) Saw tooth behaviour: This trend can be observed when a significant removal of the deposit takes place during the process. However, the fouling layer grows again and once again becomes subject to removal.

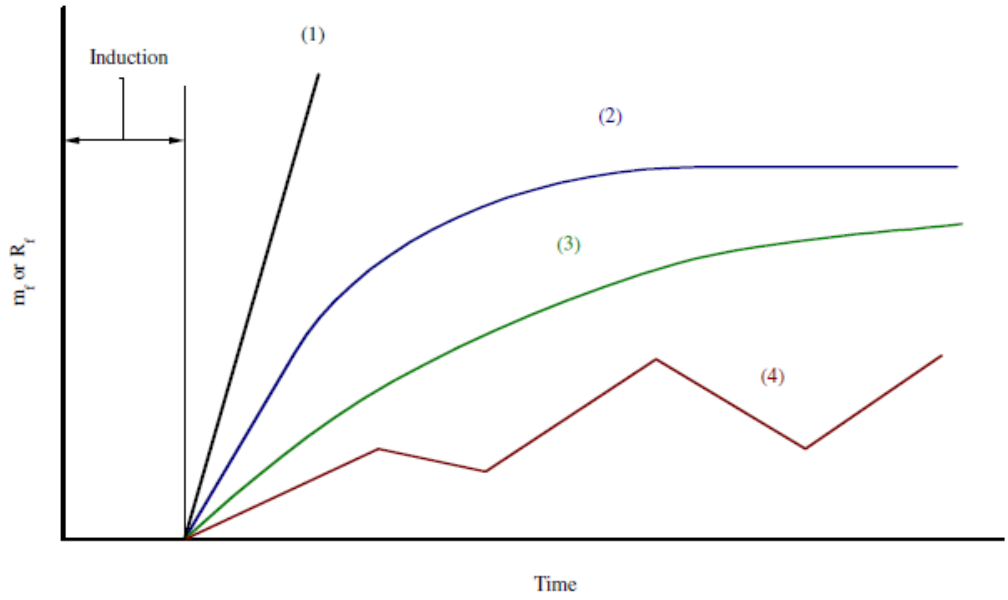

Figure 2.6: *Fouling curves [41].*

2.4 Crystallisation fouling

Crystallisation or precipitation fouling (Scaling) in membrane systems is defined as the precipitation of sparingly soluble salts at the surface of the membrane due to exceeding the solubility limits of the salts near the membrane surface as a result of the permeation and concentration polarization phenomena. One of the aims of this PhD work is to carry out a comprehensive study of $CaSO_4$ precipitation in presence of Sr^{2+} and dissolved organics (DO) at different salinity levels, thus it is necessary to understand the basic principles related to crystallisation process and to review the research work that has been done on $CaSO_4$ and $SrSO_4$ scales.

2.4.1 Crystallisation fundamentals

Crystallisation process involves the formation of a new heterogeneous phase (solid phase in a liquid). To understand the crystallisation process there is a need to understand the following three physical phenomena associated with crystallisation (1) solubility and supersaturation (2) nucleation and (3) crystal growth.

2.4.1.1 Solubility and supersaturation

A saturated solution is defined as one that has reached a dynamic equilibrium between its components: thus, the rate of precipitation equals the rate of dissolution. The solubility of any salt is the amount of the dissolved species of that salt at saturation or equilibrium. Once the concentration of the dissolved species exceeds its solubility limit the solution becomes supersaturated in that species, however, the solution may stay stable as a supersaturated solution and is then referred to as meta-stable [4].

Equation 2.15 represents a general precipitation reaction for (*MX*) salt

$$v_{+}M^{e+} + v_{-}X^{e-} \xleftarrow[Ksp]{} MX\ (s) \qquad (2.15)$$

where v_+ and v_- are the number of moles of cation and anion in 1 mole of electrolyte, respectively; e^+ and e^- is the valence of cation and anion, respectively. The thermodynamic solubility product (*Ksp*) is defined by the following equation:

$$\left(\frac{a^{v_+}{}_{M^{e+}equ.} . a^{v_-}{}_{X^{e-}equ.}}{a_{MX_{equ.}}} \right) = Ksp \qquad (2.16)$$

where $a_{M^{e+}equ}$ is the activity of M^{e+} at equilibrium $a_{X^{e-}equ}$ is the activity of X^{e-} at equilibrium and a_{MXequ} is the activity of sold precipitate. The $a_{MX\ equ}$ is unity by definition for pure salt precipitation, however, this is not precisely true for co-precipitation as is discussed in more detail in [42, 43] and will be discussed in detail in Chapter 4 of this thesis. The activity for the scaling ions is calculated as following:

$$a_{M^{e+}equ} = \gamma_{M^{e+}} [M^{e+}]_{equ} \qquad (2.17)$$

$$a_{X^{e-}equ} = \gamma_{X^{e-}} [X^{e-}]_{equ} \qquad (2.18)$$

Where $\gamma_{M^{e+}}$ is the activity coefficient of M^{e+}, $\gamma_{X^{e-}}$ is the activity coefficient of X^{e-} and $[M^{e+}]_{equ}$ &$[X^{e-}]_{equ}$ refer to the concentration of scaling ions at equilibrium.

The activity coefficient is a function of the solution composition and illustrates the interaction between the species in the solution. The Pitzer model [44] is a comprehensive model to calculate the activity coefficient in a very complex solution. Pitzer model will be discussed thoroughly and will be incorporated to calculate the activity coefficients in chapters 3 and 4 of this thesis.

Thus, the thermodynamic solubility product (*Ksp*) is a function of system temperature, pressure and composition [4, 43, 45] and all these factors should be taken into account during *Ksp* calculation. Accurate calculation of *Ksp* for the precipitation salt of interest is essential for a reliable prediction of its potential to precipitate, as it is known that the most important single factor determining the propensity for salt precipitation is the supersaturation level of the ions that form it [46]. Thus to achieve accurate prediction of the precipitation potential there is need firstly to know the composition of the solution, and thus calculate accurately the ion activity product (*IAP*) for the scaling ions of interest. The ion activity product (*IAP*) which is expressed in Eq. 2.19 is then compared with *Ksp* for the scaling ion of interest.

$$IAP = \gamma_{X^{e-}}\gamma_{M^{e+}}[M^{e+}].[X^{e-}] \qquad (2.19)$$

If the *IAP* < *Ksp*, there is no potential to precipitation (the solution is unsaturated with respect to the scaling salt of interest).
If the *IAP* = *Ksp*, the solution is in equilibrium for the scaling salt of interest.
If the *IAP* > *Ksp*, there is potential to form scale (the solution is supersaturated with the salt of interest).

Sheikholeslami [4, 5, 12, 45] has suggested the use of the Gibbs free energy change of the precipitation reaction to calculate theoretically the thermodynamic solubility product (*Ksp*). She suggested the use of the Scaling Potential Index (*SPI*) which

represents the logarithm of the quotient of the *IAP* and the *Ksp* of the scaling salt of interest, as can be seen in Eq. 2.20.

$$SPI = \log\left(\frac{IAP}{Ksp}\right) \quad (2.20)$$

This suggestion of using theoretical and fundamental equation to calculate *Ksp* opens the way to develop a theoretical approach to predict the scaling propensity of any scaling salt within full scale RO/NF [45].

SPI has previously [12, 47, 48] been compared and validated with experimental values and with other commonly and industrially used indices. The results of these experiments prove that SPI successfully predicted the onset of scale formation and the scaling type on the membrane surface in a dynamic reverse osmosis unit. For example in Run 1 (sulphate only) in Sheikholeslami 2011 [48] the permeate flux dropped dramatically as the SPI of gypsum became positive at 37% water recovery. In Run 3 (carbonate only) in the same paper the scaling caused flux decline at 8% water recovery at which stage the SPI of calcite became positive. Thus, the results showed that the decline of permeate flux took place at about the point where the SPI of these sparingly soluble salts became positive. Minor deviations are expected due to the complexity of dynamic systems, effects of impurities and inherent system fluctuations [48]. A small negative value might be chosen as criterion, to avoid a positive SPI developing at particular points or particular stages in the operating cycle. A detailed discussion of the SPI and the new approach will be included in chapter 4 of this thesis.

2.4.1.2 Nucleation

In order for crystallisation to begin there is need to have nuclei of crystallisation, minute solid bodies, in addition to the supersaturation condition [49]. These nuclei of crystallisation can take various forms such as seeds, embryos, or foreign matter present in the solution [4]. There are two types of nucleation; primary and secondary [4, 49]. Nucleation is considered secondary when the nucleus is formed on the existing crystal. Primary nucleation refers to the generation of new crystals without

effective existing crystals. Primary nucleation is subdivided into homogeneous and heterogeneous nucleation. Homogenous nucleation happens spontaneously without seeds and the heterogeneous nucleation is dependent on foreign bodies in the solution and uses them as a source of growth [4, 49].

Both types of nucleation (Primary and Secondary) are related indirectly to the solubility of the scaling salt of interest. This indirect relation could be explained according to classic nucleation theory through the relation between the induction time (t_{ind}) for the formation of a critical nucleus, the interfacial tension and the solubility. The induction time (t_{ind}) for the formation of a critical nucleus in a system is described by [50] in Eq.2.21:

$$\log t_{ind} = \frac{B}{(SPI)^2} - C \qquad (2.21)$$

where C is a constant, SPI is defined in Eq.2.20 and represent the degree of saturation with respect to the salt of interest and B is defined as following in Eq. 2.22:

$$B = \frac{\beta_f \sigma^3 V_m{}^n N_A f(\theta)}{(2.3RT)^3} \qquad (2.22)$$

where β_f is a geometric factor ($16\pi/3$ for a spherical nucleus), σ is the interfacial tension between the crystal and the aqueous solution ($J.m^{-2}$), V_m is the molar volume ($cm^3.mol^{-1}$), N_A is Avogadro's number, $f(\theta)$ is a correction factor (0.01 for heterogeneous nucleation and 1 for homogeneous nucleation). The interfacial tension is related to the solubility [51, 52] through Eq.2.23.

$$\sigma = -A\log C_s + F \qquad (2.23)$$

where A ($J.m^{-2}.m^{-1}$) and F ($J.m^{-2}$) are constants for a specific solution and C_s (m) is the salt's solubility. According to Eq. 2.22, as solubility decreases, the interfacial tension (σ) increases. A higher σ causes a high energetic barrier, thus reducing the

statistical chance for the creation of a stable nucleus. This leads to a longer induction time and a slower nucleation rate [53]. The induction time for nucleation is inversely related to rate of nucleation [4]; the reader is directed to [4] and [49] for more in depth mathematical description and discussion.

2.4.1.3 Crystal growth

Crystal growth could be due to the following probable mechanisms as described by Sheikholeslami in [4]: (1) direct ion incorporation into crystal lattice, (2) Nucleation at the surface of crystallite, (3) Particle agglomeration, and (4) Particle adsorption onto the transfer surface.

The rate of crystal growth may be affected by the ionic strength; increasing the ionic strength of the solution reduces the solubility, which results in slower kinetics [50, 53]. Reznik et al. [53] conclude that the rate of crystal growth is not only a function of the thermodynamic driving force, but also depends upon the relative concentration and characteristics of the individual ions. Zhang and Nancollas [54] suggested that the adsorption of background ions such as Na^+, and to a lesser extent K^+, onto the surface of a crystal, partially inhibits its growth rate and retards the precipitation.

2.4.2 $CaSO_4$, $SrSO_4$ scales and co-precipitation

The complex characteristics of the new types of RO/NF feed water such as Produced Water exacerbate the problem of scaling because of the high complexity of scaling prediction when salts such as $CaCO_3$, $CaSO_4$, $BaSO_4$ and $SrSO_4$ co-exist. This complexity of scaling prediction comes from the following scenario:

The mechanism of scaling is expected to be different for different salts as was demonstrated [55] for $CaCO_3$ and $CaSO_4$. Sheikholeslami [4] and her research group showed that the co-existence of $CaCO_3$ and $CaSO_4$ affects the mechanism of fouling and the thermodynamic and kinetic behaviour of each salt. In view of the fact that alkaline scales can be easily eliminated through control of the solution pH more attention should be directed toward the co-precipitation of sulphate scales thus needs to be researched further under RO/NF conditions. As has been observed [42, 56-59], there is a strong interaction between $SrSO_4$, $BaSO_4$ and $CaSO_4$ under marine and

geological conditions. Strontium sulphate and calcium sulphate scale formation have become a growing concern in oil-production systems [60]. $SrSO_4$ scale is expected to be one of the serious problems facing the desalination of Oil and Gas Produced Water. Bader [61] indicated that $SrSO_4$ and $CaSO_4$ constitute the main sulphate scale formed during Nanofiltration (NF) treatment for oil field injection operations. Thus, the experiments in this work have been designed to carry out a comprehensive study of $CaSO_4$ and $SrSO_4$ co-precipitation at different salinity levels and with or without the presence of dissolved organics.

2.4.2.1 $CaSO_4$ and $SrSO_4$ scale

Calcium sulphate causes major concerns in desalination, geochemistry and petroleum engineering. Calcium sulphate can precipitate from aqueous solution in three forms: gypsum ($CaSO_4.2H_2O$), hemihydrate ($CaSO_4.1/2H_2O$) and anhydrate ($CaSO_4$) [62].

Calcium sulphate scale may be deposited due to change in temperature, pressure and the relative concentrations of calcium or sulphate. $CaSO_4$ solubility is fairly independent of pH and hence $CaSO_4$ can readily precipitate in an acid environment.

Intensive research work has been carried out to study $CaSO_4$ precipitation in order to analyse the mechanism and determine the form of calcium sulphate at different temperatures. Partridge and White [63] found that gypsum is the usual precipitating phase in the range of $0 - 98^oC$ while anhydrite and hemihydrate are the species likely to precipitate above 98^oC. Almost all research work [63-65] indicates that gypsum is the dominant phase at temperature below 100^oC which is the range of operation of the majority of heat transfer equipment and desalination processes. In addition, many researchers [5, 62, 66-68] confirmed that the scale formed on the RO membranes is gypsum.

Strontium sulphate scale formation has become a growing concern in oil-production systems [60]. The $SrSO_4$ scale is expected to be one of the serious problems facing the desalination of Oil and Gas Produced Water. Bader [61] indicated that $SrSO_4$ and $CaSO_4$ constitute the main sulphate scale formed during Nanofiltration (NF) treatment for oil field injection operations. There are very limited studies [69-72]

related to $SrSO_4$ scale; the majority of the research work available is more focused on $SrSO_4$ scaling under oil-production systems conditions [58, 72-75].

2.4.2.2 Co-precipitation

In real industrial operations such as RO desalination systems, it is uncommon to have one single scaling salt precipitating and more usual to have a co-precipitate of common salts such as $CaSO_4$, $SrSO_4$, $BaSO_4$ and others. Unfortunately, the great majority of research work on crystallisation has been focussed on studying single salt precipitation. Only a few experimental investigations on co-precipitation of calcium sulphate and calcium carbonate under conditions related to RO/NF processes can be found in the literature [47, 48, 62, 76-82]. The results of such investigations showed that co-precipitation of $CaCO_3$ and $CaSO_4$ affect the precipitation rate, solubility, crystal structure and strength. However, the alkaline scales can be easily eliminated through control of the solution pH. The co-precipitation of sulphate scales should attract more attention and needs to be researched further under RO/NF conditions. As has been observed [42, 56-59], there is a strong interaction between $SrSO_4$, $BaSO_4$ and $CaSO_4$ under marine and geological conditions. The experiments in this work have been designed to carry out a comprehensive study of $CaSO_4$ and $SrSO_4$ co-precipitation at different salinity levels and with or without DO presence.

Thus, there is still need of better understanding to address the effect of co-precipitation on the scaling propensity. Alhseinat et al [43] have recently suggested a semi-theoretical model to incorporate the effect of co-precipitation. This model suggests that there is a need to define experimentally the co-precipitation correction factor (*Cf*). A detailed discussion of this new approach can be found in chapter 4. It has been noticed that co-precipitation may not have the same influence on all precipitated salts. For example Rushdi et al. [42] found that the co-precipitation of $SrSO_4$ and $BaSO_4$ has more influence on $BaSO_4$ than $SrSO_4$, and Sheikholeslami et al. [62] found that the co-precipitation of $CaCO_3$ and $CaSO_4$ has more influence on $CaCO_3$ than it has on $CaSO_4$. Thus, the feed water should be analysed; and the possibility for co-precipitation and its influence at the scaling salt should be addressed.

2.5 Fouling mitigation and prediction

The first step in fouling mitigation is to determine the fouling propensity of feed water. Research studies usually consider a single foulant or a single fouling mechanism and they do not take into account interactive and hydrodynamic effects. The majority of simulations mostly treat fouling in a "black box" way, only as a resistance and without, considering the science involved, simply take flux decline as a measure of fouling. Tay and Song [83] in fact point out that in some full-scale RO process it is shown that flux does not decline with fouling, and hence they state that using permeate flux decline as a measure of fouling provides erroneous results for RO fouling assessment. The inaccuracy and inadequacy of simply using flux as a measure of fouling has been scientifically explained [83]. It is now accepted that the commonly used black-box approaches of considering fouling only as a resistance are generally inapplicable to real conditions. Moreover, the current practice of assessing the fouling propensity "irrespective" of the "membrane type" is inadequate and inappropriate as there are different mechanisms for passage in different membrane processes [5]. The proper measurement, assessment, prediction and mitigation of fouling needs consideration, understanding and incorporation of fouling science and membrane types as shown and discussed in detail by [4].

2.5.1 Fouling indices

The extent of fouling in membrane processes is usually linked to the properties of the process feed and the operating conditions [12]. Several indices have been proposed for assessing the fouling propensity. Interestingly the majority of those indices which are currently applied in membrane processes were originally developed to assess the corrosive tendency of metallic structures [84].

2.5.1.1 Particulate fouling indices

Several approaches have been developed for measuring the speed with which a membrane filter becomes plugged by colloids [85].Silt Density Index (SDI) is the most common method to predict the potential of the particulate (colloidal) fouling of feed water [86]. However, there is a serious deficiency in applying SDI to the RO/NF

membrane processes [87]. The SDI test uses a 45 μm microfiltration membrane in a dead-end filtration experiment. For the details of this test procedure, the reader is referred to [85-88]. In contrast, the RO/NF processes use cross-flow systems; moreover, due to the large membrane pore size used in the SDI test the fine particles passed, which are not taken into account by the SDI value, may cause a serious fouling problem in RO/NF membranes. To overcome the main deficiencies of the SDI method, Schippers et al [85] developed the Modified Fouling Index (MFI). The MFI is proportional to the concentration of colloidal and suspended matter, and thus overcome the main problem of the SDI where there is no linear relationship between the index and the concentration of colloidal and suspended matter [85]. The MFI test procedure can be found in detail in [85-87]. Even the MFI only partially overcomes the disadvantages of the SDI method; Schippers et al emphasise that the MFI can serve only to a limited extent as an index to predict the colloidal fouling within RO/NF processes [85]. This deficiency can be due to limitations in the MFI procedure. For example, the filtration rate in RO is lower by a factor of 100 to 1000 than that in the MFI test; which mean that the stacking of particles on the membrane filter at the MFI test is less dense that on a RO membrane [85].

A detailed discussion of particulate fouling is beyond the scope of this thesis. However, the above discussion of particulate fouling indices highlights the need for new approaches that consider the variation of process parameters and geometries that must be applied in full scale processes.

2.5.1.2 Precipitation fouling (Scaling) indices

Extensive work has been carried out to try to quantify the scaling potential in membrane processes using various indices [39]. Some of theses indices are directed to a specific scalant such as $CaCO_3$ and some of them can be applied for different scalants. Here is below a brief description of the most commonly used indices and the simplifications that are employed within them.

The Langelier Saturation Index (LSI): The LSI was developed by Langelier [6] in 1946 and now is considered as the most commonly used index to predict the onset of

$CaCO_3$ scale. It is derived from the theoretical concept of saturation to provide the $CaCO_3$ degree of saturation of feed water. LSI is calculated as:

$$LSI = pH - pHs \quad (2.24)$$

where pH is the measured water pH and pHs is the pH at saturation in $CaCO_3$. pHs can be calculated by:

$$pHs = p[Ca] + p[HCO^-_3] + C \quad (2.25)$$

C is obtained empirically:

$$C = 9.3 + 0.1 (Log [TDS]-1) - 13.12 Log (T) + 34.95 \quad (2.26)$$

If LSI is negative there is no potential to form $CaCO_3$ scale: however, the system is considered corrosive. If LSI is positive there is potential to form $CaCO_3$ scale. If LSI is equal to zero the system is in equilibrium with respect to $CaCO_3$.

The LSI is purely an equilibrium index and deals only with the thermodynamic driving force for $CaCO_3$ scale formation. The LSI is only applicable to low total dissolved solid (TDS) values because, in its derivation, it does not consider the activity and assumes the activity coefficients to be unity [12].

Stiff-Davis Stability Index (S&DSI): Stiff and Davis [7] modified the LSI to account for high levels of TDS. The S&DSI can be calculated using Eq. 2.27

$$S\&DSI = pH - pHs \quad (2.27)$$

$$pHs = p[Ca] + p[HCO_3^-] + k \quad (2.28)$$

where pH and pHs has the same definition given in LSI. *k* is a function of ionic strength and temperature.

If S&DSI < 0; no potential to form $CaCO_3$ and this system is corrosive.

S&DSI > 0; there is potential to form $CaCO_3$ scale.

There are other indices that can be used to predict the propensity of $CaCO_3$ scale formation such as the Ryznar Stability Index (RSI) [8], Puckorius Scaling Index (PSI) [89], Larson-Skold Index (L&SI) [90], and Oddo-Tomson Index (O&TI) [91]. For more detail reader is the referred to the original publications cited above.

Supersaturation index (SI): The effect of supersaturation is considered to be the most important single factor that determines the propensity of crystallisation fouling [46, 78, 92, 93]. SI can be determined from Eq. 2.29 which represents the ratio between the ion activity product (*IAP*) which is expressed in Eq. 2.19 and the thermodynamic solubility product *Ksp* which is defined by Eq. 2.16 for the scaling ion of interest.

$$SI = \frac{IAP}{Ksp} \qquad (2.29)$$

Ksp as discussed before in section 2.5 is a function of temperature, pressure and ionic strength. The SI can be used to indicate the possibility of precipitation for any salt. If the SI is greater than unity for a specific salt this is a clear warning sign for scaling potential [84].

However, to successfully predict the propensity of scaling using the SI there is a need to consider the precise composition of the analysed water because the interactive effects between all existing ions must be taken into account. Unfortunately, there is shortfall in the current industrial practises; for example the Du Pont method which is considered the most frequently used model for the application of supersaturation index, [84, 94] incorporates significant simplifications. The Du Pont method is based on predicting the scalant solubility at 25 ^{o}C using a solubility product, *Kc* [94]. *Kc* expresses the dynamic equilibrium between the scalant involved ions in solution and the crystal solid phase; *Kc* is defined for (*MX*) salt using eq.2.30.

$$Kc = [M^{e+}][X^{e-}] \qquad (2.30)$$

The square brackets represent the molar ionic concentration. Thus the Du Pont index neglects the effect of electrical interactions that occur between ions even if the *Kc* is corrected to account for ionic strength effects [94].

Sheikholeslami [4, 5, 12, 45] has proposed the use of a new saturation index called the Scaling Potential Index (*SPI*) to predict the onset of scaling in RO/NF processes. The *SPI* will be modified and discussed in more detail in chapter 4 of this thesis.

2.5.2 Factors affecting fouling formation

The factors affecting the fouling formation can be classified as:

1) Operating conditions: such as pH, temperature, operating pressure, permeation rate and flow velocity [84, 95]. The temperature is an important factor that could enhance or reduce the precipitation of the scalant salts. For example increasing feed temperature will increase the precipitation of $CaSO_4$ [96]. Feed pH can affect the solubility of same salts such as $CaCO_3$ [80]. Thus fixing the feed pH can help to eliminate the precipitation of such salts. Process or operating pressure can effect the dissolved oxygen and carbon dioxide concentrations in the aqueous medium and thus enhance the biological as well as corrosion fouling or crystallisation fouling by $CaCO_3$ [4]. Process pressure, especially in high pressure membrane processes may alter the solubility of the scalant salts. The derivation and the inclusion of process pressure on the scaling propensity prediction will be discussed later in chapter 4. Permeation rate and flow velocity determine the degree of concentration polarization. Higher permeation rates mean higher CP while higher flow velocity decreases the CP as discussed before in section 2.1.2. Lee et al. [97] have demonstrated that surface crystallisation is directly influenced by concentration polarization. The effects of most of the above operating conditions on the prediction of scaling propensity in full scale RO/NF process have been included and discussed in more detail later in this thesis.

2) Feed water composition and salinity: Proper feed characterisation is essential for fouling prediction and mitigation [4]. Proper characterisation will account for ion-specific interactions and anticipate the possibility of co-precipitation and its effect. Salinity of process water is another factor that affects the solubility of scalant salts [62]. The variation of feed composition and salinity in the RO/NF process should not be ignored and must be taken into consideration in any attempt to predict the scaling

propensity within full scale RO/NF processes. In this thesis a novel approach has been developed to account for the change in individual ionic concentrations and total salinity and incorporate that with a fundamental approach to predict the onset of scaling propensity within a full scale RO/NF process.

3) Membrane characteristics: Clean membrane resistance is a characteristic of the RO membranes and various ranges are available on the market [83]. Clean membrane resistance specifies the permeability of the membrane and thus can be related to the effect of concentration polarisation as well. Also the membrane rejection capability for specific salts is important to determine the variation of concentrate composition and thus facilitate the scaling propensity prediction. Surface roughness, surface energy and charge, hydrophilicity and hydrophobicity greatly affect the magnitude of intermolecular forces between the surface and foulants. The reader is refereed to [4] for a more in depth discussion of the effect of surface characteristics on fouling.

2.5.3 Fouling in full scale RO/NF processes

The variation of processes variables and parameters in full scale RO/NF processes make it harder to implement the currently used approach for fouling prediction and mitigation. Unfortunately, even though there are a few attempts to model the fouling in full scale RO/NF processes, these attempts always treat fouling as a black-box manner and ignore the science of fouling and the interaction effects in fouling processes. For example, recently, Hoek et al [32] tried to model the effects of fouling on full scale reverse osmosis processes. In their paper they use a global approach and treat fouling in a black-box manner. They even have a subsection 2.3.2 entitled “internal fouling by physical compaction” which in itself is erroneous because there is no such thing as internal fouling for RO, as it is a non-porous membrane, and physical compaction cannot be fouling. Internal fouling only exists in porous membranes where the pores become blocked. Fouling is defined scientifically and means in the English language deposition of unwanted material, never compaction. Further any RO membrane, even in absence of any foulant, becomes compacted. A proper assessment of fouling is conducted after operating the RO membranes with

distilled and filtered ultra-pure water for a period of time to compact them and eliminate flux reduction due to compaction in the measurements. Further the paper totally ignores water quality parameters. In addition, it uses the concept of particle deposition in dead end micro-filtration to cross-flow RO. In dead-end micro-filtration deposition is by micron-sized particles and in RO by colloidal particles that move subject to a completely different mechanism. In addition, dead-end micro-filtration fluid mechanics are very different from cross-flow RO.

Chen et al [11] and Tay and Song [83], in their attempts to model the fouling in full scale RO processes, neglect fouling science and consider the fouling in best case as a new resistance to permeation. Chen et al [11] in their paper firstly treat the "fouling layer" in a black-box way without consideration of fouling science. They also use the usual approach of a serial fouling and membrane resistances and introduce a factor determined experimentally by a test within a small RO unit based on its asymptotic fouling resistance. This ignores the fouling science and its importance in formation, build up and resistance of the fouled layer. Tay and Song [83] in their paper discuss the fact that, in full-scale RO processes, it has been operationally shown that using permeate flux decline as a measure of fouling, such as done by Hoek et al [32] provides erroneous results for RO fouling assessment. They suggest a term "filtration coefficient" and combine it with their global approach discussed above. However, these papers highlight the importance of thermodynamic effects in full scale processes and also pointing out the fact that flux is not a parameter to be used in isolation for the characterization of fouling – flux decline is just a symptom. Bhattacharjee and Johnston [98] have used a coupled model of concentration polarization, fouling by scale formation, and pore transport of ionic solutes to predict the flux decline and ion separation during nanofiltration operations involving a ternary mixture of Na_2SO_4 and $CaSO_4$. Their work has highlighted the importance of predicting the fouling behaviour at different axial position in crossflow filtration channel.

Mane et al [99] have recently developed a mechanistic predictive model to simulate the rejection of boron by a spiral wound reverse osmosis (RO) membrane element

under varying water quality and operating conditions. Their paper has no relevance to fouling. However, their paper highlights the use of alkali at different stages for boron removal and therefore indirectly points out the inadequacy of empirically based indices that do not have the capacity to assess varying conditions and water chemistry along the membrane module; thus, there is a further reason for having a new theoretically based approach that has the capability to incorporate water chemistry for assessing fouling by sparingly soluble salts at any location within the module with a further capability of taking into account also membrane-specific ion passages effects along the module.

2.5.4 Fouling mitigation

Fouling mitigation strategies start with understanding the factors affecting the fouling mechanisms. According to Sheikholeslami [4] these factors include the type, actual concentration of foulant, flow conditions, hydrodynamics, surface geometry and characteristics, temperature, pH, pressure, and any factor that could modify any of these parameters.

The most common scale mitigation techniques can be grouped into three categories [84]:

1. Altering feed water characteristics through pre-treatment,
2. Optimising operating parameters and system design and
3. Antiscalant addition.

The choice of the mitigation strategy should be built on three factors: the effectiveness in fouling prevention, economics and environmental viability. No general approach can be given to choose the right mitigation strategy and every process should be examined on its own merits [4]. Thus, a reliable approach that can account for the type and the propensities of the foulant would help to facilitate the decision taking. For further discussion of the mitigation strategies reader is referred to [4, 84].

2.6 Summary

This chapter indicates the knowledge required in order to facilitate the development of new approaches for fouling propensity prediction within full scale RO/NF processes. The history and fundamentals of RO/NF processes have been reviewed. Also, fouling science and types have been discussed. The currently used indices for fouling prediction have been reviewed. The important of considering the specific ionic-interactions and the process hydrodynamics in fouling propensity prediction have been highlighted.

The next chapter will introduce a new approach for accounting for the variation of specific ion interactions within a full scale RO/NF processes. Then in chapter 4 the new approach will be coupled with a fundamental method for fouling propensity prediction and the effect of the operational parameters, co-precipitation and process pressure will be incorporated and discussed. The rest of the thesis will aimed to enhancing understanding of crystallisation fouling and the effect of co-precipitation. A comprehensive experimental study of $CaSO_4$ and $SrSO_4$ co-precipitation will be discussed. Then the proposed approaches will be experimentally validated using laboratory membrane rig.

Chapter 3

Reliable thermodynamic description of RO/NF concentrates along full scale module using the Pitzer Model

3. Thermodynamic description of RO/NF concentrates using the Pitzer model

In this chapter a reliable thermodynamic description of RO/NF concentrates along full scale module will be described and achieved using the Pitzer model. The primary novelty of the developed approach is its ability to predict the local thermodynamic behaviour (Activity coefficient and Osmotic coefficients) at different axial position in a long membrane filtration channel. The Matlab programs that have been developed to achieve this reliable description will be illustrated and verified in this chapter. This chapter has been divided to seven sections. The first section gives general introduction where the motivation of creating this approach has been highlighted and discussed, also the important and general logic of the purposed approach has been discussed. The second section of this chapter was divided to two subsections where a brief discussion of the activity models has been provided. The three next sections (3.3,3.4, and 3.5) discuss the developed Matlab programs for activity coefficients and osmotic coefficients calculations, the modelling of the species concentration change along full scale RO/NF module, and the developed Matlab program that account for the change of activity coefficients, osmotic coefficients and species concentrations along full scale RO/NF filtration channel. Section 3.6 discuses the confidence of the simulation and section 3.7 gives a brief summary of the chapter.

3.1 Introduction

Fouling in membranes is not as historically important as it is in other types of process equipment, because membrane separation is a relatively newer process than others. Presumably for this reason the majority, if not almost all, of models and simulations on membrane fouling treat fouling without any consideration of the fouling mechanism and purely as an extra resistance. Furthermore, within a module these approaches assume uniform flow properties and fouling rate throughout the module

and over the membrane surface while in a membrane channel system variables and parameters change substantially along its length. Ignoring the science of fouling and making these further assumptions renders the existing models unrealistic in the assessment of fouling in a full-scale RO/NF process. For crystallization fouling, the normal practice is to use empirical indices to assess the fouling potential of feed water due to sparingly soluble dissolved salts. As shown and discussed in [100], these empirical relationships are not suitable for membrane processes. Furthermore, nanofiltration (NF) and RO membranes should not be treated identically as highlighted in Chapter 2. Even as discussed elsewhere [4, 5] the LSI and S & DSI, which use the theoretical concept of saturation, include significant simplifications and empirical relationships in their derivation and do not reflect the high salinities, the interactive effects and the operational conditions within the membrane module. Therefore, it is inadequate to apply these indices to predict what may happen in the membrane desalination module train and their predictions are incorrect. Thus there is a further reason for having a theoretically based approach that has the capability to incorporate water chemistry for assessing fouling by sparingly soluble salts at any location within the module with the further capability of also taking into account the effect of membrane specific ion passages along the module.

In order to achieve reliable prediction of fouling propensity in full scale membrane channel, a reliable prediction of the local thermodynamic behaviour (Activity coefficient and Osmotic coefficients) at different axial position in the membrane filtration channel is needed. This chapter introduces a novel approach to predict the local thermodynamic behaviour (Activity coefficient and Osmotic coefficients) at different axial position in a long membrane filtration channel.

3.1.1 The present approach

This approach is based on an almost theoretical approach for calculating the activity coefficients and osmotic coefficients propensity within a full-scale RO/NF desalination module. In this approach a thermodynamic modelling of RO/NF concentrates is accomplished using the Pitzer model for ionic activity coefficients

and osmotic pressure coefficient. A Matlab program is written to simultaneously account for the change in ionic concentrations along the membrane channel and thus the change in water chemistry and to consider changes of the operating variables. This program has been designed to account for the activity coefficients of all ionic species present in the concentrate. The changes of concentrate density and viscosity have been calculated and taken into account using the extended equation of state for seawater at elevated temperature and salinity [101]. The confidence of the simulation has been tested through a comparison between the calculated data and some published data at the same simulation conditions. The goal of this program is to achieve a reliable thermodynamic description of the RO/NF concentrate.

This approach will assist to consider the science of fouling by considering the solution chemistry, and thermodynamics and combines those with principles of osmosis, mass transport across the membrane and conservation of mass within the RO/NF module. It results in a simulation model for scientifically and theoretically predicting the onset of crystallization fouling within RO/NF modules, as will be discussed further in Chapter 4. This approach is a very powerful tool that could help in the specific design of RO/NF processes as well as in simulations of the operating variables for optimization of the RO/NF system. It could easily be developed to be more user- friendly.

3.2 Activity coefficients models

Activity coefficients of electrolytes dissolved in water are a special subject of study in the electrochemical literature [102]. There are several semi-empirical models in the literature that can be used to predict the activity coefficients of electrolytes dissolved in water, most of them were discussed in [103]. For studies involving ion-selective membranes with different ionic permeabilities, it is often difficult to predict the activity coefficients of the ions within these models [102]. However, these activity coefficients are necessary for the calculation of the electrochemical potential which is a very important parameter in determining the thermodynamic equilibrium

[102]. Thus, reliable prediction of the activity coefficients is essential to achieve a reliable prediction of the potential of scaling within the membranes models.

The Poisson Boltzman equation and the Debye-Hückel theory are the basis of a number of successful semi-empirical equations for a variety of thermodynamic properties [104]. The more popular of these are discussed in references [103, 104]. Perhaps the most widely applicable of these equations are those developed by Pitzer and coworkers since 1973 [104]. Pitzer [44, 105-108] discusses the origin of these equations and their application in some detail.

3.2.1 Debye-Huckel theory

Debye- Hückel theories assume the ions to be charged species with a fixed diameter in a continuous dielectric medium [104]. The original Debye- Hückel formulation is valid only for very low concentrations below 0.001 m, due to assuming the ions to be point charges. The extended Debye- Hückel theory assigns a value to the ionic diameter and thus can be applied for concentrations up to 0.1 m. The Debye- Hückel limiting law gives the activity coefficients γ_i in terms of the ionic strength, *I*, which defined by Eq.3.1.

$$I = \frac{1}{2}\sum_i m_i z_i^2 \qquad (3.1)$$

where z_i is the charge on ion *i*, and m_i is the molality of ion *i*.

The activity coefficient can be calculated by the Debye-Hückel Limiting Law using Eq.3.2

$$\log \gamma_i = -A.z_i^2.I^{1/2} \qquad (3.2)$$

where A = 0.509 / (mol kg^{-1})$^{1/2}$ for an aqueous solution at 25 ^{o}C. In general, *A* depends on the relative permittivity of solvent and the temperature.

The activity coefficient may be estimated from the extended Debye-Hückel law using Eq.3.3.

$$\log \gamma_i = \frac{-A.z_i^2.I^{1/2}}{1+b.I^{1/2}} \qquad (3.3)$$

where b is a measure of distance between ions. In the limit of small concentration $I^{1/2} << 1$, and, in the denominator of Eq.3.3, $I^{1/2}$ can be neglected; the extended Debye-Hückel Law tends to the Debye-Hückel Limiting Law at low concentrations.

The Debye- Hückel and the extended Debye-Hückel theory are the basis of a number of successful semi-empirical equations for a variety of thermodynamic properties [104]. Pitzer and his research team established very widely applicable equations for high concentrations up to 6 m. Pitzer in his publication [44, 105] discusses the origin of these equations and their application in some detail [104]. Here is below a brief description of Pitzer equations that have been used in this work.

3.2.2 Pitzer model

The Pitzer model can be considered as an extension of the Debye-Hückel model. The general formulation of the Pitzer model can be described by Eq.3.4 which correlates the total excess Gibbs energy with the ionic composition. The first part of this equation corresponds to the Debye- Hückel model and is function of ionic strength and the dielectric constant of the solvent [109]. The second and the third terms are introduced to model binary and ternary interactions which were neglected in the initial Debye- Hückel model. Pitzer introduced and formulated these two terms in order to describe the behaviour of solutions at high concentrations [109].

$$\frac{G^{ex}}{n_w R_g T} = f(I) + \sum_i \sum_j \lambda_{ij} m_i m_j + \sum_i \sum_j \sum_k \mu_{ijk} m_i m_j m_k \qquad (3.4)$$

where $f(I)$ is a function of ionic strength, expressing the effect of the long-range electrostatic forces; i,j and k are different anions (or cations), m_i denotes molality of the ith ion (moles per kilogram) and n_w is number of kilograms of water. λ_{ij} is a second virial coefficient which expresses the effect of the short-range forces between species i and j. λ_{ij} is dependent on the ionic strength. μ_{ijk} is third virial coefficient which allows for triple ion interactions; μ_{ijk} is independent of the ionic strength [108].

The activity coefficient equations are obtained by appropriate derivations from Eq.3.1 which are described in detail in [44, 105, 107, 108]. Equations (3.5-3.6) are used to obtain the ionic activity coefficients for cations M and anions X:

$$\ln(\gamma_M) = z_M^{\,2} F + \sum_a m_a (2B_{Ma} + ZC_{Ma}) + \sum_c m_c (2\Phi_{Mc} + \sum_a m_a \psi_{Mca}) + \sum_{a<} \sum_{a'} m_a m_{a'} \psi_{aa'M} + z_M \sum_c \sum_a m_c m_a C_{ca} \quad (3.5)$$

$$\ln(\gamma_X) = z_X^{\,2} F + \sum_c m_c (2B_{cX} + ZC_{cX}) + \sum_a m_a (2\Phi_{Xa} + \sum_c m_c \psi_{Xac}) + \sum_{c<} \sum_{c'} m_c m_{c'} \psi_{cc'X} + |z_X| \sum_c \sum_a m_c m_a C_{ca} \quad (3.6)$$

The osmotic coefficient $\varphi_{osmotic}$ which characterises the deviation of solvent from ideal behaviour can be calculated using Eq. 3.7. The calculation of osmotic coefficient is important in calculation of the osmotic pressure within the RO/NF module, as will be discussed in more detail in section 3.4.

$$(\varphi_{osmotic} - 1) = \frac{2}{\sum_i m_i} \left[\frac{-A_\phi I^{3/2}}{(1 + bI^{1/2})} + \sum_c \sum_a m_c m_a (B^\phi_{ca} + ZC_{ca}) + \sum_{c<} \sum_{c'} m_c m_{c'} (\Phi^\phi_{cc'} + \sum_a m_a \psi_{cc'a}) + \sum_{a<} \sum_{a'} m_a m_{a'} (\Phi^\phi_{aa'} + \sum_c m_c \psi_{caa}) \right] \quad (3.7)$$

The various terms in Eqs.3.5-3.7 are defined as follows:

I is the ionic strength which defined by Eq.3.1 as $I = \frac{1}{2} \sum_i m_i z_i^2$

The term F in equations 3.5 and 3.6 is defined by Eq.3.8

$$F = f^\gamma + \sum_c \sum_a m_c m_a B'_{ca} + \sum_{c<} \sum_{c'} m_c m_{c'} \Phi'_{cc'} + \sum_{a<} \sum_{a'} m_a m_{a'} \Phi'_{aa'} \quad (3.8)$$

where f^γ is defined by Eq.3.9

$$f^\gamma = -A_\phi \left[\frac{I^{1/2}}{1 + bI^{1/2}} + \frac{2}{b} \ln(1 + bI^{1/2}) \right] \quad (3.9)$$

where b is 1.2 and A_ϕ , which is the Debye- Hückel slope. The variation of the Debye- Hückel slope, A_ϕ , for the activity coefficient with temperature can be expressed in Eq. 3.10 [110].

$$A_\phi = 3.6901531\times10^{-1} - 6.32100430\times10^{-4}T + \frac{9.1425359}{T} - 1.35143986\times10^{-2}\ln T + \frac{2.26089788\times10^{-3}}{T-263} + 1.92118597\times10^{-6}T^2 + \frac{4.52586464\times10^{1}}{680-T} \quad (3.10)$$

where *T* is the absolute temperature in Kelvins.

The variables B_{MX}, B^{ϕ}_{MX}, and C_{MX} which define the thermodynamic properties of single-salts solution are given below by

$$B_{MX} = \beta^{(0)}_{MX} + \beta^{(1)}_{MX} g(\alpha_1 I^{1/2}) + \beta^{(2)}_{MX} g(\alpha_2 I^{1/2}) \quad (3.11)$$

in which:

$$g(x) = 2\left[1-(1-x)e^{-x}\right]/x^2 \quad (3.12)$$

$$g'(x) = -2\left[1-(1+x+0.5x^2)e^{-x}\right]/x^2 \quad (3.13)$$

$$B'(x) = \beta^{(1)}_{MX} g'(\alpha_1 I^{1/2})/I + \beta^{(2)}_{MX} g'(\alpha_2 I^{1/2})/I \quad (3.14)$$

$$B^{\phi}_{MX} = \beta^{(0)}_{MX} + \beta^{(1)}_{MX}\exp(-\alpha_1 I^{1/2}) + \beta^{(2)}_{MX}\exp(-\alpha_2 I^{1/2}) \quad (3.15)$$

$$C_{MX} = \frac{C^{\phi}}{2\left|z_M z_X\right|^{1/2}} \quad (3.16)$$

The parameters $\beta^{(0)}$, $\beta^{(1)}$, $\beta^{(2)}$, and C^{ϕ} that define the variables *B* and *C* are fitted from single-salt data [111] and the literature values of these parameters are tabulated here in Table 3.1. For any salt containing a monovalent ion such as 1-1 (e.g. NaCl), 1-2 (e.g Na_2SO_4) or 2-1 (e.g. $CaCl_2$) α_1 = 2 and α_2 = 0. For 2-2 (e.g $CaSO_4$) electrolytes α_1 =1.4 and α_2 =12.0. For 3-2 and 4-2 electrolytes α_1 =2 and α_2 =50 [106].

The coefficient to C_{MX}, Z, in Eqs. 3.5-3.7 is defined by Eq. (3.17) below

$$Z = \sum_i m_i \left| z_i \right| \tag{3.17}$$

The parameters Φ and ψ are determined from two-salt systems. Φ accounts for cation-cation and anion-anion interaction while the parameter ψ is defined for cation-cation-anion and anion-anion-cation interaction. Values of Φ_{ij} can be determined using Eqs.3.18-3.25

$$\Phi_{ij}^{\phi} = \theta_{ij} + I\,{}^{E}\theta_{ij}^{'}(I) + {}^{E}\theta_{ij}(I) \tag{3.18}$$

$$\Phi_{ij} = \theta_{ij} + {}^{E}\theta_{ij}(I) \tag{3.19}$$

$$\Phi_{ij}^{'} = {}^{E}\theta_{ij}^{'}(I) \tag{3.20}$$

$${}^{E}\theta_{ij}(I) = \left(\frac{\left|z_i z_j\right|}{4I}\right)\left[J(x_{ij}) - 0.5J(x_{ii}) - 0.5J(x_{jj})\right] \tag{3.21}$$

$${}^{E}\theta_{ij}^{'} = \left(\frac{-{}^{E}\theta_{ij}}{I}\right) + \left(\frac{\left|z_i z_j\right|}{8I^2}\right)\left[x_{ij}J^{''}(x_{ij}) - 0.5x_{ii}J^{''}(x_{ii}) - 0.5x_{jj}J^{''}(x_{jj})\right] \tag{3.22}$$

$$x_{ij} = 6\left|z_i z_j\right| A_{\phi} I^{0.5} \tag{3.23}$$

$$J(x) = x\left[4 + 4.581\ x^{-0.7237}\ \exp(-0.0120\ x^{0.528})\right]^{-1} \tag{3.24}$$

$$J''(x) = \frac{4 + \left[4.581x^{-0.7237}\exp(-0.0120x^{0.528})\right]\left[0.006336x^{0.528} + 1.7237\right]}{\left[4 + 4.581x^{-0.7237}\exp(-0.012x^{0.528})\right]^2} \tag{3.25}$$

In the above equations m_i denotes molality of the i^{th} ion (moles per kilogram) where the subscripts M, c and c' refer to cations and the subscripts X, a and a' to anions. The summation index, c, denotes the sum over all cations in the system while the double summation index, c<c', denotes the sum over all distinguishable pairs of dissimilar cations. Similar definitions apply to the summation indices for anions X, a and a'. *B* and *f* represent measurable combinations of the second virial coefficients λ . *C* and ψ represent measurable combinations of the third virial coefficients μ [109]. The

terms ${}^{E}\theta_{ij}$ and ${}^{E}\theta'_{ij}$ account for electrostatic mixing effects of unsymmetrical cation-cation and anion-anion pairs [107]. Values of ${}^{E}\theta_{ij}$ and ${}^{E}\theta'_{ij}$ depend only on ion charge and total ionic strength and are zero when *ij* cation or anion pairs have the same charge [111].

Pitzer ion interaction parameters $\beta^{(0)}$, $\beta^{(1)}$, $\beta^{(2)}$, θ, ψ, and C^{ϕ} are functions of temperature. Different empirical functions have been used to describe the variation of these parameters with respect to temperature [112]. The following ten parameter expression has been used to recast these function [112].

$$X(T) = a_1 + a_2 T + \frac{a_3}{T} + a_4 \ln T + \frac{a_5}{T-263} + a_6 T^2 + \frac{a_7}{680-T} + \frac{a_8}{T-227} + a_9 T^3 + a_{10} T^4$$

(3.26)

With *X(T)* being one of Pitzer's parameters $\beta^{(0)}$, $\beta^{(1)}$, $\beta^{(2)}$, θ, ψ, and C^{ϕ}. The a_i constants in Eq.3.26 are given in Table 3.1 for binary interaction parameters and in Table 3.2 for ternary interaction parameters. T is the temperature in Kelvins.

Three separate Matlab programs have been written for calculating the anion and cation activity coefficients and the osmotic coefficient in the RO/NF concentrate stream using Eqs.3.1-3.26. These programs can be used to calculate the activity coefficient and osmotic pressure for any solution with known composition. The logic of these programs will be discussed here below and the details Matlab programs will be included in the appendix (B).

Table 3.1: *Values of fitting constants (Eq.3.26) for the binary interaction parameters for aqueous electrolytes*

		Constants (T in degrees Kelvin)				
		a1	a2	a3	a4	a5
		a6	a7	a8	a9	a10
A_ϕ [110]		3.37E-01	-6.32E-04	9.14E+00	-1.35E-02	2.26E-03
		1.92E-06	4.53E+01	0.00E+00	0.00E+00	0.00E+00
Na,Cl [110]	$\beta^{(0)}$	1.44E+01	5.61E-03	-4.22E+02	-2.51E+00	0.00E+00
		-2.62E-06	4.44E+00	-1.71E+00	0.00E+00	0.00E+00
	$\beta^{(1)}$	-4.53E-01	1.41E-03	1.19E+02	0.00E+00	0.00E+00
		0.00E+00	0.00E+00	-4.23E+00	0.00E+00	0.00E+00
	C^ϕ	-1.01E-01	-1.81E-05	8.61E+00	1.25E-02	0.00E+00
		3.41E-08	6.83E-02	2.94E-01	0.00E+00	0.00E+00
Na,SO4 [110]	$\beta^{(0)}$	8.17E+01	3.01E-02	-2.32E+03	-1.44E+01	-6.66E-01
		-1.04E-05	0.00E+00	0.00E+00	0.00E+00	0.00E+00
	$\beta^{(1)}$	1.00E+03	5.77E-01	-2.18E+04	-1.89E+02	-2.04E-01
		-3.24E-04	1.47E+03	0.00E+00	0.00E+00	0.00E+00
	C^ϕ	-8.08E+01	-3.55E-02	2.02E+03	1.46E+01	-9.17E-02
		1.44E-05	-2.42E+00	0.00E+00	0.00E+00	0.00E+00
KCl [113]	$\beta^{(0)}$	2.67E+01	1.01E-02	-7.58E+02	-4.71E+00	0.00E+00
		-3.76E-06	0.00E+00	0.00E+00	0.00E+00	0.00E+00
	$\beta^{(1)}$	-7.42E+00	0.00E+00	3.23E+02	1.16E+00	0.00E+00
		0.00E+00	0.00E+00	-5.95E+00	0.00E+00	0.00E+00
	C^ϕ	-3.31E+00	-1.30E-03	9.13E+01	5.86E-01	0.00E+00
		4.96E-07	0.00E+00	0.00E+00	0.00E+00	0.00E+00
K,SO4 [113]	$\beta^{(0)}$	4.08E+01	8.27E-03	-1.42E+03	-6.75E+00	0.00E+00
		0.00E+00	0.00E+00	0.00E+00	0.00E+00	0.00E+00
	$\beta^{(1)}$	-1.32E+01	2.36E-02	2.07E+03	0.00E+00	0.00E+00
		0.00E+00	0.00E+00	0.00E+00	0.00E+00	0.00E+00
	C^ϕ	-1.88E-02	0.00E+00	0.00E+00	0.00E+00	0.00E+00
		0.00E+00	0.00E+00	0.00E+00	0.00E+00	0.00E+00
Ca,Cl [110]	$\beta^{(0)}$	-9.42E+01	-4.05E-02	2.35E+03	1.71E+01	-9.23E-01
		1.51E-05	-1.39E+00	0.00E+00	0.00E+00	0.00E+00
	$\beta^{(1)}$	3.48E+00	-1.54E-02	0.00E+00	0.00E+00	0.00E+00
		3.18E-05	0.00E+00	0.00E+00	0.00E+00	0.00E+00
	C^ϕ	1.93E+01	9.77E-03	-4.28E+02	-3.58E+00	8.82E-02
		-4.62E-06	9.91E+00	0.00E+00	0.00E+00	0.00E+00
Ca,SO4 [110]	$\beta^{(0)}$	1.50E-01	0.00E+00	0.00E+00	0.00E+00	0.00E+00
		0.00E+00	0.00E+00	0.00E+00	0.00E+00	0.00E+00
	$\beta^{(1)}$	3.00E+00	0.00E+00	0.00E+00	0.00E+00	0.00E+00
		0.00E+00	0.00E+00	0.00E+00	0.00E+00	0.00E+00
	C^ϕ	-1.29E+02	4.00E-01	0.00E+00	0.00E+00	0.00E+00
		0.00E+00	0.00E+00	0.00E+00	0.00E+00	0.00E+00

Table 3.1 (continued)

		Constants (T in degrees Kelvin)				
		a1	a2	a3	a4	a5
		a6	a7	a8	a9	a10
Mg,Cl [114]	$\beta^{(0)}$	5.76E-01	-9.32E-04	0.00E+00	0.00E+00	0.00E+00
		5.94E-07	0.00E+00	0.00E+00	0.00E+00	0.00E+00
	$\beta^{(1)}$	2.60E+00	-1.09E-02	0.00E+00	0.00E+00	0.00E+00
		2.60E-05	0.00E+00	0.00E+00	0.00E+00	0.00E+00
	C^{ϕ}	5.95E-02	-2.50E-04	0.00E+00	0.00E+00	0.00E+00
		2.42E-07	0.00E+00	0.00E+00	0.00E+00	0.00E+00
Mg,SO_4 [114]	$\beta^{(0)}$	9.39E+01	-5.14E-01	-6.85E+03	0.00E+00	0.00E+00
		1.41E-03	0.00E+00	0.00E+00	-1.95E-06	1.08E-09
	$\beta^{(1)}$	5.29E+02	-1.48E-01	-5.78E+03	0.00E+00	0.00E+00
		1.58E-04	0.00E+00	0.00E+00	0.00E+00	0.00E+00
	$\beta^{(2)}$	1.06E+03	-6.88E+00	-6.79E+04	0.00E+00	0.00E+00
		2.02E-02	0.00E+00	0.00E+00	-2.30E-05	0.00E+00
	C^{ϕ}	-3.72E+01	2.11E-01	2.63E+03	0.00E+00	0.00E+00
		-5.95E-04	0.00E+00	0.00E+00	8.37E-07	-4.69E-10
Sr,Cl [115]	$\beta^{(0)}$	4.43E+00	-1.10E-02	-5.12E+02	0.00E+00	0.00E+00
		9.44E-06	0.00E+00	0.00E+00	0.00E+00	0.00E+00
	$\beta^{(1)}$	1.14E+01	-3.36E-02	-1.06E+03	0.00E+00	0.00E+00
		4.24E-05	0.00E+00	0.00E+00	0.00E+00	0.00E+00
	C^{ϕ}	-1.54E-02	0.00E+00	4.51E+00	0.00E+00	0.00E+00
		0.00E+00	0.00E+00	0.00E+00	0.00E+00	0.00E+00
Ba,Cl [116]	$\beta^{(0)}$	3.44E+01	6.38E-04	-1.34E+03	-5.30E+00	0.00E+00
		4.61E-06	0.00E+00	0.00E+00	0.00E+00	0.00E+00
	$\beta^{(1)}$	-1.04E+02	3.23E-03	4.37E+03	1.59E+01	0.00E+00
		-6.77E-06	0.00E+00	0.00E+00	0.00E+00	0.00E+00
	C^{ϕ}	-2.41E+01	-1.54E-04	7.84E+02	3.90E+00	0.00E+00
		-1.10E-05	0.00E+00	0.00E+00	8.76E-09	0.00E+00
Na,HSO_4 [117]	$\beta^{(0)}$	9.48E-01	-5.97E-03	1.19E-05	-8.61E-09	0.00E+00
		0.00E+00	0.00E+00	0.00E+00	0.00E+00	0.00E+00
	$\beta^{(1)}$	-5.99E+00	3.18E-02	-4.08E-05	5.43E-09	0.00E+00
		0.00E+00	0.00E+00	0.00E+00	0.00E+00	0.00E+00
	C^{ϕ}	-1.55E-01	1.06E-03	-2.40E-06	1.82E-09	0.00E+00
		0.00E+00	0.00E+00	0.00E+00	0.00E+00	0.00E+00
Ca,HSO_4 [118]	$\beta^{(0)}$	-4.22E+01	-1.43E-02	0.00E+00	0.00E+00	9.88E+02
		7.62E+00	0.00E+00	0.00E+00	0.00E+00	0.00E+00
	$\beta^{(1)}$	9.33E+02	2.48E-01	0.00E+00	0.00E+00	-2.58E+04
		-1.61E+02	0.00E+00	0.00E+00	0.00E+00	0.00E+00
Ca,OH [118]	$\beta^{(0)}$	-1.58E+00	2.64E-04	0.00E+00	0.00E+00	4.15E+02
		0.00E+00	0.00E+00	0.00E+00	0.00E+00	0.00E+00
	$\beta^{(1)}$	-2.30E-01	0.00E+00	0.00E+00	0.00E+00	0.00E+00
		0.00E+00	0.00E+00	0.00E+00	0.00E+00	0.00E+00

Table 3.1 (continued)

		Constants (T in degrees Kelvin)				
		a_1	a_2	a_3	a_4	a_5
		a_6	a_7	a_8	a_9	a_{10}
Na,OH [117]	$\beta^{(0)}$	7.48E-01	-1.05E-03	0.00E+00	0.00E+00	-9.89E+01
		0.00E+00	0.00E+00	0.00E+00	0.00E+00	0.00E+00
	$\beta^{(1)}$	1.20E+00	-1.30E-03	0.00E+00	0.00E+00	-2.06E+02
		0.00E+00	0.00E+00	0.00E+00	0.00E+00	0.00E+00
	C^{ϕ}	-9.11E-02	1.18E-04	0.00E+00	0.00E+00	1.73E+01
		0.00E+00	0.00E+00	0.00E+00	0.00E+00	0.00E+00
H,Cl [117]	$\beta^{(0)}$	5.21E-02	6.27E-04	-2.18E-06	0.00E+00	0.00E+00
		0.00E+00	1.00E-01	4.88E+01	0.00E+00	0.00E+00
	$\beta^{(1)}$	2.20E+00	-7.78E-03	1.85E-05	0.00E+00	0.00E+00
		0.00E+00	-4.07E-01	-4.61E+02	0.00E+00	0.00E+00
H,SO_4 [117]	$\beta^{(0)}$	-1.48E+00	1.78E-02	-6.30E-05	7.04E-08	0.00E+00
		0.00E+00	0.00E+00	0.00E+00	0.00E+00	0.00E+00
	C^{ϕ}	-2.54E+00	2.14E-02	-5.70E-05	4.81E-08	0.00E+00
		0.00E+00	0.00E+00	0.00E+00	0.00E+00	0.00E+00
H,HSO_4 [117]	$\beta^{(0)}$	1.05E+00	-6.32E-03	1.61E-05	-1.46E-08	0.00E+00
		0.00E+00	0.00E+00	0.00E+00	0.00E+00	0.00E+00
	$\beta^{(1)}$	2.02E-01	1.60E-03	-2.68E-06	0.00E+00	0.00E+00
		0.00E+00	0.00E+00	0.00E+00	0.00E+00	0.00E+00
K,HSO_4 [117]	$\beta^{(0)}$	-3.00E-04	0.00E+00	0.00E+00	0.00E+00	0.00E+00
		0.00E+00	0.00E+00	0.00E+00	0.00E+00	0.00E+00
	$\beta^{(1)}$	4.81E+00	0.00E+00	0.00E+00	0.00E+00	-1.35E+03
		0.00E+00	0.00E+00	0.00E+00	0.00E+00	0.00E+00
	C^{ϕ}	2.21E-02	-1.67E-05	0.00E+00	0.00E+00	-4.95E+00
		0.00E+00	0.00E+00	0.00E+00	0.00E+00	0.00E+00
K,OH [117]	$\beta^{(0)}$	-5.91E-01	7.88E-04	0.00E+00	0.00E+00	1.47E+02
		0.00E+00	0.00E+00	0.00E+00	0.00E+00	0.00E+00
	$\beta^{(1)}$	1.27E+01	-1.71E-02	0.00E+00	0.00E+00	-2.15E+03
		0.00E+00	0.00E+00	0.00E+00	0.00E+00	0.00E+00
	C^{ϕ}	1.37E-01	-2.00E-04	0.00E+00	0.00E+00	-2.23E+01
		0.00E+00	0.00E+00	0.00E+00	0.00E+00	0.00E+00

Table 3.2: *Value of fitting constants (Eq.3.26) for ternary interaction parameters for aqueous electrolyte.*

	Constants (T in degrees Kelvin)				
	a1	a2	a3	a4	a5
	a6	a7	a8	a9	a10
θ (Cl,SO_4) [113]	7.00E-02	0.00E+00	0.00E+00	0.00E+00	0.00E+00
25-150 °C	0.00E+00	0.00E+00	0.00E+00	0.00E+00	0.00E+00
θ (Na,K)[113]	-5.02E-02	0.00E+00	1.40E+01	0.00E+00	0.00E+00
	0.00E+00	0.00E+00	0.00E+00	0.00E+00	0.00E+00
θ (Na,Ca)[113]	5.00E-02	0.00E+00	0.00E+00	0.00E+00	0.00E+00
	0.00E+00	0.00E+00	0.00E+00	0.00E+00	0.00E+00
θ (Na,Mg)[114]	7.00E-02	0.00E+00	0.00E+00	0.00E+00	0.00E+00
	0.00E+00	0.00E+00	0.00E+00	0.00E+00	0.00E+00
θ (Na,Sr)[119]	5.10E-02	0.00E+00	0.00E+00	0.00E+00	0.00E+00
	0.00E+00	0.00E+00	0.00E+00	0.00E+00	0.00E+00
θ (K,Ca)[113]	1.16E-01	0.00E+00	0.00E+00	0.00E+00	0.00E+00
	0.00E+00	0.00E+00	0.00E+00	0.00E+00	0.00E+00
θ (Na,H)[117]	4.81E-02	0.00E+00	0.00E+00	0.00E+00	-4.05E+00
	0.00E+00	0.00E+00	0.00E+00	0.00E+00	0.00E+00
θ (Cl,OH)[117]	1.10E-01	0.00E+00	0.00E+00	0.00E+00	-4.94E+01
	0.00E+00	0.00E+00	0.00E+00	0.00E+00	0.00E+00
θ (SO_4,OH)[117]	2.30E-01	-1.23E-03	7.78E-07	0.00E+00	0.00E+00
	0.00E+00	0.00E+00	2.10E+01	0.00E+00	0.00E+00
θ (Ca,H) [118]	9.69E-02	0.00E+00	0.00E+00	0.00E+00	0.00E+00
	0.00E+00	0.00E+00	0.00E+00	0.00E+00	0.00E+00
θ (SO_4,HSO_4)[117]	-3.65E-01	9.96E-04	0.00E+00	0.00E+00	1.11E+01
	0.00E+00	-5.71E-01	-2.75E+01	0.00E+00	0.00E+00
θ (K,H)[117]	2.03E-01	0.00E+00	0.00E+00	0.00E+00	-5.59E+01
	0.00E+00	0.00E+00	0.00E+00	0.00E+00	0.00E+00
ψ (Na,Cl,SO_4)[113]	-9.00E-03	0.00E+00	0.00E+00	0.00E+00	0.00E+00
25-150 °C	0.00E+00	0.00E+00	0.00E+00	0.00E+00	0.00E+00
ψ (K,Cl,SO_4)[113]	-2.12E-01	2.49E-04	3.76E+01	0.00E+00	0.00E+00
	0.00E+00	0.00E+00	0.00E+00	0.00E+00	0.00E+00
ψ (Ca,Cl,SO_4)[113]	-1.80E-02	0.00E+00	0.00E+00	0.00E+00	0.00E+00
	0.00E+00	0.00E+00	0.00E+00	0.00E+00	0.00E+00
ψ (Mg,Cl,SO_4)[114]	-1.17E-01	0.00E+00	3.26E+01	0.00E+00	0.00E+00
	0.00E+00	0.00E+00	0.00E+00	0.00E+00	0.00E+00
ψ (Na,K,Cl)[113]	1.34E-02	0.00E+00	-5.10E+00	0.00E+00	0.00E+00
	0.00E+00	0.00E+00	0.00E+00	0.00E+00	0.00E+00
ψ (Na,K,SO_4)[113]	3.48E-02	0.00E+00	-8.22E+00	0.00E+00	0.00E+00
	0.00E+00	0.00E+00	0.00E+00	0.00E+00	0.00E+00
ψ (Na,Ca,Cl)[113]	-3.00E-03	0.00E+00	0.00E+00	0.00E+00	0.00E+00
	0.00E+00	0.00E+00	0.00E+00	0.00E+00	0.00E+00
ψ (Na,Ca,SO_4)[113]	-1.20E-02	0.00E+00	0.00E+00	0.00E+00	0.00E+00
	0.00E+00	0.00E+00	0.00E+00	0.00E+00	0.00E+00

Table 3.2 (Continued)

	Constants (T in degrees Kelvin)				
	a1	a2	a3	a4	a5
	a6	a7	a8	a9	a10
ψ (Na,Mg,Cl)[114]	1.99E-02	0.00E+00	-9.51E+00	0.00E+00	0.00E+00
	0.00E+00	0.00E+00	0.00E+00	0.00E+00	0.00E+00
ψ (Na,Sr,Cl)[119]	-2.10E-03	0.00E+00	0.00E+00	0.00E+00	0.00E+00
	0.00E+00	0.00E+00	0.00E+00	0.00E+00	0.00E+00
ψ (Na,Ba,Cl)[116]	1.28E-02	0.00E+00	0.00E+00	0.00E+00	0.00E+00
	0.00E+00	0.00E+00	0.00E+00	0.00E+00	0.00E+00
ψ (K,Ca,Cl)[113]	4.76E-02	0.00E+00	-2.71E+01	0.00E+00	0.00E+00
	0.00E+00	0.00E+00	0.00E+00	0.00E+00	0.00E+00
ψ (K,Mg,Cl)[114]	2.59E-02	0.00E+00	-1.43E+01	0.00E+00	0.00E+00
	0.00E+00	0.00E+00	0.00E+00	0.00E+00	0.00E+00
ψ (Na,K,OH)[117]	1.09E+00	-1.60E-03	0.00E+00	0.00E+00	-1.84E+02
	0.00E+00	0.00E+00	0.00E+00	0.00E+00	0.00E+00
ψ (Na,H,Cl)[117]	-1.46E-02	0.00E+00	0.00E+00	0.00E+00	3.59E+00
	0.00E+00	0.00E+00	0.00E+00	0.00E+00	0.00E+00
ψ (Na,H,SO_4)[117]	4.76E-03	0.00E+00	0.00E+00	0.00E+00	3.59E+00
	0.00E+00	0.00E+00	0.00E+00	0.00E+00	0.00E+00
ψ (Na,H,HSO_4)[117]	-1.46E-02	0.00E+00	0.00E+00	0.00E+00	0.00E+00
	0.00E+00	0.00E+00	0.00E+00	0.00E+00	0.00E+00
ψ (Na,Cl,OH)[117]	1.28E+01	3.67E-03	0.00E+00	0.00E+00	-3.55E+02
	-2.21E+00	3.23E-03	-2.72E+01	0.00E+00	0.00E+00
ψ (Na,SO4,OH)[117]	1.02E-01	-7.30E-05	0.00E+00	0.00E+00	-2.53E+01
	0.00E+00	0.00E+00	0.00E+00	0.00E+00	0.00E+00
ψ (Ca,SO4,HSO_4)[118]	4.51E+01	7.00E-03	0.00E+00	0.00E+00	-1.76E+03
	-7.28E+00	0.00E+00	0.00E+00	0.00E+00	0.00E+00
ψ (Ca,H,Cl)[118]	-2.08E-01	1.08E-04	0.00E+00	0.00E+00	1.98E+01
	1.72E-02	0.00E+00	0.00E+00	0.00E+00	0.00E+00
ψ (Ca,Cl,OH)[118]	-8.20E-01	1.52E-03	0.00E+00	0.00E+00	9.82E+01
	0.00E+00	0.00E+00	0.00E+00	0.00E+00	0.00E+00
ψ (Na,SO4,HSO_4)[117]	-1.03E-01	1.40E-04	0.00E+00	0.00E+00	1.99E+01
	0.00E+00	0.00E+00	0.00E+00	0.00E+00	0.00E+00
ψ (K,H,Cl)[117]	-8.03E-01	2.12E-05	0.00E+00	0.00E+00	4.36E+01
	1.12E-01	0.00E+00	0.00E+00	0.00E+00	0.00E+00
ψ (K,H,SO_4)[117]	1.30E-01	0.00E+00	0.00E+00	0.00E+00	-4.05E+01
	0.00E+00	0.00E+00	0.00E+00	0.00E+00	0.00E+00
ψ (K,H,HSO_4)[117]	3.48E-02	0.00E+00	0.00E+00	0.00E+00	-1.86E+01
	0.00E+00	0.00E+00	0.00E+00	0.00E+00	0.00E+00
ψ (K,Cl,OH)[117]	-3.54E-03	2.02E-05	0.00E+00	0.00E+00	-1.70E+00
	0.00E+00	0.00E+00	0.00E+00	0.00E+00	0.00E+00
ψ (K,SO_4,OH)[117]	1.31E-01	0.00E+00	0.00E+00	0.00E+00	-4.21E+01
	0.00E+00	0.00E+00	0.00E+00	0.00E+00	0.00E+00

3.3 Activity coefficient and Osmotic coefficient Matlab programs

In order to achieve a thermodynamic modelling of saline waters two Matlab programs have been written for calculating the activity coefficient of all anions and cations that exist in saline water. A third program has been written to calculate the osmotic coefficient. A detail description of the Matlab programs can be found in the in Appendix (B).

The following steps are followed by the developed Matlab program in every run:
(a) The Matlab program will start by asking the user to input the number of cations and anions that exist in his system.

(b) The Matlab program will ask the user to specify the cations and anions, the user will be asked to input a specific number for every specific cation or anion.

(c) The Matlab program will ask the user to input the temperature in degree Celsius (^{o}C) and then convert it to (Kelvin), density (g/L) and the salinity (ppm).

(d) The Matlab program will ask the user to input the concentration of every cations and anion involved in the calculation in units of molarity ($mol/L_{solution}$).

(e) The program will ask the user to enter the molecular weight of every cation and anion involved in the calculation.

(f) The program will convert the entered concentrations to molality unit ($mol/Kg_{solvent}$) using the entered data where is needed.

(g) The program will initiate matrices for the Pitzer interaction parameters for all cations and anions involved in the calculation. An Excel spreadsheet has been designed to include and update the Pitzer interaction parameters according to the temperature and ionic strength of the system according to Eqs.3.10-3.26.

(h) The program then will start calculating activity coefficients using Eq.3.5 for cations, Eq.3.6 for anion and Eq.3.7 for the osmotic coefficients, part by part.

(i) The output of the program will be either the activity of the cations or the activity of the inions or the osmotic coefficient, depending in the chosen program at the beginning of the run.

To illustrate the calculations performed, the program was applied to a specific seawater composition and the results were compared with some published experimental and computerised data for seawater with almost the same composition. The comparison will be discussed later in this chapter.

The whole Matlab programs with their commands will be included in the appendix (B) of this thesis. These programs have been incorporated with a simulation for a full scale RO/NF process in order to predict the type and propensity of the scales within the system. The details of the mathematical model and Matlab simulation will be discussed in the following sections.

3.4 Modelling for variation of concentration along a membrane channel

In order to calculate the change in local scaling propensity with position, there is a need to have a correlation describing the variation of concentration of scaling salts as a function of location along the membrane channel. The real RO/NF feed membrane channel could be described as shown in Fig. 3.1 and it consists of two parallel membranes within which there is a feed spacer. The channel has a symmetric plane in the middle of it. For ease of depiction, the feed spacer is not shown in Fig. 3.1. Thus, all the relevant transport and conservation equations for the RO/NF feed channel, like any other symmetrical channel, are solved for half the channel where flux at the symmetrical boundary is zero.

The aim of this work, as explained previously, is to combine the theoretical principles and thermodynamics of crystallization fouling with the principles of membrane transport and conservation along the RO/NF channel to predict the scaling propensity and onset of the scale formation along the module. Thus, this work does not intend to include the effect of time, and scale build-up with time, within the RO/NF channel. Only steady state simulations are discussed in this chapter and Chapter 4 of this thesis. This prediction is very important for the process optimization and design of both process and equipment, by predicting the scaling propensity along the module so that proper measures can be taken to minimize the onset of scale formation. The information in this work is required for preventative measures – it is a mitigation technique.

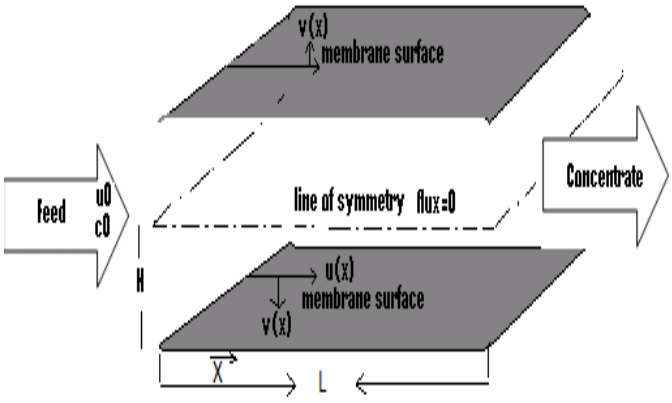

Figure 3.1: *Simplified schematics of RO/NF membrane channel*

The full scale RO/NF transport model of Song et al. [10] is modified here to able to account the change of water chemistry along the model. The membrane transport and continuity equations that are used in this model and also were used by Song et al [10, 11, 120] to obtain the variations of concentrations along the membrane feed channel are discussed below.

Complete transverse mixing in the filtration channel is assumed. This assumption can be considered valid in this case due to the small channel height; thus, the governing equations in the x direction are sufficient to define the case [10, 32, 45].

Concentration of any given species at location x along a membrane channel is modelled using Eq 3.28, derived through applying the principles of mass conservation to that species.

$$c(x) = \frac{1}{u(x)H}\left[c_0 u_0 H - (1-r)\int_0^x c(\xi)v(\xi)d\xi\right] \qquad (3.28)$$

In the above equation, *u(x)* is the cross flow velocity at location *x* along the channel; *H* is the height of the membrane channel; u_0 is the feed flow velocity; c_0 is the species concentration at the feed channel entrance; *v* is permeate flux; *r* the fraction of the species rejected by and not passed through the membrane; and ξ is a dummy integration variable. The two terms in the square brackets are respectively the total amounts of a given species entering the membrane feed channel and those passing through the membrane to the permeate channel.

It should be noted that the effect of concentration polarization is "implicitly" taken into account in Equations 3.32-3.33 by using the local species concentration at the membrane surface which is obtained through Eq. 3.29. With the small channel height and the spacers used a complete depolarization (uniform distribution across the feed channel height) prevails. However, for the purpose of completeness and accuracy Eq. 3.29 is used, where $c_w(x)$ is the concentration on membrane surface at location *x*, to check and confirm the value of concentration polarization within the system.

$$c_w(x) = c_0 + \exp(-v(x)H/D)\frac{rc_0}{uH}\int_0^x v(\xi)d\xi + \frac{rc_0 v(x)}{uD}\int_0^x v(\xi)d\xi \qquad (3.29)$$

This relationship for local wall concentration (Eq. 3.29) has also been used elsewhere [27]. The effect of undisturbed concentration polarization in a channel filled with spacers is described as a combination of two extreme cases, namely the undisturbed concentration polarization and complete depolarization (uniform distribution across the channel height).

In this work the local salt concentrations were calculated using both Equations 3.28 and 3.29 and results confirmed that, within the simulated system, there was complete depolarization. All the concentration related values used in the following equations refer to the values at the wall.

Similarly, the application of mass conservation principle for water results in the following expression for cross flow velocity at any location along the membrane channel:

$$u(x) = u_0 - \frac{1}{H}\int_0^x v(\xi)\, d\xi \tag{3.30}$$

The trans-membrane static pressure (p_f - p_p) at any location is defined by Δp. The static pressure in the feed channel (p_f) changes substantially from that at entrance (p_{f0}) to that at any location along the feed channel ($p_f(x)$) due to frictional losses; but the changes in the static pressure in the permeate channel (p_p) is negligible compared with Δp and hence p_p is assumed constant along the channel. Therefore (Δp_0) – ($\Delta p(x)$) which is the change in the trans-membrane pressure differential up to a point along the channel has the same value as the frictional losses (Δp_{fric}) along the feed channel between the two points. Hence $\Delta p(x)$ is defined by Eq. 3.31 where the parameter in the bracket is (Δp_{fric}) up to location x along the feed channel due to friction by the membrane surfaces and spacers [121].

$$\Delta p(x) = \Delta p_0 - [\frac{12\, k_{spacer}\, \eta}{H^2}\int_0^x u(\xi) d\xi] \tag{3.31}$$

where k_{spacer} is the friction coefficient due to spacer, and η is the dynamic viscosity.

Finally, from the principles of membrane transport, the permeate flux at location x along the membrane feed channel is given by Eq. 3.32 where R_m is membrane resistance to water passage; $\Delta\pi$ is the osmotic pressure difference and is calculated by Eq 3.33; α relates the osmotic pressure to concentration through application of the van't Hoff formula through Eq. 3.34; N is the number of ions in solution that can result from one salt molecule (N is 2 for NaCl); R_g is the universal gas constant; T is

the absolute temperature; *Mw* is the molecular weight of the solute; and $\varphi_{osmotic}$ is the Pitzer osmotic coefficient.

$$v(x) = \frac{\Delta p(x) - \Delta \pi(x)}{R_m} \tag{3.32}$$

$$\Delta \pi(x) = \alpha \Delta c(x) \tag{3.33}$$

$$\alpha = \frac{N \varphi_{osmotic} R_g T}{Mw} \tag{3.34}$$

It should be noted that α is a function of stream composition and the effect of variations in feed composition should be taken into account. This has been included in this work by using the Pitzer equation and obtaining the osmotic coefficient $\varphi_{osmotic}$ as function of local stream concentration using Eq.3.7.

The local ionic activity coefficients, osmotic pressure and scaling propensity can be determined through solving Eqs. 3.28-3.34 for scaling species concentration next to the membrane wall along the filtration channel. In this work, as the aim is just to describe the distribution of scaling propensity along the filtration channel immediately before the onset of the scaling/precipitation reaction, the change of scaling salt species concentration due to actual formation of foulant does not need to be taken into account; however, in expanding the current model to transient conditions and modelling the build-up of the fouling layer that change can be incorporated as well. The next section describes the numerical solution and the Matlab program that have been used to simulate a full scale RO/NF process.

3.5 Model algorithm

The following finite difference solution procedure has been used to solve Eqs 3.28-3.34. The membrane channel was divided into n segments of equal intervals represented by Δx. The start of the first segment and the end of the last segment are respectively denoted as 0 and n+1. Accordingly, the concentration, cross-flow

velocity, driving force pressure and permeate velocity in segment *i*, where it ranges from 1 to n, are denoted as c_i, u_i, Δp_i and v_i respectively. Fig.3.2 shows the recursive algorithm that has been used in this simulation. The simulation parameters can be chosen for given specific operating conditions and from the manufacturers' specifications for modules as shown in Table 3.3.

Table 3.3: *Parameter values for model Simulations for section 3.5*

Length of RO system, L (m)	6
Channel height, H (m)	7×10^{-4}
Applied (pump) pressure, p_0 (Pa)	5.516×10^{6}
Feed Salinity (mg/l)	10000
Cross flow velocity at entrance,(m/s)	0.1
Membrane intrinsic resistance,(Pa s/m)	1.8×10^{11}
Number of channel segments used in the simulations	300
Temperature, °C	25
Water viscosity at 25 °C, Pa.s	0.89×10^{-3}
Friction coefficient due to spacers	5
Initial Ca^{2+} concentration, ppm	600
Initial SO_4^{2-} concentration, ppm	1000

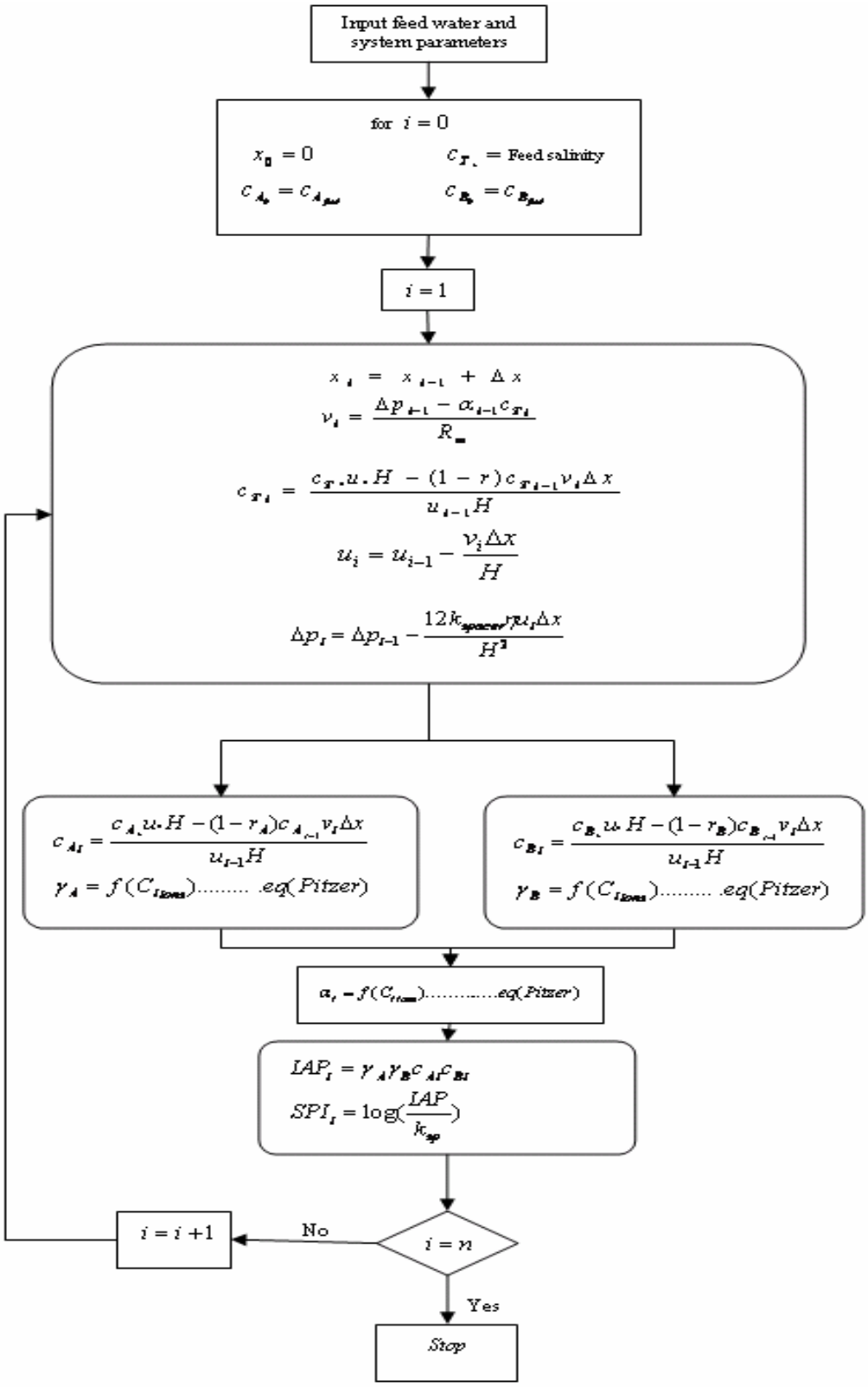

Figure 3.2: *A recursive algorithm for solving the mathematical model*

A Matlab program has been written to solve the mathematical model shown in Fig.3.2. As seen in Fig. 3.2, the Matlab program will first ask the user to input the feed water composition and the RO/NF system parameters which include the following:

(a) The length of the membrane channel.

(b) The membrane channel height.

(c) The initial applied pressure.

(d) The initial cross flow velocity.

(e) The membrane intrinsic resistance.

(f) Membrane rejection for every species in case of NF.

(g) Initial water density, viscosity, and salinity.

The Matlab will use these initial conditions to initiate the solution loop. The equations in Fig.3.2 will be solved initially considering salinity or total dissolved solid (TDS) as the major parameter representing all dissolved species (scaling and non-scaling salts) which exist in the solution. Thus the calculated permeate velocity, cross flow velocity and trans-membrane pressure as function of salinity will be used to find the change of each scaling salt species concentration along the filtration channel. At every segment the activity coefficients of all dissolved species and the osmotic coefficient will be calculated using the Matlab programs discussed in section 3.3. The change in water density and viscosity has been taking into account and calculated at every segment along the membrane channel using the extended equation of state for seawater at elevated temperature and salinity [101]. This program will be used to predict the scaling type and propensity along full scale filtration channel as will be discussed in more details in chapter 4.

3.6 Confidence of the simulation

3.6.1 Salinity comparison

In this simulations we used the same channel RO parameters as those tested previously [10, 11, 27, 120] to ensure we could compare our results for local

permeate flux (Fig 3.3) and local salinity (Fig 3.4) with previous work [11]. The simulation results shown here in Figs 3.3 and 3.4 are identical to the simulations results in [11] shown in their Figures 4 and 6 at the start (t = 0 time, day zero).

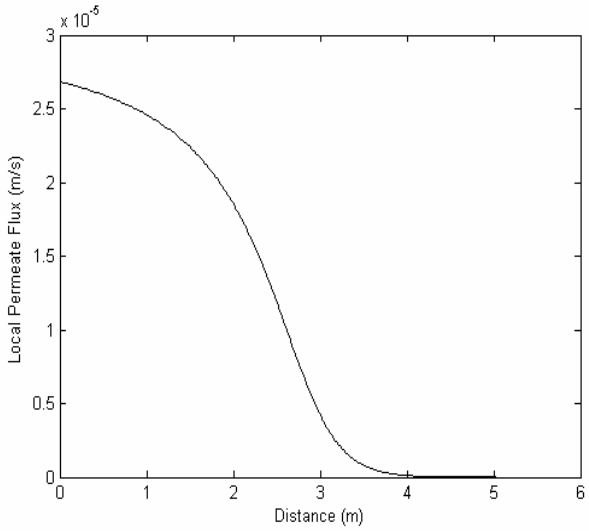

Figure 3.3: *Local permeate flux (m/s) change along the membrane filtration channel*

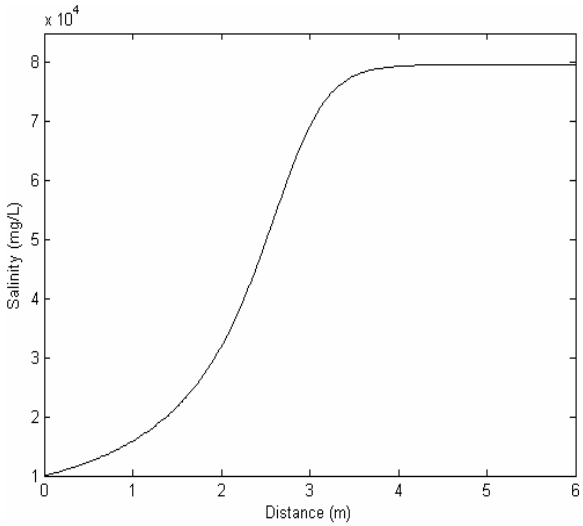

Figure 3.4: *Local salinity along 6 m membrane filtration channel*

Convergence tests have been conducted to find the optimum mesh size (the intervals and number of segments). The standard (default) local error control method in MATLAB® was used to monitor the error at each step; this method sets the relative tolerance as 0.1% (1e-3) and if the local error at the end of each step is greater than the threshold acceptable error, then the solver reduces the step and reiterates. It

should be noted that, though the accuracy and rigour have been carefully tested, the importance of the rigor is secondary in the current work to the novelty of the work. Its "primary" importance is its introduction of a fundamental and realistic approach: that of using a reliable description of the water chemistry within the RO/NF desalination module. While the rigor and accuracy of the simulations is of "secondary" importance, as in this case, the confidence and convergence tests are not usually conducted as, for example, they are in the case of Song et al. [11], since the main aim was to show the effect of thermodynamics on the performance limitation of the full-scale reverse osmosis process.

3.6.2 Activity coefficient and osmotic coefficient comparison

The activity coefficients and the osmotic coefficients of different published saline water compositions have been calculated and tabulated in Table 3.4 and Table 3.5. As can be seen in these two tables, the developed programs give very good estimation of the activity coefficients and osmotic coefficient at different salinity levels and different water compositions.

Table 3.4: *Single ion activity coefficients calculated using our programs and by others*

Reference	I (mol/Kg)	m Na^+	γ Na^+	m K^+	γ K^+	m Ca^{2+}	γ Ca^{2+}	m Mg^{2+}	γ Mg^{2+}	m Cl^-	γ Cl^-	m SO_4^{2-}	γ SO_4^{2-}
Hamrouni and dhahbi [109]	0.730	0.493	0.640	0.017	0.599	0.011	0.190	0.056	0.206	0.576	0.691	0.029	0.121
This work	0.730	0.493	0.646	0.017	0.518	0.011	0.197	0.056	0.204	0.576	0.518	0.029	0.097
Millero and Schreiber [122]	0.700	-	0.690		0.615	-	0.228	-	0.255	-	0.628	-	0.085
Hajbi et al. [123]	1.050	0.651	0.619	0.017	0.557	0.017	0.183	0.090	0.198	0.816	0.691	0.047	0.085
This work	1.040	-	0.631		0.475	-	0.188	-	0.201	-	0.585	-	0.078
Hajbi et al. [123]	1.580	0.830	0.636	0.027	0.540	0.025	0.227	0.133	0.265	1.397	0.673	0.061	0.060
This work	1.570	0.830	0.647	0.027	0.566	0.025	0.226	0.133	0.257	1.400	0.531	0.061	0.055

Hamrouni and Dhahbi [109] and Hajbi et al. [123] used the Pitzer model for the activity coefficient calculation, while Millero and Schreiber [122] used the ion pairing model to estimate the activity coefficients. The difference between the current work and the others is due to the assumptions used by each author. In this work, for the essay in computation, whole ions are assumed to be free in the water and thus all species are assumed fully ionised. However, these programs could be developed to account for more accurate species distribution. The current programs give adequate estimation for the activity and osmotic coefficient and specify the requirement that have been designed for as explained before in section 3.6.

Table 3.5: *Osmotic coefficients as calculated using the developed program and some literature values*

Reference	NaCl (mol/Kg)	φ_{osmoti}
Hajbi et al. [123]	0.65	0.973
Hamer and We [124]	0.6	0.923
Hamer and We [124]	0.7	0.926
This work	0.65	0.916
Hajbi et al. [123]	0.83	0.956
Hamer and We [124]	0.8	0.929
This work	0.83	0.946

3.7 Summary

This chapter introduced a new approach for assessing the local ionic activity coefficients and osmotic coefficients for saline water in RO/NF full scale processes. The Matlab programs developed and used have been discussed and validated through the encouraging comparison with existing published data. This approach will enable us to study locally on the membrane surface the effect of hydrodynamics and solution pH, salinity, temperature and concentration of the sparingly soluble salts on fouling potential at the membrane surface along the feed module from fundamental principles, as will be discussed in more detail in the next chapter. Moreover, in view of the fact that different ions have specific retentions, this approach would incorporate the effect of relative solution composition along a membrane module; this is very significant for a nanofiltration (NF) module which has different retentions for mono-valent and di-valent ions.

Chapter 4

A New Reliable Approach for Assessing the Fouling Propensity along a Full-Scale RO/NF Processes

4. Fouling propensity assessment along a full-scale RO/NF processes

This Chapter aims to develop a new reliable approach for assessing scaling (crystallization/precipitation fouling) propensity through the programs previously proposed and tested in chapter 3. This approach incorporates the local variation of foulant properties along the membrane filtration channel into fundamental transport and conservation equations to achieve a unified and scientifically based assessment of the scaling potential. Thus, a highly accurate simulation of the local fouling propensity along a full-scale RO/NF module will be obtained. This work has overcome the challenge of determining and incorporating the locally varying foulant concentration (and factors affecting it) and the effect of concentration polarization to predict the local fouling propensity along the membrane channel. The only available theoretical index, the Scaling Potential Index (SPI) has been modified and incorporated so that reliable prediction of pure salt precipitation can be achieved without any need for empirical parameters and/or constants. A semi theoretical approach is suggested to overcome the effect of scaling salt co-precipitation. The effect of process pressure on solubility product is incorporated theoretically to predict the onset of scaling in a full scale RO/NF process. The consequences of ignoring the effect of process pressure on solubility product and scaling propensity prediction are highlighted and discussed. Therefore, a fundamental and more realistic description of fouling propensity and onset of fouling at the membrane surface along the feed channel is developed and explained. Moreover, the effects of initial applied pressure, initial cross flow velocity, initial feed water salinity, clean membrane resistance and feed water temperature on fouling propensity and onset of fouling along the channel are investigated and discussed. This suggested model is a very powerful tool that could help in the specific design of RO/NF process as well as in simulations of the operating variables for optimization of RO/NF systems.

4.1 Introduction

In terms of crystallization fouling (commonly referred to as scaling) as discussed by many other researchers [4, 125-128] most of the fouling models that are proposed expand the black-box approach and do not consider the effect of varying hydrodynamics on fouling mechanisms and processes within the equipment. The scaling propensity of sparingly soluble salts in any membrane process could be more accurately simulated through considering the varying local parameters and scaling salts concentrations and their interactions.

The approach developed in this thesis introduces a reliable assessment of the scaling propensity within a full-scale RO/NF desalination module. This approach considers the science of fouling through considering the varying chemistry and thermodynamics of the treated concentrate. Then combining them with the principles of osmosis, mass transport across the membrane and conservation of mass to assess the local scaling potential of the sparingly soluble salt of concern within the RO/NF module as discussed before in chapter 3. It results in a simulated model for scientifically and theoretically predicting the onset of crystallisation fouling within RO/NF modules.

4.1.1 Content

The intent is to incorporate the effects of locally varying concentrations and of concentration polarization to predict the scaling propensity of sparingly soluble salts along the length of a membrane channel. Since the local scaling salts concentration and the concentration polarisation vary along a membrane channel, the scaling propensity will not be uniform along the channel. Thus, the scaling propensity at any location along the membrane channel can be predicted only by consideration of the local values. For reliable modelling of the scaling propensity the variation of the ionic interactive forces and the salinity along the filtration channel will be calculated and taken into account as discussed previously in chapter 3.

The potential for onset of crystallisation fouling for pure precipitation will be determined using Sheikholeslami's theoretical index [5, 12] whose accuracy was previously tested experimentally in membrane modules and reported elsewhere [47, 48, 76, 77]. This theoretical index, referred to as theoretical SPI, is developed using thermodynamic principles including the use of the Gibbs free Energy concept and will be briefly discussed in Section 4.2.1 A new approach to overcome the effect of co-precipitation will be suggested and discussed in section 4.2.2. The SPI is modified to incorporate theoretically effect of process pressure for the first time in section 4.2.3.

Sections 4.3 and 4.4 respectively include the simulation results and discussions and the chapter summary.

4.2. Scaling propensity prediction

Sheikholeslami suggested and tested [5, 12] her theoretical index based on a fundamental and unified approach for assessing the scaling potential of any salt by incorporating the ion activities and principles of thermodynamics including Gibbs free Energies as introduced above and will be described below in Equations 4.1-4.8. In these equations the ions constituting the sparingly soluble salts (Y_cZ_a) are represented by "Y" and "Z", and "c" and "a" are respectively the number of cations and anions in one mole of electrolyte in the following equation showing the chemical reaction for precipitation/crystallization of the salt; e+ and e- are the valences for cation and anion, respectively.

$$cY^{e+} + aZ^{e-} \underset{Ksp}{\longleftrightarrow} Y_cZ_a(s) \qquad (4.1)$$

Sheikholeslami [62, 79-82, 129-131] noticed through experimental observations that the thermodynamic solubility product (*Ksp*) for the precipitation/crystallization reaction changes significantly due to the presence of other components and the conditions. She concluded that, for any given sparingly soluble salt, the *Ksp* of

precipitation varies depending on the solution composition and that even the presence of trace materials had significant effects. That led to her hypothesis [78, 100, 129] that since the "structure" of precipitate is dependent on and varies in presence of trace materials, the *Ksp* of the precipitate must vary; therefore the concept of "constant" solubility product even in the presence of trace compounds, does not hold. As shown in Eq. 4.2 when the "product" changes even if the reactants are under the same conditions, the standard Gibbs free energy change of the reaction $\Delta_{reac} G^{\phi}$ shown in Eq. 4.3 will change and hence *Ksp* for this reaction would change.

$$\Delta_{reac} G^{\phi} = (\Delta_f G^{\phi})_{products} - (\Delta_f G^{\phi})_{reactants} \qquad (4.2)$$

$$- R_g T \ \ln(\ Ksp\ ) \ = \ \Delta_{\ reac}\ G^{\ \phi} \qquad (4.3)$$

Therefore, she concluded [62, 78, 79, 100, 129, 130] that the onset of precipitation varies and then proposed her theoretical index represented by Eq 4.4, tested it under controlled experimental conditions for calcium carbonate and reported its accuracy [12].

$$SPI = \log(I\ AP / KSP) = \log(IAP / EXP(-\Delta_{reac} G^{\phi} / R_g T) \qquad (4.4)$$

Gibbs free energy of reaction ($\Delta_{reac}G^{\Phi}$) according to Eq. (4.2) is related to the standard Gibbs free energies of formation ($\Delta_f G^{\Phi}$) and *IAP* is the ion activity products.

4.2.1 Pure precipitation

Sheikholeslami [5, 12, 62, 78-80, 130] then used thermodynamic principles and relationships and proposed the following for RO desalination: (1) Eq.4.5 [12] to incorporate the effect of temperature on the Gibbs free energy; (2) Eq.4.6 [5, 62, 78-80, 130] to determine ion activity products; and (3) Eq.4.7 [5, 12, 62] to incorporate high ionic strengths and salinity effects in RO desalination through the effects of

ionic strength as well as the electrostatic effects and short and long range ion interaction forces.

$$-R_g T \ln(Ksp) = \Delta_{reac} G^T = \frac{T}{298.15} \Delta_{reac} G^{298} + \Delta_{reac} H^{298} \left(1 - \frac{T}{298.15}\right) \quad (4.5)$$

$$IAP = \{Y^{e+}\}^c \{Z^{e-}\}^a = \left(\gamma_{Y^+}[Y^{e+}]\right)^c \left(\gamma_{Z^-}[Z^{e-}]\right)^a \quad (4.6)$$

$\gamma = f$ (salinity and concentration of species) (4.7)

In the above equations R_g is the gas constant (1.987×10^{-3} kcal/mol.K), and T is the temperature (K) which significantly affects temperature Gibbs free energy; standard Gibbs free energies are at 298K, (ΔH_{reac}) is the enthalpy of reaction, the curly bracketed parameters are ion activities and related to concentrations by activity coefficients (γ).

Sheikholeslami's theoretical index, as shown in Eq.4.4, can be used to assess the potential for scale formation of a given salt such as that shown in Eq.4.1. The *SPI* is related to the supersaturation [5] which is defined by Eq.4.8

$$SS = \left\{I\,AP / Ksp\right\}^{\frac{1}{c+a}} = \left\{IAP / EXP\left(-\Delta_{reac} G^{\phi} / R_g T\right)\right\}^{\frac{1}{c+a}} \quad (4.8)$$

It is reported [5] that the above procedure is suitable, applicable and accurate also for very high salinities common in RO desalination. The Pitzer model, which is used in the calculation of activity coefficients, is assessed to be valid for concentrated electrolyte mixtures of up to 6m [114].

The challenge arises when mixed precipitates are formed for which the Gibbs free energy is different from that of a pure compound [62, 79-82, 129-131] and thus the Gibbs free energy of reaction and the thermodynamic solubility product of the pure precipitate formation are different from those in the presence of impurities and in co-precipitating systems. Until a completely theoretical approach is developed to

calculate the solubility product of co-precipitation, it is suggested that the semi theoretical approach below can be followed.

4.2.2 Co- precipitation

The coexistence of precipitating salts (co-precipitation) produce a product different from that of single salt precipitation [4]. Sheikholeslami [4] has concluded that the thermodynamic equilibrium constant of the co-precipitation is different from that of single salt precipitation.

Equations 4.10 and 4.11 represent the theoretical solubility product for MX salt, which precipitates according to Eq. 4.9, in pure precipitation and co-precipitation systems respectively. For pure precipitation the convention is to assume the activity $a_{MX_{equ(pure)}}$ of the solid as unity; however, in co-precipitation scenario the activity $a_{MX_{eq(mix)}}$ of solid cannot be assumed to be unity [42].

$$M^{e+} + X^{e-} \xleftrightarrow[Ksp]{} MX(s) \tag{4.9}$$

$$Ksp_{theo} = \left(\frac{a_{M^{e+}{}_{equ.}} . a_{X^{e-}{}_{equ.}}}{a_{MX_{equ.(pure)}}} \right) = a_{M^{e+}{}_{equ.}} . a_{X^{e-}{}_{equ.}} = Exp\left(-\frac{\Delta_r G^{\phi}}{R_g T}\right) \tag{4.10}$$

$$Ksp_{\exp} = \left(\frac{a_{M^{e+}{}_{equ.}} . a_{X^{e-}{}_{equ.}}}{a_{MX_{equ.(mix)}}} \right) \tag{4.11}$$

Dividing equation (4.11) by equation (4.10)

$$\frac{Ksp_{\exp}}{Ksp_{theo}} = \frac{1}{a_{MX_{equ.(mix)}}} \tag{4.12}$$

By defining the Co-precipitation Correction Factor (*Cf*) as

$$Cf = \frac{1}{a_{MX_{equ(mix)}}} \tag{4.13}$$

$$Ksp_{\exp} = Cf . Exp\left(-\frac{\Delta_r G^{\phi}}{R_g T}\right) \tag{4.14}$$

where T is the temperature in (*K*) and R_g is the Universal gas constant. $Ksp_{\exp}$ is the experimental solubility product for impure solid scaling salt resulted from co-precipitation and Ksp_{theo} is the solubility product for pure solid scaling salt calculated from Gibbs free energy $\Delta_r G^{\phi}$ as seen in Eq. 4.10 and discussed in details elsewhere [5, 12, 45].

$Ksp_{\exp}$ may be calculated for a specific feed water scenario using the experimental procedure which will be later discussed in chapters 5 and 6 of this thesis. Thus, by using the Co-precipitation Correction Factor (*Cf*) a reliable prediction for scaling propensity for any scaling salt may be reached; and moreover the effect of temperature, pressure and salinity can be still included as described in the details for pure scaling salts at [45] and here above.

4.2.3 Effect of process pressure

The SPI can be modified to include the effect of pressure on solubility product by integrating the following Eqs (4.15-4.16),

$$\left(\frac{\partial \ln Ksp(T,P)}{\partial P}\right)_r = \frac{-\Delta V_r^o(T,P)}{R_g T} \qquad (4.15)$$

and

$$\left(\frac{\partial \Delta V_r{}^o(T,P)}{\partial P}\right)_T = -\Delta K_r{}^o(T,P) \qquad (4.16)$$

where ΔV_r^0 and ΔK_r^o stand for the standard volume and compressibility changes of the precipitation reaction of the of the solid considered (MX) [45].

The integration of Eqs.4.15 and 4.16 leads to the following expression [42, 45, 112].

$$\ln Ksp(T,P) = \ln Ksp(T,P_o) - \frac{\Delta \overline{V_r^o}}{R_g T}(P-P_o) + \frac{\Delta \overline{K_r^o}}{2R_g}(P-P_o)^2 \qquad (4.17)$$

where $\Delta\overline{V_r^o}$ is the standard molal volume change of the precipitation reaction and $\Delta\overline{K_r^o}$ is its standard molal compressibility change. The effect of $\Delta\overline{K_r^o}$ can be neglected at RO pressures as its reported [112] to be negligible at moderate pressures, which includes the RO pressure range. $\Delta\overline{V_r^o}$ is expressed for any scaling salt (MX) as:

$$\Delta\overline{V_r^o} = V^o(MX,s) - \overline{V^o}(MX,aq) \qquad (4.18)$$

The values of $V^o(MX,s)$ for the most common scaling salt in RO/NF are tabulated in Table 4.1, and the value of $\overline{V^o}(MX,aq)$, the standard molal volume of aqueous *MX*, is calculated at *T* and P_o from those of sodium sulfate and sodium chloride and of M-chloride at the same temperature and pressure using the additivity rule which is expresses by:

$$\overline{V^o}(MX,aq) = \overline{V^o}(MCl_2,aq) + \overline{V^o}(Na_2SO_4,aq) - 2\overline{V^o}(NaCl,aq) \qquad (4.19)$$

where the values of ($\overline{V^o}$) the standard molal volume of designated aqueous electrolyte are calculated at 25°C using the algebraic transformation of [112] and tabulated in Table 4.1.

Table 4.1: *The Standard molal volume change of the precipitation reaction for common scaling salts*

Scaling Salt	$V^o(MX,s)^*$ cm^3/mol at 25 °C and 1bar	$\overline{V^o}(MX,aq)^{**}$ cm^3/mol at 25 °C	$\Delta\overline{V_r^o}$ cm^3/mol
Gypsum	74.94 [132]	$2.14x10^{+03}$	$2.06x10^{+03}$
Barite	52.1 [112, 133]	$5.32x10^{+02}$	$4.80x10^{+02}$
Celestite	46.25[112, 133]	$2.03x10^{+03}$	$1.98x10^{+03}$

* $V^o(MX,s)$ is considered to be constant over the temperature and pressure ranges of RO desalination following [112] for ranges including the RO range.

** $\overline{V^o}(MX,aq)$ could be calculated at any temperature up to 250°C see [112].

The solubility product, *Ksp* (T,P_o) at temperature *T(K)* and reference pressure P_o (1 bar) can be calculated either from the Gibbs free energy change of reaction as described before and elsewhere [5, 12, 45] or by using Eqs 4.20-4.23 as described by [112]. Assuming the heat capacity is constant over the investigated temperature range, which is the case in RO process, and then *Ksp* (T, P_o) is given by:

$$\ln Ksp(T,P_o) = A + B\ln T + \frac{C}{T} \qquad (4.20)$$

With

$$A = \frac{\Delta_r S^o}{R_g} - \frac{\Delta_r C_p^o}{R_g}[1+\ln T_o] \qquad (4.21)$$

$$B = \frac{\Delta_r C_p^o}{R_g} \qquad (4.22)$$

$$C = -\frac{\Delta_r H^o}{R_g} + \frac{T_o \Delta_r C_p^o}{R_g} \qquad (4.23)$$

where $\Delta_r S^o$, $\Delta_r H^o$ and $\Delta_r C_p^o$ respectively refer to standard entropy, enthalpy and heat capacity changes of the precipitation reaction. R_g is the gas constant and T_o the reference temperature (298.15 *K*) [112].

4.3. Simulation results and discussion

Numerical simulations have been conducted to investigate the onset of local scaling propensity along a full-scale RO process under various conditions. Table 4.2 shows the given conditions for the module and the feed water parameters used in these simulations; however, other parameters applicable to other cases could also be used.

Table 4.2: *Parameter values for model Simulations for section 4.3.1-4.3.6*

Length of RO system, L (m)	6
Channel height, H (m)	7×10^{-4}
Applied (pump) pressure, P_0 (Pa)	5.516×10^{6}
Feed Salinity (mg/l)	10000
Cross flow velocity at entrance,(m/s)	0.1
Membrane intrinsic resistance,(Pa s/m)	1.8×10^{11}
Number of elements along RO system	300
Temperature, °C	25
Water viscosity at 25 °C, Pa.s	0.89×10^{-3}
Friction coefficient due to spacers	5
Initial Ca^{2+} concentration, ppm	600
Initial SO_4^{2-} concentration, ppm	1000

4.3.1. Scaling propensity on a membrane along its channel

The theoretical index gives a conservative estimate for assessing onset of the scaling potential. If *SPI* is negative the scale will not form; when it is zero the system is at equilibrium but in certain circumstances scale may have the potential to form; behaviour at equilibrium is discussed in detail elsewhere [4, 5, 12, 78]. At the point where the *SPI* becomes positive the sparingly soluble salts certainly have the "potential" to form scale [5]. These results focus on the potential and the thermodynamic aspects. The aspects related to scale thickness development and kinetics are the transient aspects which, as discussed previously, can be demonstrated in the future work.

Figure 4.1 shows the effects of local permeate flux (LPF) along the 6m length of module on the local potential for scale formation (local SPI). Firstly as expected, it shows that the local flux declines due to concentration effects, and hence increases in the osmotic pressure, along the channel. At about 3.6m point along the channel, pressure driving force ($\Delta P(x) - \Delta\pi(x)$) between the feed and permeate and hence LPF

would approach zero, at which point the desalination system reaches thermodynamic equilibrium. The local SPI rises as the LPF drops and reaches an asymptotic value of 0.5 at the point (about 3.6m) where there will no longer be any permeation in the channel as the system is controlled thermodynamically which is what Song et al. reported [29] actually to take place in practice. The local SPI at the feed inlet has a value of -0.39 and rapidly increases but remains negative for another 1.65m length, within which there is no potential for scale formation. From 1.65m onwards the local SPI has positive value and there is potential for scale formation - in fact with the presence of spacers and with the magnitude of surface area [4] in contact with the solution this potential is very strong. The increase in SPI is very rapid initially but then slows gradually until it reaches an asymptotic value of 0.5 at 3.6m. Permeation affects the local SPI in two different ways: (1) by concentrating the sparingly soluble (scaling) species, which increases the potential for fouling; and (2) by concentrating the non-scaling species (NaCl, etc) so that their concentration reduces the potential for scale formation [5, 62]. The second effect is minor in comparison to the first one; however, it has been taken into account in the simulations. These results are to show the onset of local SPI and not the issues related to actual precipitation kinetics and "formation" of any fouling layer.

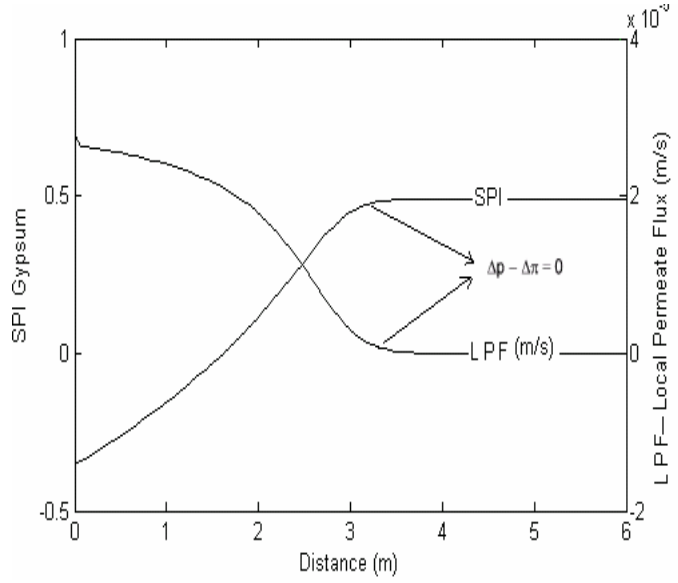

Figure 4.1: *Local SPI along 6 m membrane filtration channel and Local permeate flux (LPF) (m/s) along the channel*

Figure 4.2 shows the local SPI and the normalized "cumulative" flux, which is an important parameter for the overall performance of RO process, along the module. Figure 4.2 shows that the cumulative permeate flux reaches its maximum value within the first 3-4 m and the rest (2-3m) of the permeation channel will suffer severe scaling since the SPI is at its highest value.

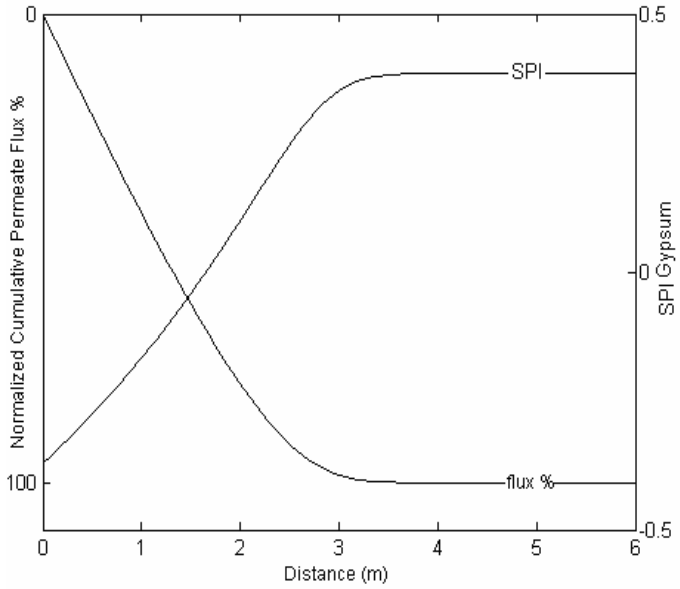

Figure 4.2: *Normalized cumulative permeate flux and local SPI along 6 m membrane filtration channel.*

4.3.2. Effect of feed water salinity on scaling propensity

It is important to show the effect feed water salinity has on local SPI, as RO desalination is applied to lightly brackish seawater and also industrial waters, some of which are even much more saline than seawater. Also, as briefly discussed previously and in detail elsewhere, [5, 12, 62, 78] the presence of saline non-scaling species (such as NaCl) affects the scaling potential of a given scaling species, It also affects nucleation and the kinetics of precipitation.

Figure 4.3 shows the local SPI along the module for various feed salinities. As discussed in previous sections, the theoretical index incorporates salinity effects on thermodynamics and hence the local SPI for various feed waters; its purpose is not to

cover all the salinity ranges for RO desalination but to show the significance of salinity on local SPI.

It should be noted that in Figure 4.3 the only variable between the curves is the concentration of "non-scaling" species; the concentration of scaling species and other parameters are the same in all the curves on the figure. It is shown, as expected, that at higher feed water salinities, the lower is the local scaling propensity at a given point along the membrane feed channel. Also, the rate of increase in local SPI along the channel decreases as the feed salinity is increased.

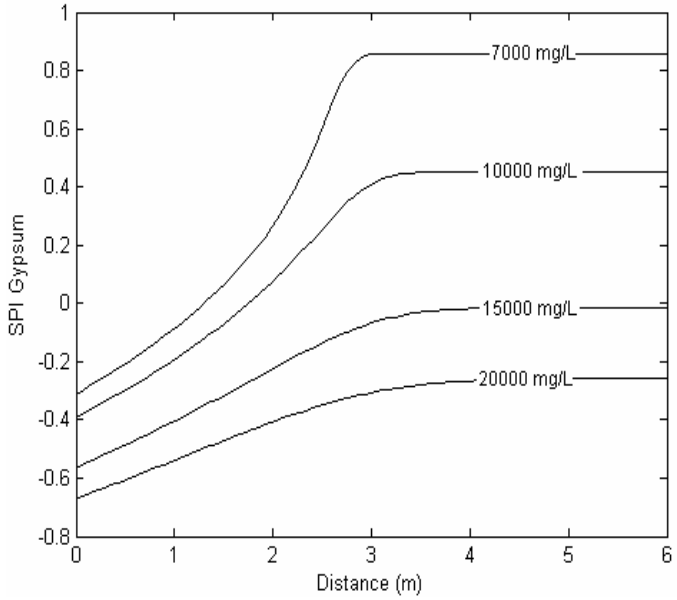

Figure 4.3: *Effect of feed water salinity on local SPI along 6 m membrane channel*

In comparing these curves it should be noted that the feed salinity affects the onset of scaling along the channel via two different routes: (1) through the thermodynamics and kinetics of precipitation as discussed above; and (2) through changes in the driving force ($\Delta p(x)-\alpha c(x)$). Reduction in permeate flux for a given feed scaling salt concentration reduces the "concentration factor" of the scaling ions along the length of feed channel and hence the scaling propensity (*SPI*)[47, 48, 76, 77].

Fig 4.3 is in accordance with theory and experimental observations showing that, for a given concentration of scaling species and non-scaling species, the SPI will

increase as the concentration of scaling ions increases along the channel in parallel with total salinity increase; this will continue until the osmotic pressure equals the applied pressure as explained before. However, the effect non-scaling species concentrations (salinity) for a given concentration of scaling species is governed by thermodynamics as discussed above.

4.3.3. Effect of membrane resistance on scaling propensity

Clean membrane resistance is a characteristic of the RO membranes and various ranges are available in the market. Figure 4.4 depicts a comparison between two membranes and their different effects on local SPI along the membrane channel for otherwise identical conditions. One curve is for the membrane used in these simulations (with clean membrane resistance of 1.8 x 10^{11} Pa s/m, which is one of those currently available in the market) and the other is a typical one used for RO process 10-20 years ago (8 x 10^{11} Pa s/m).

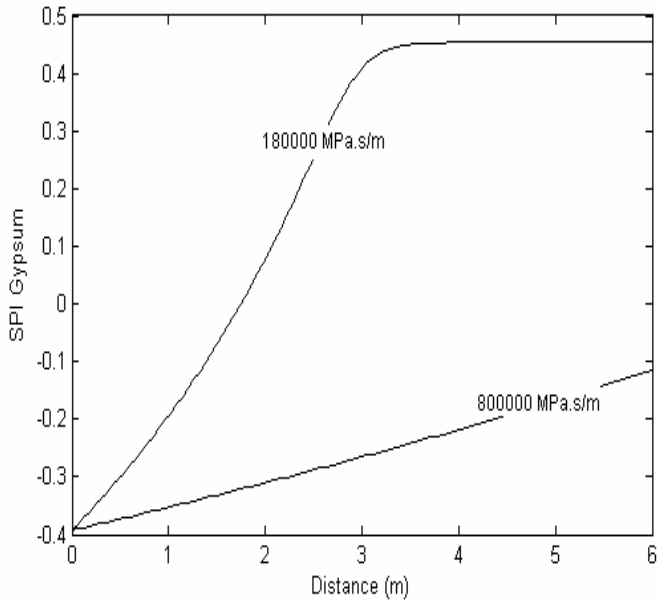

Figure 4.4: *Effect of clean membrane resistance on local SPI*

It can be seen from the figure that under otherwise identical conditions the scaling propensity is higher for the currently used membranes which have less specific resistance. This is due higher local flux giving rise to a higher concentration factor for the more permeable membrane. As can be seen, higher permeability values which

are favoured by industry and are applicable particularly in many brackish water systems increase the potential for the onset of scaling.

4.3.4. Effect of initial cross flow velocity on scaling propensity

Figure 4.5 shows the effect of various initial cross flow velocities (feed flow rates) on the local SPI along a 6m permeation channel. Cross flow velocity affects the onset of fouling for several reasons [4] and, under otherwise identical conditions, the higher it is the lower becomes the potential for fouling. For example, in our simulations under otherwise identical conditions, when the feed water velocity is doubled from that of Table 4.2 (0.1 m/s) water could travel about 3.6m, more than about twice the previous length (about 1.3m), without having any potential for scale formation. This observation could be used as a reference to give the safe operational limit.

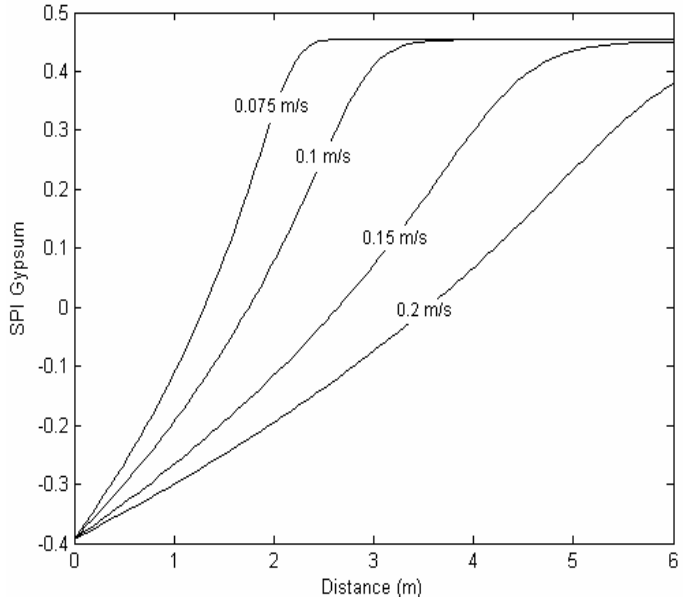

Figure 4.5: *Effect of initial cross flow velocity on local SPI along 6 m membrane feed channel*

As mentioned above, the curves on the figure are for otherwise identical conditions.

4.3.5 Effect of applied pump pressure on scaling propensity

One of the operating parameters that affects the scaling potential and severity is the trans-membrane pressure and Fig 4.6 shows simulated results for various pump pressures under otherwise identical conditions. As may be seen, at the highest applied pump pressure the membrane is more prone to scale formation. Also, our simulations show that the onset of local fouling potential along the module is moved downstream at lower pump pressures. Thus, theoretical assessment of the scaling potential enables one to assess and set operational parameters within safe limits.

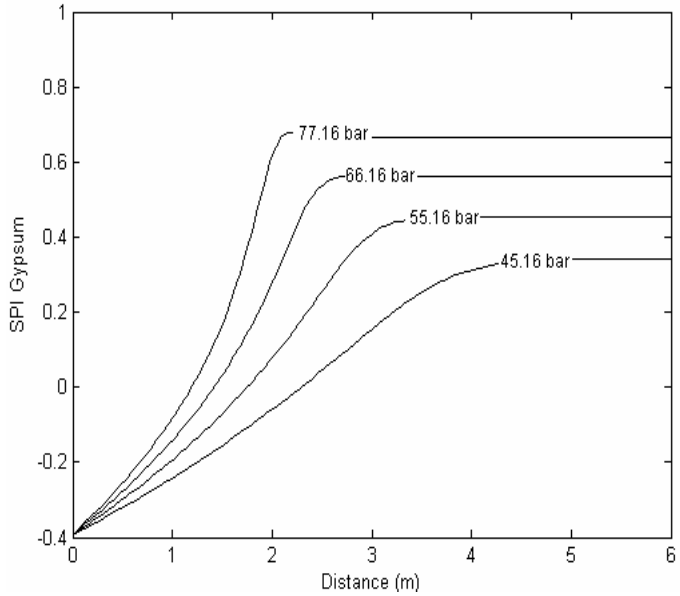

Figure 4.6: *Effect of initial applied pressure on local SPI along 6 m membrane channel*

4.3.6 Effect of feed water temperature on scaling propensity

Figure 4.7 shows the effect of feed temperature on local *SPI* along a 6m feed channel. The thermodynamic solubility product (*Ksp*) was calculated using Eq.4.5 for both temperatures; the effect of temperature on density and viscosity was also taken into account. Increasing the temperature from 25^{o}C to 70^{o}C did not appreciably affect the scaling propensity. Gypsum is an inverse solubility salt and the figure shows that at any given point along the channel, the scaling propensity is slightly higher for the simulation at higher temperature. In these simulations a given

membrane was used for all comparative assessments; therefore further attention should be given to the effect of high temperatures on the membrane structure and performance and also its inter-relation with the scaling propensity.

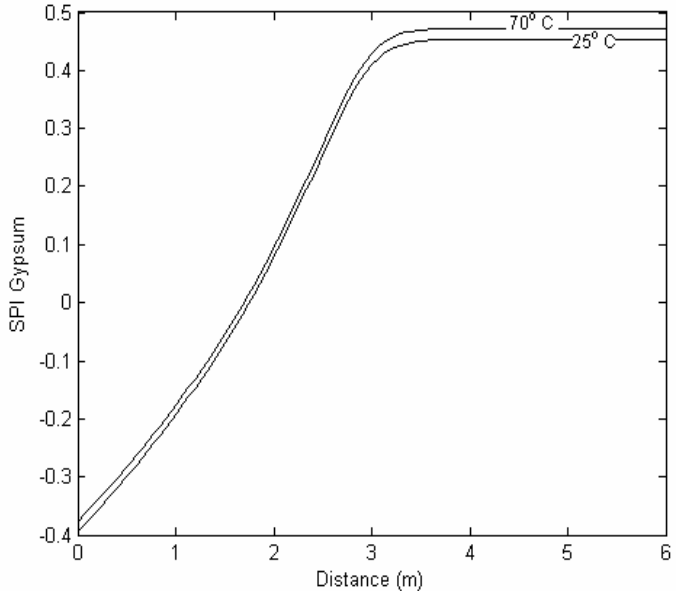

Figure 4.7: *Effect of feed water temperature on local SPI along 6m filtration channel*

4.3.7 Effect of process pressure on scaling propensity prediction

In this chapter, the effect of pressure has been incorporated theoretically, for the first time, to predict the onset of scaling in a full scale RO process. Table 4.3 shows the parameter values for the model simulations in sections 4.3.7 and 4.3.8. The effect of pressure has usually been ignored and believed to be insignificant in RO processes. However, this is not the case as seen in Figs. 4.8-4.10 for different scaling salts. It can be seen from Figs. 4.8-4.10 that neglect of the pressure effect can result in significant errors in the RO operation and design. Indeed, excluding the pressure effect will lead to a significant error in scaling propensity estimation. For celestite and gypsum, as seen in Fig. 4.8 and Fig. 4.10 respectively, ignoring the effect of pressure will lead to a positive *SPI* curve from the first meter downstream and further along the membrane channel, which indicates a high potential for scale formation. This prediction of high scale formation potential would indicate action such as installation of a pre-treatment process, decreasing of the system recovery, adding of

an antiscalant…etc to mitigate the expected high scale formation, which mean additional cost to the capital and production budgets. In reality, after incorporating the pressure effect the *SPI* curve is negative, for both celestite and gypsum, along the whole membrane channel; indicating that no celestite and gypsum scales will form.

Table 4.3: *Parameter values for model Simulations for sections 4.3.7 and 4.3.8*

Length of RO system, L (m)	6
Channel height, H (m)	7×10^{-4}
Applied (pump) pressure, P_o (Pa)	5.516×10^{6}
Feed Salinity (mg/l)	30000
Cross flow velocity at entrance,(m/s)	0.1
Membrane intrinsic resistance,(Pa s/m)	1.8×10^{11}
Number of elements along RO system	400
Temperature, °C	25
pH	7.1
Friction coefficient due to spacers	5
Initial Na^{+} concentration, ppm	9850
Initial Ca^{2+} concentration, ppm	1500
Initial Ba^{2+}, ppm	0.02
Initial Sr^{2+}, ppm	30
Initial Cl^{-}, ppm	15800
Initial SO_4^{2-}, ppm	2000

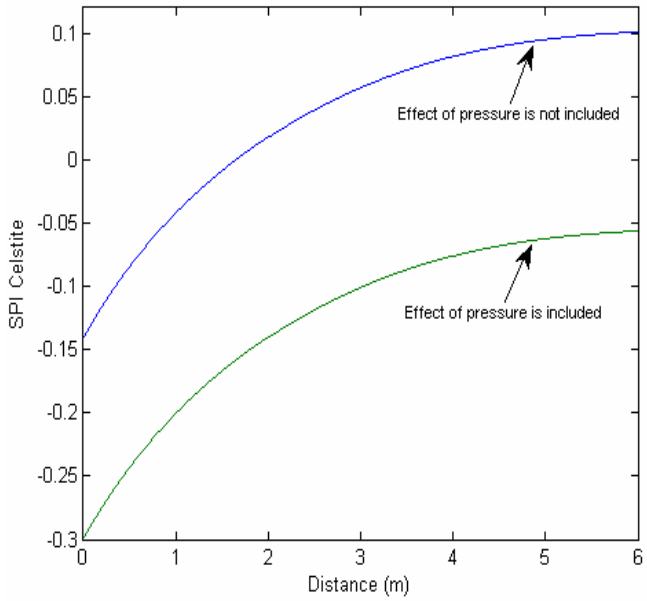

Figure 4.8: *Scaling propensity of celestite at 55 bar with and without inclusion of the pressure effect along a 6m membrane channel.*

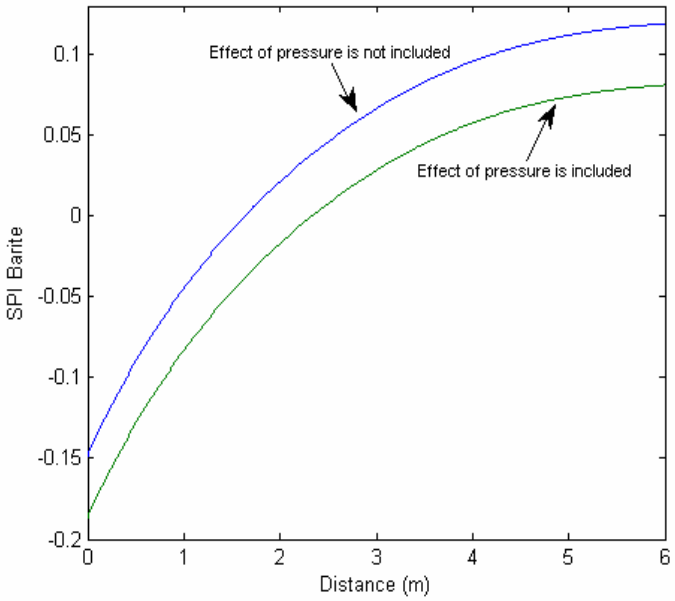

Figure 4.9: *Scaling propensity of barite at 55 bar with and without inclusion of the pressure effect along a 6m membrane channel.*

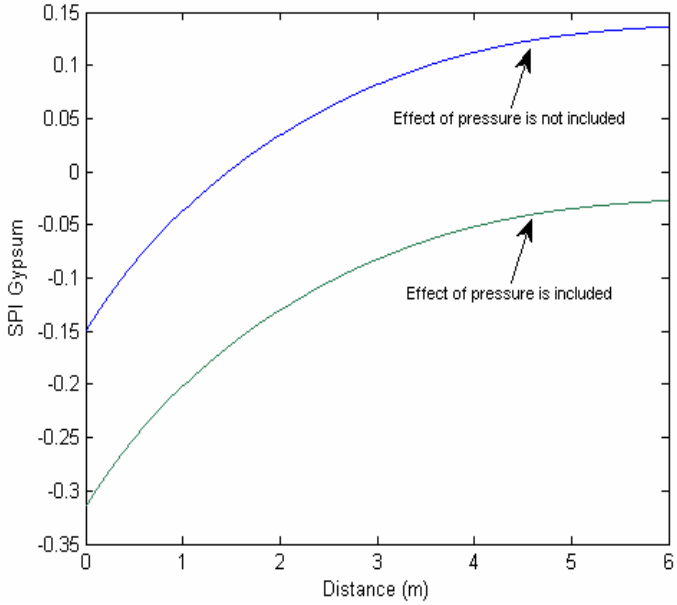

Figure 4.10: *Scaling propensity of gypsum at 55 bar with and without inclusion of the pressure effect along a 6m membrane channel.*

4.3.8 Effect of salt co-existence in scaling propensity prediction

As an example of the effect of co-precipitation, Rushdi et al. [42] found that the estimated barite activities at equilibrium with seawater at 20^{o}C and 25^{o}C are

respectively 1.25 and 1.36 and that for celestite, the activity is 1.001. For Barite, involvement of other cations, such as Ca and K, in the crystal structure could affect its activity, but it has been reported that Sr is likely to be the primary contaminant [134, 135]. Rushdi et al. [42] Barite and Celestite activity values have been used to calculate the co-precipitation correction factor (*Cf*) as explained before in section 4.2.2.

Fig. 4.11 shows the scaling propensity prediction of Barite with and without taking into account the effect of Celestite- Barite co-precipitation. As seen in Fig. 4.11 the effect of co-precipitation on the Barite scaling propensity is a crucial factor and should not be ignored; as can be observed, ignoring the effect of co-precipitation gives a serious underestimate of the onset of Barite scaling. However, in case of Celestite precipitation it seems, as seen in Fig.4.12, that there is no effect of Barite co-precipitation on the onset of Celestite scaling.

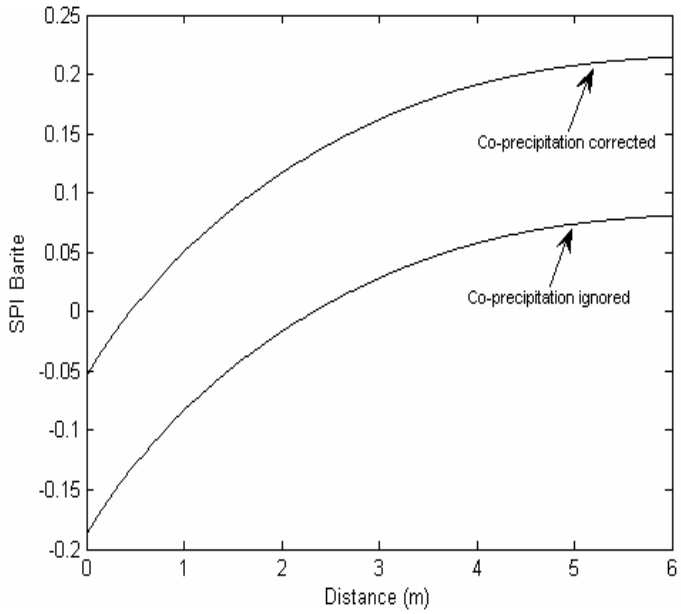

Figure 4.11: *Scaling propensity prediction of Barite with and without taking into account the effect of Celestite- Barite co-precipitation*

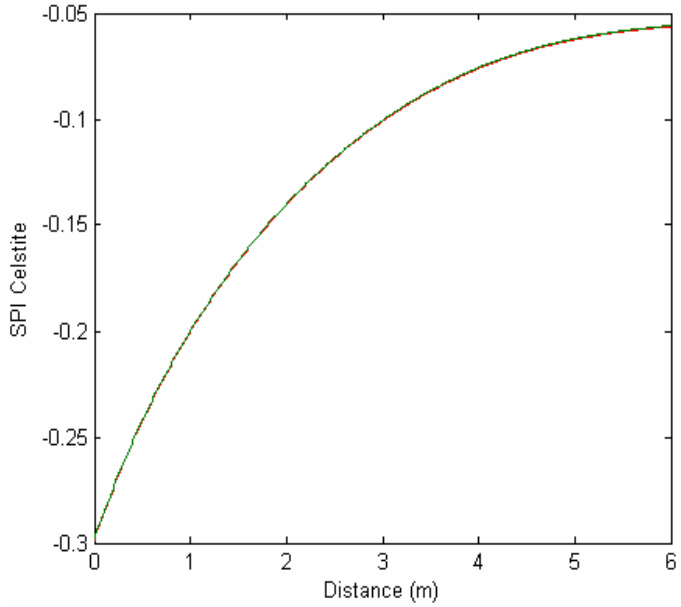

Figure 4.12: *Scaling propensity prediction of Celestite with and without taking into account the effect of Celestite- Barite co-precipitation*

4.4. Summary

This chapter modifies and incorporates the only available theoretical index (which was previously proposed and its accuracy tested) for fouling (scaling) by sparingly soluble salts with the fundamental equations of transport and continuity to reliably simulate and assess the onset of scaling propensity locally on the membrane surface along a full-scale RO membrane. This realistic simulation is fundamentally based and does not include any experimentally determined parameters or constants in the case of pure precipitation or while ignoring the co-precipitation effect. This approach enables us to study locally on the membrane surface the effect of hydrodynamics and salinity, temperature and concentration of the sparingly soluble salts on fouling potential along the feed module at the membrane surface from fundamental principles. Moreover, in view of the fact that different ions have specific retention factors, this approach would incorporate the effect of relative solution composition along a membrane module; this is even more significant for a nanofiltration (NF) module which has different retentions for mono-valent and di-valent ions.

The suggested model is a very powerful tool that could help in design of the specifics of RO/NF processes as well as in the simulation and optimisation of the operational variables. In this chapter the effects of membrane resistance, pump feed pressure, feed mass flow rate, salinity and temperature on the onset of fouling (scaling) propensity for a given sparingly salt on the membrane surface, locally along the module, have been shown and discussed.

Also in this chapter, a new procedure for incorporating the effect of co-precipitation of the scaling salts on scaling propensity prediction was introduced and discussed. The consequence of ignoring the effect of RO process pressure on solubility product and scaling propensity prediction during RO processes was highlighted and discussed. Taking into account the effect of co-precipitation and the pressure effect are essential to a reliable prediction of the scaling propensity. The current industrial practice of using solubility data for single salt precipitation, where co-precipitation can exist, and ignoring the effect of pressure within the RO system in predicting the onset of scaling leads to a significant error in scaling propensity prediction, which adds extra costs to the RO/NF processes in pre-treatment and scheduled shutoffs.

The next three chapters in this thesis introduce the experimental work that has been done to enhance the understating of crystallisation fouling. Chapter 5 will describe the material and methodology for the experimental work. Chapter 6 will give an example and describe the experimental procedure that could be followed to specify the Co-precipitation Correction Factor as mention before in section 4.2.2. Also this chapter will enhance the understanding of the $CaSO_4$ and $SrSO_4$ co-precipitation. Chapter 7 will describe the testing of the proposed approach in an experimental membrane rig.

Chapter 5

Material and Methodology for the Experimental Work

5. Material and methodology for the experimental work

The experimental work in this thesis consists of two sections; the batch section and the hydrodynamic section. This chapter describes the material and the methodology that have been used during the batch and hydrodynamic experiments.

5.1 Materials and model solutions preparation

5.1.1 Chemicals and standard solutions

Table 5.1 presents the major reagents used for this work, including quality and manufacturer. NaCl, $CaCl_2$, Na_2SO_4, and $SrCl_2$ were used to synthesise the model solutions. Valeric (pentanoic) acid, 99% was used to simulate the effect of the presence of dissolved organics (DO). Fatty acids are the major components of dissolved organics in produced water, contributing over 90% of the total organic content [136]. In these experiments, pentanoic acid was used as a simulator to study the effect of dissolved organics on the formation of pure and mixed $SrSO_4$ and $CaSO_4$ deposits at different salinity levels.

Other common reagents include pH buffer solutions 4, 7, 10 for pH electrode calibration; Ca^{2+},Sr^{2+}, Na^{+} and S standard solutions for inductivity coupled plasma (ICP) analysis, HCl and NaOH. The water used was deionised and filtered with 0.2-μm pore size membrane before use.

Stocks of $CaCl_2$, Na_2SO_4, $SrCl_2$ and NaCl solutions with known concentration within their solubility limits were prepared and kept for quick synthesis of model solutions. These stock solutions were prepared by dissolving the respective salts in deionised water and further filtering with a 0.2 μm filter after preparation to ensure no impurities or un-dissolved salt were present.

Table 5.1: *Lists of major Chemical reagents*

Chemical Reagent	Grade	Manufacture
NaCl	Analytical	Fisher Scientific
$CaCl_2$	Analytical	Fisher Scientific
Na_2SO_4	Analytical	Fisher Scientific
$SrCl_2$	Analytical	Fisher Scientific
Valeric acid	Analytical	Acros Organics

5.1.2 Preparation of the model solutions

The model solutions were prepared through mixing the already prepared stock solutions to achieve the required supersaturated solutions of calcium sulphate ($CaSO_4$) and strontium sulphate ($SrSO_4$) in sodium chloride (NaCl).

The prepared solutions were analytically analysed for all components immediately after preparation and their compositions were monitored during the experimentation. Water quality is determined by measuring pH, conductivity and ionic concentrations (calcium, strontium and sulphate by ICP).

5.2 Methodology

5.2.1 Batch tests

A series of batch tests has been carried out according to a very controlled experimental procedure which is described in the two sections below.

5.2.1.1 Experimental apparatus

Figure 5.1 show a series of plastic test tubes that were used to simulate a constant-volume batch reactor. A set of thermo-baths were used to keep a constant temperature for the whole run, thus assuring isothermal reaction.

Figure 5.1:*Test tubes in water thermo-bath*

5.2.1.2 Experimental procedure

For the batch experiments the mixed model solutions were carefully transferred to a series of 30 ml plastic test tubes and the test tubes were placed in temperature baths at constant temperature (30^{o}C). All test tubes were fully filled to ensure that there was no air and to permit analysis of data based on the assumption of a constant-volume batch reactor. Great attention was given to avoiding air bubble formation during the transfer process, as the air bubbles will affect the equilibrium of CO_2 with the solutions and hence the precipitation of carbonate scales.

These constant-volume batch reactors were used for chemical analysis as the run progressed. Water quality was monitored for each sample taken during the run. The water quality tests were carried out until equilibrium was attained. A few coupons (1.5 cm x 3 cm) of a flat sheet of the membrane used were inserted into a number of the test tubes to assess the scaling attachment. The solid precipitates were collected using Thermo Scientific Nalgene Disposable Filter Units with 0.2 μm membrane pore size. The collected precipitates were left on the filter paper and dried using a vacuum dryer. These dried solid samples were used to carry out SEM and EDS

(Energy dispersive X-ray spectrometry) analysis. This procedure was also followed by Sheikholeslami and her research group [62, 79, 82].

5.2.2 Hydrodynamics tests

5.2.2.1 Laboratory membrane rig

Hydrodynamic tests were conducted in a laboratory-based research loop system (Fig. 5.2) which consists of a feed solution reservoir with a capacity of 50 L, a low pressure pump, capable of delivering a flow of water up to 10 L/min and 10 bar, a high pressure, variable speed pump capable of delivering a flow of water between 0.5 and 6.0 L/min in the region of 100 bar, a SEPA CF II Membrane Cell which is designed by the manufacturer for research and small-scale production with a full 140 cm^2 of membrane effective area, a heat exchanger for cooling water to reduce the process water temperature to ambient (15-20 ^oC), and a series of pressure, temperature and flow measuring and control devices connected to data acquisition software (Fig. 5.3). A full description of the hydrodynamic system is included in Appendix C. This unit was designed to operate in either full recycling mode or in partial recycling mode. A full description of the operation modes and conditions is included in chapter 7 of this thesis.

Figure 5.2: *Laboratory membrane rig*

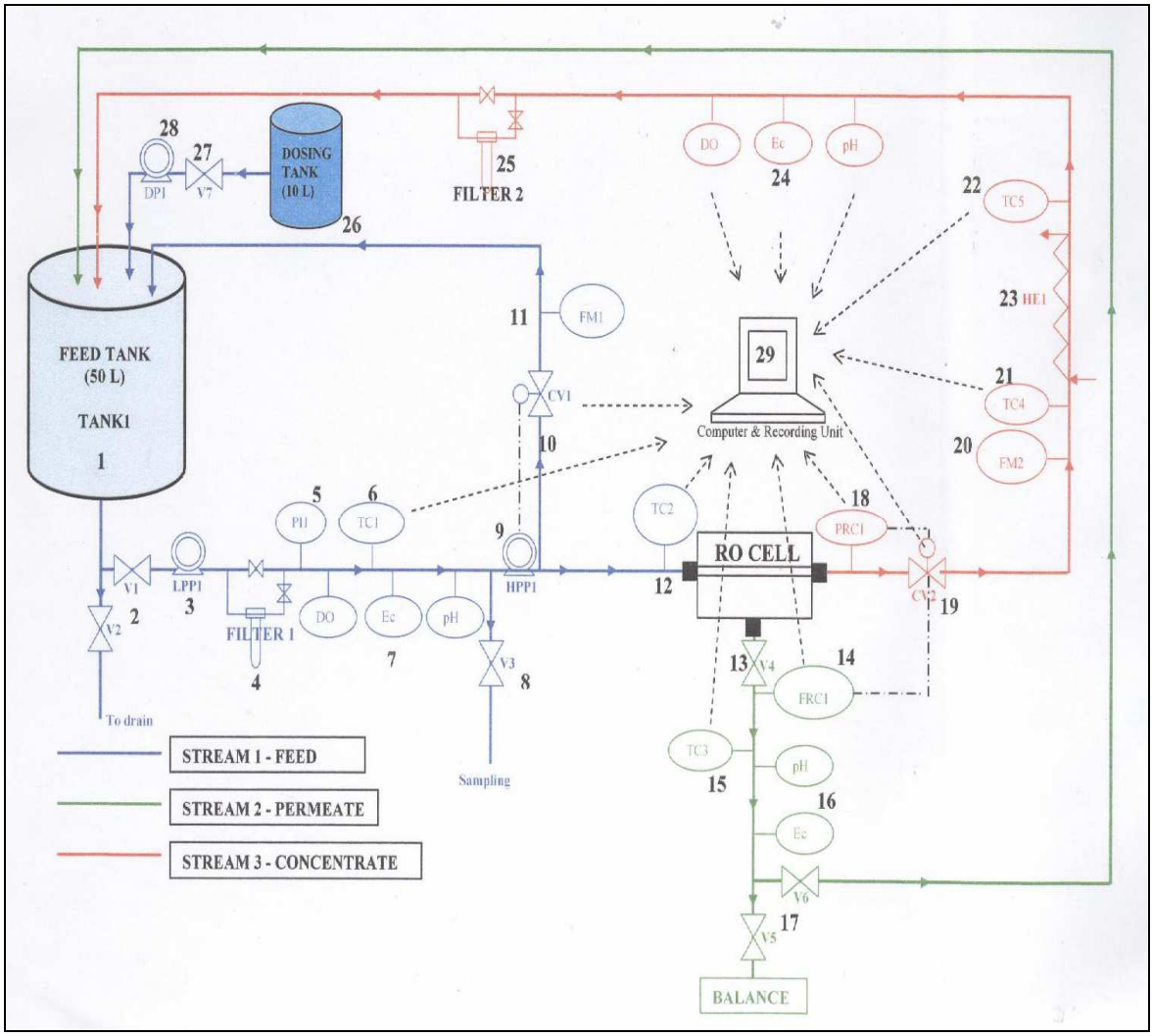

Figure 5.3: *Schematic diagram of the membrane rig*

5.2.2.2 Test procedure

The test procedure consisted of solution preparation, membrane conditioning, actual test run and system cleaning. Solution preparation was carried out following the procedure mentioned above for batch experiments. For dynamic tests, normally stock concentrated solutions were prepared below the saturation limit of the salts as discussed in section 5.1.1. Then the mixed model solutions were directly transferred to the feed tank.

5.2.2.2.1 Membrane conditioning

The RO membrane used is a composite polyamide RO membrane provided by Hydranautics (Catalogue designation: ESPA2). The data sheet of the membrane used can be found in Appendix D. The membranes were cut to the required size and rinsed using pure water. Then, the membranes were installed into the cell and conditioned by pure water for 24 hours by fully recycling 15L pure water under the predetermined operating conditions.

5.3 Instrumental analysis

5.3.1 Sampling

Samples of the testing solution were taken before the test and also during the test as explained before. For sample preparation, for both batch and hydrodynamic tests a sample of 5-30 ml was taken and directly filtered using a Thermo Scientific Nalgene Disposable Filter Unit with 0.2 μm membrane pore size and then diluted with 0.5% HNO_3 solution to stop any possible reaction. The amount of dilution was chosen according to the expected maximum concentration that fits within the ICP calibration curve.

5.3.2 Inductivity Coupled Plasma (ICP)

A Thermo Scientific iCap6000 series spectrometer with a Cetac ASX-520 Auto-sampler has been used to obtain calcium, strontium, sodium and sulphur ion concentrations. The experimental errors arise from ICP analysis can be up to 10%. This experimental error is composed of errors in sample dilution, the calibration of the ICP, and the drift and fluctuation of ICP readings.

Figure 5.4: *Thermo Scientific iCap6000 series spectrometer with a Cetac ASX-520 Auto-sampler*

Ca^{2+},Sr^{2+}, Na^{+} and S certified single element standards solutions supplied by Fisher Scientific for ICP analysis were used to calibrate the ICP. The calibration was made according to the expected concentrations that are being analysed. A sample of the ICP calibration curve can be seen in Fig. 5.5.

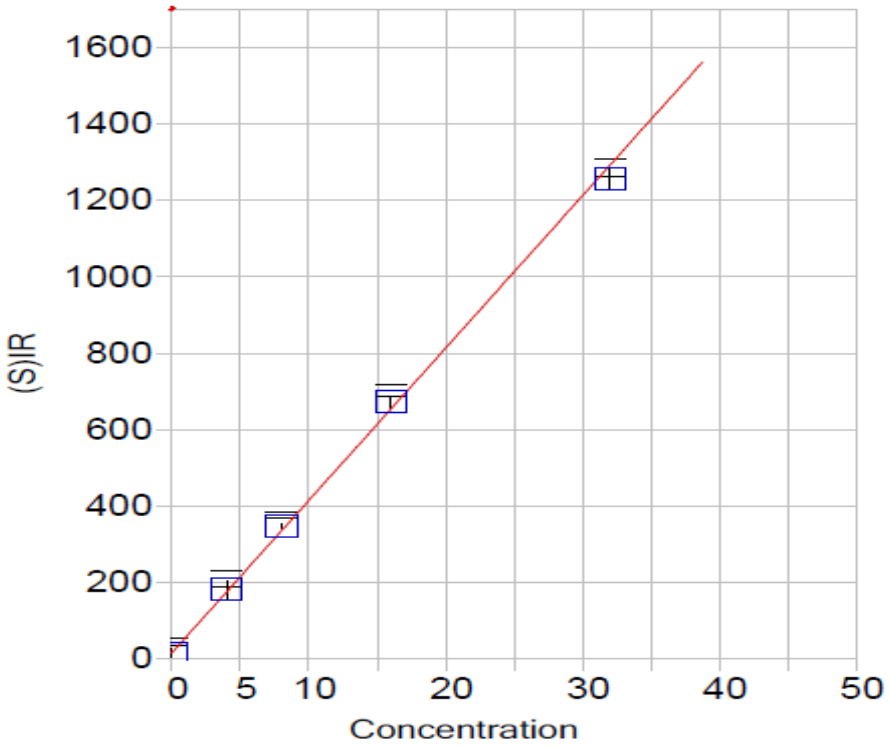

Figure 5.5: Sample of the ICP calibration curves

5.3.3 pH measurements

A Sartorius Professional pH meter has been used to measure the solution pH. Three point calibration was carried out using pH 4, 7 and 10 buffer standard solutions. Solution pH was initially adjusted between 7 and 7.5 using concentrated HCl and NaOH for all tested solutions, even though the pH has no effect on sulphate scale as long as the pH is above 3; since sulphuric acid is a strong acid and at pH>3, SO_4^{2-} is the predominant species [81].

5.3.4 SEM-EDS analysis

Micrographic imaging and elemental analysis of the collected precipitates were determined by Scanning Electronic Microscope (SEM) in conjunction with energy dispersive X-ray spectrometery (EDS). SEM analysis gives a qualitative assessment of the type and size of the crystals formed. EDS determines the composition of the crystals. The collected crystals were coated with carbon before being tested. The SEM-EDS instrument used is located in the Grant Institute of Earth Sciences at the University of Edinburgh. A full description of the SEM-EDS specification can be found in the School of GeoSciences web site:

http://www.geos.ed.ac.uk/facilities/sem/

Chapter 6

A Comprehensive Study of the Precipitation and Co-Precipitation of $CaSO_4$ and $SrSO_4$ with and without the presence of Dissolved organics at Different Salinity Levels

6. Precipitation and co-precipitation of $CaSO_4$ and $SrSO_4$

This chapter aims to study comprehensively the effect of salinity and Dissolved organics (DO) on $CaSO_4$ and $SrSO_4$ precipitation and co-precipitation. A series of isothermal batch tests at 30^oC have been carried out with or without the presence of Dissolved organics (DO) for salinity value ranging between 0.35-1.5 M of NaCl, 0.0475 M $CaSO_4$ concentration and two values of $SrSO_4$ concentration (0.005 M and 0.02 M). The decline of the scaling ions' concentrations (Sr^{2+}, Ca^{2+}, SO_4^{2-}) have been monitored with time until equilibrium has been reached. Quantitative and qualitative thermodynamics and kinetics analyses combined with deposits structural analyses have been carried out to investigate the effect of salinity, DO presence and co-precipitation on $SrSO_4$ and $CaSO_4$ precipitation. The Pitzer model has been used to calculate the activity coefficient of the scaling ions of interest. Thermodynamic solubility products for $CaSO_4$ and $SrSO_4$ were determined using the calculated activity coefficient and the measured concentrations at equilibrium. The $CaSO_4$ precipitation is found to be more affected by the salinity level than the $SrSO_4$ in a co-precipitation situation. Also the co-precipitation of $CaSO_4$ and $SrSO_4$ alters the precipitation thermodynamic solubility product and the kinetics of the precipitation reaction for pure salts. The co-precipitation and DO present clearly affects the adhesion of the precipitate of $CaSO_4$ and $SrSO_4$. Images of the precipitates resulting from pure and mixed precipitation have been produced using high-resolution digital imaging camera coupled with an optical microscope and using Scanning Electron Microscopy (SEM). The produced images show that salinity increases affect the $SrSO_4$ crystals' size and shape and affect the size of $CaSO_4$ crystals. Also, Energy Dispersive Spectroscopy (EDS) analyses have been carried out in order to investigate the composition of the precipitates. The EDS analyses confirm that there is an interaction between the $CaSO_4$ and $SrSO_4$ during the co-precipitation of these two salts. There is no detected change in crystal composition as a result of salinity

increase. These combined effects of Salinity, presence of DO and co-precipitation affect the Gibbs free energy changes in associated with the crystallisation process and thus alter the thermodynamics and the kinetics of the precipitation. The observations in this study are very important for deeper understanding of the effect of scaling salts' coexistence, salinity and DO presence on the behaviour of the scaling salts. This is crucial to reaching a reliable prediction of the scaling propensity within membrane processes.

6.1. Introduction

Reverse osmosis (RO) desalination has recently become very attractive for water reclamation for different types of waste water, in addition to its traditional use of desalting seawater and brackish water. For example, a recent study carried out by a BP research and development team [137] found that the injection of desalted water in an oil field can increase the recovery up to 10% over the non-desalted case. This interesting observation opens the way to benefiting from the huge amount of waste water produced during the production of oil and gas (commonly referred to as Produced Water). In fact, desalination of Produced Water may convert Produced Water from a grave problem, that burdens the oil and gas industry, to a useful commodity for increasing the oil recovery, and as part of a solution to the problem of fresh water shortage [138]. However, these new applications of RO technology bring further challenges that should be addressed and solved to achieve the best performance of the RO process. One of these challenges is the complexity of the feed water; which will increase the severity of the fouling. Indeed, fouling is considered a fundamental limitation to the economic viability of membranes in Produced Water treatment [3].

Crystallization fouling (commonly referred to as scaling) is the most serious type of fouling that can face RO desalination. Scaling occurs once the precipitating salt exceeds its saturation limits. Scaling mitigation begins with predicting the scaling propensity of feed water and modifying and optimising the process accordingly [78].

The complex characteristics of the new types of RO feed water such as Produced Water exacerbates the problem of scaling because of the high complexity of scaling prediction when salts such as $CaCO_3$, $CaSO_4$, $BaSO_4$ and $SrSO_4$ co-exist. This complexity of scaling prediction comes from the following facts: the mechanism of scaling is expected to be different for different salts as was demonstrated [55] for $CaCO_3$ and $CaSO_4$. Sheikholeslami [4] and her research group showed that the co-existence of $CaCO_3$ and $CaSO_4$ affects the mechanism of fouling and the thermodynamic and kinetic behaviour of each salt; hence, single salt data is not applicable to the situation where salts co-exist. Thus, the application of current industrial practice which ignores the science of fouling for assessing scaling propensity in a desalination plant, is limited and may only be able to crudely approximate the scaling propensity for simple feed water at the entrance to the RO desalination unit [5, 45, 78].

This chapter aims to carry out a comprehensive study of $CaSO_4$ precipitation in presence of Sr^{2+} and dissolved organics (DO) at different salinities up to 1.5 M, as a part of a fully comprehensive study of the possible scaling scenarios that may face the RO desalination of complex waste water. This comprehensive study is important for a better understanding of the interactive effect between scaling salts. Understanding the interactive effect between the precipitation salts will produce a more reliable prediction of the scaling potential within the RO/NF processes. This study includes quantitative and qualitative thermodynamic, kinetic and deposit structure analyses; with more focus on thermodynamics and deposit structure as the main aim here is to deeply understand and incorporate the effect of co-precipitation on the recent approach developed by the authors [43, 45] for a reliable scaling propensity prediction within a full scale RO/NF processes. The quantitative analysis of kinetics is beyond the scope of this work but kinetics can be comprehensively studied later to develop a model to predict scaling development and its effect on the operation of full scale RO process.

6.2 Experimental conditions and model solutions for batch tests

All the reagents that have been used on this research work are analytical grades supplied by Fisher Scientific. Table 5.1 presents all reagents used for this work, including quality and manufacturer. NaCl, $CaCl_2$, Na_2SO_4 and $SrCl_2$ were used to prepare synthetic solutions according to the procedure that is described before in detail in chapter 5. Table 6.1 shows the experimental conditions and the model solutions that were prepared according to the methodology described in chapter 5. Other common reagents include pH buffer solution 4, 7, 10 for pH electrode calibration; Ca^{2+}, Sr^{2+}, Na^{+} and SO_4^{2-} standard solution, HCl and NaOH were used through this experimental work.

Prepared solutions were analytically tested for all components immediately after preparation and their compositions were monitored during experimentation. Solutions concentration, and pH were measured directly after mixing the solutions; a sample of mixed solution was withdrawn, filtered with 0.22 μm filter and then analysed for water quality. Water quality is determined by measuring of pH, calcium, Sodium, Strontium and sulphate. A detailed description of the methodology is included in chapter 5 of this thesis.

Table 6.1: *Experimental conditions and model solutions for batch tests*

No	Temperature (°C)	NaCl (M)	$[Sr^{2+}]$ M	Pentanoic acid (mg/L)	$[SO_4^{2-}]$ M	$[Ca^{2+}]$ M
1	30	0.35	0.000	0	0.0475	0.0475
2	30	0.35	0.020	0	0.0475	0.0475
3	30	0.35	0.005	0	0.0475	0.0475
4	30	0.35	0.000	450	0.0475	0.0475
5	30	0.35	0.020	450	0.0475	0.0475
6	30	0.35	0.005	450	0.0475	0.0475
7	30	0.35	0.005	0	0.0475	0.0000
8	30	0.35	0.005	450	0.0475	0.0000
9	30	0.5	0.000	0	0.0475	0.0475
10	30	0.5	0.020	0	0.0475	0.0475
11	30	0.5	0.005	0	0.0475	0.0475
12	30	0.5	0.000	450	0.0475	0.0475
13	30	0.5	0.020	450	0.0475	0.0475
14	30	0.5	0.005	450	0.0475	0.0475
15	30	1.5	0.000	0	0.0475	0.0475
16	30	1.5	0.020	0	0.0475	0.0475
17	30	1.5	0.005	0	0.0475	0.0475
16	30	1.5	0.000	450	0.0475	0.0475
17	30	1.5	0.020	450	0.0475	0.0475
18	30	1.5	0.005	450	0.0475	0.0475

6.3. Results and discussion

6.3.1 Decline in concentration of scaling ions

6.3.1.1 The effect of salinity on scaling ions declines for pure $CaSO_4$ precipitation with and without the presence of DO.

Calcium and sulphate concentrations were monitored during the precipitation of $CaSO_4$ at different salinity levels. Fig. 6.1 and Fig. 6.2 show that the concentrations of calcium and sulphate ions were strongly affected by the increase of salinity. In Fig. 6.1 the Ca^{2+} concentration at salinity 0.35 decreased from the initial value of 0.041 M to the equilibrium concentration of 0.029 M in around 50 hr, demonstrating that approximately 30% had precipitated within 50 hr from the mixing. Also in Fig.

6.1 the Ca^{2+} concentration at salinity 0.5 decreased from the initial value of 0.042 M to the equilibrium concentration of 0.033 M in around 90 hr demonstrating, that approximately 21% had precipitated within 90 hr from the mixing. It can also be observed from Fig. 6.1 that there was small change in the Ca^{2+} concentration at salinity 1.5 within 1300 hr from the mixing. The same observation can be made from Fig. 6.2 for the sulphate ion and also from Figs. 6.3 and 6.4 where DO is also present. Therefore, it seems that $CaSO_4$ precipitation decreases with an increase of salinity level; and moreover, that salinity affects the time required to reach equilibrium (the kinetics of the reaction). This explains the behaviour of both Ca^{2+} and SO_4^{2-} ions in Figs. 6.1-6.4, where the decline of ionic concentration is less observed at higher salinity.

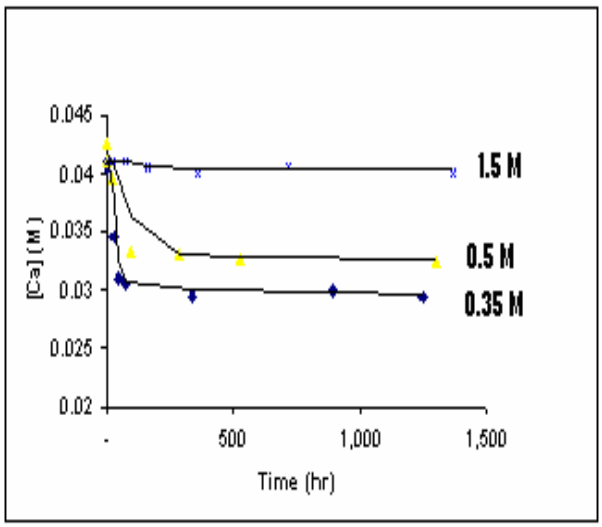

Figure 6.1: *Effect of salinity level on the profile of [Ca^{2+}] decline during pure $CaSO_4$ precipitation in the absence of DO.*

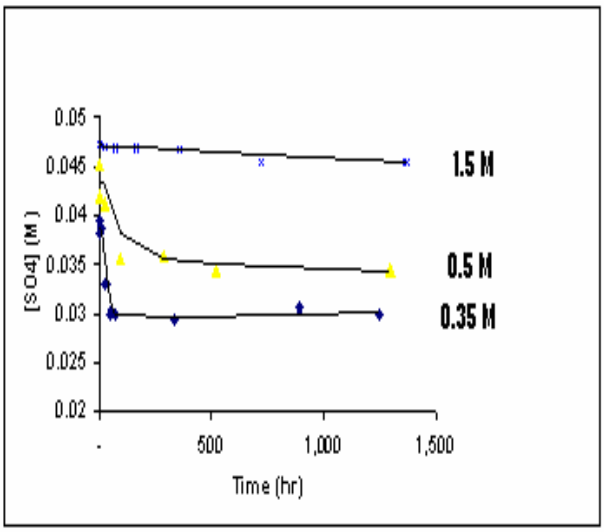

Figure 6.2: *Effect of salinity level on the profile of [SO_4^{2-}] decline during pure $CaSO_4$ precipitation in the absence of DO.*

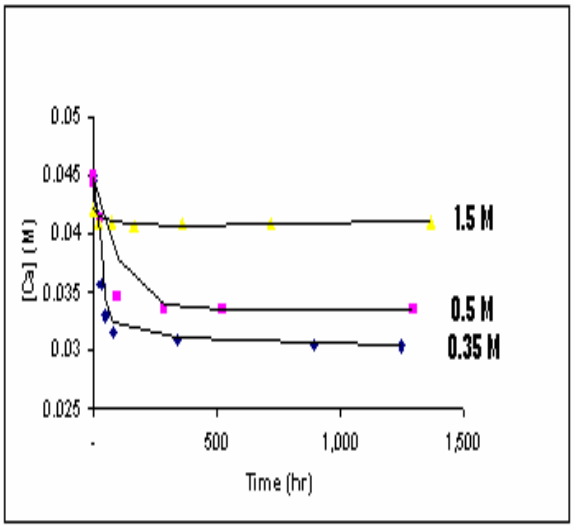

Figure 6.3: *Effect of salinity level on the profile of [Ca^{2+}] decline during pure $CaSO_4$ precipitation in the presence of DO.*

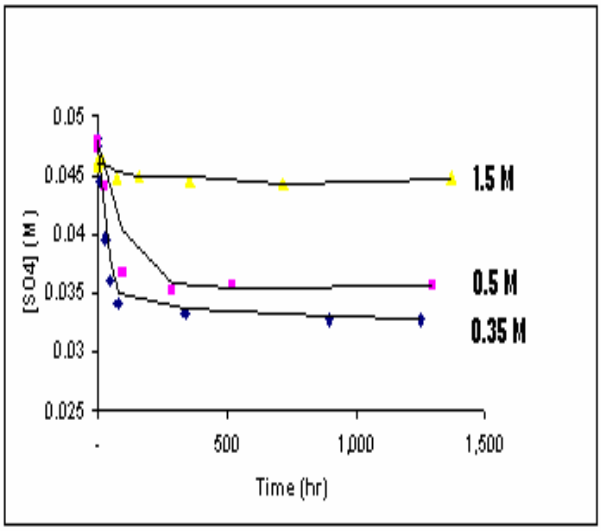

Figure 6.4: *Effect of salinity level on the profile of [SO_4^{2-}] decline during pure $CaSO_4$ precipitation in the presence of DO.*

6.2.1.2 Effect of salinity on the decline of scaling ion concentrations for $CaSO_4$ and $SrSO_4$ co-precipitation with and without presence of DO.

In order to investigate the effect of salinity on $CaSO_4$ and $SrSO_4$ co-precipitation, the concentration of Ca^{2+}, Sr^{2+} and SO_4^{2-} ions were monitored during co-precipitation of $CaSO_4$ and $SrSO_4$ at different salinity levels. Figs. 6.5-6.16 show the change of the scaling ion (Ca^{2+}, Sr^{2+} or SO_4^{2-}) concentrations with time at three different salinity levels (0.35M, 0.5M and 1.5M) with and without the presence of DO. Two different initial Sr^{2+} concentrations (0.02 M and 0.005 M) were chosen to investigate the effect of salinity on $CaSO_4$ and $SrSO_4$ co-precipitation; the initial Ca^{2+} and SO_4^{2-} ion concentrations were kept as constant as possible.

In the case of an initial concentration of 0.02 M of Sr^{2+} ions; it can be seen in Fig. 6.5 and Fig. 6.8 that Ca^{2+} concentration almost remains constant for about 1300hr from the mixing of the model solutions. This observation can be made for the three salinity levels 0.35M, 0.5M and 1.5M, however, it is seen that increasing the salinity up to 1.5 M almost eliminates the precipitation of $CaSO_4$. However, increasing salinity has not inhibited the $SrSO_4$ precipitation at such high supersaturation as can be observed on Figs. 6.6-6.7 and Figs.6.9-6.10. The Sr^{2+} concentration at salinity 0.35 decreased from the initial value of 0.018 M to the concentration of 0.0011 M in around 48 hr,

demonstrating that approximately 94% had precipitated within 48 hr from the mixing.

In the case of a low initial Sr^{2+} concentration (0.005 M), Figs. 6.11 and 6.14 illustrate that the Ca^{2+} ions showed the same trend of decreasing Ca^{2+} consumption as the salinity increased as was observed for pure precipitation. Figs. 6.12 and 6.15 show that the Sr^{2+} ions have the same trend as well, as the salinity increases less Sr^{2+} will be consumed. However, it seems that salinity increase has greater influence in term of precipitation decrease on $CaSO_4$ than $SrSO_4$ during co-precipitation.

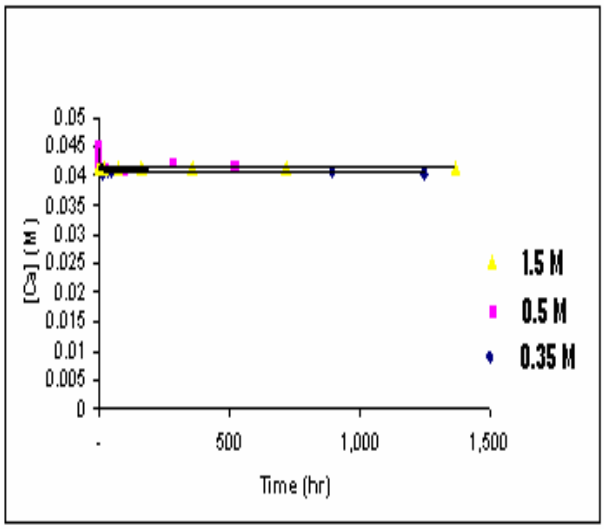

Figure 6.5: *Effect of salinity level on the profile of [Ca^{2+}] decline during $CaSO_4$ and $SrSO_4$ co-precipitation in the absence of DO (0.02 M initial [Sr^{2+}]).*

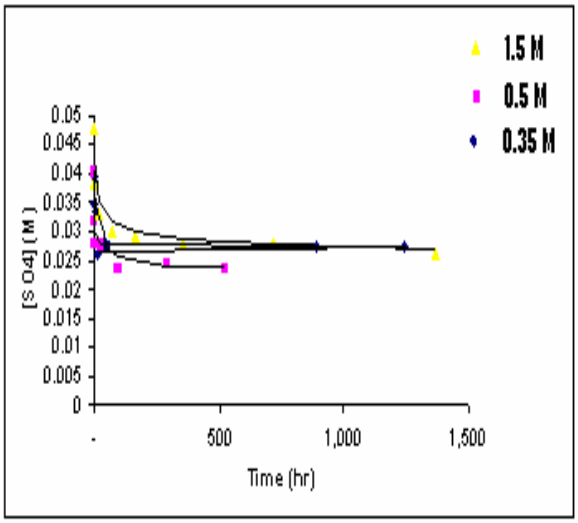

Figure 6.6: *Effect of salinity level on the profile of [SO_4^{2-}] decline during $CaSO_4$ and $SrSO_4$ co-precipitation in the absence of DO (0.02 M initial [Sr^{2+}]).*

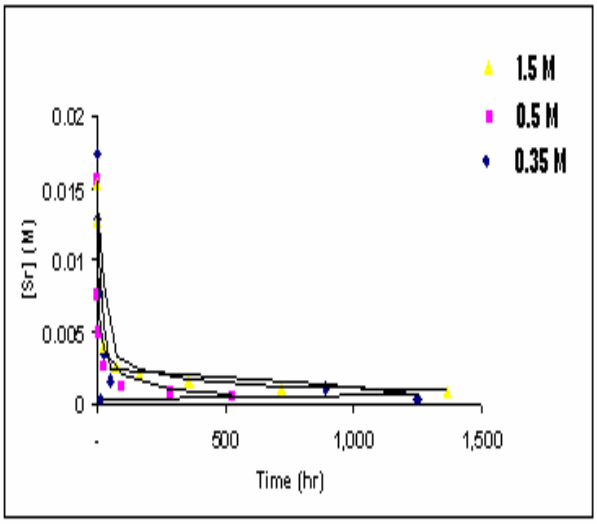

Figure 6.7: *Effect of salinity level on the profile of [Sr^{2+}] decline during $CaSO_4$ and $SrSO_4$ co-precipitation in the absence of DO (0.02 M initial [Sr^{2+}]).*

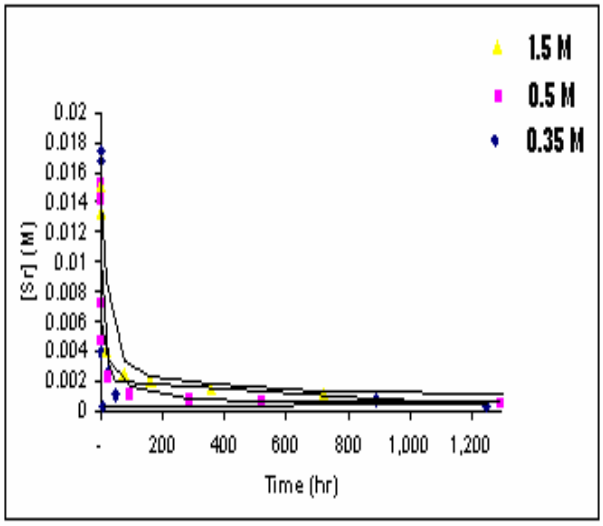

Figure 6.9: *Effect of salinity level on the profile of [Sr^{2+}] decline during $CaSO_4$ and $SrSO_4$ co-precipitation in the presence of DO (0.02 M initial [Sr^{2+}]).*

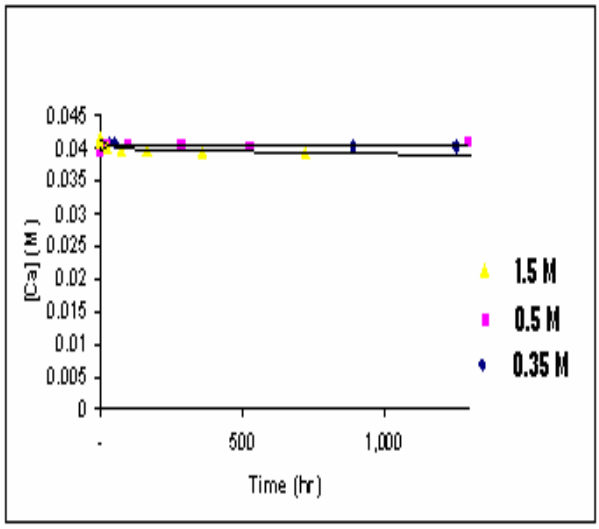

Figure 6.8: *Effect of salinity level on the profile of [Ca^{2+}] decline during $CaSO_4$ and $SrSO_4$ co-precipitation in the presence of DO (0.02 M initial [Sr^{2+}]).*

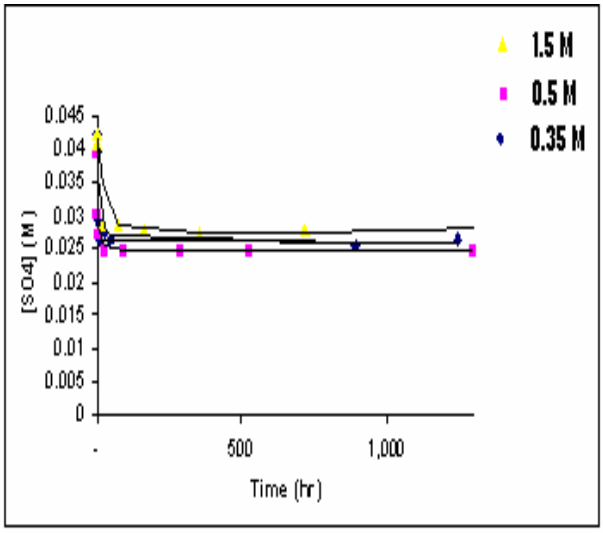

Figure 6.10: *Effect of salinity level on the profile of [SO_4^{2-}] decline during $CaSO_4$ and $SrSO_4$ co-precipitation in the presence of DO (0.02 M initial [Sr^{2+}]).*

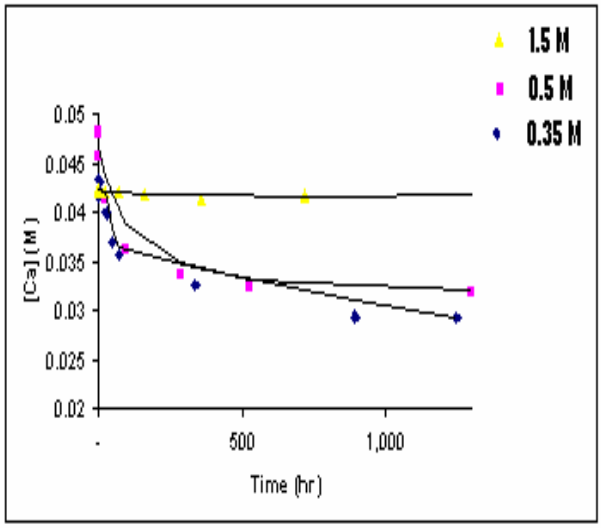

Figure 6.11: *Effect of salinity level on the profile of [Ca^{2+}] decline during $CaSO_4$ and $SrSO_4$ co-precipitation in the absence of DO (0.005 M initial [Sr^{2+}]).*

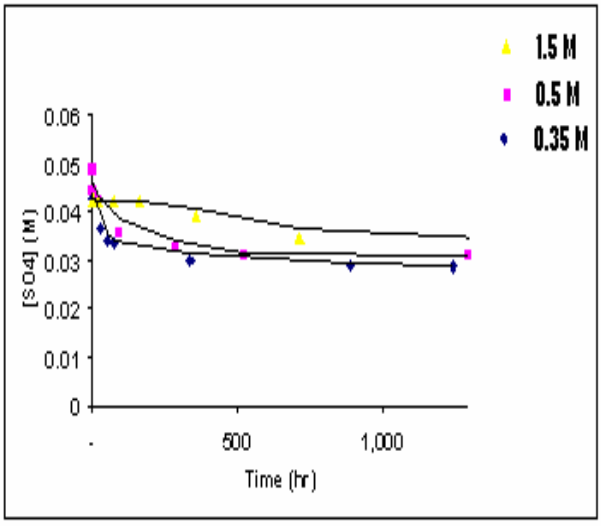

Figure 6.13: *Effect of salinity level on the profile of [SO_4^{2-}] decline during $CaSO_4$ and $SrSO_4$ co-precipitation in the absence of DO (0.005 M initial [Sr^{2+}]).*

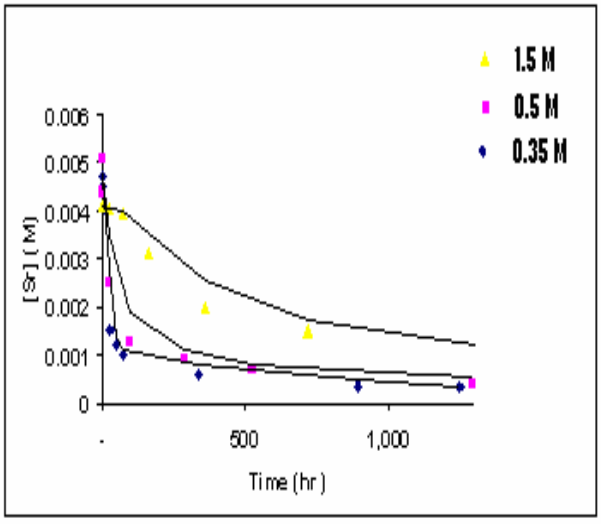

Figure 6.12: *Effect of salinity level on the profile of [Sr^{2+}] decline during $CaSO_4$ and $SrSO_4$ co-precipitation in the absence of DO (0.005 M initial [Sr^{2+}]).*

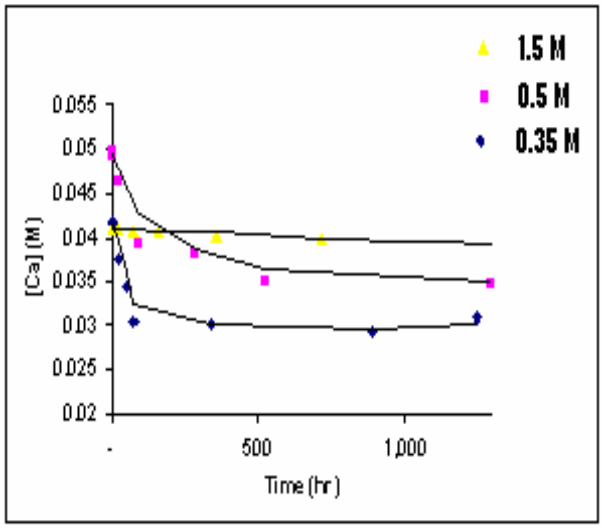

Figure 6.14: *Effect of salinity level on the profile of [Ca^{2+}] decline during $CaSO_4$ and $SrSO_4$ co-precipitation in the presence of DO (0.005 M initial [Sr^{2+}]).*

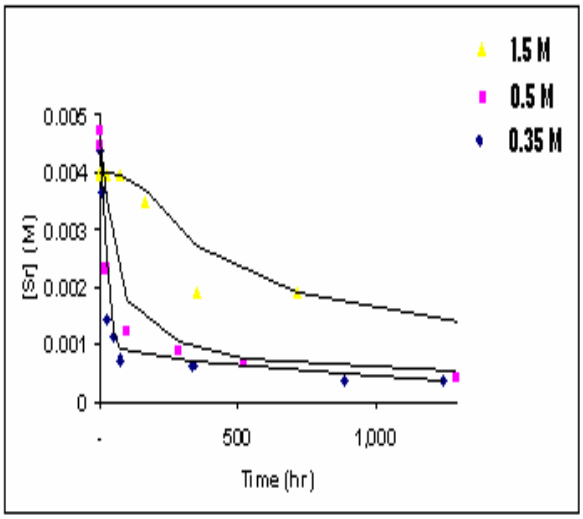

Figure 6.15: *Effect of salinity level on the profile of [Sr^{2+}] decline during $CaSO_4$ and $SrSO_4$ co-precipitation in the presence of DO (0.005 M initial [Sr^{2+}]).*

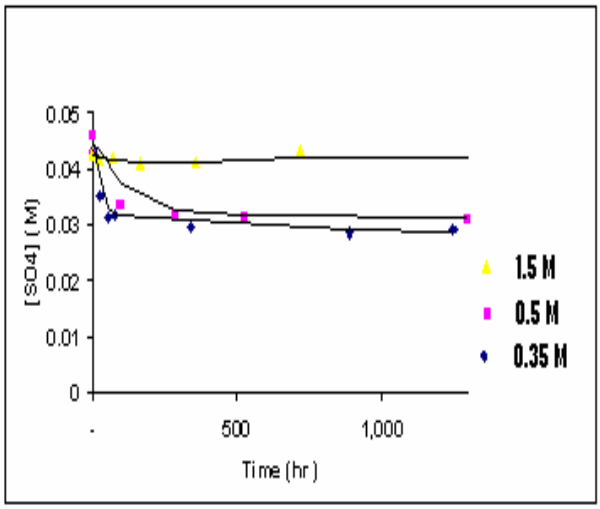

Figure 6.16: *Effect of salinity level on the profile of [SO_4^{2-}] decline during $CaSO_4$ and $SrSO_4$ co-precipitation in the presence of DO (0.005 M initial [Sr^{2+}]).*

6.3.1.3 Effect of $CaSO_4$ and $SrSO_4$ co-precipitation on the decline of scaling ion concentrations with and without presence of DO at different salinity levels.

The decline of scaling ion concentrations was monitored during the co-precipitation of $CaSO_4$ and $SrSO_4$. The initial Ca^{2+} and SO_4^{2-} ion concentrations were kept almost constant and the initial Sr^{2+} concentration was changed to study the $CaSO_4$ and $SrSO_4$ co-precipitation at three salinity levels. Figs. 6.17-6.20 show the decline in Ca^{2+} and SO_4^{2-} ion concentrations at different initial Sr^{2+} concentrations and at a salinity of 0.35 M and with and without the presence of DO. It can be observed from Figs. 6.17 and 6.19 that the decline of Ca^{2+} concentration has been affected by the presence of Sr^{2+}; as the concentration of Sr^{2+} increases the decline in Ca^{2+} decrease, this is maybe due to the reaction of Sr^{2+} with the SO_4^{2-} to form $SrSO_4$ which reduce the concentration of SO_4^{2-} as can be seen in Figs.6.18 and 6.20.

The same observation can be noticed at higher salinity (0.5 and 1.5) see Figs. 6.21-6.28, where it can be seen that the decline in Ca^{2+} decreases as Sr^{2+} concentration increases. However, the main observation that could be made from Figs. 6.17-6.28 was that the existence of Sr^{2+} ions will reduce the $CaSO_4$ precipitation and may eliminate it at high salinity. This is due to several factors including the common ion

effect, the increase in ionic strength and the influence of co-precipitation on the thermodynamic solubility product of both precipitate salts.

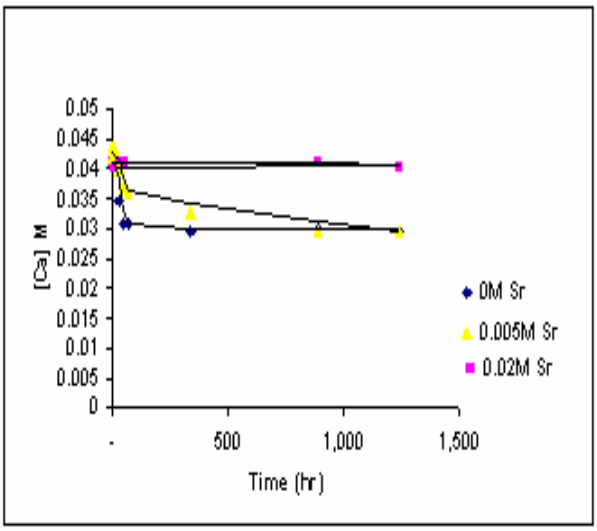

Figure 6.17: *Effect of $CaSO_4$ and $SrSO_4$ co-precipitation on $[Ca^{2+}]$ decline in the absence of DO at 0.35M salinity.*

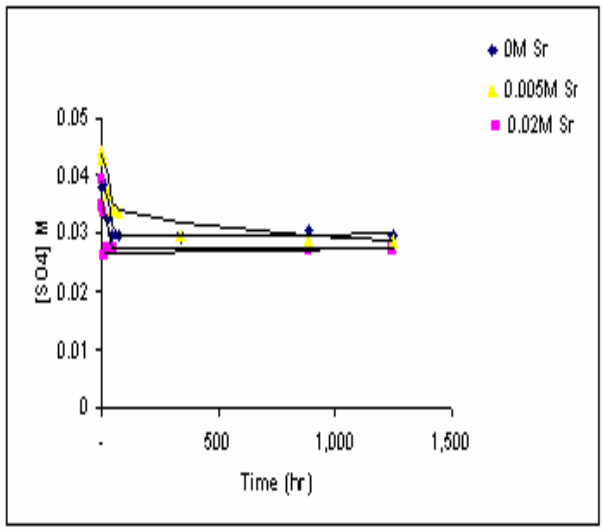

Figure 6.18: *Effect of $CaSO_4$ and $SrSO_4$ co-precipitation on $[SO_4^{2-}]$ decline in the absence of DO at 0.35M salinity.*

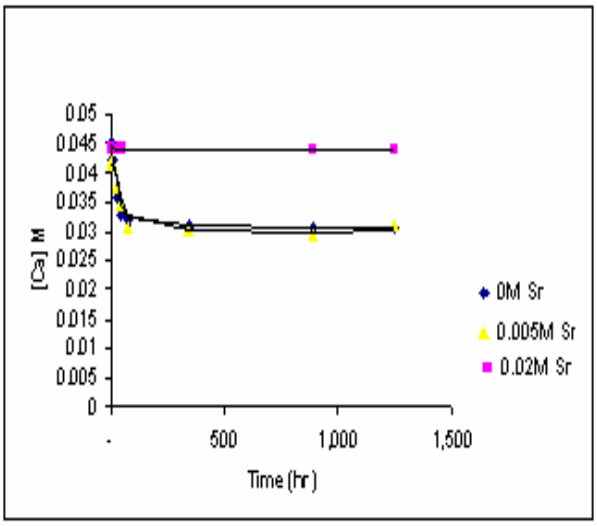

Figure 6.19: *Effect of $CaSO_4$ and $SrSO_4$ co-precipitation on $[Ca^{2+}]$ decline in the presence of DO at 0.35M salinity.*

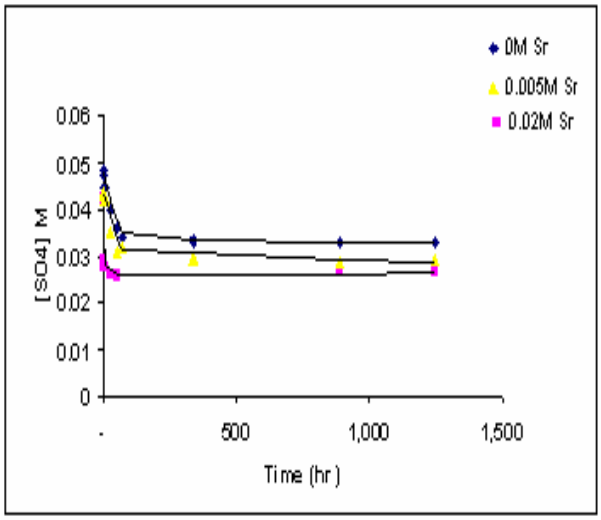

Figure 6.20: *Effect of $CaSO_4$ and $SrSO_4$ co-precipitation on $[SO_4^{2-}]$ decline in the presence of DO at 0.35M salinity.*

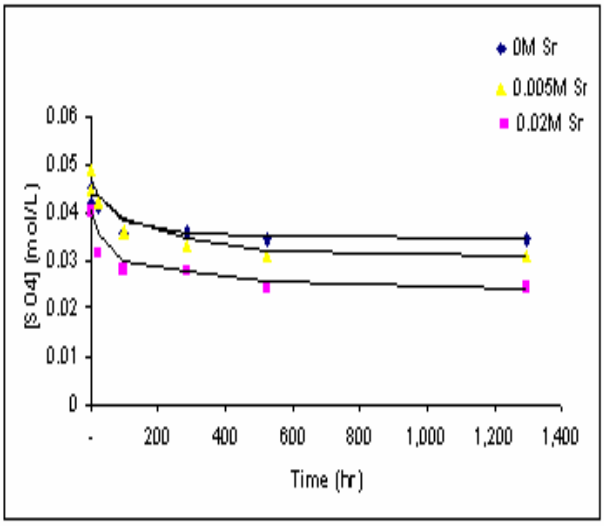

Figure 6.22: *Effect of $CaSO_4$ and $SrSO_4$ co-precipitation on $[SO_4^{2-}]$ decline in the absence of DO at 0.5M salinity.*

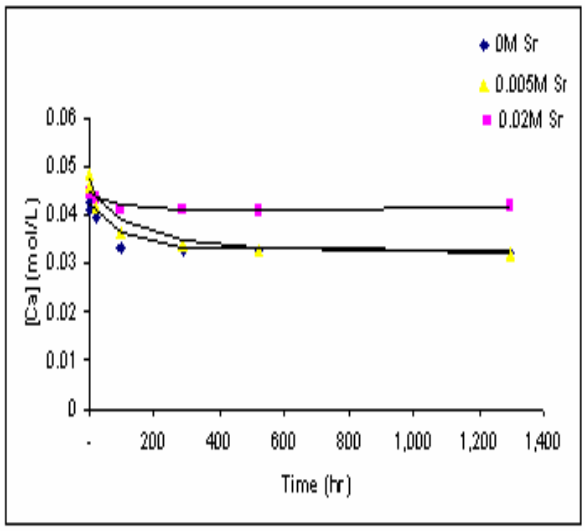

Figure 6.21: *Effect of $CaSO_4$ and $SrSO_4$ co-precipitation on $[Ca^{2+}]$ decline in the absence of DO at 0.5M salinity.*

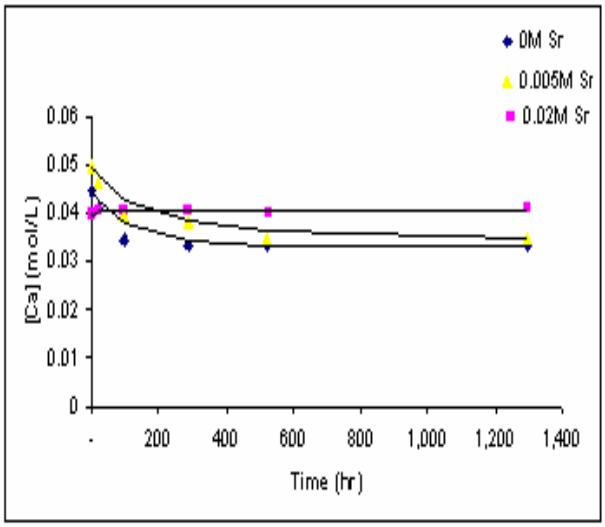

Figure 6.23: *Effect of $CaSO_4$ and $SrSO_4$ co-precipitation on $[Ca^{2+}]$ decline in the presence of DO at 0.5M salinity.*

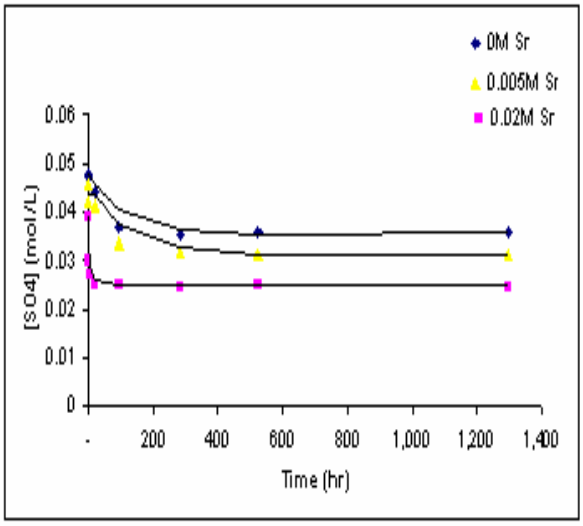

Figure 6.24: *Effect of $CaSO_4$ and $SrSO_4$ co-precipitation on $[SO_4^{2-}]$ decline in the presence of DO at 0.5M salinity.*

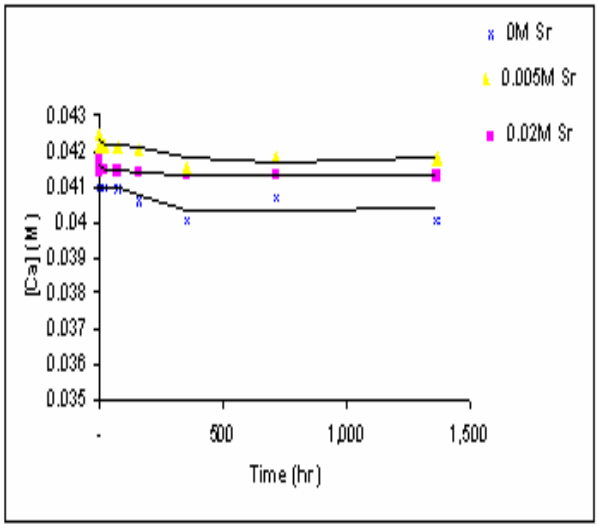

Figure 6.25: *Effect of $CaSO_4$ and $SrSO_4$ co-precipitation on $[Ca^{2+}]$ decline in the absence of DO at 1.5M salinity.*

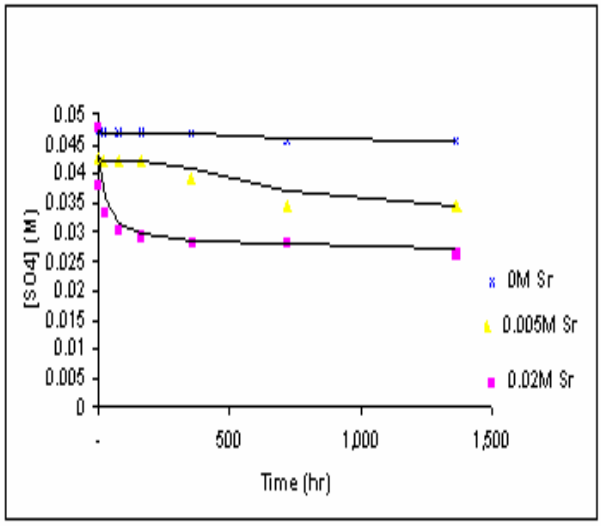

Figure 6.26: *Effect of $CaSO_4$ and $SrSO_4$ co-precipitation on $[SO_4^{2-}]$ decline in the absence of DO at 1.5M salinity.*

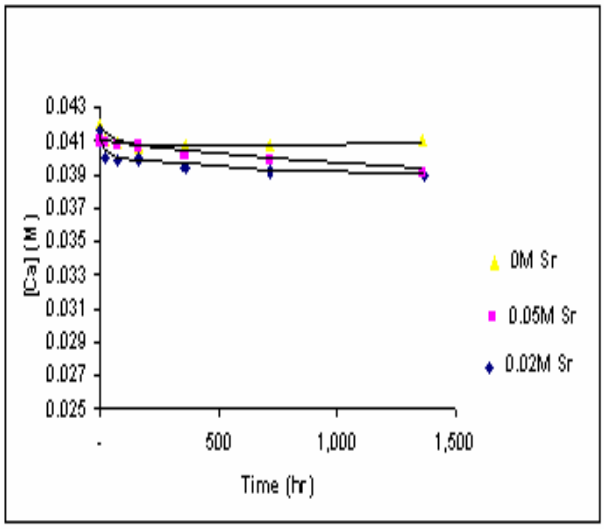

Figure 6.27: *Effect of $CaSO_4$ and $SrSO_4$ co-precipitation on $[Ca^{2+}]$ decline in the presence of DO at 1.5M salinity.*

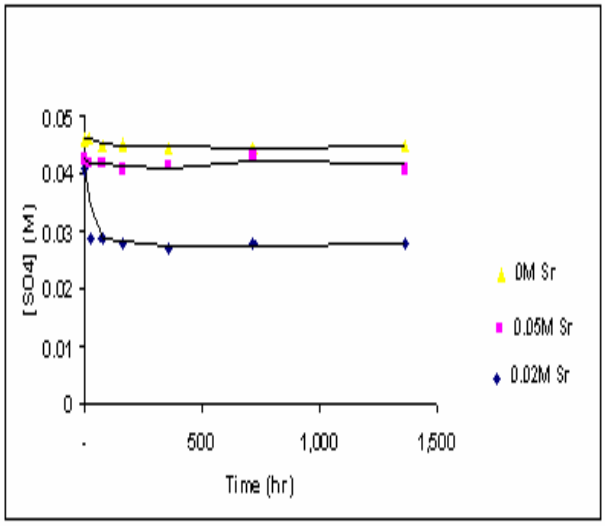

Figure 6.28: *Effect of $CaSO_4$ and $SrSO_4$ co-precipitation on $[SO_4^{2-}]$ decline in the presence of DO at 1.5M salinity.*

6.3.1.4 Effect of the presence of DO on the decline of scaling ion concentrations during $CaSO_4$ and $SrSO_4$ co-precipitation at different salinity levels.

The effect of the presence of Dissolved organics (DO) on $CaSO_4$ and $SrSO_4$ co-precipitation has been studied. Figs 6.29-6.37 show the effect of DO on the decline of scaling ion (Ca^{2+}, Sr^{2+} and SO_4^{2-}) concentrations at different salinity levels. The main observation is that the DO has minor influence on the co-precipitation of $CaSO_4$ and $SrSO_4$; even though, the existence of DO has an inhibition effect on both precipitates. However, it is clearly noted that the DO presence affect the adhesion of the precipitate on the reactor and membrane surface. The presence of DO reduced the adhesion of scaling on the reactor and membrane surfaces, and this was apparent during surface cleaning. Also it has been noticed that DO reduced the adhesion of $CaSO_4$ more than both $SrSO_4$ and the co-precipitation products. The effects of DO on Scaling structure will be discussed in detail later.

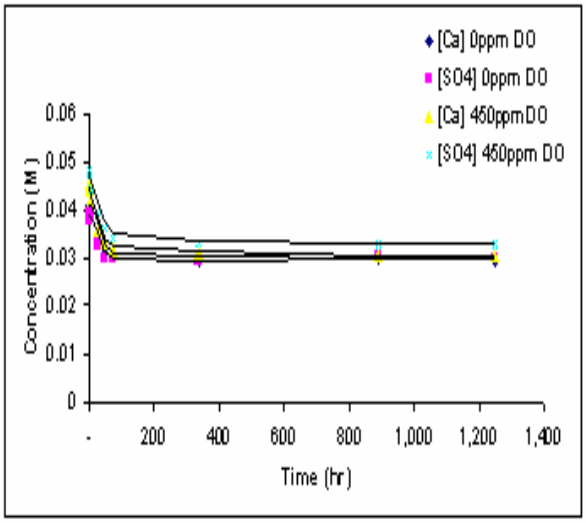

Figure 6.29: *Effect of the presence of DO on the decline of scaling ion concentrations during $CaSO_4$ precipitation at 0.35M salinity.*

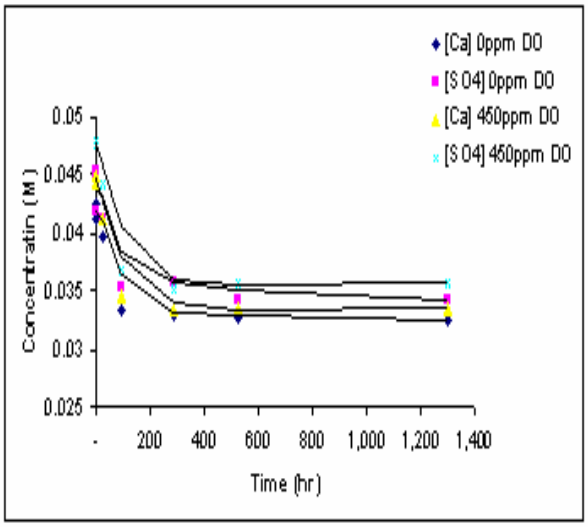

Figure 6.30: *Effect of the presence of DO on the decline of scaling ion concentrations during $CaSO_4$ precipitation at 0.5M salinity.*

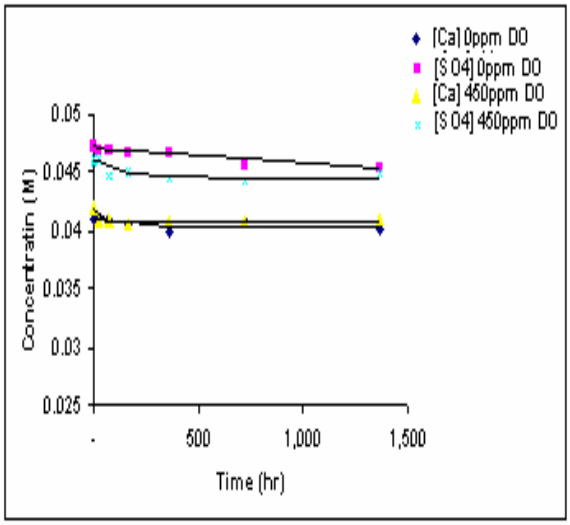

Figure 6.31: *Effect of the presence of DO on the decline of scaling ion concentrations during $CaSO_4$ precipitation at 1.5M salinity.*

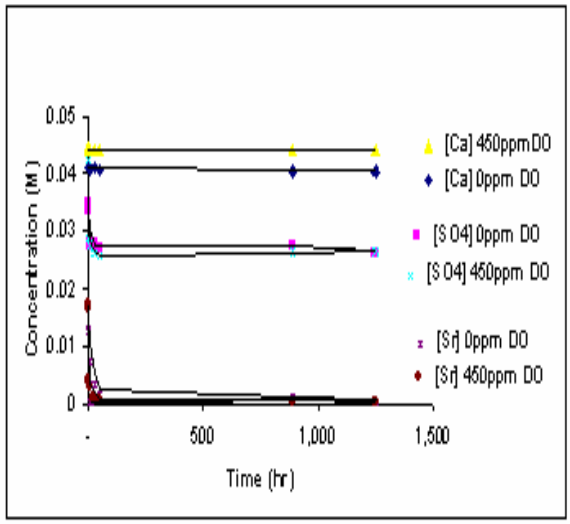

Figure 6.32: *Effect of the presence of DO on the decline of scaling ion concentrations during $CaSO_4$ and $SrSO_4$ co-precipitation at 0.35M salinity and 0.02M $[Sr^{2+}]$.*

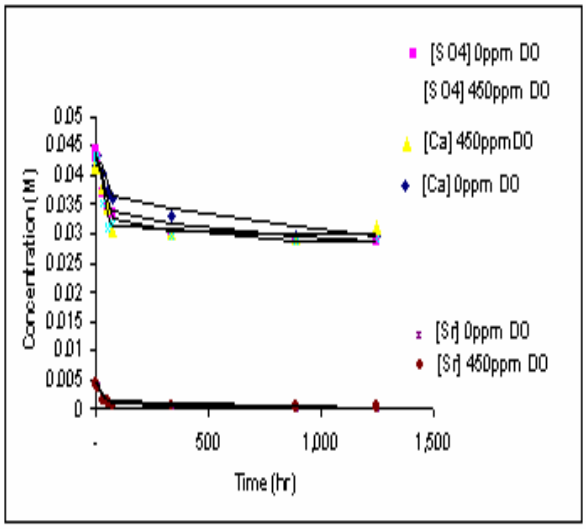

Figure 6.33: *Effect of the presence of DO on the decline of scaling ion concentrations during $CaSO_4$ and $SrSO_4$ co-precipitation at 0.35M salinity and 0.005M of $[Sr^{2+}]$.*

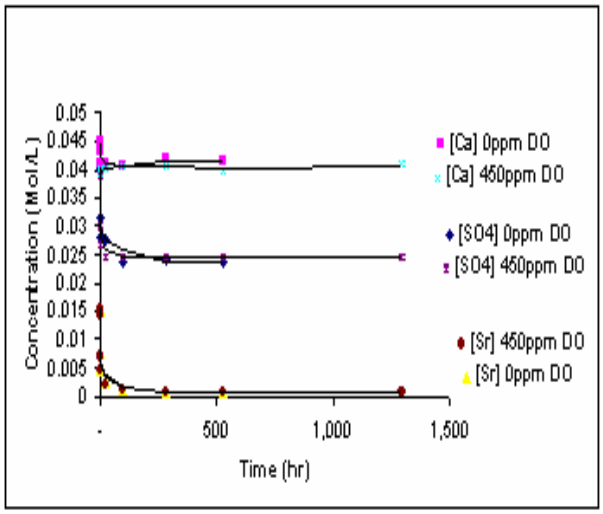

Figure 6.34: *Effect of the presence of DO on the decline of scaling ion concentrations during $CaSO_4$ and $SrSO_4$ co-precipitation at 0.5M salinity and 0.02M $[Sr^{2+}]$.*

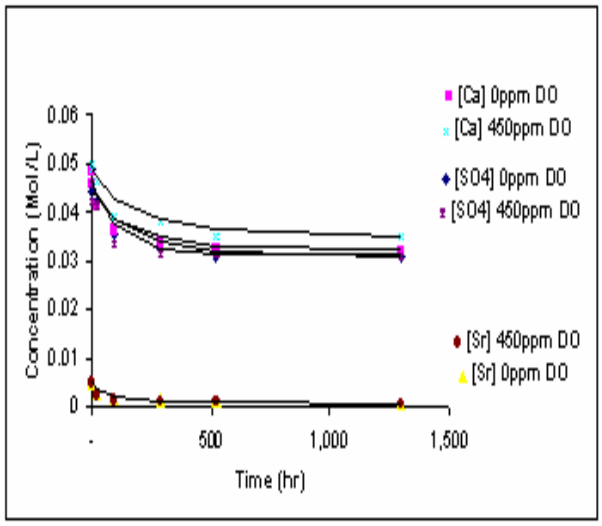

Figure 6.35: *Effect of the presence of DO on the decline of scaling ion concentrations during $CaSO_4$ and $SrSO_4$ co-precipitation at 0.5M salinity and 0.005M $[Sr^{2+}]$.*

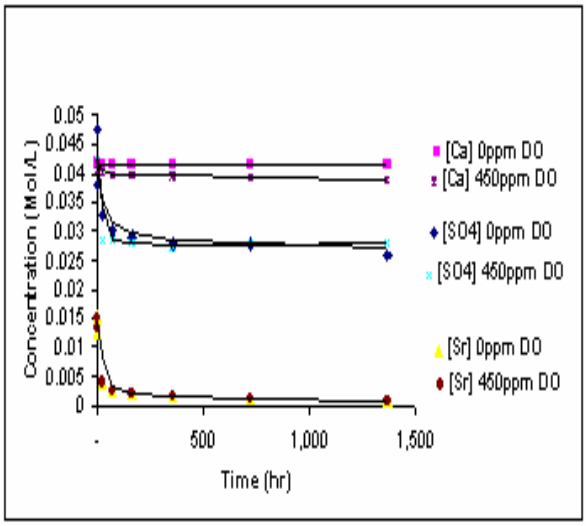

Figure 6.36: *Effect of the presence of DO on the decline of scaling ion concentrations during $CaSO_4$ and $SrSO_4$ co-precipitation at 1.5M salinity and 0.02M $[Sr^{2+}]$*

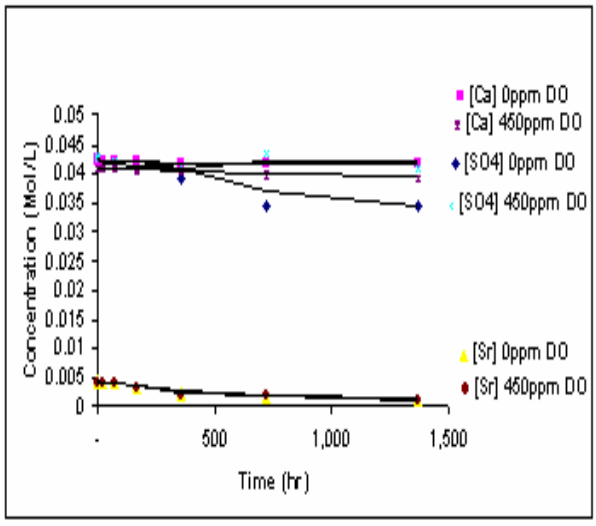

Figure 6.37: *Effect of the presence of DO on the decline of scaling ion concentrations decline during $CaSO_4$ and $SrSO_4$ co-precipitation at 1.5M salinity and 0.005M $[Sr^{2+}]$*

6.4 Thermodynamic analysis

The thermodynamic solubility products (*Ksp*) have been calculated for pure $CaSO_4$ precipitation and co-precipitation of $CaSO_4$ and $SrSO_4$ at different salinity levels. The experiments which are shown in table 6.1 have been conducted until equilibrium was reached. The measured concentrations at equilibrium have been used to calculate the activity coefficients (γ) using the Pitzer equations for each ion. Table 6.2 shows the values of the calculated activity coefficient for the scaling ions of interest (Ca^{2+},Sr^{2+}, SO_4^{2-}); these calculated values showed excellent agreement with published data [122, 123] where comparison is possible. The thermodynamic solubility products for each salt (*Ksp*) were calculated using equations (2.16-2.18) as discussed in detail in section 2.4.1.1.

Table 6.3 summarises the calculated thermodynamic solubility product (*Ksp*). The calculated *Ksp* for pure $CaSO_4$ at 0.5M salinity was found to be $2.638x10^{-05}$ $(mol/L)^2$ which is in very good agreement with $2.18x10^{-5}(mol/L)^2$ the published value in [62]. Effect of salinity, DO presence and the effect of co-precipitation of $CaSO_4$ and $SrSO_4$ on the *Ksp* values of both salts were investigated. Salinity increases increased the *Ksp* for both salts; as can be seen in table 6.3 all tested solutions showed the same trend of increasing *Ksp* as the salinity increased. The salinity effect is believed to be due to the increase in non-scaling ionic species which increases the interaction between all existing species and also due to the influence of salinity on the crystal size and shape as will be discussed in more detail later. It has been observed that salinity increases have more influence on $CaSO_4$ precipitation than on $SrSO_4$ precipitation; the calculated *Ksp* values in table 6.3 support this observation as the change of *Ksp* for $CaSO_4$ is more noticeable than the change of *Ksp* of $SrSO_4$ as result of salinity increase.

The effect of dissolved organics on the *Ksp* values for pure $CaSO_4$ precipitation and $CaSO_4$ and $SrSO_4$ co-precipitation was tested at different salinity levels. As shown in table 6.3, the effect of dissolved organics present was greater on the $CaSO_4$ than on the $SrSO_4$. The effect of dissolved organics on the *Ksp* is believed to be due to the inhibition effect that DO has in the precipitation formation [139] and thus the size of

the formed crystal. The mechanism of the inhibition caused by the DO is believed to be either due to the complexing of calcium ions which in theory should lead to reduce the saturation state of the solution and consequently decrease the reaction rate [139]. However, this believed not to be the case in our experiments since as shown in Figs. 6.29-6.37 the concentration of free calcium ions is higher in the presence of dissolved organics. It is expected that the inhibition effect in this case is due to coverage of the active sites of the crystal surface, which alters the size of the crystal. This hypothesis is supported by the findings of the morphological analysis and will be discussed later in the scale morphology section.

Table 6.2: *Calculated activity coefficients for scaling ions during pure and co-precipitation of $CaSO_4$ and $SrSO_4$ at different salinity levels and 30^oC*

	Activity coefficients for scaling ions (Ca^{2+},Sr^{2+}, SO_4^{2-})								
	salinity (0.35 M)			salinity (0.5 M)			salinity (1.5 M)		
	Ca^{2+}	SO_4^{2-}	Sr^{2+}	Ca^{2+}	SO_4^{2-}	Sr^{2+}	Ca^{2+}	SO_4^{2-}	Sr^{2+}
Pure $CaSO_4$	0.2310	0.1270	-	0.2190	0.0997	-	0.2260	0.0506	-
Pure $CaSO_4$ with DO presence	0.2290	0.1260	-	0.2190	0.0992	-	0.2260	0.0507	-
Co- precipitation (0.02 M Sr^{2+})	0.2250	0.1220	0.1990	0.2160	0.0984	0.1906	0.2250	0.0512	0.1892
Co- precipitation (0.02 M Sr^{2+}) with DO	0.2230	0.1197	0.1969	0.2160	0.0984	0.1902	0.2251	0.0514	0.1889
Co- precipitation (0.005 M Sr^{2+})	0.2310	0.1272	0.2021	0.2190	0.1007	0.1896	0.2252	0.0510	0.1864
Co- precipitation (0.005 M Sr^{2+}) with DO	0.2297	0.1262	0.2011	0.2182	0.0996	0.1886	0.2259	0.0510	0.1847

Indeed, co-precipitation of $CaSO_4$ and $SrSO_4$ affects the *Ksp* values of both salts. This variation of *Ksp* values for $CaSO_4$ and $SrSO_4$ in mixed solution is believed to be due to change in the crystal structure and size. This is, has been observed during the SEM and EDS analyses and will be discussed later in the coming sections.

Table 6.3: *Thermodynamic solubility product (Ksp) during pure and co-precipitation of $CaSO_4$ and $SrSO_4$ at 30^oC*

	Ksp for $CaSO_4$			*Ksp* for $SrSO_4$		
	salinity (0.35 M)	salinity (0.5 M)	salinity (1.5 M)	salinity (0.35 M)	salinity (0.5 M)	salinity (1.5 M)
Pure $CaSO_4$	$2.553x10^{-05}$	$2.428x10^{-05}$	$2.078x10^{-05}$			
Pure $CaSO_4$ with DO presence	$2.866x10^{-05}$	$2.590x10^{-05}$	$2.108x10^{-05}$			
Co- precipitation (0.02 M Sr^{2+})	$2.894x10^{-05}$	$2.075x10^{-05}$	$1.238x10^{-05}$	$2.228x10^{-07}$	$2.227x10^{-07}$	$2.179x10^{-07}$
Co- precipitation (0.02 M Sr^{2+}) with DO presence	$3.120x10^{-05}$	$2.128x10^{-05}$	$1.258x10^{-05}$	$2.336x10^{-07}$	$2.316x10^{-07}$	$2.493x10^{-07}$
Co- precipitation (0.005 M Sr^{2+})	$2.470x10^{-05}$	$2.165x10^{-05}$	$1.658x10^{-05}$	$2.415x10^{-07}$	$2.405x10^{-07}$	$2.630x10^{-07}$
Co- precipitation (0.005 M Sr^{2+}) with DO presence	$2.603x10^{-05}$	$2.327x10^{-05}$	$1.838x10^{-05}$	$2.716x10^{-07}$	$2.499x10^{-07}$	$3.116x10^{-07}$

6.5 Kinetic study

Detail quantitative analysis of precipitation kinetics is beyond the scope of this work, since this chapter is part of ingoing research focussed on developing a reliable approach to predict the onset of scaling propensity, thus, the kinetics of scale

development and build up is beyond the major scope of this work and may be addressed later. However, the effect of salinity, DO, and co-precipitation on the kinetics of $CaSO_4$ and $SrSO_4$ precipitation was qualitatively assessed. The change in the induction period and the change of scaling salt concentration are used to assess the effects of salinity, DO, and co-precipitation on kinetics of $CaSO_4$ and $SrSO_4$ precipitation.

6.5.1 Effects on induction periods

As was discussed in section 2.4.1.2 from chapter 2, the induction period for the precipitation reaction refers to the period of metastability before the precipitation occurs. The change of induction period was observed as the salinity was increased for the both precipitating salts ($CaSO_4$ and $SrSO_4$). It was observed that the induction period for pure $CaSO_4$ precipitation changed from around 9 hr at 0.35 M salinity to about 15 hr at 0.5 M salinity and to above 500 hr for 1.5 M salinity; which indicates an enormous impact of salinity on the metastability of the solution. However, it may be worthwhile to mention that these numbers represent visual observations and that, for more accurate readings, there is a need to monitor the change of scaling salt concentrations, or even solution turbidity, instantaneously during the precipitation reaction. DO presence in the solution during the precipitation has increased the induction time. This is believed to be due to coverage of the active nucleation sites by which the growth of the nucleus is delayed.

Co-precipitation of $CaSO_4$ and $SrSO_4$ also has influence on the induction time. Two different Sr^{2+} concentrations (0.02 M and 0.005M) have been added to almost the same solution containing the same Ca^{2+} and SO_4^{2-} concentrations. At high [Sr^{2+}] there was a huge increase in $CaSO_4$ induction time. That is due to the common ion effect; the Sr^{2+} consumed quantities of SO_4^{2-} to form $SrSO_4$ which reduced the concentration of SO_4^{2-} and decreased the possibility to form $CaSO_4$. In the case of low [Sr^{2+}] there was a noticeable shift in the induction period for pure $CaSO_4$. This shift in induction time is believed to be due not just to the influence of Sr^{2+} in term of ion interaction which is limited as seen in table 6.2 and needs more study to calculate all the interaction parameters in such complex solutions, but also due to the influence

of Sr^{2+} on the crystal formation of $CaSO_4$ which is obscure but still very important as will be discussed later in sections 6.6 and 6.7.

6.5.2 Qualitative reaction rate analysis

As seen in Figs. 6.1-6.2 as the salinity increases while pure $CaSO_4$ precipitation takes place, the reaction kinetics slow-down and the equilibrium concentrations of Ca^{2+} and SO_4^{2-} increased. This may be due to the increase of the $CaSO_4$ solubility product as the salinity increase, as was discussed before in section 6.4. Also an increase in $[Na^+]$ has an inhibition effect on $CaSO_4$ crystal growth as Zhang and Nancollas [54], suggested. They proposed that the Na^+ adsorbs onto the surface of gypsum and thus partially inhibits its growth rate and thus, as the salinity increases, the Na^+ adsorption increases and the precipitation rate decreases [53]. Also, the same observation has been noted during $CaSO_4$ and $SrSO_4$ co-precipitation; where, as can be seen in Figs. 6.17, 6.19, 6.21, 6.23, 6.25 and 6.27, the equilibrium concentration of Ca^{2+} has been increased which indicates a decline in the amount of $CaSO_4$ precipitation. Also it could be concluded from Figs 6.29-6.37 that DO has decreased the precipitation rate because of the inhibition effects it has on $CaSO_4$ and $SrSO_4$ precipitation as discussed before.

6.6. Morphology effects

The precipitates resulted from pure and co-precipitation of $CaSO_4$ and $SrSO_4$ have been examined using a high-resolution digital imaging camera coupled with an optical microscope, SEM and EDS.

6.6.1 High-resolution digital imaging

Figs 6.38-6.52 show digitised images for the precipitates during pure and co-precipitation of $CaSO_4$ and $SrSO_4$ at 0.35M, 0.5M and 1.5M salinity and with and without the presence of DO. Figs 6.38, 6.41, 6.44 and 6.46 show that the pure $CaSO_4$ precipitation forms a long needle shaped crystal; which may indicate the formation of calcium sulphate dihydrate or gypsum. The effect of salinity on the crystal structure of pure $CaSO_4$ precipitate is mainly on the crystal size as can be seen from the comparison between Fig. 6.38 and Fig. 6.44. However, at salinity 1.5M there was

no observation of $CaSO_4$ crystals, which is consistent with the effect of salinity obtained from the thermodynamic and kinetic analyses. Also, from the comparisons between Fig. 6.38 and Fig.6.41 and between Fig. 6.44 and Fig. 6.46, it was observed that DO presence affects the crystal size during pure $CaSO_4$ precipitation, which is also consistent with the effect of DO as discussed before. The variation in crystal size could affect the changes in Gibbs free energy associated with the crystallisation process [140] as has been observed and discussed in section 6.4.

In co-precipitation where a high concentration of Sr^{2+} is present, there was no observation of $CaSO_4$ crystals within the precipitate as can be seen in Figs. 6.39, 6.42, 6.47, 6.49, and 6.51; and $SrSO_4$ was observed as the only precipitate in this case. In the case of co-precipitation where a low concentration of Sr^{2+} is present, there was observation of both $CaSO_4$ and $SrSO_4$ crystals see Figs. 6.40, 6.43, 6.48, 6.50 and 6.52. It was observed that in addition to the free $SrSO_4$ and $CaSO_4$ crystals; there was an interaction between the $SrSO_4$ crystals and the $CaSO_4$ crystals, which indicates that the co-existence of these salts enhanced the heterogeneous nucleation of both salts. The $SrSO_4$ increases the tenacity of the $CaSO_4$ precipitate since the $SrSO_4$ acts as a cementing agent and connects the $CaSO_4$ crystals as seen in Figs. 6.40, 6.43, 6.45 and 6.48.

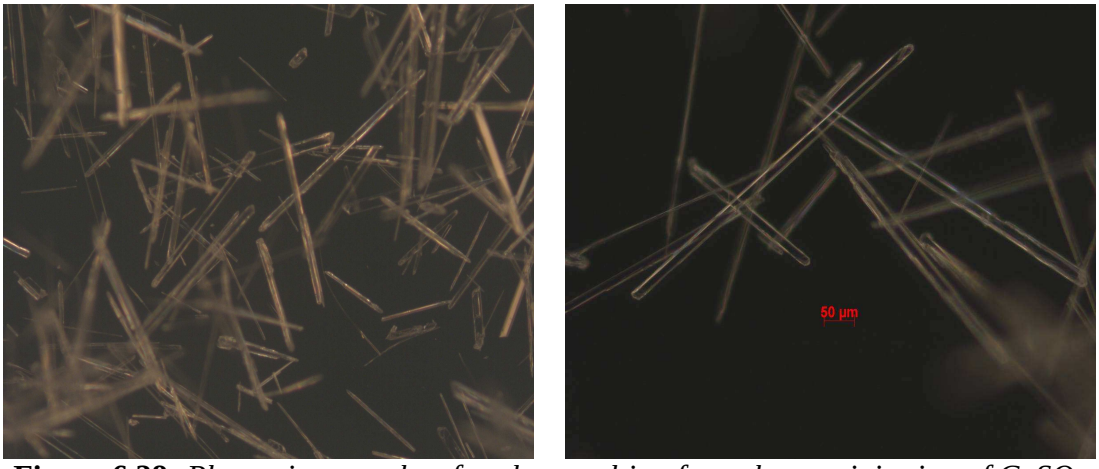

Figure 6.38: *Photomicrographs of scales resulting from the precipitation of $CaSO_4$ at 0.35 M salinity (0.047M Ca^{2+} and 0.047M SO_4^{2-}); magnifications 10x and 20x.*

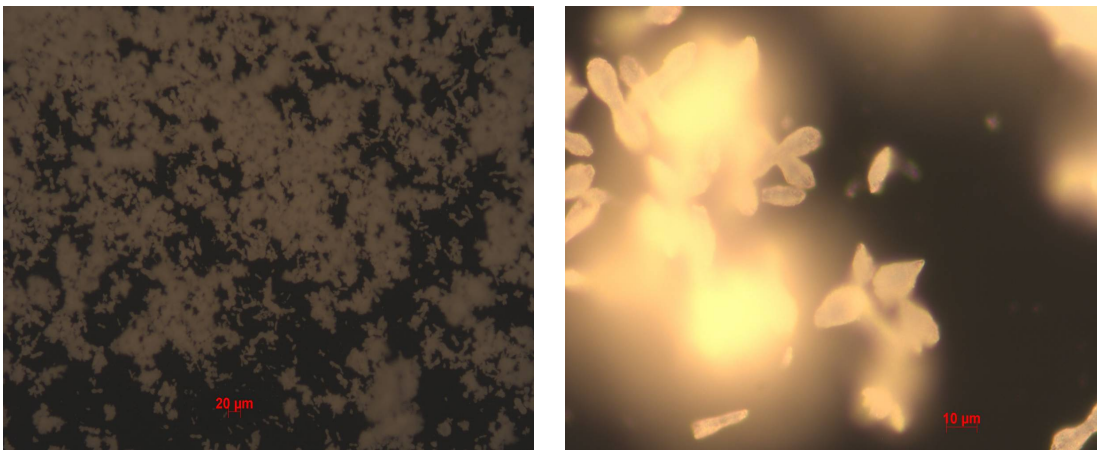

Figure 6.39: *Photomicrographs of scales resulting from the precipitation of mixed $SrSO_4$ and $CaSO_4$ at 0.35 M salinity (0.02M Sr^{2+}, 0.047M Ca^{2+} and 0.047M SO_4^{2-}); magnifications 5x and 50x.*

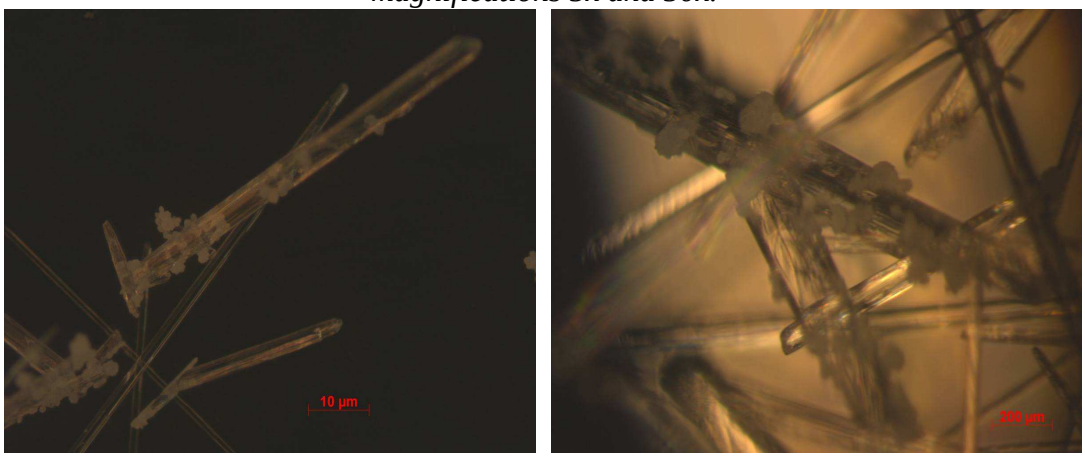

Figure 6.40: *Photomicrographs of scales resulting from the precipitation of mixed $SrSO_4$ and $CaSO_4$ at 0.35 M salinity (0.005M Sr^{2+}, 0.047M Ca^{2+} and 0.047M SO_4^{2-}); magnifications 20x and 50x respectively.*

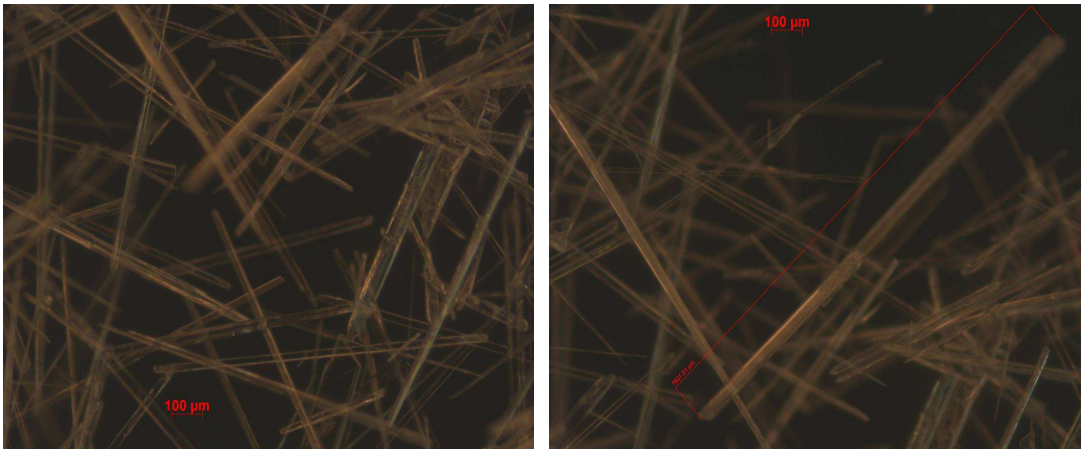

Figure 6.41: *Photomicrographs of scales resulting from the precipitation of $CaSO_4$ in the presence of DO at 0.35 M salinity (0.047M Ca^{2+} and 0.047M SO_4^{2-}); magnifications 10x for both photos.*

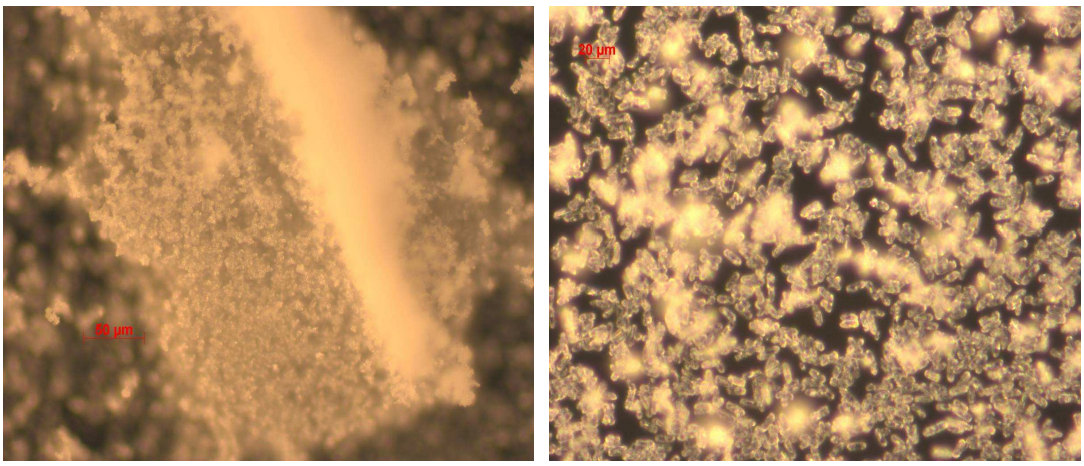

Figure 6.42: *Photomicrographs of scales resulting from the precipitation of mixed $SrSO_4$ and $CaSO_4$ in the presence of DO at 0.35 M salinity (0.02M Sr^{2+}, 0.047M Ca^{2+} and 0.047M SO_4^{2-}); magnifications 10x and 20x.*

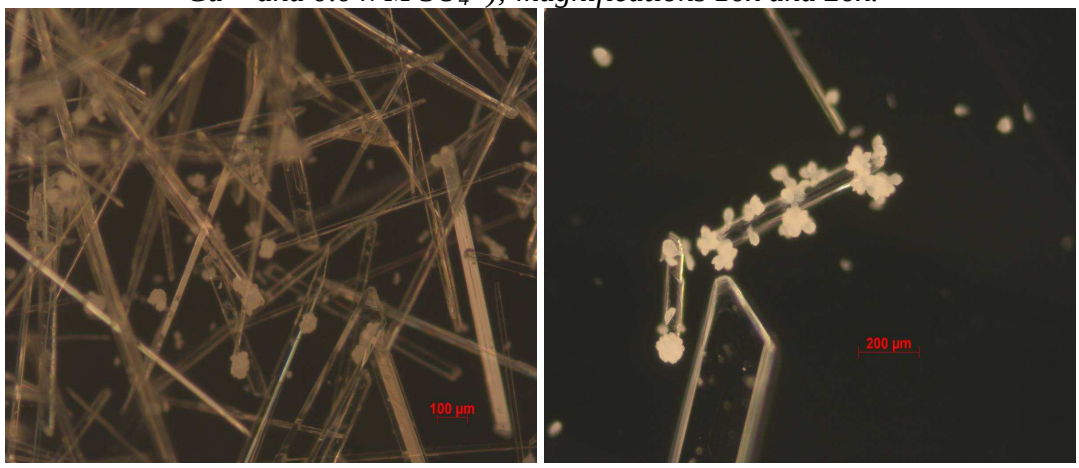

Figure 6.43: *Photomicrographs of scales resulting from the precipitation of mixed $SrSO_4$ and $CaSO_4$ in presence of DO at 0.35 M salinity (0.005M Sr^{2+}, 0.047M Ca^{2+} and 0.047M SO_4^{2-}); magnifications 10x and 20x.*

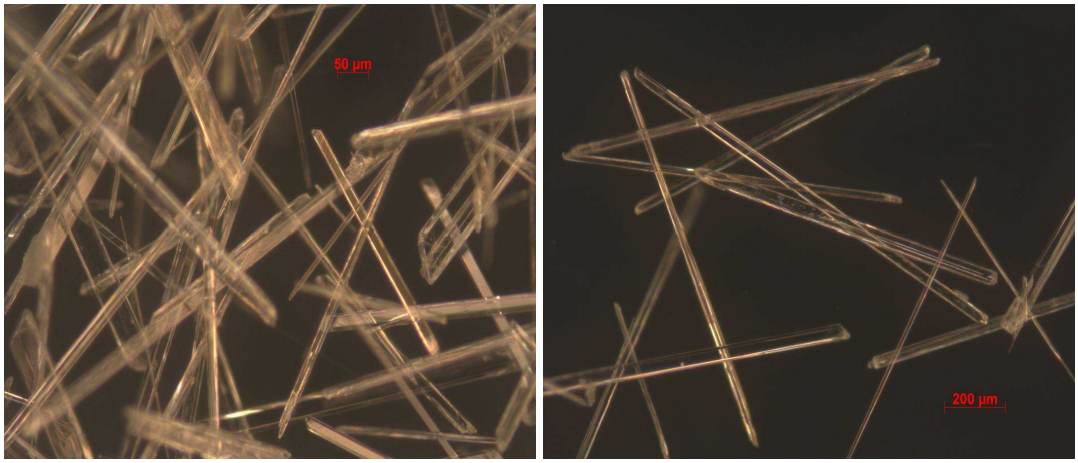

Figure 6.44: *Photomicrographs of scales resulting from the precipitation of $CaSO_4$ at 0.5 M salinity (0.047M Ca^{2+} and 0.047M SO_4^{2-}); magnifications 10x and 20x.*

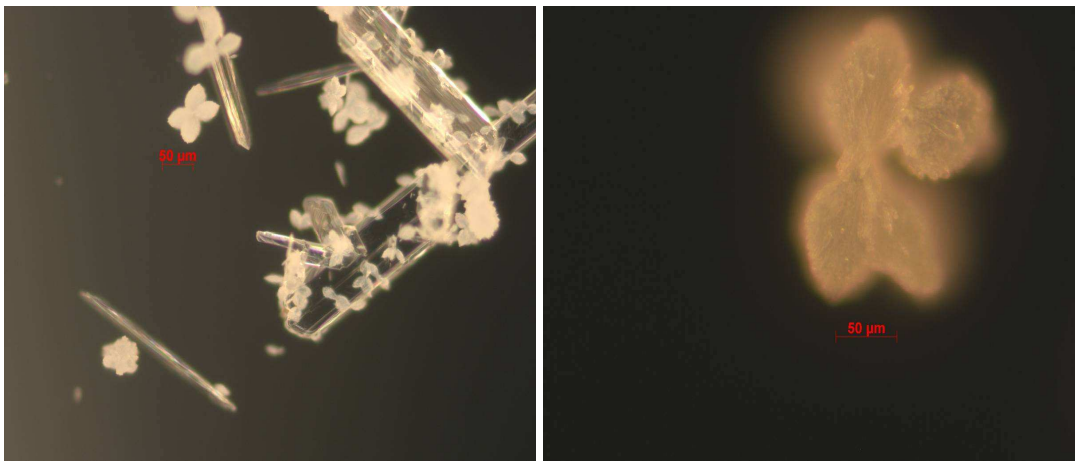

Figure 6.45: *Photomicrographs of scales resulting from the precipitation of mixed $SrSO_4$ and $CaSO_4$ at 0.5 M salinity (0.005M Sr^{2+}, 0.047M Ca^{2+} and 0.047M SO_4^{2-}); magnifications 20x and 50x*

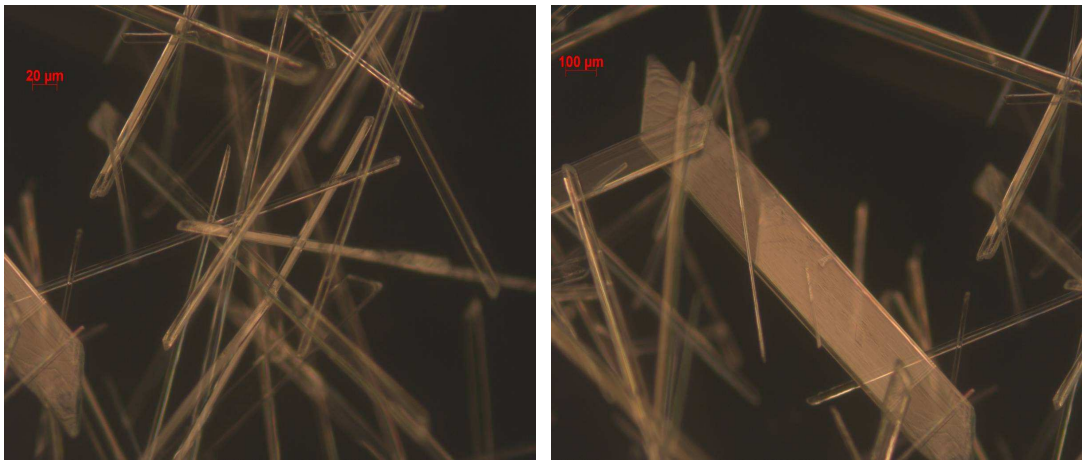

Figure 6.46: *Photomicrographs of scales resulting from the precipitation of $CaSO_4$ in the presence of DO at 0.5 M salinity (0.047M Ca^{2+} and 0.047M SO_4^{2-}); magnifications 10x and 20x.*

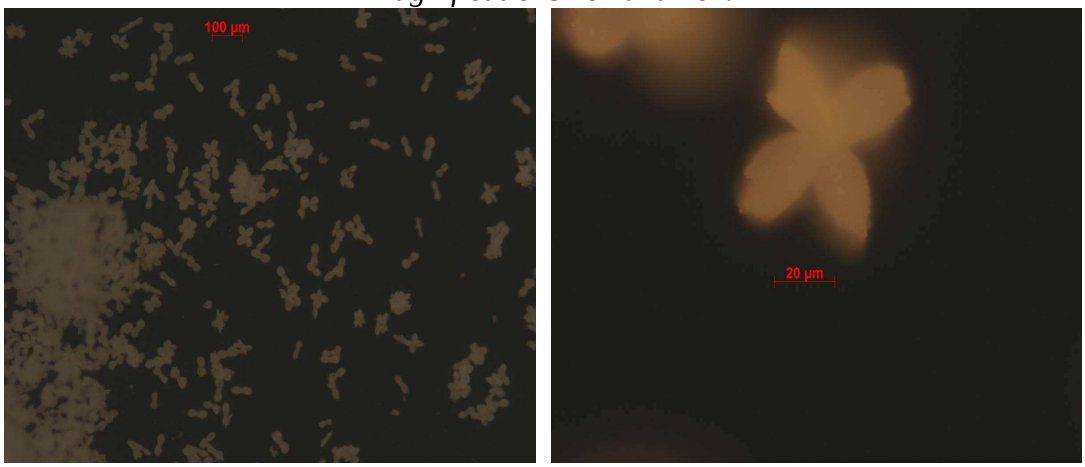

Figure 6.47: *Photomicrographs of scales resulting from the precipitation of mixed $SrSO_4$ and $CaSO_4$ at 0.5 M in the presence of DO at 0.5 M salinity (0.02M Sr^{2+}, 0.047M Ca^{2+} and 0.047M SO_4^{2-}); magnifications 5x and 50x.*

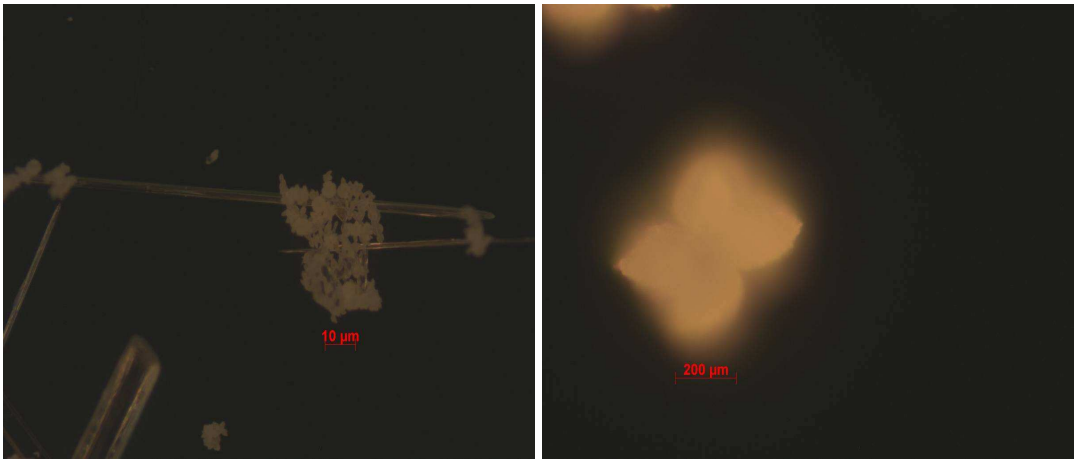

Figure 6.48: *Photomicrographs of scales resulting from the precipitation of mixed $SrSO_4$ and $CaSO_4$ at 0.5 M in the presence of DO at 0.5 M salinity (0.005M Sr^{2+}, 0.047M Ca^{2+} and 0.047M SO_4^{2-}); magnifications 10x and 50x.*

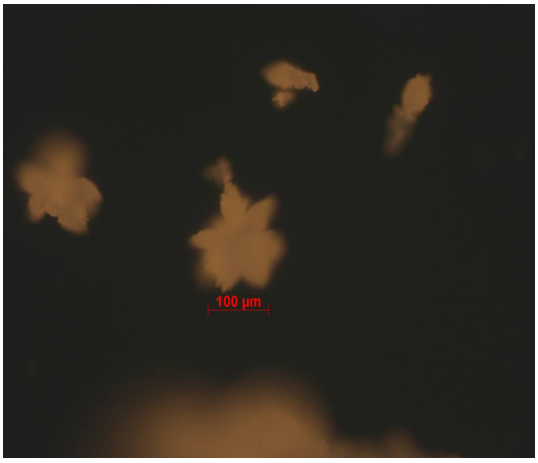

Figure 6.49: P*hotomicrographs of scales resulting from the precipitation of mixed $SrSO_4$ and $CaSO_4$ at 1.5 M salinity (0.02M Sr^{2+}, 0.047M Ca^{2+} and 0.047M SO_4^{2-}); magnifications 100x.*

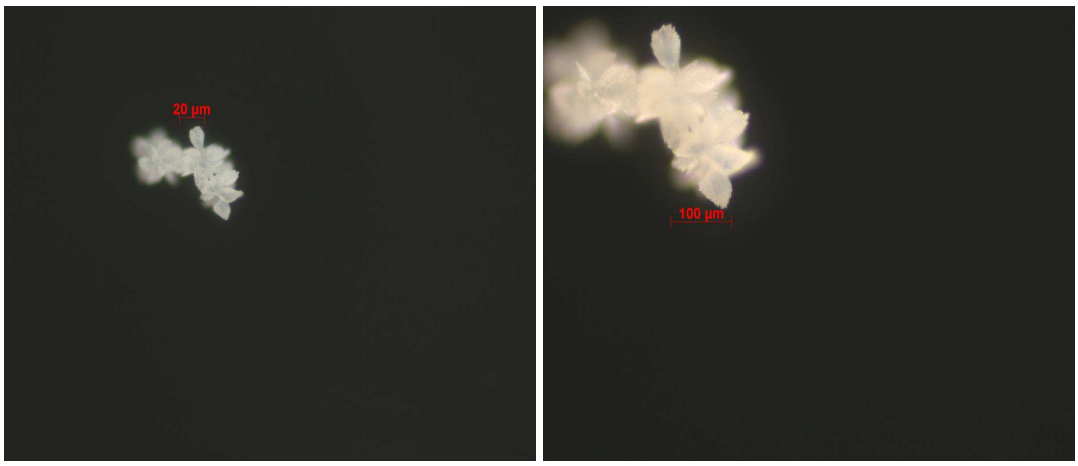

Figure 6.50: *Photomicrographs of scales resulting from the precipitation of mixed $SrSO_4$ and $CaSO_4$ at 1.5 M salinity (0.005M Sr^{2+}, 0.047M Ca^{2+} and 0.047M SO_4^{2-}); magnifications 20x, and 50x.*

Figure 6.51: *Photomicrographs of scales resulting from the precipitation of mixed $SrSO_4$ and $CaSO_4$ in the presence of DO at 1.5 M salinity (0.02M Sr^{2+}, 0.047M Ca^{2+} and 0.047M SO_4^{2-}); magnifications 10x and 20x.*

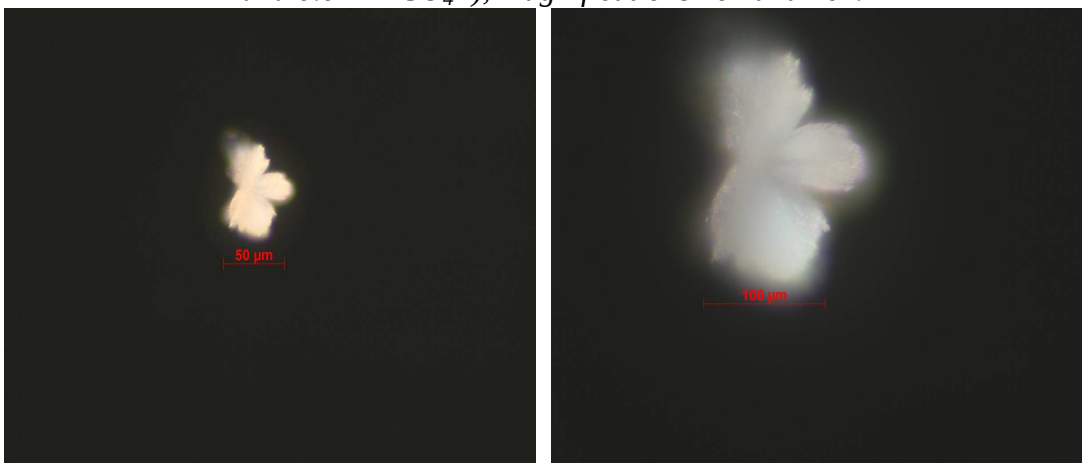

Figure 6.52: *Photomicrographs of scales resulting from the precipitation of mixed $SrSO_4$ and $CaSO_4$ in the presence of DO at 1.5 M salinity (0.005M Sr^{2+}, 0.047M Ca^{2+} and 0.047M SO_4^{2-}); magnifications 20x, and 50x.*

6.5.2 SEM analysis

Figures 6.53-6.69 show the SEM images for the precipitates resulting from the precipitation of pure $CaSO_4$, pure $SrSO_4$, and mixed $CaSO_4$ and $SrSO_4$ with and without the presence of DO at different salinity levels.

In pure $CaSO_4$ crystallization it is observed from Figs. 6.53 and 6.61 that the $CaSO_4$ crystals have a needle shape which is a typical gypsum structure [62]. Increased salinity affects the crystal size as can be observed from the comparison between Fig. 6.53 at 0.35M salinity and Fig. 6.61 at 0.5M salinity. An increase of salinity up to 1.5M almost eliminates the precipitation of $CaSO_4$ and thus no precipitate has been collected. The presence of DO also affects the crystal size which is shown by comparison of Fig. 6.53 and Fig. 6.57 at 0.35M salinity and of Fig. 6.61 and Fig. 6.63 at 0.5M salinity. These observations support the results of the thermodynamic and kinetic analyses which have been discussed in detail in sections 6.4 and 6.5.

In mixed $CaSO_4$ and $SrSO_4$ precipitation, it has been observed from Figs. 6.55, 6.64 and 6.66 that at high initial Sr^{2+} concentration, $SrSO_4$ was the only precipitate observed at 0.35M, 0.5M, and 1.5M salinity levels. At low initial Sr^{2+} concentration there is clear evidence of the presence of both $CaSO_4$ crystals and $SrSO_4$ crystals at 0.35M and 0.5M salinity as can be seen in Figs. 6.56, 6.60, 6.62, and 6.65. However, Figs. 6.67 and 6.69 show no evidence of $CaSO_4$ at high salinity (1.5M), which supports the hypothesis that salinity has more effect on $CaSO_4$ than $SrSO_4$. Nevertheless, increased salinity affects the size and the shape of the $SrSO_4$ precipitate as can be observed from the comparison between Figs. 6.54, 6.55, 6.62, 6.64, 6.66, and 6.67.

Interestingly, the co-precipitation of $CaSO_4$ and $SrSO_4$ altered the shape and the size of the $SrSO_4$ precipitate as can be seen from figs. 6.54 and 6.56 and has less influence on the $CaSO_4$ precipitate. In figs. 6.56, 6.60, 6.62, 6.65, and 6.68 an interaction can be observed between the $CaSO_4$ precipitate and $SrSO_4$ precipitate, so it can be suggested that in mixed $CaSO_4$ and $SrSO_4$ precipitation the presence of

$CaSO_4$ crystals and $SrSO_4$ crystal act as seed and therefore both homogeneous and heterogeneous nucleation of $CaSO_4$ and $SrSO_4$ take place.

The effect of DO presence in the precipitate resulting from co-precipitation of $CaSO_4$ and $SrSO_4$ is the same as on pure $CaSO_4$ and $SrSO_4$ precipitates as can be observed through comparison between Figs. 6.54,6.58 and Figs. 6.56,6.60 for $SrSO_4$ and between Figs. 6.53,6.57 and Figs. 6.56,6.60 for $CaSO_4$. The presence of DO alters the size of the precipitates, which supports the hypothesis that the inhibition effect of DO is due to the coverage of active crystallisation sites. Interestingly, there was evidence of $CaSO_4$ crystals in Fig. 6.68 where DO is present at high salinity (1.5 M). This means that the high salinity does not totally eliminate the $CaSO_4$ precipitation and this explains the slight decrease in Ca^{2+} concentration at high salinity observed in section 6.3.

It is worthwhile to mention that it has been observed that the presence of DO, salinity and co-precipitation affect the adhesion strength of the precipitate. DO presence decreases the adhesion strength between the precipitate, the reactor wall and the membrane surface. Salinity increases the adhesion of the precipitate at the surfaces and makes it harder to clean the deposits. The co-precipitation of $CaSO_4$ and $SrSO_4$ slightly increases the adhesion of $CaSO_4$ and decreases the adhesion of $SrSO_4$.

These combined effects of salinity, presence of DO, and co-precipitation may affect the changes in Gibbs free energy associated with the crystallisation process and thus alter the thermodynamics and the kinetics of the precipitation.

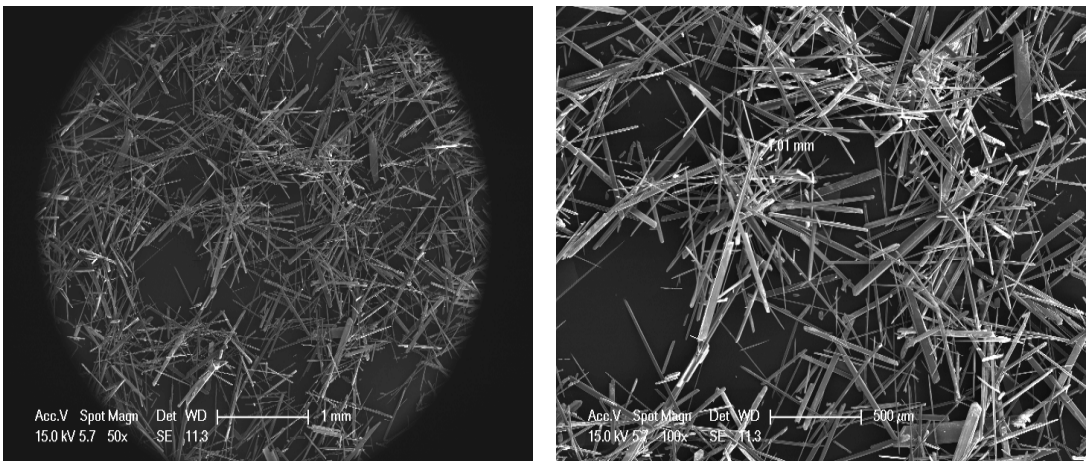

Figure 6.53: *SEM images of scales resulting from the precipitation of $CaSO_4$ (0.047M Ca^{2+} and 0.047M SO_4^{2-}) at 0.35 M salinity; magnifications 50x and 100x.*

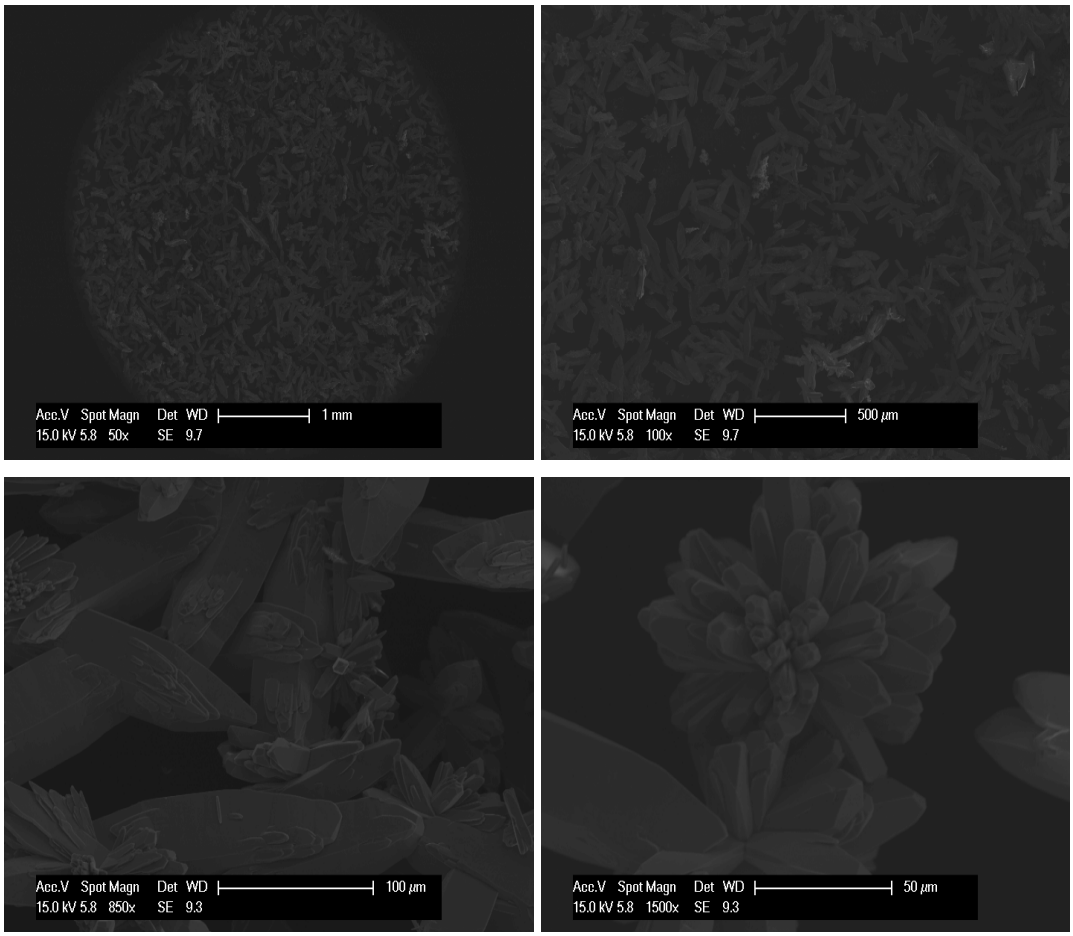

Figure 6.54: *SEM images of scales resulting from the precipitation of $SrSO_4$ (0.005M Sr^{2+} and 0.047M SO_4^{2-}) at 0.35 M salinity; magnifications 50x and 100x, 850x, and 1500x.*

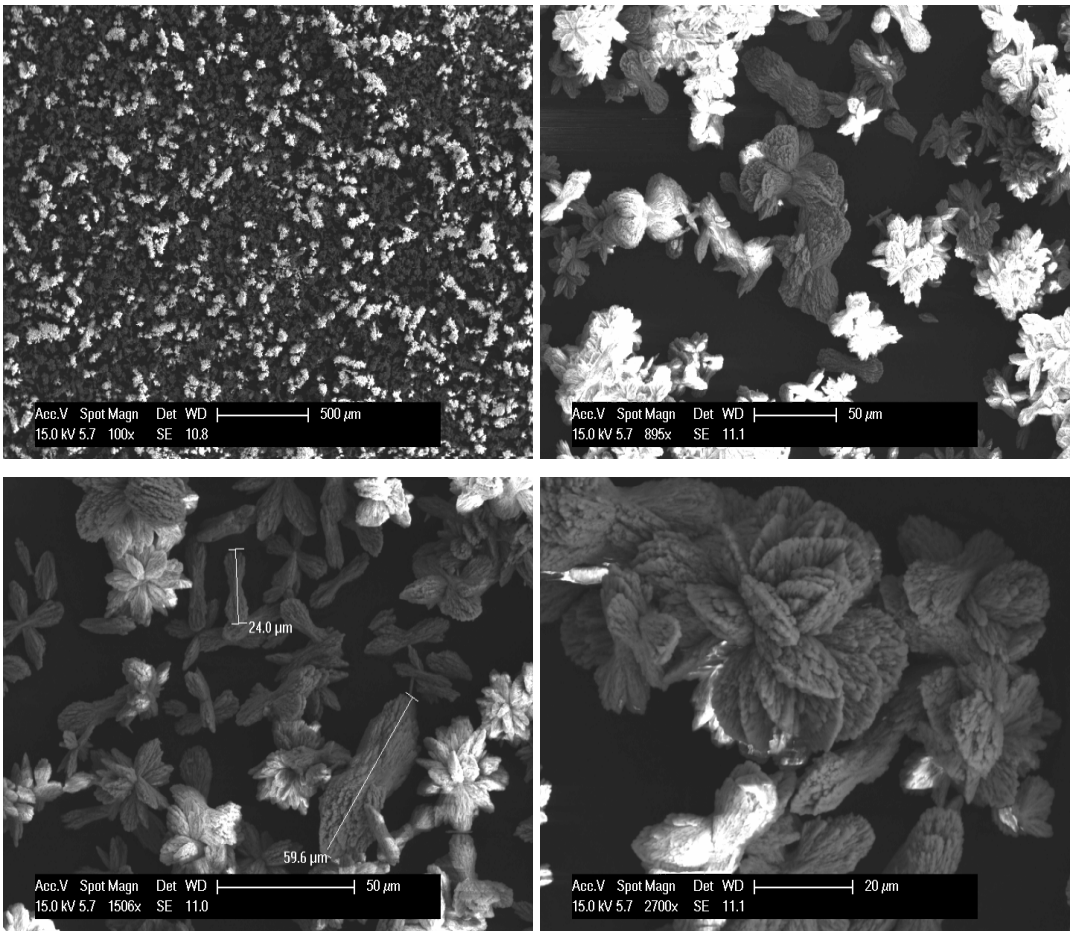

Figure 6.55: *SEM images of scales resulting from the precipitation of mixed $SrSO_4$ and $CaSO_4$ (0.02M Sr^{2+}, 0.047M Ca^{2+} and 0.047M SO_4^{2-}) at 0.35 M salinity; magnifications 100x, 850x, 1500x and 2700x.*

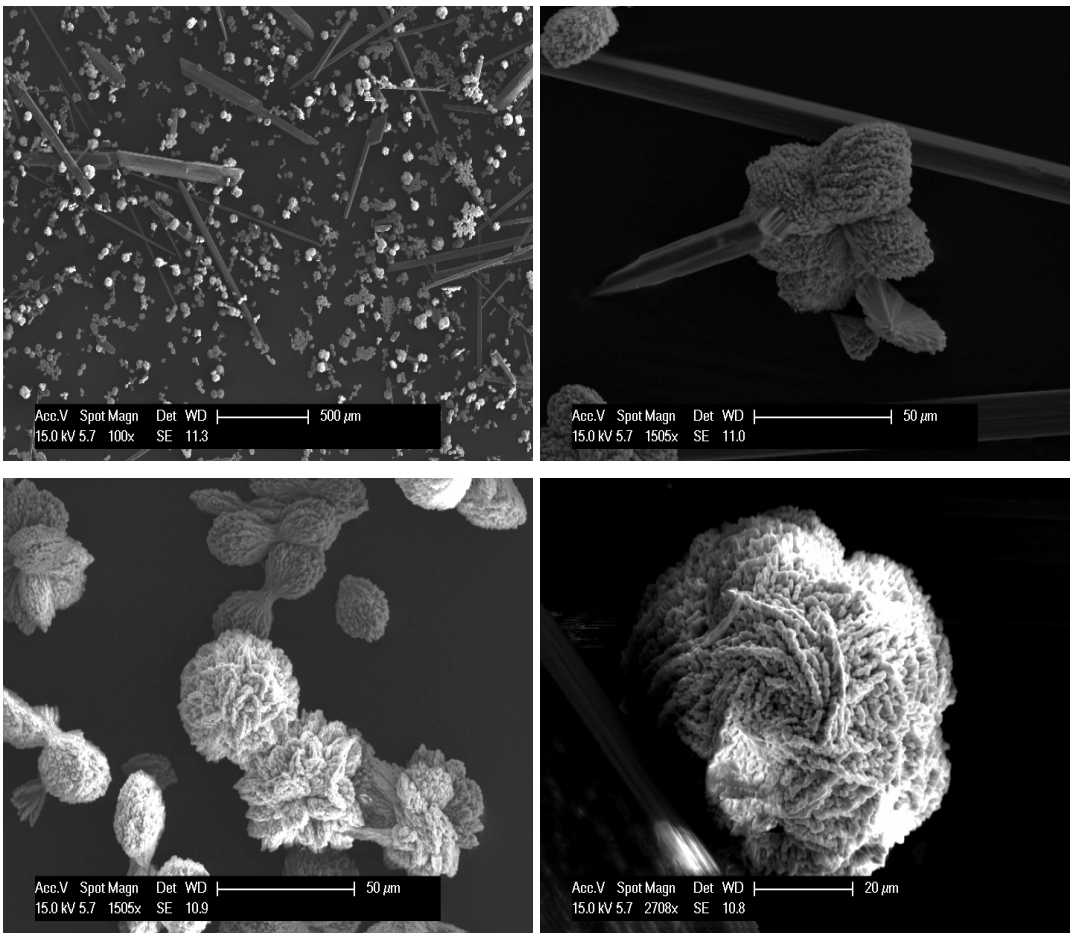

Figure 6.56: *SEM images of scales resulting from the precipitation of mixed $SrSO_4$ and $CaSO_4$ (0.005M Sr^{2+}, 0.047M Ca^{2+} and 0.047M SO_4^{2-}) at 0.35 M salinity; magnifications 100x , 1500x, 1500x and 2700x respectively.*

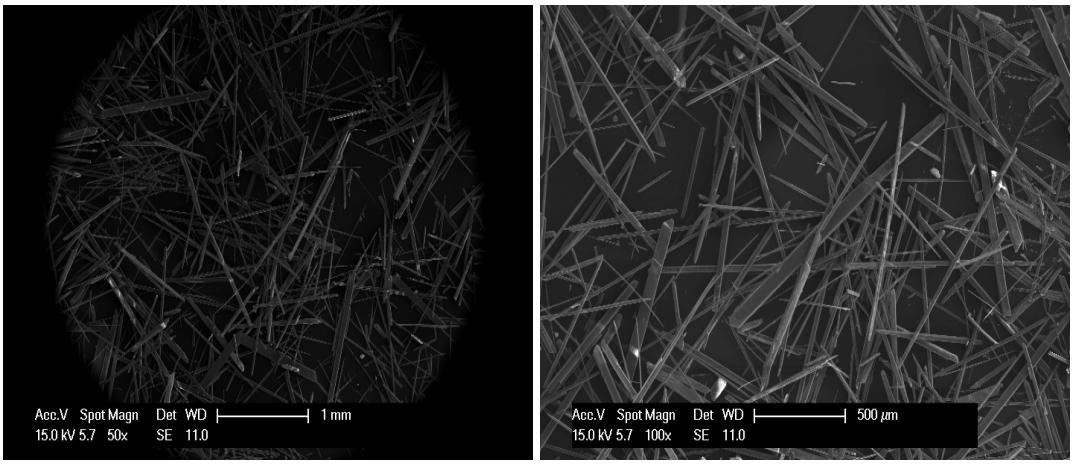

Figure 6.57: *SEM images of scales resulting from the precipitation of $CaSO_4$ (0.047M Ca^{2+} and 0.047M SO_4^{2-}) in the presence of DO at 0.35 M salinity; magnifications 50x and 100x.*

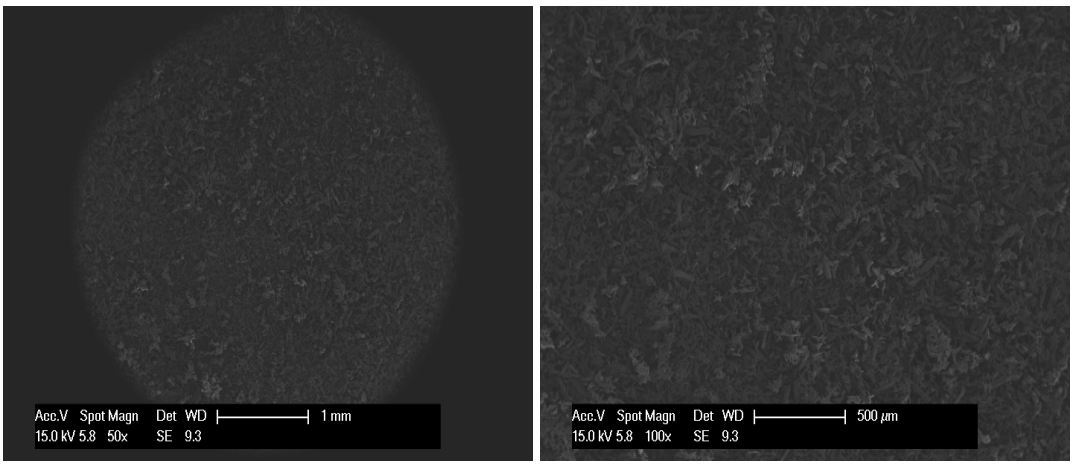

Figure 6.58: *SEM images of scales resulting from the precipitation of $SrSO_4$ (0.005M Sr^{2+} and 0.047M SO_4^{2-}) in the presence of DO at 0.35 M salinity; magnifications 50x and 100x.*

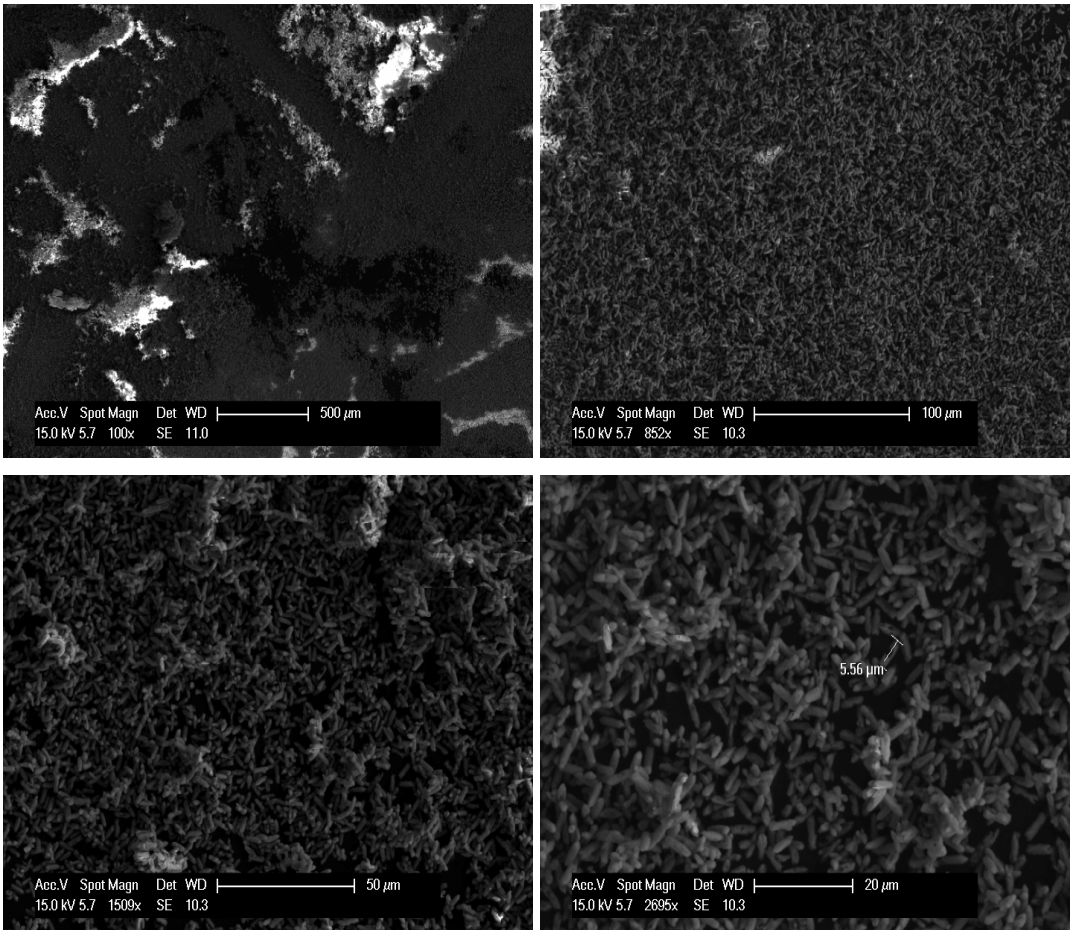

Figure 6.59: *SEM images of scales resulting from the precipitation of mixed $SrSO_4$ and $CaSO_4$ (0.02M Sr^{2+}, 0.047M Ca^{2+} and 0.047M SO_4^{2-}) in the presence of DO at 0.35 M salinity; magnifications 100x, 850x, 1500 and 2700x.*

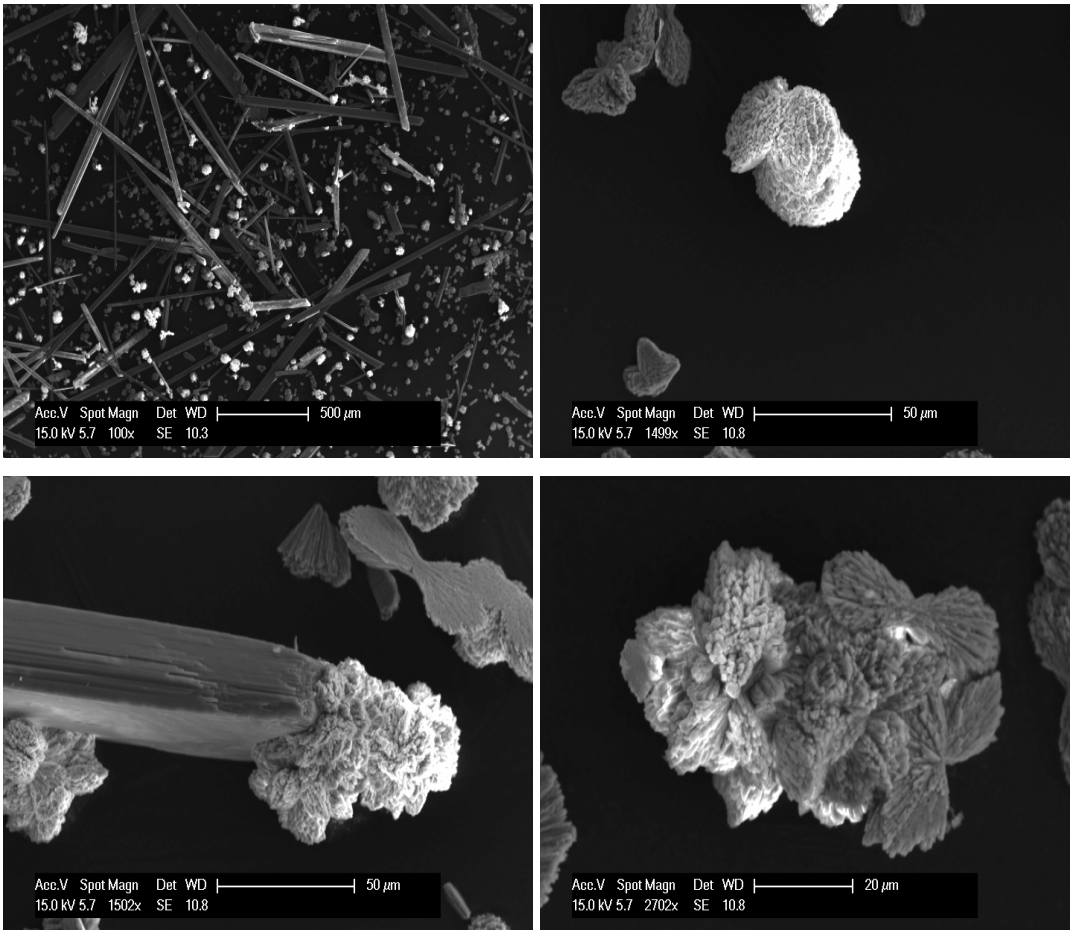

Figure 6.60: *SEM images of scales resulting from the precipitation of mixed $SrSO_4$ and $CaSO_4$ (0.005M Sr^{2+}, 0.047M Ca^{2+} and 0.047M SO_4^{2-}) in the presence of DO at 0.35 M salinity; magnifications 100x, 1500x, 1500x and 2700x.*

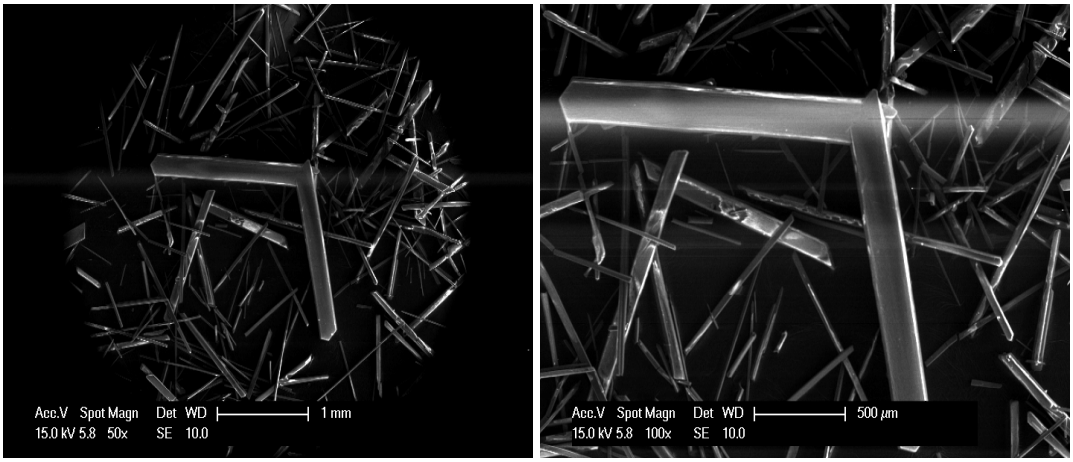

Figure 6.61: *SEM images of scales resulting from the precipitation of $CaSO_4$ (0.047M Ca^{2+} and 0.047M SO_4^{2-}) at 0.5 M salinity; magnifications 50x and 100x*

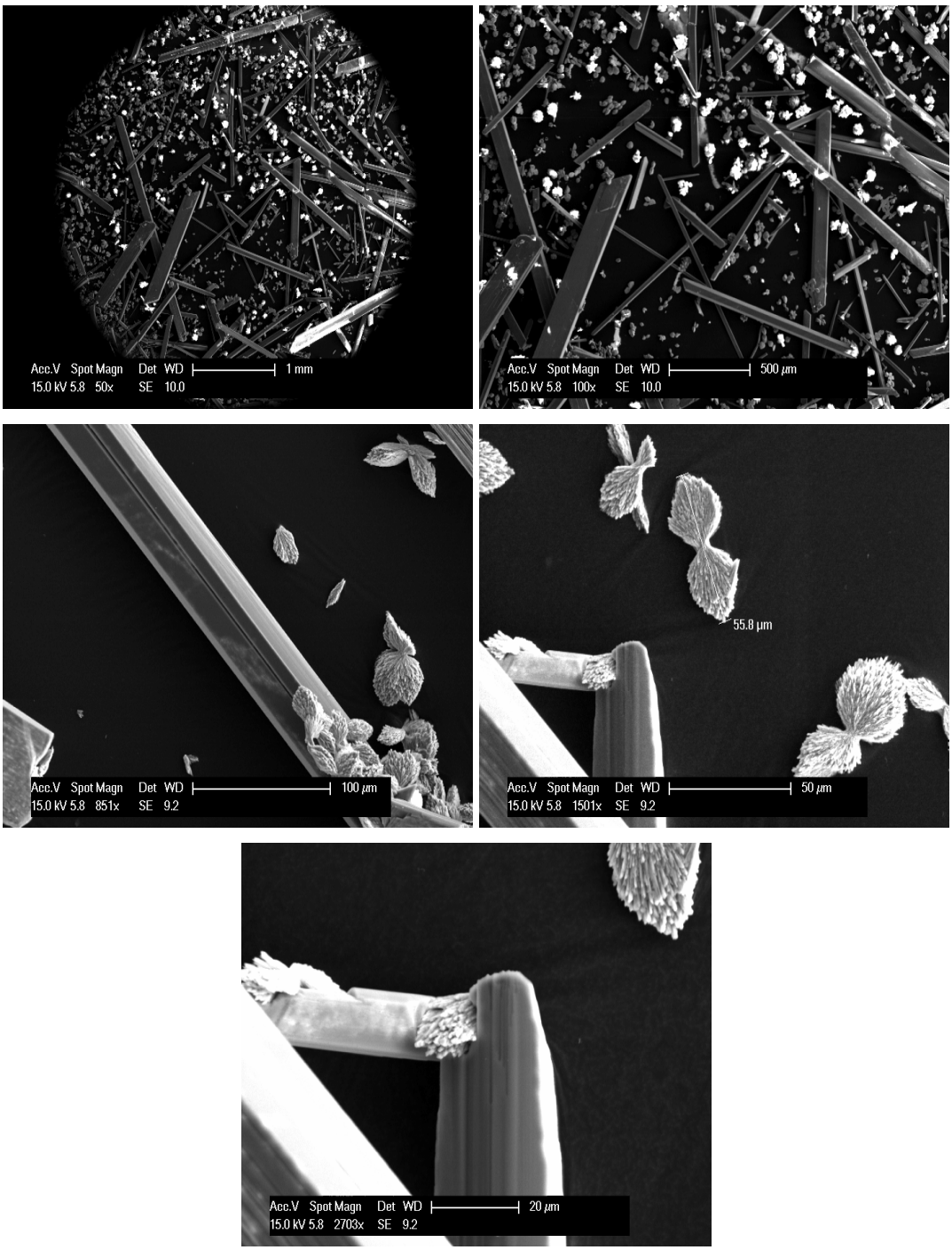

Figure 6.62: *SEM images of scales resulting from the precipitation of mixed $SrSO_4$ and $CaSO_4$ (0.005M Sr^{2+}, 0.047M Ca^{2+} and 0.047M SO_4^{2-}) at 0.5 M salinity; magnifications 50x, 100x, 850x, 1500x and 2700x.*

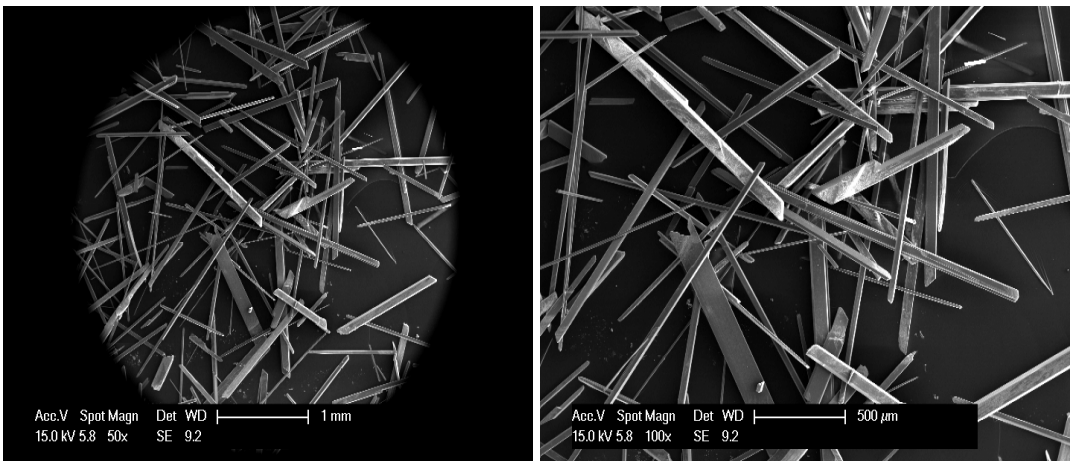

Figure 6.63: *SEM images of scales resulting from the precipitation of $CaSO_4$ and DO presence (0.047M Ca^{2+} and 0.047M SO_4^{2-}) at 0.5 M salinity; magnifications 50x and 100x.*

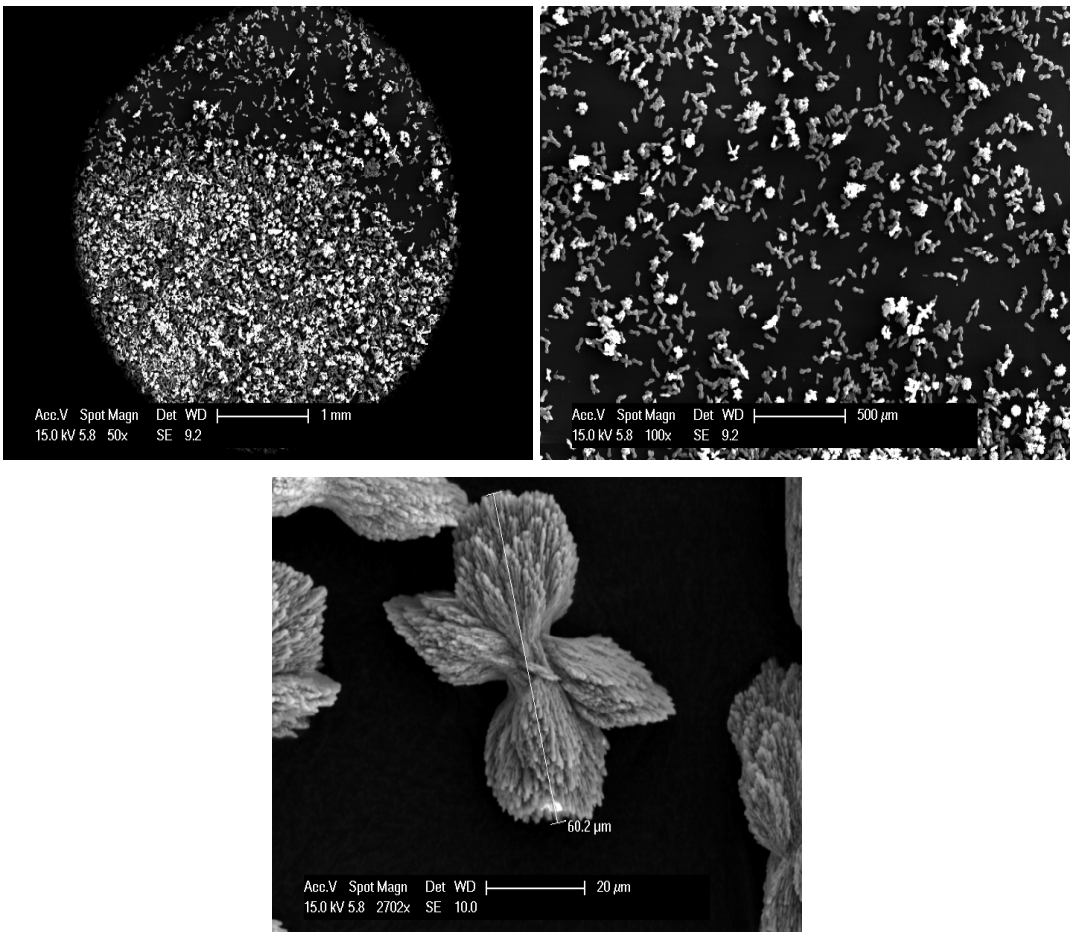

Figure 6.64: *SEM images of scales resulting from the precipitation of mixed $SrSO_4$ and $CaSO_4$ (0.02M Sr^{2+}, 0.047M Ca^{2+} and 0.047M SO_4^{2-}) in the presence of DO at 0.5 M salinity; magnifications 50x, 100x and 2700x.*

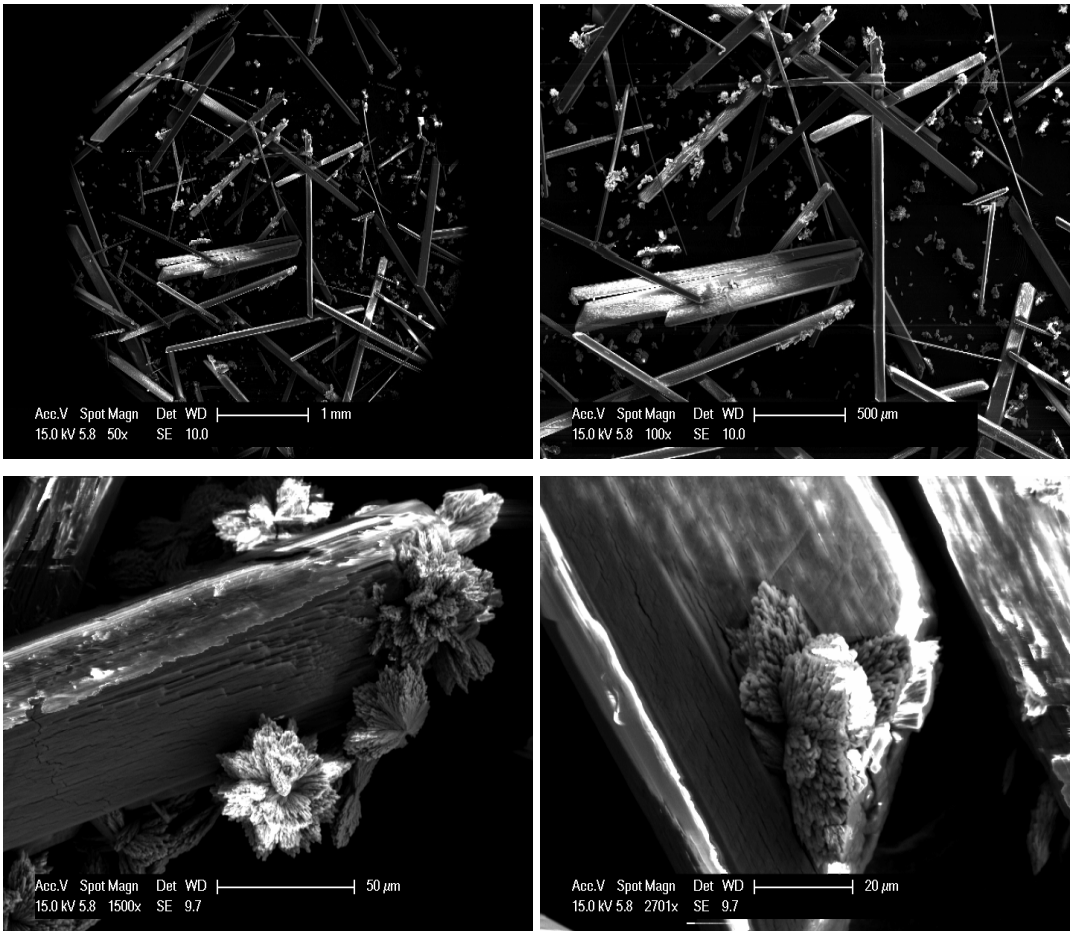

Figure 6.65: *SEM images of scales resulting from the precipitation of mixed $SrSO_4$ and $CaSO_4$ (0.005M Sr^{2+}, 0.047M Ca^{2+} and 0.047M SO_4^{2-}) in the presence of DO at 0.5 M salinity; magnifications 50x, 100x, 1500x and 2700x.*

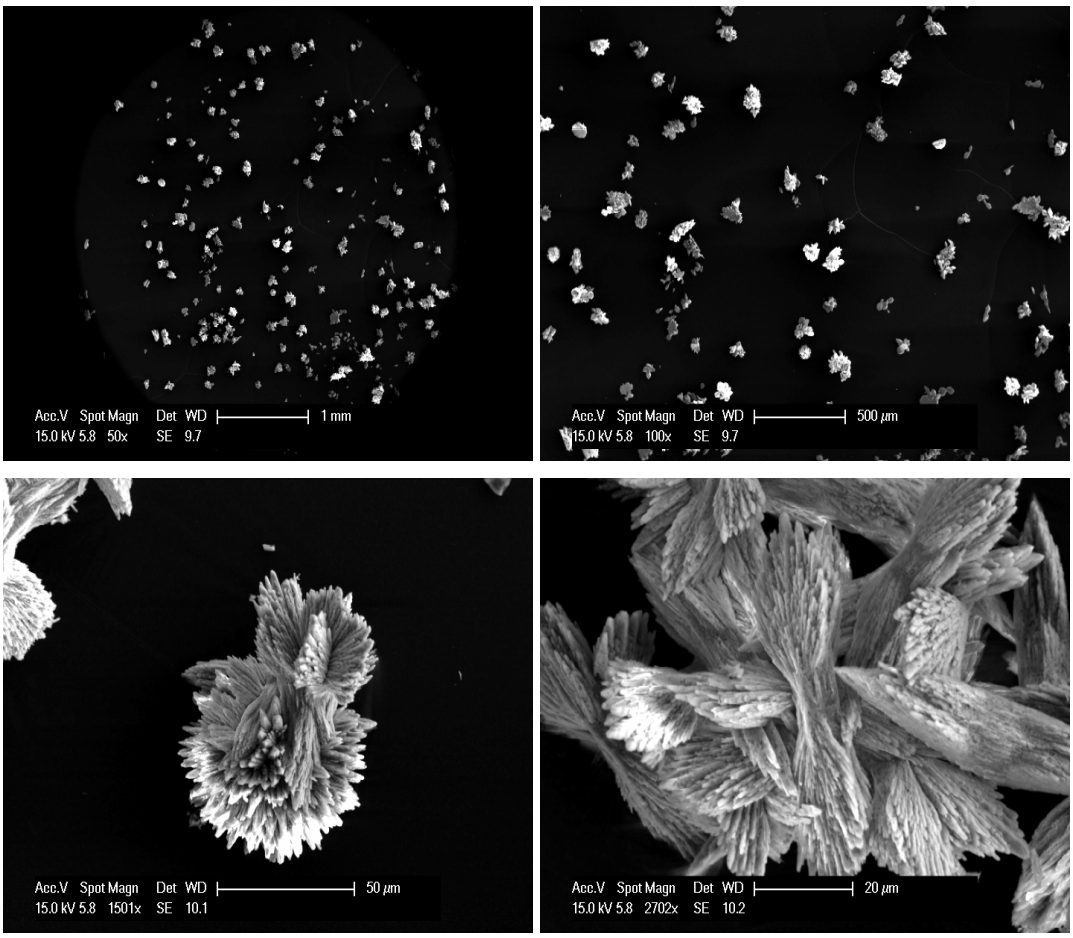

Figure 6.66: *SEM images of scales resulting from the precipitation of $SrSO_4$ and $CaSO_4$ (0.02M Sr^{2+}, 0.047M Ca^{2+} and 0.047M SO_4^{2-}) at 1.5 M salinity; magnifications 50x, 100x, 1500x, and 2700x.*

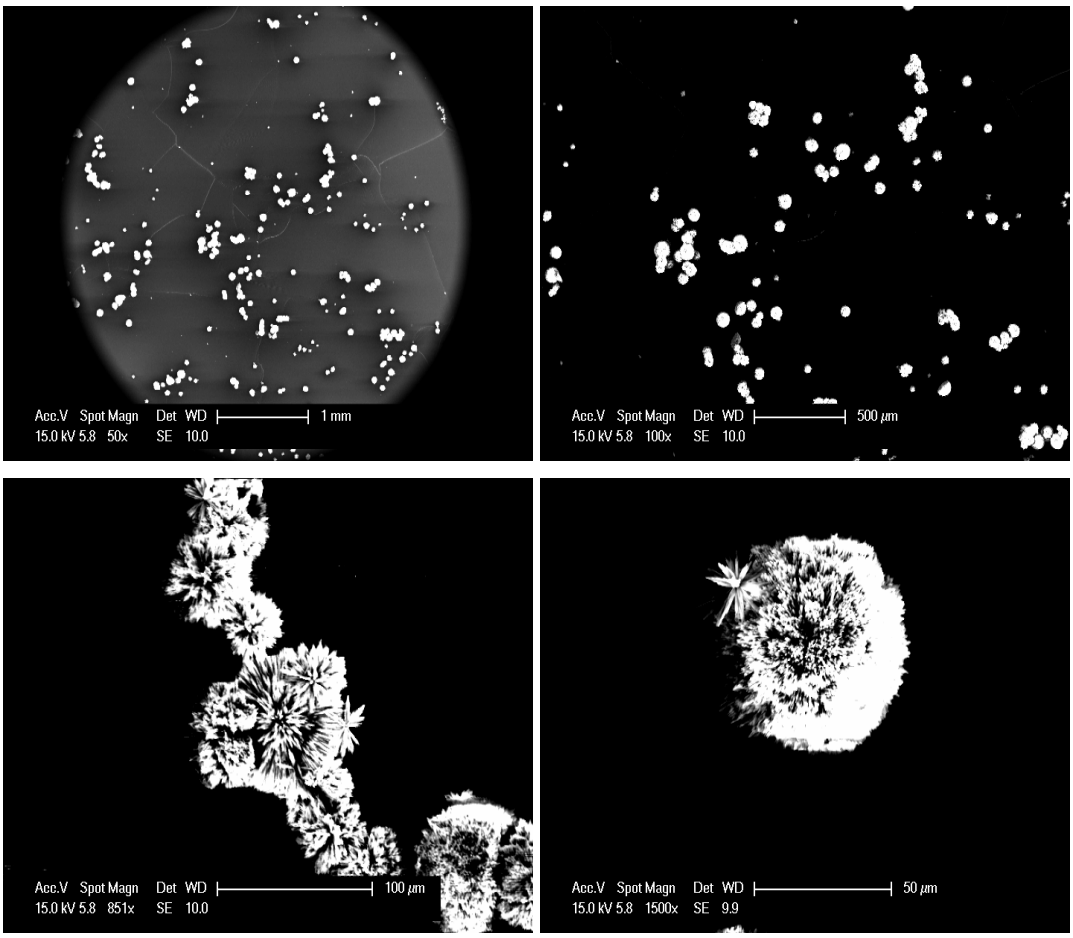

Figure 6.67: *SEM images of scales resulting from the precipitation of $SrSO_4$ and $CaSO_4$ at (0.005M Sr^{2+}, 0.047M Ca^{2+} and 0.047M SO_4^{2-}) 1.5 M salinity; magnifications 50x, 100x, 850x and 1500x.*

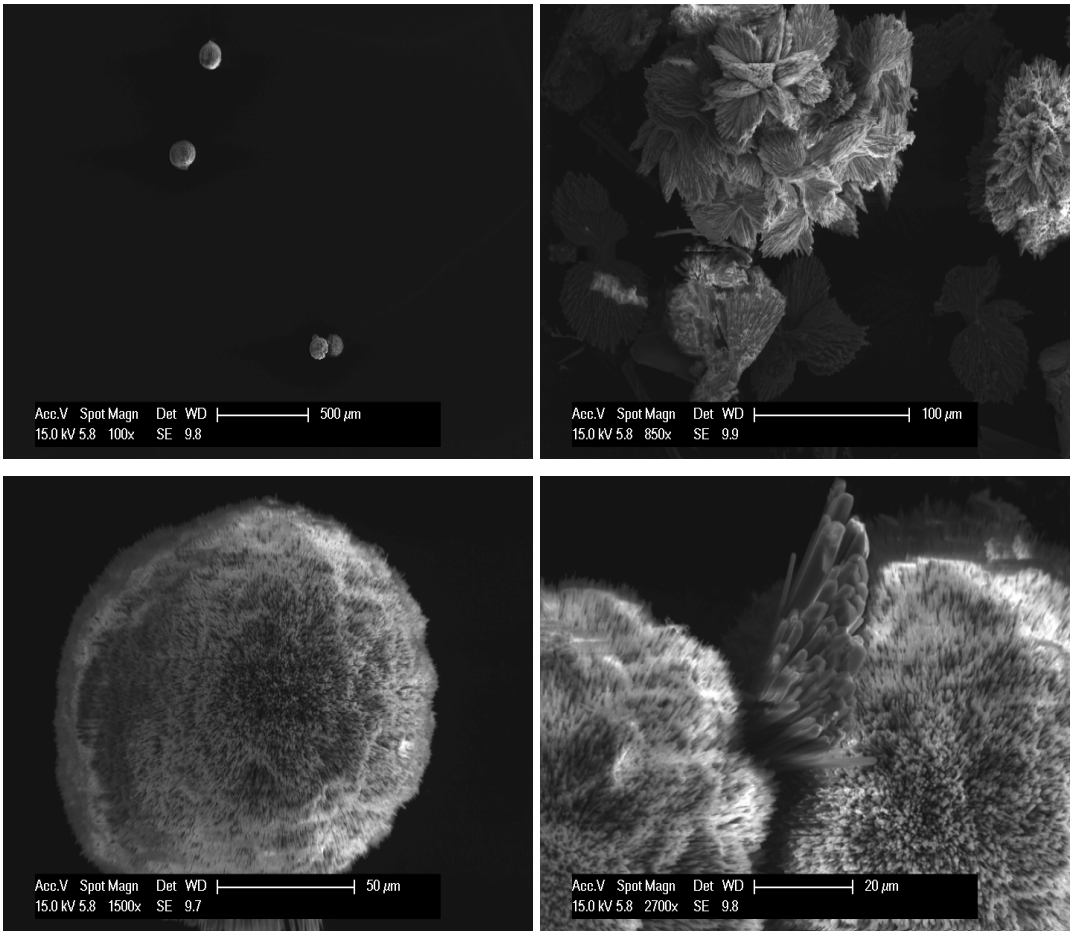

Figure 6.68: *SEM images of scales resulting from the precipitation of mixed $SrSO_4$ and $CaSO_4$ (0.02M Sr^{2+}, 0.047M Ca^{2+} and 0.047M SO_4^{2-}) in the presence of DO at 1.5 M salinity; magnifications 100x, 850x, 1500x and 2700x.*

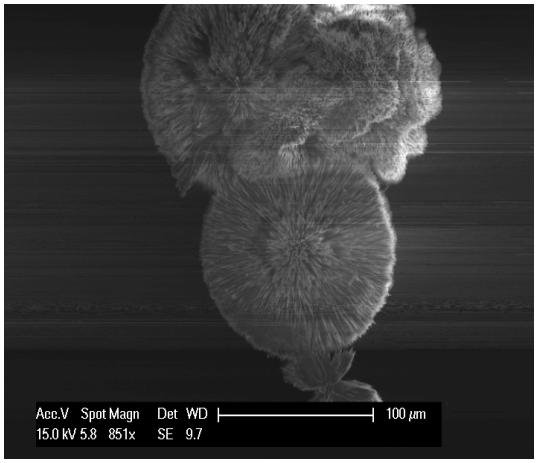

Figure 6.69: *SEM images of scales resulting from the precipitation of $SrSO_4$ and $CaSO_4$ (0.05M Sr^{2+}, 0.047M Ca^{2+} and 0.047M SO_4^{2-}) in the presence of DO at 1.5 M salinity; magnifications 850x.*

6.5.3 EDS analysis

EDS analysis has been carried out in order to investigate the composition of the precipitates. Figs. 6.70, 6.73, 6.76, and 6.78 show the composition of the precipitate resulting from pure $CaSO_4$ precipitation at different salinity level and with or without DO presence; it is clear that $CaSO_4$ is the only precipitate formed under these conditions. Figs. 6.85 and 6.86 show that only $SrSO_4$ precipitate has been formed during the precipitation of pure $SrSO_4$ at 0.35M salinity and with or without the presence of DO.

In case of co-precipitation at low initial Sr^{2+} concentration both $CaSO_4$ and $SrSO_4$ crystals have been formed at 0.35M and 0.5M salinity and with or without the presence of DO as seen in Figs. 6.72, 6.75, 6.77, 6.80. However, at high salinity 1.5M there was no evidence of $CaSO_4$ precipitate. At high initial Sr^{2+} concentration was observed for $SrSO_4$ precipitate as can be seen in Figs. 6.71, 6.74, 6.79, 6.81, and 6.82. Interestingly, Fig. 6.83 shows the presence of $CaSO_4$ precipitate at high salinity level and in the presence of DO. The EDS analysis is highly affected by the position on the crystal surface of the sample analyzed but some inference can be drawn from the relative magnitude of the peaks indicating the relative quantity of the constituents [62]. Thus, it can be concluded from the EDS analysis that there is a form of interaction between the $CaSO_4$ and $SrSO_4$ during the co-precipitation of these two salts.

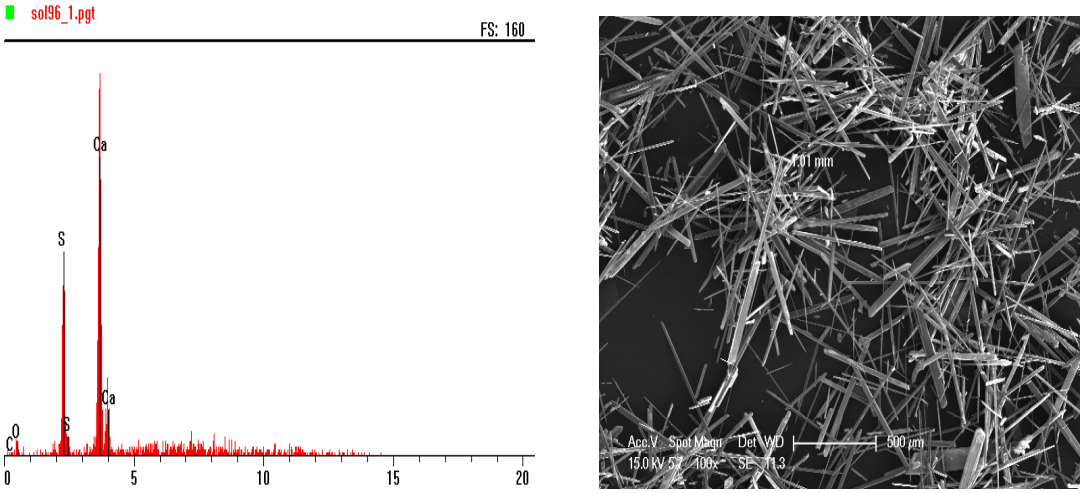

Figure 6.70: *EDS analysis for scales resulting from the precipitation $CaSO_4$ (0.047M Ca^{2+} and 0.047M SO_4^{2-}) at 0.35 M salinity.*

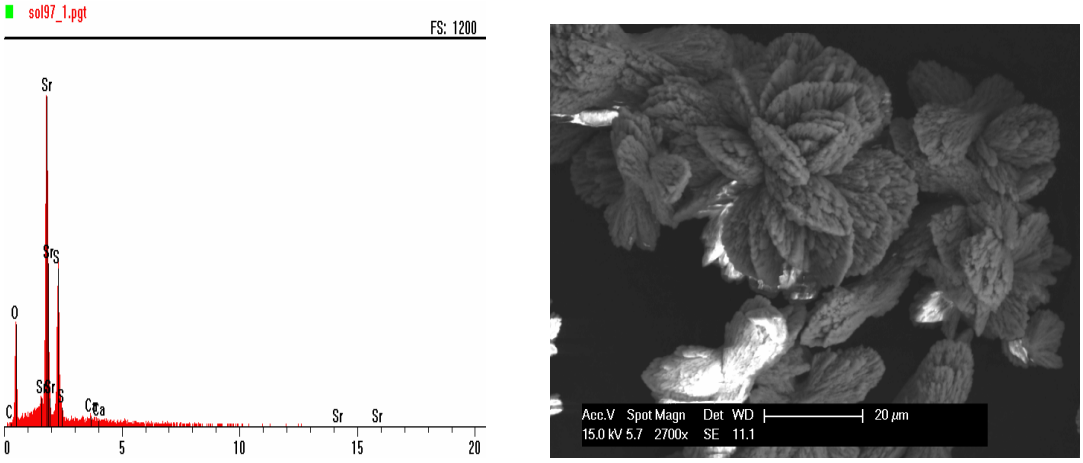

Figure 6.71: *EDS analysis for scales resulting from the precipitation of mixed $SrSO_4$ and $CaSO_4$ (0.02M Sr^{2+}, 0.047M Ca^{2+} and 0.047M SO_4^{2-}) at 0.35 M salinity.*

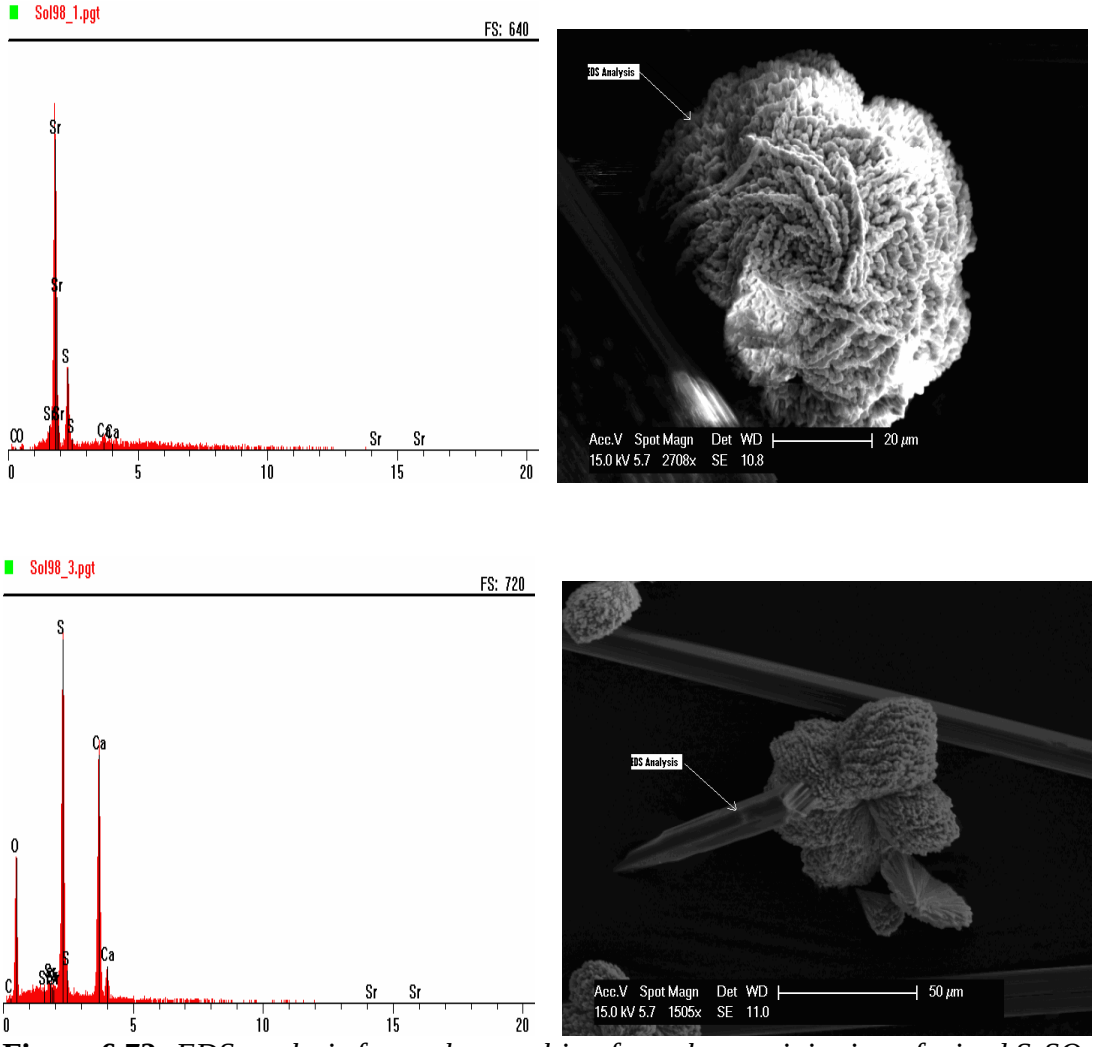

Figure 6.72: *EDS analysis for scales resulting from the precipitation of mixed $SrSO_4$ and $CaSO_4$ (0.005M Sr^{2+}, 0.047M Ca^{2+} and 0.047M SO_4^{2-}) at 0.35 M salinity.*

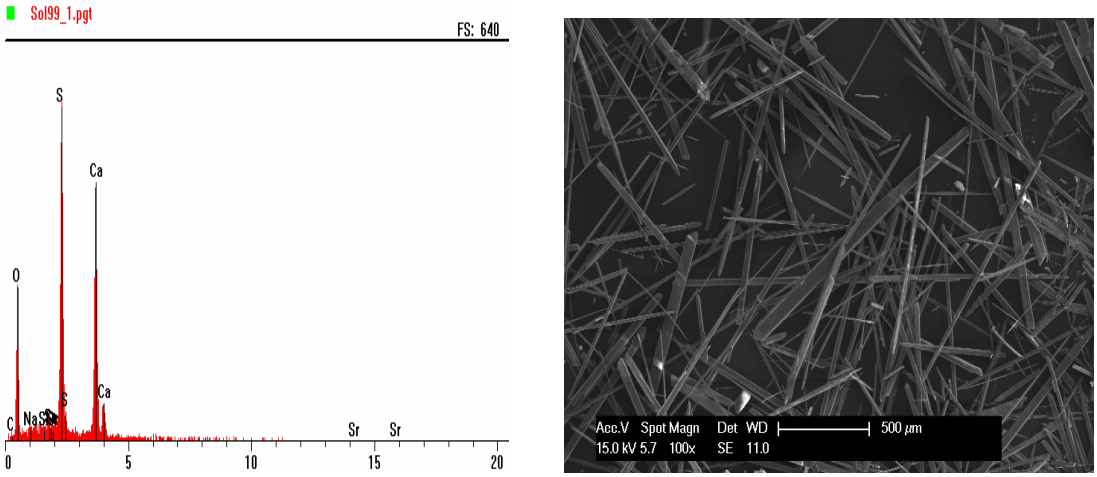

Figure 6.73: *EDS analysis for scales resulting from the precipitation of $CaSO_4$ (0.047M Ca^{2+} and 0.047M SO_4^{2-}) in the presence of DO at 0.35 M salinity.*

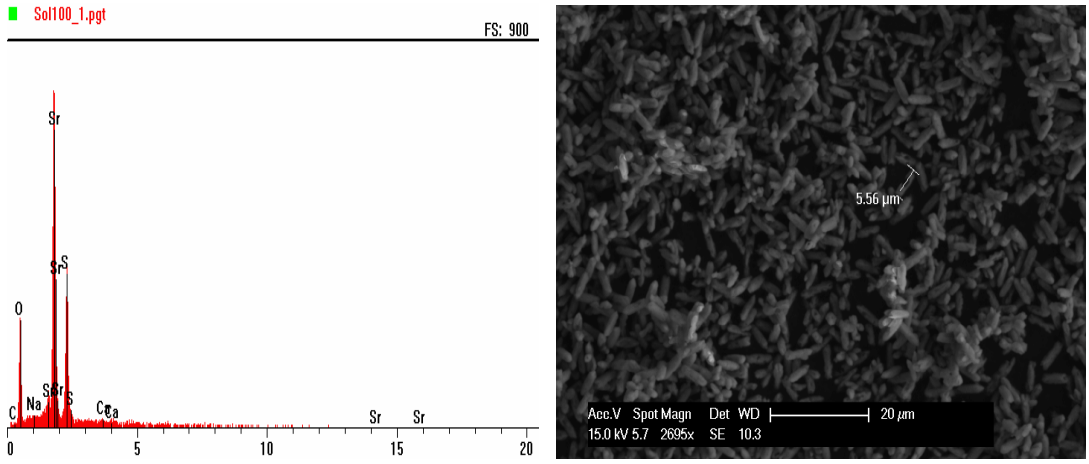

Figure 6.74: *EDS analysis for scales resulting from the precipitation of mixed $SrSO_4$ and $CaSO_4$ (0.02M Sr^{2+}, 0.047M Ca^{2+} and 0.047M SO_4^{2-}) in the presence of DO at 0.35 M salinity.*

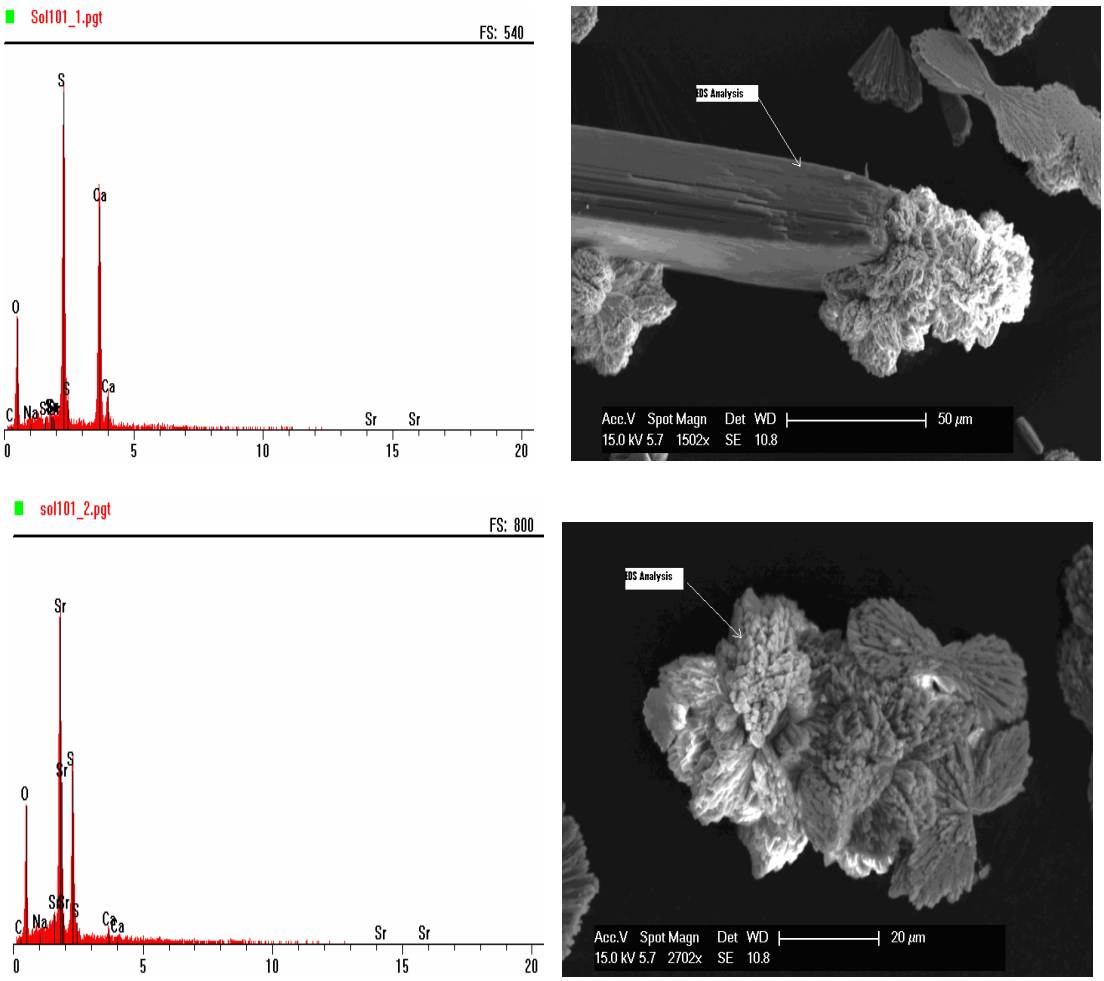

Figure 6.75: *EDS analysis for scales resulting from the precipitation of mixed $SrSO_4$ and $CaSO_4$ (0.005M Sr^{2+}, 0.047M Ca^{2+} and 0.047M SO_4^{2-}) in the presence of DO at 0.35 M salinity.*

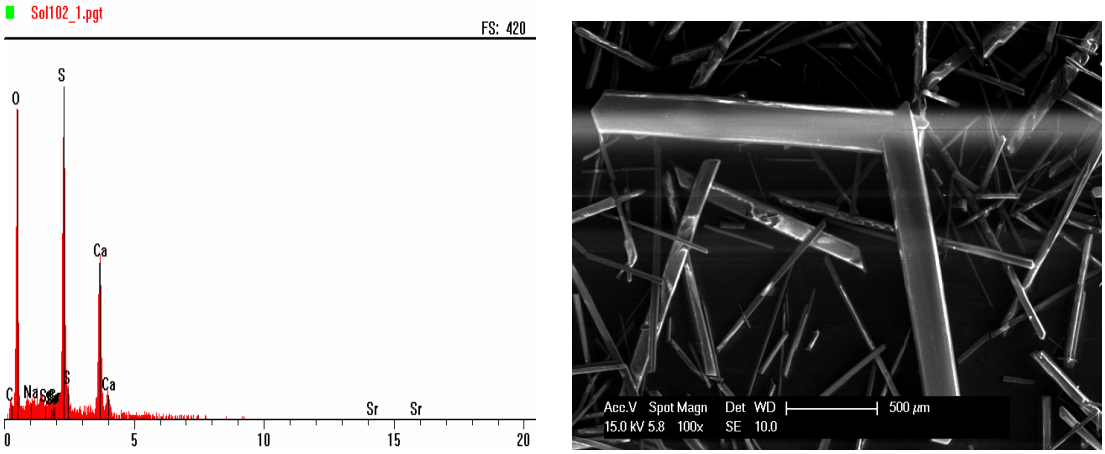

Figure 6.76: *EDS analysis for scales resulting from the precipitation of $CaSO_4$ (0.047M Ca^{2+} and 0.047M SO_4^{2-}) at 0.5 M salinity.*

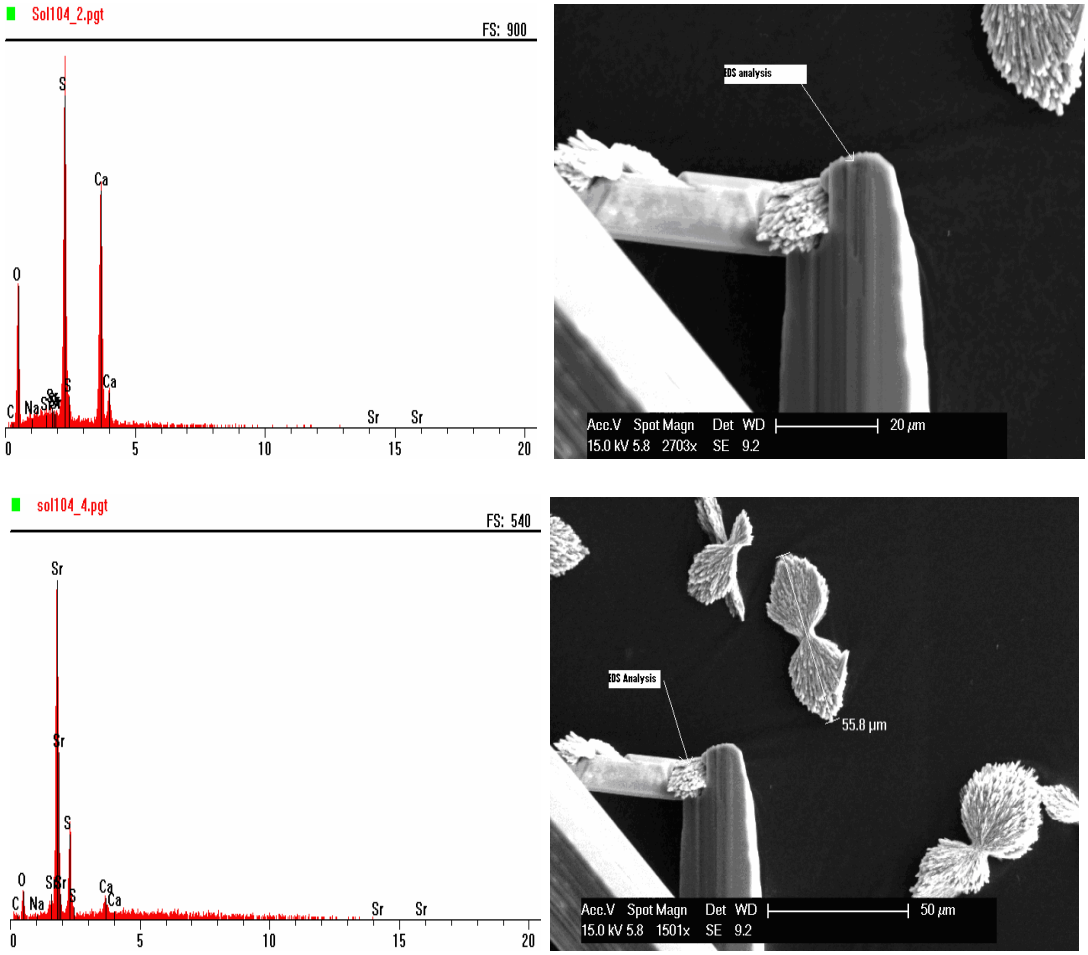

Figure 6.77: *EDS analysis for scales resulting from the precipitation of mixed $SrSO_4$ and $CaSO_4$ (0.005M Sr^{2+}, 0.047M Ca^{2+} and 0.047M SO_4^{2-}) at 0.5 M salinity.*

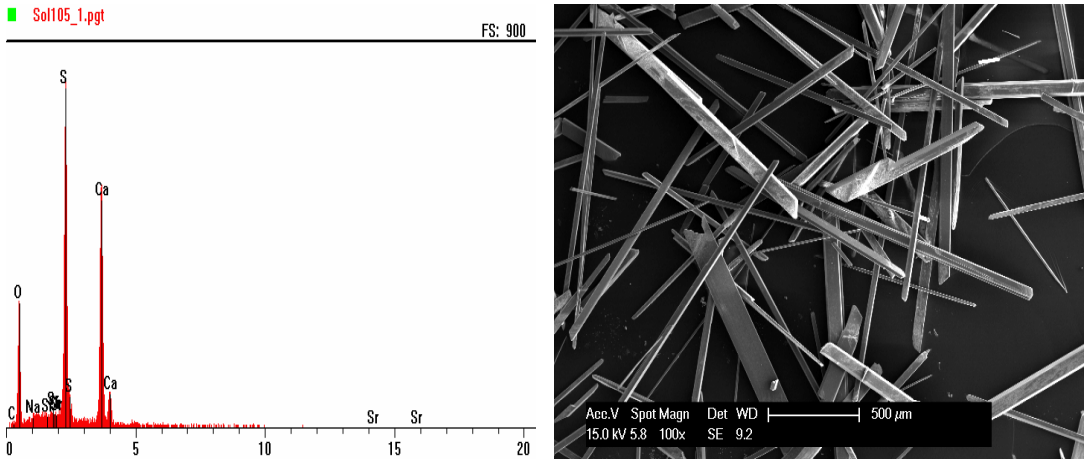

Figure 6.78: *EDS analysis for scales resulting from the precipitation of $CaSO_4$ (0.047M Ca^{2+} and 0.047M SO_4^{2-}) in the presence of DO at 0.5 M salinity.*

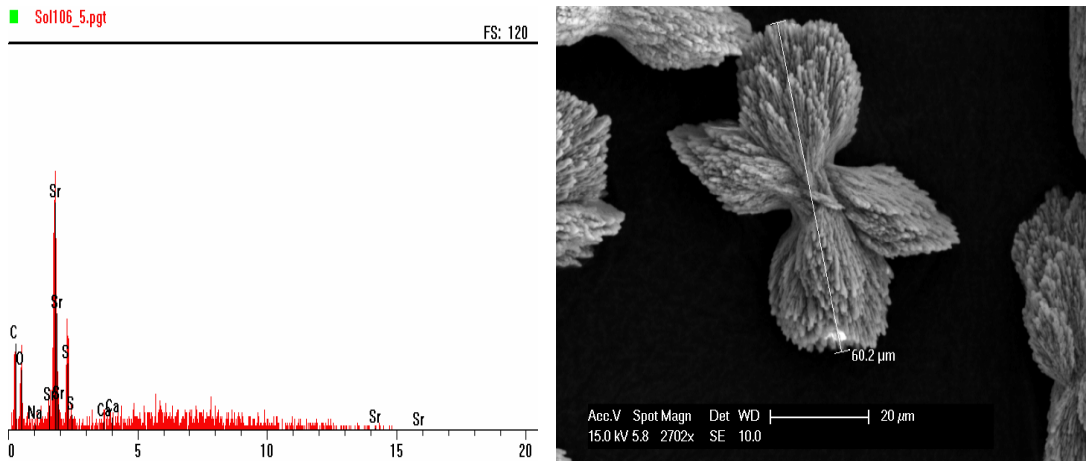

Figure 6.79: *EDS analysis for scales resulting from the precipitation of mixed $SrSO_4$ and $CaSO_4$ (0.02M Sr^{2+}, 0.047M Ca^{2+} and 0.047M SO_4^{2-}) in the presence of DO at 0.5 M salinity.*

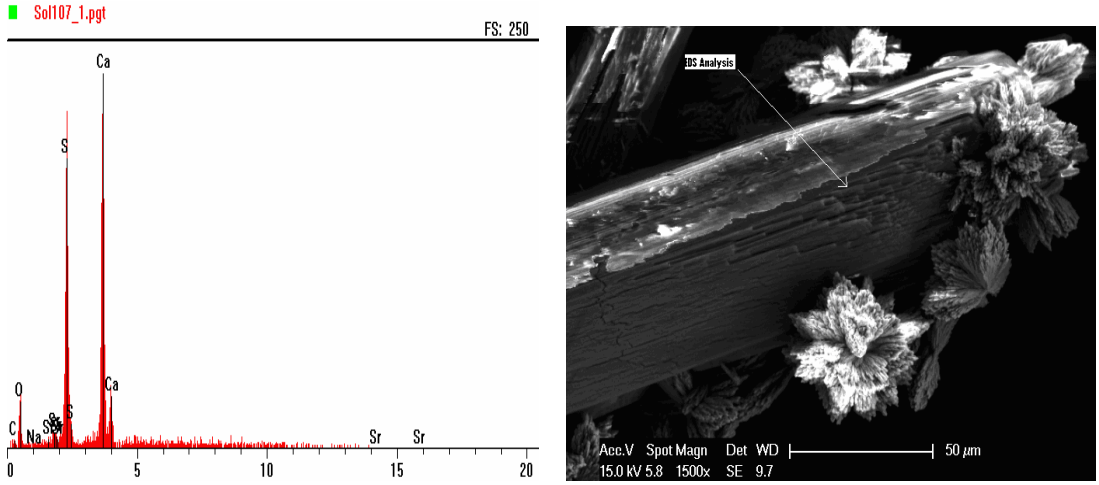

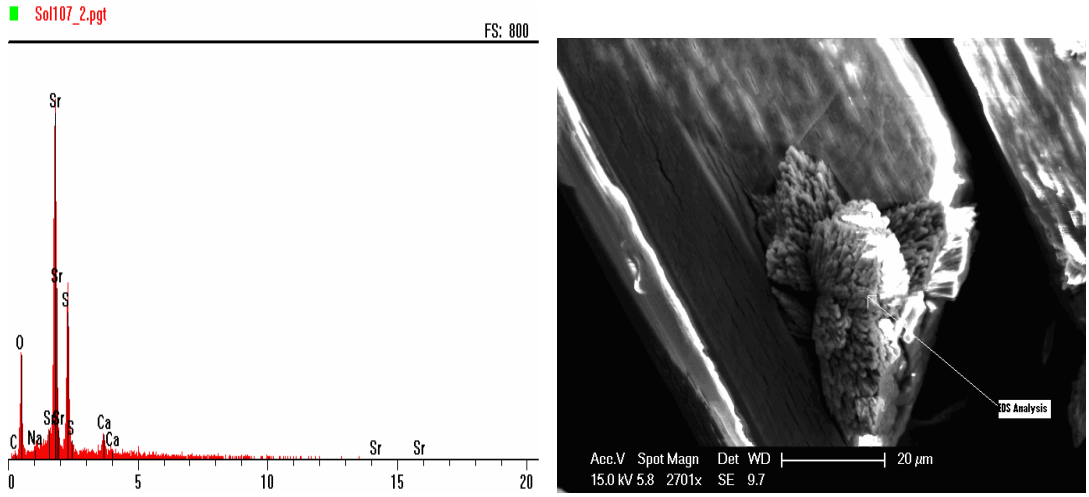

Figure 6.80: *EDS analysis for scales resulting from the precipitation of mixed $SrSO_4$ and $CaSO_4$ (0.005M Sr^{2+}, 0.047M Ca^{2+} and 0.047M SO_4^{2-}) in the presence of DO at 0.5 M salinity.*

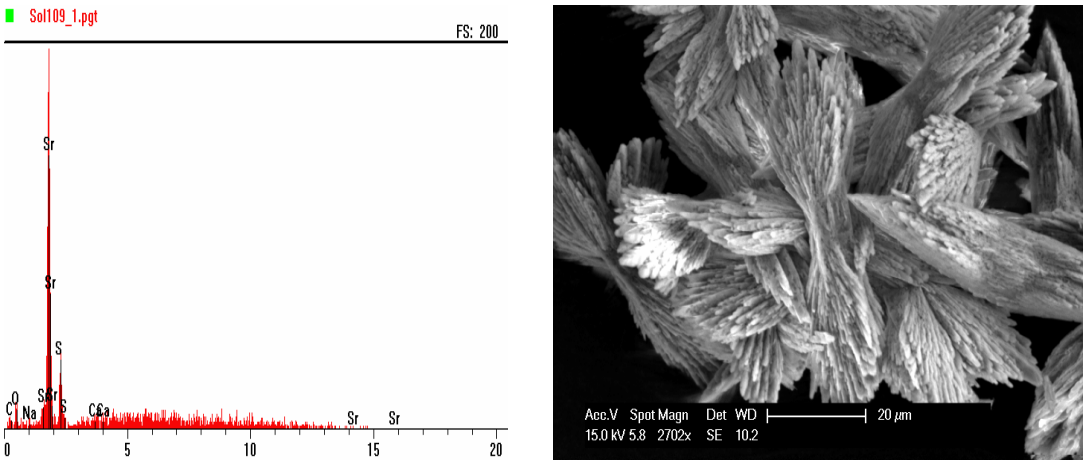

Figure 6.81: *SEM images for scales resulting from the precipitation of $SrSO_4$ and $CaSO_4$ (0.02M Sr^{2+}, 0.047M Ca^{2+} and 0.047M SO_4^{2-}) at 1.5 M salinity.*

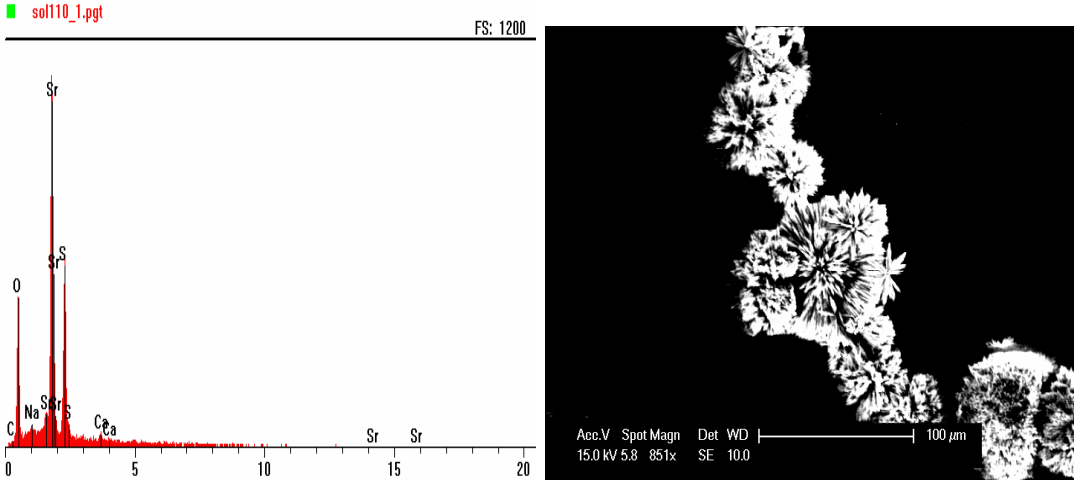

Figure 6.82: *EDS analysis for scales resulting from the precipitation of mixed $SrSO_4$ and $CaSO_4$ (0.005M Sr^{2+}, 0.047M Ca^{2+} and 0.047M SO_4^{2-}) at 1.5 M salinity.*

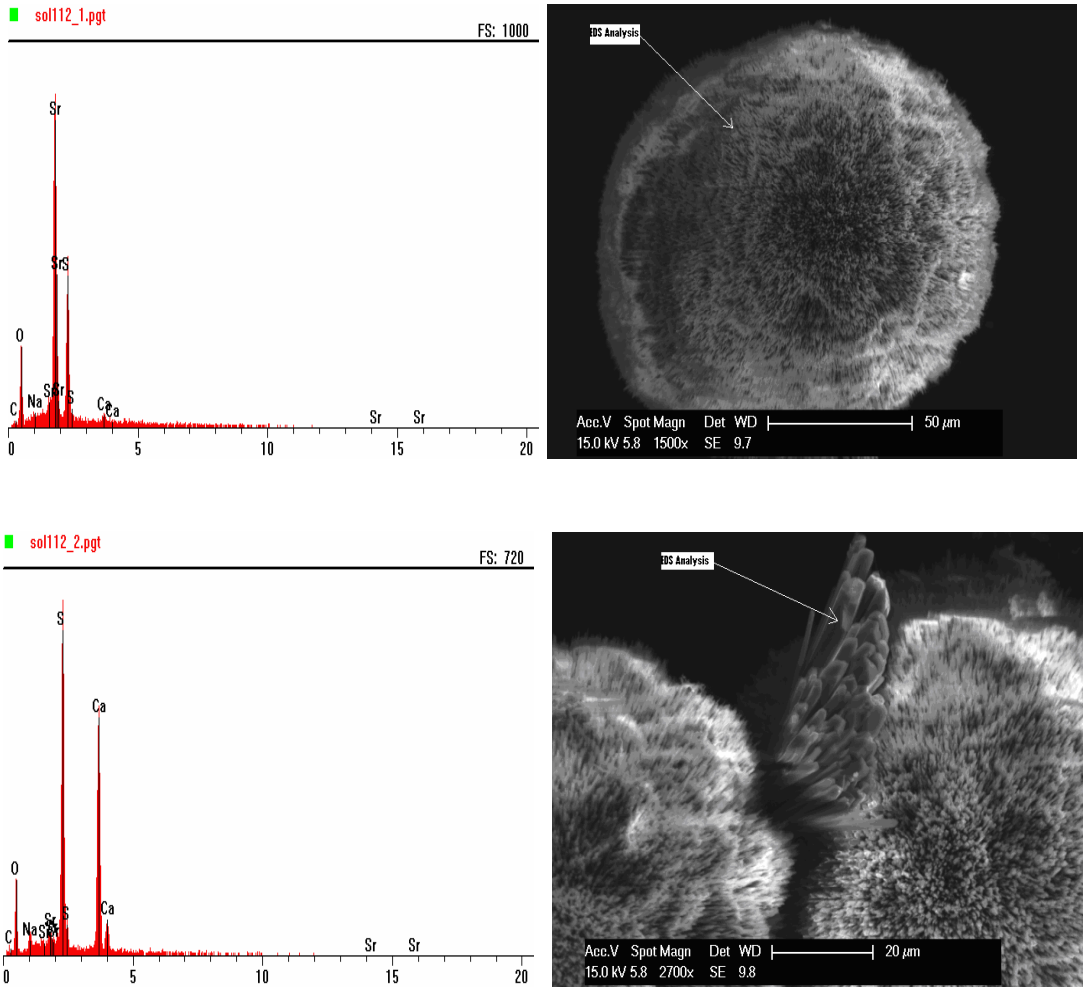

Figure 6.83: *EDS analysis for scales resulting from the precipitation of mixed $SrSO_4$ and $CaSO_4$ (0.02M Sr^{2+}, 0.047M Ca^{2+} and 0.047M SO_4^{2-}) in the presence of DO at 1.5 M salinity.*

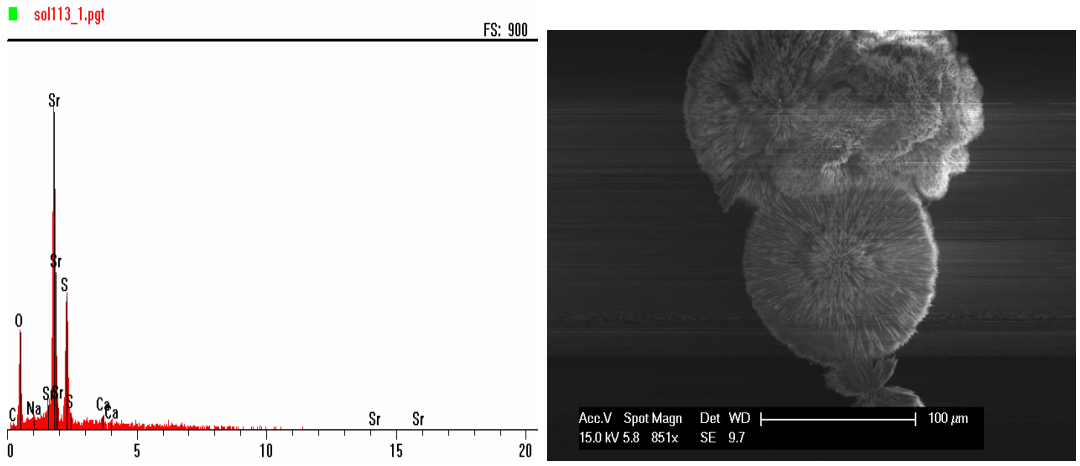

Figure 6.84: *EDS analysis for scales resulting from the precipitation of mixed $SrSO_4$ and $CaSO_4$ (0.05M Sr^{2+}, 0.047M Ca^{2+} and 0.047M SO_4^{2-}) in the presence of DO at 1.5 M salinity.*

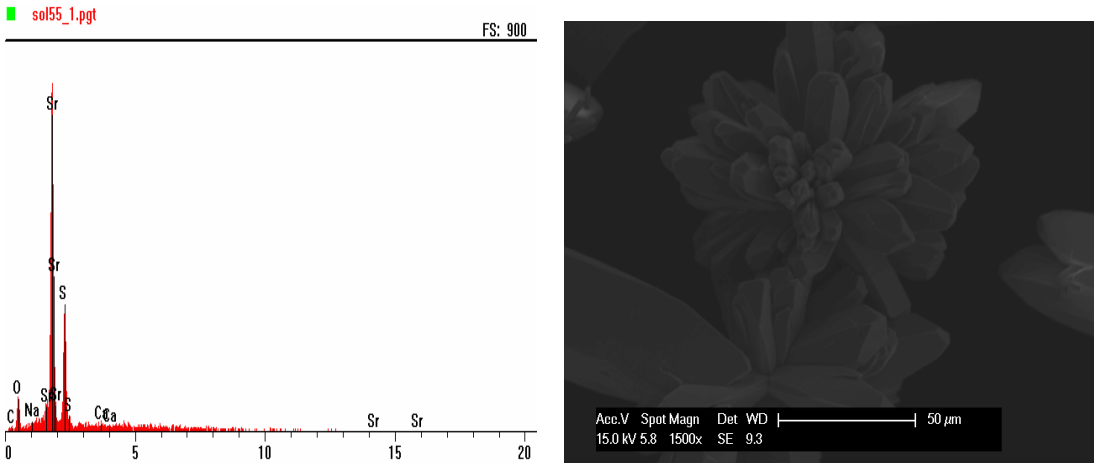

Figure 6.85: *EDS analysis for scales resulting from the precipitation of $SrSO_4$ (0.005M Sr^{2+} and 0.047M SO_4^{2-}) at 0.35 M salinity.*

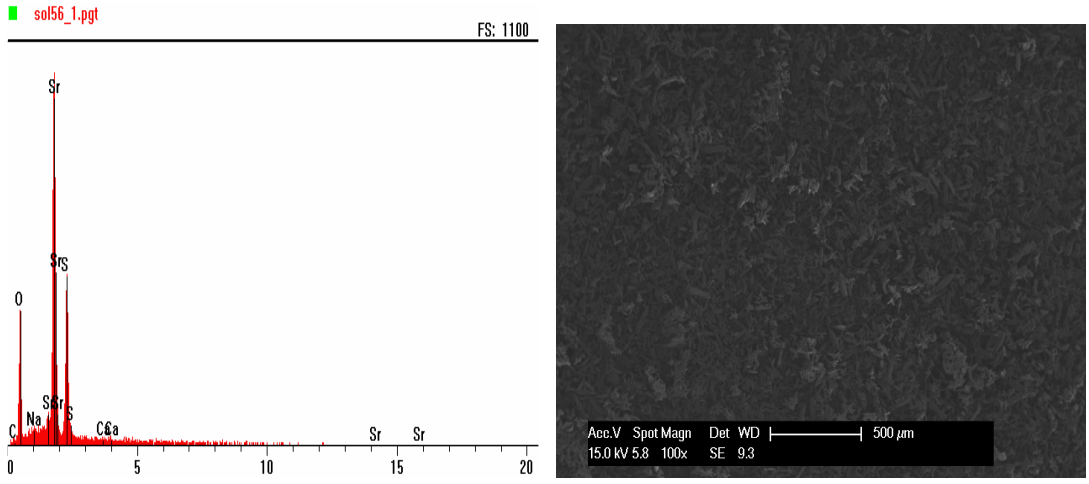

Figure 6.86: *EDS analysis for scales resulting from the precipitation of $SrSO_4$ (0.005M Sr^{2+} and 0.047M SO_4^{2-}) in the presence of DO at 0.35 M salinity.*

6.6. Summary

This chapter presents experimental work that has been carried out to study the precipitation and co-precipitation of $CaSO_4$ and $SrSO_4$ with or without the presence of DO at different salinity levels. It has been observed that a salinity increase has a greater effect on the precipitation of $CaSO_4$ than it dose on $SrSO_4$. The presence of DO inhibits the precipitation of both $CaSO_4$ and $SrSO_4$. The DO seems to cover the active crystallisation sites which increases the induction time and thus the crystal size. The co-precipitation of $CaSO_4$ and $SrSO_4$ altered the solubility product of both salts at different salinity levels. The SEM images show changes in crystals size and shape for the $SrSO_4$ as a result of co-precipitation and increased salinity. Also, the

SEM images show that the co-precipitation and salinity increase changed the size of $CaSO_4$ crystals. The EDS analyses show an interaction between the $CaSO_4$ and $SrSO_4$ during the co-precipitation of these two salts. These combined effects of salinity, DO and co-precipitation may affect the changes in Gibbs free energy associated with the crystallisation process and thus alter the thermodynamics and the kinetics of the precipitation. Thus, taking into account the effects of co-existing precipitation salts and the presence of DO are essential to have a reliable predication of the scaling propensity. The current industrial practice of using the solubility data of a single precipitating salt to predict the scaling propensity of a co-precipitation system will lead to a significant error in scaling propensity prediction. This will add unnecessary extra cost to the RO process for pre-treatment and unscheduled shut-downs and membrane replacement. The use of the experimental work in this chapter to understand and determine the possibility of interaction between co-existence scaling salts in the feed water is very important to achieve reliable scaling propensity prediction. This experimental work could be done as a pre-design measurement to have accurate solubility data reflecting the real feed water.

Chapter 7
Validation of the proposed approach using laboratory membrane rig

7. Validation of the proposed approach using laboratory membrane rig

The main aim of this chapter is the attempt to validate the Matlab program developed in Chapter three and Chapter four of this thesis using set of hydrodynamic tests. This set of tests has been carried out using a newly installed laboratory membrane rig. In this chapter a new technique to simulate full scale membrane processes is proposed using a laboratory membrane rig combined with the program previously developed in this thesis. This new approach can be used to study the effect of process hydrodynamics on scaling and process performance of full scale membrane processes using laboratory rig.

7.1 Test apparatus

Figure 5.2 shows the experimental apparatus which has been used for the hydrodynamic runs. As seen in Fig 5.2 the experimental apparatus is a closed-loop circulation system which consists of a storage tank, low pressure and high pressure circulation pumps, a double-pipe heat exchanger, an Osmaonics® patented SEPA® CF II membrane cell, a series of pressure, temperature, conductivity, pH and flow measuring and control devices and optional micro-filters (5µm pore size, Puente.)

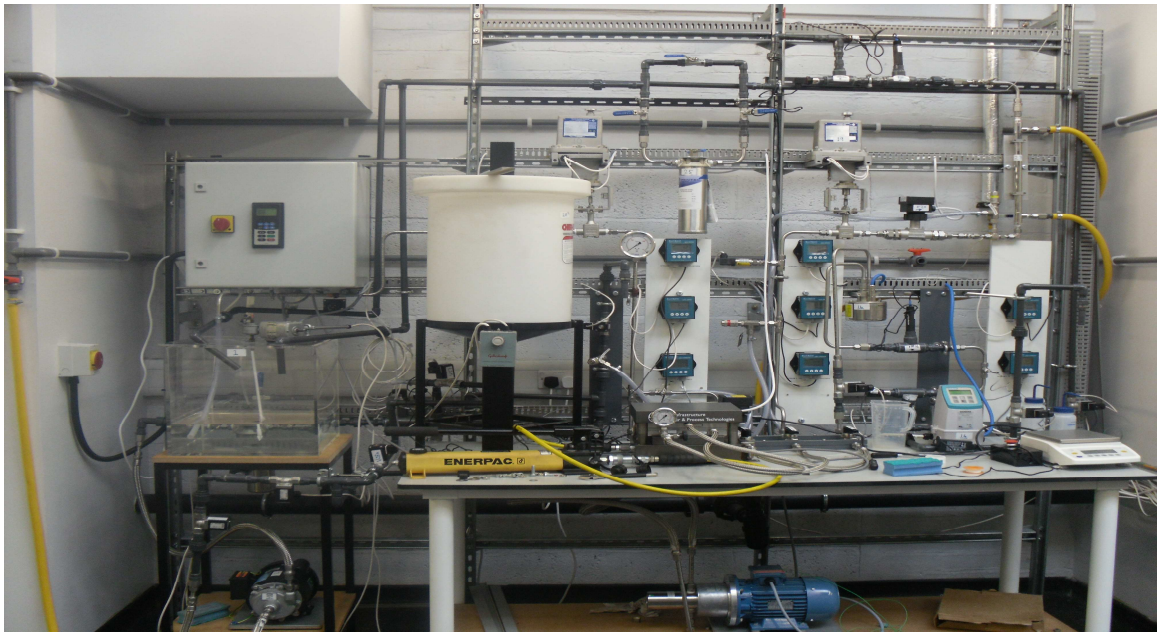

Figure 5.2: *Photograph of membrane test apparatus*

This laboratory membrane rig is designed to operate either in full recycle mode (recycle the concentrate and permeate streams) or in a partial recycle mode (withdraw the permeate stream). A schematic diagram for the experimental rig is shown in Fig 5.3.

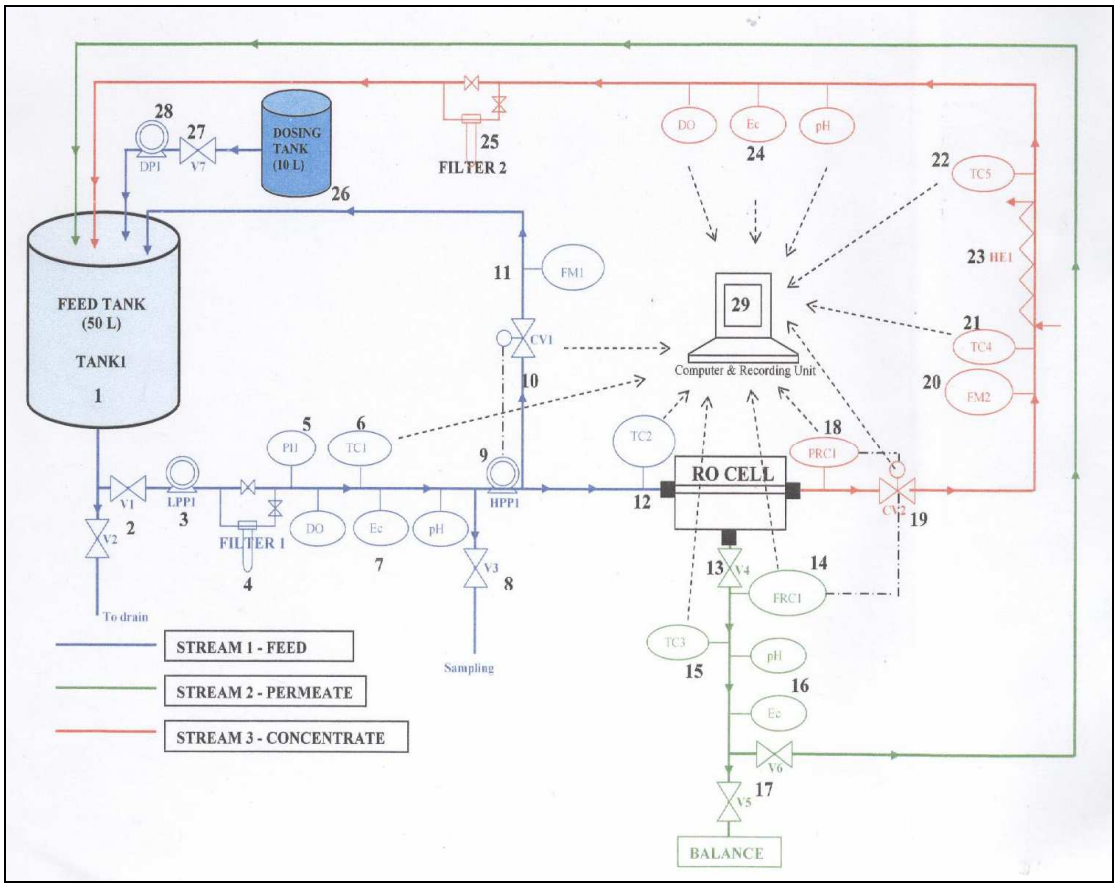

Figure 5.3: *Schematic diagram of experimental membrane rig*

All the piping, fittings, and test cell were manufactured either from stainless steel or PVC to prevent corrosion. A data acquisition and control system was designed using Labview to control the feed pressure, concentrate flowrate and feed flowrate at set values and to collect the data of permeate flux and solution pH, conductivity and temperature. The results are constantly displayed on the computer screen and recorded into the computer's hard disk at given time intervals. More details about the membrane rig will be included in appendix (C).

7.2 Test procedures and conditions

7.2.1 Membrane preparation

A composite polyamide RO membrane provided by Hydranautics (Catalogue designation: ESPA2) was used in this experimental work. The membrane was cut to the required size and rinsed using pure water. Then, the membrane was installed into the cell and conditioned by pure water for 24 hours in full recycling mode under the test operating conditions.

7.2.2 Reagents

All the reagents used on this research work are analytical grades supplied by Fisher Scientific. Table 5.1 presents all reagents used for this work, including quality and manufacturer. NaCl, $CaCl_2$, Na_2SO_4 and $SrCl_2$ were used to prepare a synthetic feed water solution according to the procedure described in detail in chapter 5. Other common reagents include pH buffer solution 4, 7, 10 for pH electrode calibration; Ca^{2+} ,Sr^{2+}, Na^{+} and SO_4^{2-} standard solutions, HCl and NaOH were used through this experimental work.

7.2.3 Methodology

Solutions of calcium sulphate ($CaSO_4$) and strontium sulphate ($SrSO_4$) in sodium chloride (NaCl) were prepared by mixing solutions of $CaCl_2$, $SrCl_2$ Na_2SO_4, and NaCl which had been prepared by dissolving the respective salts in micro-filtered (with an 0.2 micrometer filter) desalted water and further filtered with an 0.2 micrometer filter after preparation to ensure no impurities or un-dissolved salt were present.

The prepared solutions were analytically tested for all components immediately after preparation and their compositions were monitored during experimentation. Solutions concentration, conductivity and pH were measured directly after mixing the solutions; a sample of mixed solution was withdrawn, filtered with an 0.2 μm filter and then analyzed for water quality. Water quality is determined by measuring pH, conductivity, calcium, sodium, strontium and sulphate. A detailed description of the methodology has been included in chapter 5 of this thesis.

7.2.4 General test procedure

The scaling propensity and other important parameters along a full scale membrane process can be simulated based on the laboratory technique proposed by A. Drak et al, [93] and the Matlab programs previously developed in this thesis. This laboratory technique consists of recycling the feed solution while continuously withdrawing permeate. The increase of ionic concentrations induced by permeate removal increases the scaling potential [93]. After a certain period of time, permeate is recycled, with the concentrate, to the feed tank to expose the membrane to a totally recycling solution for another fixed period of time which represents a certain recovery level. This recovery level is used to locate the simulated position along a full scale membrane channel using the developed Matlab program, as will be explained in detail later in this chapter. The recovery level can be increased by repeating the permeate withdrawal while recycling the concentrate. Increasing the recovery level means moving forward along the full scale membrane channel and thus the full scale membrane process can be simulated. The composition of the recycling solution and the permeate flow are recorded at every recovery level.

A set of experiments was carried out to validate this new approach. At the beginning of every run the prepared feed solution was transferred to the feed storage tank. The data logging program was then initiated. The operating pressure and feed velocity were controlled at set values according to the run conditions. In order to mix the bulk solution completely and stabilize the system, the system was operated in full recycling mode for a certain period of time. The changes of Ca^{2+}, Sr^{2+} and SO_4^{2-} concentrations and solution conductivity, pH, temperature and permeate flow during the run were monitored using the Labveiw program and through periodic samples withdrawn from the test solution. The withdrawn samples were immediately filtered through 0.2 μm filter and diluted using 0.5%HNO_3.

7.3 Experimental work

7.3.1 Permeate flowrate and R_m calculations

Table 7.1 shows the operational conditions that were used to calculate the permeate flowrate of the membrane used and then to calculate the value of the membrane resistance (R_m) which was to be used in the Matlab simulation. The averaged measured permeate flowrate (0.556 L/hr) shows a very good agreement with the manufacturer value (0.536 L/hr) at the same operation conditions.

Table 7.1: *Operation conditions for membrane permeability and Rm calculations*

Test No.	1
Feed pressure, (bar)	10.5
Brine flow rate , (L/s)	0.087
Temp., (^oC)	25
Feed salinity , (ppm)	1500
Permeate Recovery	15%
Initial pH	6.5

The operational conditions used in test No. 1 are the same as those used by the manufacturer of the membrane (Hydranautics). A copy of the membrane data sheet is attached in the Appendix (D).

To calculate R_m using Eq. 3.32, there is a need to calculate the osmotic pressure difference $\Delta\pi$ using Eq 3.33; in which α relates the osmotic pressure to concentration through application of the van't Hoff formula through Eq. 3.34; R_g is the universal gas constant; T is the absolute temperature; Mw is the molecular weight of the solute; N is the number of ions in solution that can result from one salt molecule (N is 2 for NaCl); and $\varphi_{osmotic}$ is the Pitzer osmotic coefficient (calculated using the Matlab program). The calculated R_m value for the membrane species tested under test 1 operating conditions was $8.61 \times 10^{+10}$ Pa.s/m and the R_m calculated from the manufacturer's data sheet is $8.74 \times 10^{+10}$ Pa.s/m. Sample of the calculation can be found in section 7.6 of this chapter.

$$v = \frac{\Delta P - \Delta \pi}{R_m} \qquad (3.32)$$

$$\Delta \pi = \alpha \Delta c \qquad (3.33)$$

$$\alpha = \frac{N \varphi_{osmotic} R_g T}{Mw} \qquad (3.34)$$

The same calculations have been carried out to find out R_m for all the membrane samples used in this experimental work.

7.3.2 Concentration polarisation and mass transfer coefficient calculations

The concentration polarisation CP can be calculated experimentally as discussed before in Chapter 2. The experimental determination of CP involves measuring the mass transfer coefficient, K_m. The technique suggested by Sutzkover et al [18] has been tested in this work for laminar flow since Sutzkover et al, tested their technique under turbulent flow conditions only. This technique is based on evaluation of the permeate flux decline induced by the addition of a salt solution to an initially salt-free water feed. According to this approach the mass transfer coefficient is given by Eq. 2.12:

$$K_m = \frac{v_{salt}}{\ln\left\{\frac{\Delta p}{\pi_b - \pi_p}\left[1 - \frac{v_{salt}}{v_{H_2O}}\right]\right\}} \qquad (2.12)$$

Thus, the value of K_m can be evaluated from the osmotic pressures π_b and π_p of the saline feed and of the permeate respectively and by measuring the permeate flux of pure water, v_{H_2O}, and the permeate flux of saline solution, v_{salt}.

$$CP = \mathrm{Exp}(v_{salt}/K_m) \qquad (2.13)$$

Table 7.3 shows the initial operating conditions for the experiment that was carried out to calculate the concentration polarisation factor CP, the mass transfer coefficient K_m, and the membrane resistance R_m. The permeate flux of pure water v_{H_2O} found to be 3.32×10^{-05} (m/s). Table 7.4 gives the values of the v_{salt} measured during increasing the recovery and the calculated CP, K_m and R_m. The averaged value of the R_m was

found to be $9.08 \times 10^{+10}$ (Pa.s/m); this value was used in the Matlab simulation in order to simulate the experimental work. The comparison between the CP and K_m values calculated using the Sutzkover et al technique with the CP and K_m values calculated by the Dresner model [26] indicates a minor difference which can be attributed to the assumption made by each author. Sutzkover et al, assume that the osmotic pressure is linearly proportional to salt concentration and thus they directly substitute the ratio between the osmotic pressures with the ratio of the concentrations. Drenser [26] assumed a complete rejection of the solute by the membrane and a constant permeate flux and a fully developed velocity profile along the whole filtration channel. According to Dresner and as discussed in chapter 2 of this thesis, CP can be calculated at locations downstream in the filtration channel by Eq. 7.1. The length of the entrance region was found to be 0.003-0.007 m through Eq.7.2 [20], which is very small compared to the length of the membrane channel used (0.14 m), and thus only the values of CP and K_m downstream in the filtration channel have been included in Table 7.3.

$$CP = 1 + \frac{v^3 . H . L}{3 . u . D^2} \qquad (7.1)$$

$$\frac{EL}{d_h} = \frac{1000 \, to \, 2500}{\mathrm{Re}^{0.875}} \qquad (7.2)$$

where H is the height of the channel, L is the length of the channel, D is the solute diffusivity coefficient in the solvent (1.2×10^{-9} m^2/s at experiment conditions), v is the permeate flux and u is the feed flux, EL is the entrance region length and d_h is the hydraulic diameter.

The Sutzkover et al technique have been tested in a more reliable approach by calculating the difference between the osmotic pressures at each side of the membrane wall (concentrate and permeate sides) using Eq.7.3, then calculating the equivalent c_w using Eq3.33, the c_p can be assumed to be the same as the measured value during the experiments. Then the calculated c_w and measured c_b and c_p can be used to calculate the CP and K_m using Eq 2.10.

$$\pi_w - \pi_p = \Delta P.\left[1 - \frac{v_{salt}}{v_{H_2O}}\right] \qquad (7.3)$$

$$\frac{c_w - c_p}{c_b - c_p} = \exp\left(\frac{v}{K_m}\right) \qquad (2.10)$$

Table 7.2: *Initial operating conditions for Concentration polarisation measurements.*

Test No.	2	3
Feed pressure, (bar)	25	25
Brine flow rate , (L/s)	0.076	0.076
Temp., (^oC)	25	25
Feed salinity , (ppm)	0.0	12970
Permeate Recovery	0.0	0.0
Initial pH	6.5	6.5

Table 7.3: *The measured v_{salt} and calculated CP, K_m, and R_m at different recovery levels under table 7.3 operation conditions.*

Recovery%	v_{salt} (m/s)	CP Using Eqs 7.3 and 2.10	K_m (m/s) Using Eqs 7.3 and 2.10	CP Sutzkover et al	K_m (m/s) Sutzkover et al	CP Dresner	K_m (m/s) Dresner	R_m (Pa.s/m)
0.00	$1.98x10^{-05}$	1.59	$4.26x10^{-05}$	1.52	$4.74x10^{-05}$	1.23	$9.56x10^{-05}$	$9.28x10^{+10}$
13.30	$1.77x10^{-05}$	1.59	$3.85x10^{-05}$	1.52	$4.25x10^{-05}$	1.17	$1.14x10^{-04}$	$9.75x10^{+10}$
22.67	$1.69x10^{-05}$	1.58	$3.72x10^{-05}$	1.52	$4.03x10^{-05}$	1.14	$1.26x10^{-04}$	$10.0x10^{+10}$
33.33	$1.60x10^{-05}$	1.52	$3.85x10^{-05}$	1.46	$4.21x10^{-05}$	1.12	$1.39x10^{-04}$	$10.1x10^{+10}$
46.67	$1.50x10^{-05}$	1.35	$5.04x10^{-05}$	1.32	$5.36x10^{-05}$	1.10	$1.57x10^{-04}$	$9.75x10^{+10}$
58.67	$1.35x10^{-05}$	1.14	$1.03x10^{-04}$	1.14	$1.01x10^{-04}$	1.07	$1.92x10^{-04}$	$8.89x10^{+10}$
64.00	$1.24x10^{-05}$	1.07	$1.82x10^{-04}$	1.08	$1.64x10^{-04}$	1.06	$2.25x10^{-04}$	$8.43x10^{+10}$
68.67	$1.08x10^{-05}$	1.05	$2.38x10^{-04}$	1.05	$2.08x10^{-04}$	1.04	$2.93x10^{-04}$	$8.30x10^{+10}$
73.33	$9.90x10^{-06}$	1.07	$1.54x10^{-04}$	1.07	$1.48x10^{-04}$	1.03	$3.47x10^{-04}$	$8.65x10^{+10}$
82.00	$8.63x10^{-06}$	1.05	$1.75x10^{-04}$	1.05	$1.68x10^{-04}$	1.02	$4.55x10^{-04}$	$7.60x10^{+10}$

As can be seen in Table 7.4 Sutzkover et al., technique gives reasonable estimation for the CP and K_m values in laminar flow.

As can be seen in Table 7.3; K_m values decrease with increases in the recovery. This may be due to the decrease of permeate flux as a result of the osmotic pressure increases. This effect will be combined with an increase of the boundary layer thickness (δ) as a result of the increase in salts concentration and its effect on the fluid viscosity. All values in Table 7.3 show high consistency and agree well with literature values [20] where comparison is possible.

7.4 Experimental validation of the proposed model

Table 7.5 shows the operating and feed conditions that have been used in experimental work and Matlab simulation. The same parameters have been used in the Matlab program to simulate the experiment.

Table 7.4: *Operating and feed conditions for the experimental work and Matlab simulation.*

Test No.	4
Feed pressure, (bar)	25
Brine flow rate (L/s)	0.076
Temp., (^{o}C)	18
Na^{+}, (M)	0.154
Ca^{2+}, (M)	0.013
Sr^{2+}, (M)	0.00013
Cl^{-}, (M)	0.18
SO_4^{-2}, (M)	0.0155
Brine velocity, (m/s)	0.925
Channel height (m)	0.00085

7.4.1 Salinity prediction validation

The change in salinity induced by permeate removal has been calculated by two approaches; firstly through the change of total ionic concentration obtained from analysing periodic samples at different recovery levels and from the conductivity recorded by the Labview program during the run. The recoded conductivities were converted to salinity using the UNESCO International Equation of State (IES 80)

[141] as described in Fofonoff [142] using the online Sea Water Equation of State Calculator [143]. Figure 7.1 shows both the predicated feed salinity change and measured feed salinity at different recovery levels. As can be seen in Fig. 7.1 the prediction salinity shows a very good agreement with the measured salinity values.

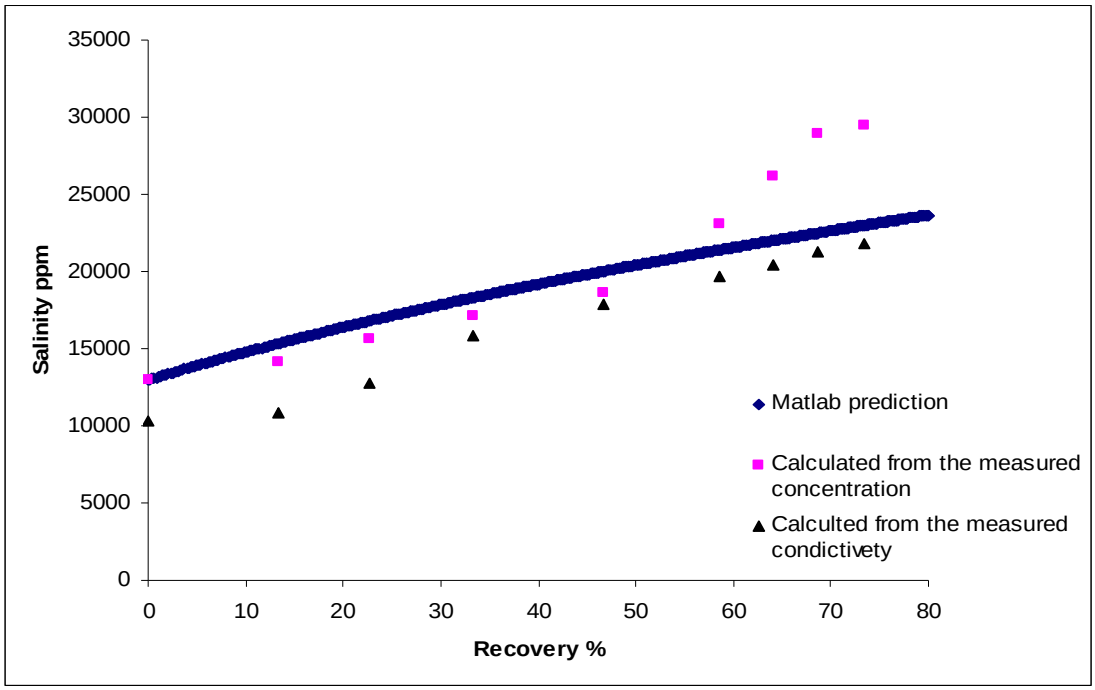

Figure 7.1: *The predicted feed salinity change and measured feed salinity at different recovery percentages.*

7.4.2 Permeate flow prediction validation

To validate the permeate flow prediction resulted from the Matlab simulation, the permeate flow has been measured experimentally at different recovery levels. Figure 7.2 shows the predicted permeate flow and the measured permeate flow at different recovery levels. As can be seen in Figure 7.2 our program gives a very good prediction for the permeate flow.

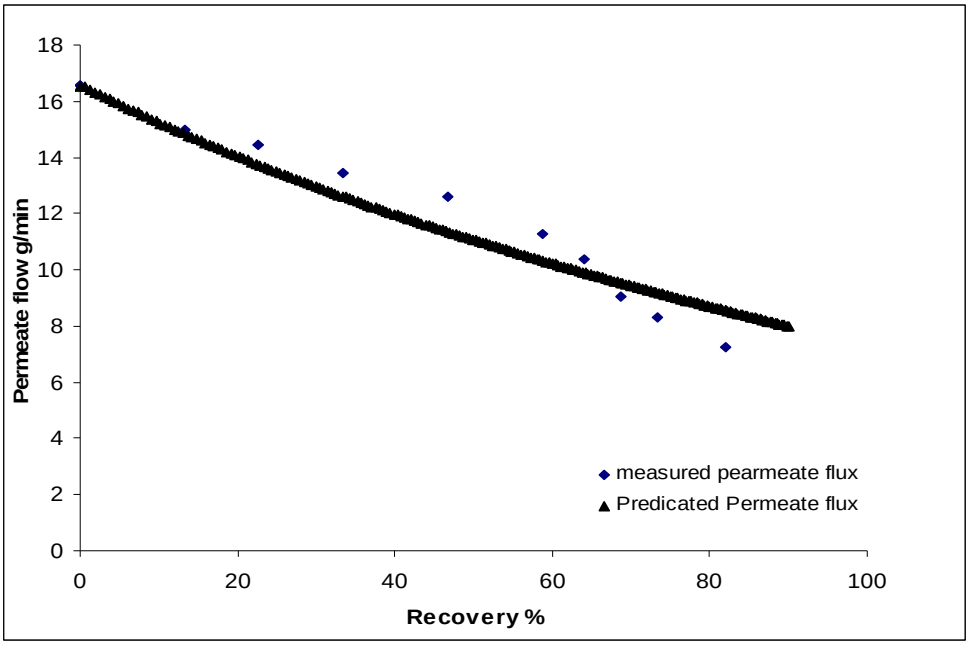

Figure 7.2: *The predicted permeate flux and the measured permeate flux at different recovery levels.*

7.4.3 Scaling propensity validation

The measured ionic concentrations were used to calculate the Scaling Propensity Index (SPI) at different recovery levels. The initial measured ionic concentrations were used in the Matlab simulation to predict the SPI along the channel. Figure 7.3 shows that there is a very good agreement between the measured SPI values and the predicted one. As can be seen in Fig. 7.3, the calculated SPI increases with recovery as a result of the increase in scaling salts concentrations. However, SPI values remain negative along the channel which is consistent with the experimental observation that no scale was formed.

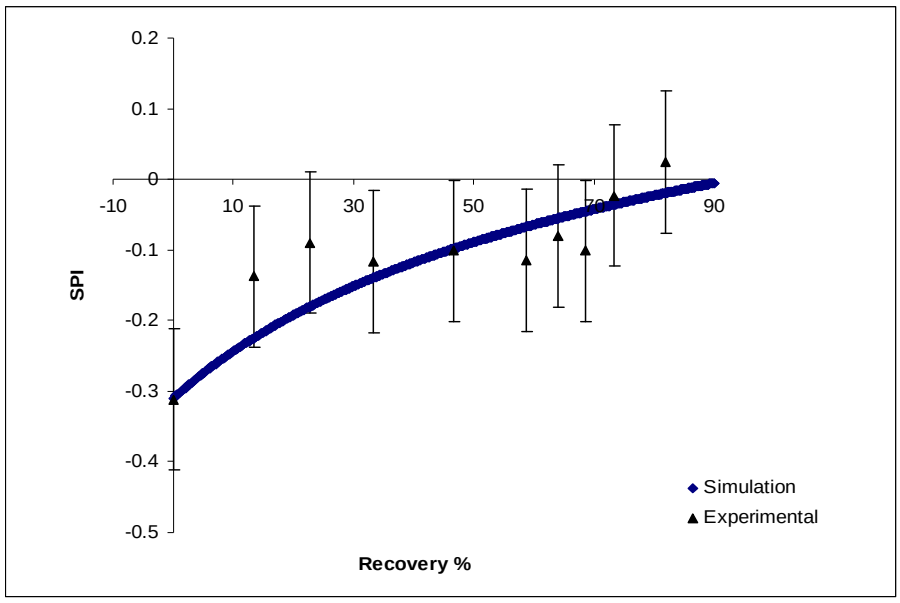

Figure 7.3: *Calculated and predicted Scaling Propensity Index (SPI) at different recovery levels.*

7.5 Summary

In this chapter the developed Matlab program in chapter 3 and chapter 4 has been verified experimentally. The predicted change of salinity, permeate flow and scaling propensity have been supported by the experimental obtained profiles. The Sutzkover et al. [20], technique for measuring the concentration polarisation factor CP and mass transfer coefficient K_m has been tested under laminar flow condition. Reasonable estimations for the CP and K_m values have been achieved using this technique under test conditions. A new approach to simulate and to study the performance of full scale membrane process using a laboratory membrane rig has been suggested. This new approach depends in the developed Matlab program to locate the position along the filtration channel within full scale membrane process using the recovery levels optioned from the laboratory membrane rig.

Chapter 8

Thesis Conclusions and Future Work

8. Thesis conclusion and future work

8.1 Thesis conclusion

In this thesis a new approach for assessing local ionic activity coefficients and osmotic coefficients for saline water in full-scale RO/NF processes has been introduced. A set of Matlab programs has been created in order to calculate the ionic activity coefficients and osmotic coefficients for saline water. These programs have been validated through encouraging comparisons with existing published data. This approach enables us to study from first principles the effect of hydrodynamics, salinity, temperature and concentrations of dissolved salts on local fouling potential at the membrane surface along the feed module. Moreover, this approach is able to incorporate the effect of relative solution composition along a membrane module; this is very significant for nanofiltration (NF) modules having different retentions for mono-valent and di-valent ions.

Also in this thesis, the only available theoretical index for prediction of fouling (scaling) by sparingly soluble salts has been modified and combined with the fundamental equations of transport and continuity to reliably simulate and assess the onset of scaling propensity locally on the membrane surface along a full-scale RO membrane. This realistic simulation is fundamentally based and does not include any experimentally determined parameters or constants in the case of pure precipitation, i.e. while ignoring the co-precipitation effect. This model has been used to study the effects of membrane resistance, pump feed pressure, feed mass flow rate, salinity and temperature on the onset of fouling (scaling) propensity for a given sparingly salt on the membrane surface.

Furthermore, a new procedure for incorporating the effect of co-precipitation on scaling propensity prediction has been introduced and discussed. The effect of process pressure on solubility products at the onset of scaling during the full scale RO process has been theoretically included and analysed for the first time. The

consequence of ignoring the effect of process pressure on solubility product and scaling propensity prediction during RO processes was highlighted and discussed. It must be emphasised that taking into account the effect of co-precipitation and the pressure effect are essential to a reliable prediction of the scaling propensity. This model can help in process optimisation and the design of both processes and equipment, by predicting the scaling propensity along the module so that proper measures can be taken to minimise the onset of scale formation. The information that can be achieved from this model can be used for preventive measures and thus can be applied as a fouling mitigation technique.

In the course of research aimed at studying the effect of co-precipitation, a set of experiments has been carried out to study the precipitation and co-precipitation of $CaSO_4$ and $SrSO_4$ with and without the presence of dissolved organics (DO), at different salinity levels. It has been observed that a salinity increase has a greater effect on the precipitation of $CaSO_4$ than it does on $SrSO_4$. The presence of dissolved organics inhibits the precipitation of both $CaSO_4$ and $SrSO_4$. These dissolved organics seem to cover the active crystallisation sites, increasing the induction time and thus the crystal size. The co-precipitation of $CaSO_4$ and $SrSO_4$ alter the solubility product of both salts at different salinity levels. SEM images show changes in crystals size and shape for the $SrSO_4$ as a result of co-precipitation and increased salinity. Also, the SEM images show that the co-precipitation and salinity increase changed the size of $CaSO_4$ crystals. The EDS (Energy dispersive X-ray scattering) analyses show an interaction between the $CaSO_4$ and $SrSO_4$ during the co-precipitation of these two salts. This leads to the hypothesis that salinity, DO and co-precipitation may affect the changes in Gibbs free energy associated with the crystallisation process and thus alter the thermodynamics and the kinetics of the precipitation. The current industrial practice of using the solubility data of a single precipitating salt to predict the scaling propensity of a co-precipitation system will lead to a significant error in scaling propensity prediction. This will add unnecessary extra cost to the RO process for pre-treatment and unscheduled shut-downs and membrane replacement. The experimental techniques described in this thesis can be used to aid understanding and determine the possibility of interaction between co-

existence scaling salts in the feed water, which is very important in achieving reliable scaling propensity predictions. This experimental work could be done as a pre-design measurement to secure accurate solubility data reflecting the real feed water.

Finally, in this thesis the Matlab programs developed in chapters three and four have been verified experimentally. The predicted changes of salinity, permeate flow and scaling propensity have been supported by the experimentally measured profiles. The Sutzkover et al. [20], technique for measuring the concentration polarisation factor CP and mass transfer coefficient K_m has been tested under laminar flow conditions. Reasonable estimates for the CP and K_m values have been achieved using this technique under test conditions. A new approach to simulation and study of the performance of full-scale membrane processes using a laboratory membrane rig has been suggested. This new approach depends on the developed Matlab program to locate the position along the filtration channel within full-scale membrane process corresponding to recovery levels measured by the laboratory membrane rig. Data reproducibility has been checked through the duplication of selected experiments as can be seen in appendix (E).

8.2 Future work

The techniques proposed in the course of this thesis can easily be developed to be more user- friendly and applicable to real processes, for deciding on preventative measures as a fouling mitigation technique. However, the following points should be covered in future work.

1) A completely theoretical approach must be developed and incorporated into the model to calculate the solubility product, taking into account the effects of co-precipitation, salinity, DO and the presence of any species that may affect the Gibbs free energy change of precipitation. This can be done as suggested in [4, 62] through advances in computational chemistry.

2) The current model can be expanded to include transient conditions and model the build-up of the fouling layer. This can be done by incorporating actual

precipitation kinetics. Thus the change of the fouling layer type and thickness can be simulated.

3) A novel experimental apparatus should be developed to investigate the added resistance of the predicted type of scale to the membrane resistance under process operating conditions.

4) The Experimental work in Chapter 6 of this thesis can be followed to characterise all the possibilities of co-precipitation and their effects on thermodynamics and kinetics. This characterisation of the feed water is essential to reach reliable prediction of the scaling propensity. Also more comprehensive work needs to be done to quantitatively study the effect of co-precipitation, salinity, and DO on the kinetics of precipitation The same procedure of using isothermal batch reactors described in chapter 6 can be used to calculate the constant of the precipitation reaction rate and the order of the reaction, but this will need extensive number of tests so for example, the method of initial rates can be used for detailed kinetics analysis. X-Ray Diffraction (XRD) can be used to analyse the structure of the precipitate.

5) The dissolved organics (DO) effects should be more analysed through using various structures, polarities and the length of the nonpolar chain. Also radio-labelled organics can be used to work out precisely how and where the DO are incorporated in growing crystals.

6) The membrane rig described in Chapter 7 can be used to study the effect of process hydrodynamics and operating conditions on the co-precipitation of targeted-scales.

9. References

[1] R. Sheikholeslami, Strategies for future research and development in desalination - Challenges ahead, Desalination, 248 (2009) 218-224.

[2] A.D. Khawaji, I.K. Kutubkhanah, J.-M. Wie, Advances in seawater desalination technologies, Desalination, 221 (2008) 47-69.

[3] A. Fakhru'l-Razi, A. Pendashteh, L.C. Abdullah, D.R.A. Biak, S.S. Madaeni, Z.Z. Abidin, Review of technologies for oil and gas produced water treatment, Journal of Hazardous Materials, 170 (2009) 530-551.

[4] R. Sheikholeslami, Fouling in Membranes and Thermal Units: A Unified Approach- its Principles Assessment, Control and Mitigation, Balaban Desalination publications, L'Aquila, Italy, 2007.

[5] R. Sheikholeslami, Assessment of the scaling potential for sparingly soluble salts in RO and NF units, Desalination, 167 (2004) 247-256.

[6] W.E. Langelier, Chemical equilibria in water treatment, J. AWWA, 38 (1946) 169.

[7] J.H.A. Stiff, L.E. Davis, A method for predicting the tendency of oil field water to deposit calcium carbonate, Pet Trans AIME, 195 (1952) 213.

[8] J.W. Ryznar, A new index for determining amount of calcium carbonate scale formed by a water, AWWA, 36 (1944) 472.

[9] P.R. Puckorius, J.M. Brooke, A new practical index for calcium carbonate scale producing in cooling tower systems, Corrosion, 74 (1991) 280-284.

[10] L. Song, S. Hong, J. Hu, S. Ong, W. Ng, Simulations of Full-Scale Reverse Osmosis Membrane Process, Journal of Environmental Engineering 128 (2002) 960-966.

[11] K.L. Chen, L. Song, S.L. Ong, W.J. Ng, The development of membrane fouling in full-scale RO processes, Journal of Membrane Science, 232 (2004) 63-72.

[12] R. Sheikholeslami, Scaling potential index (SPI) for $CaCO_3$ based on Gibbs free energies, AIChE Journal, 51 (2005) 1782-1789.

[13] AWWA, R. Bergman, M46-Reverse Osmosis and Nanofiltration, 2 ed., American Water Works Association, 2007.

[14] A.I. Schäfer, Natural organics removal using membranes : principles, performance and cost Lancaster, Pa. : Technomic Publishing, 2001.

[15] R.W. Baker, Membrane Technology and Applications, 2nd ed., John Wiley & Sons, Ltd., 2004.

[16] K.P. Lee, T.C. Arnot, D. Mattia, A review of reverse osmosis membrane materials for desalinationt-Development to date and future potential, Journal of Membrane Science, 370 (2011) 1-22.

[17] G.-d. Kang, Y.-m. Cao, Development of antifouling reverse osmosis membranes for water treatment: A review, Water Research, 46 (2012) 584-600.

[18] D. Rana, T. Matsuura, Surface Modifications for Antifouling Membranes, Chemical Reviews, 110 (2010) 2448-2471.

[19] C. Fritzmann, J. Löwenberg, T. Wintgens, T. Melin, State-of-the-art of reverse osmosis desalination, Desalination, 216 (2007) 1-76.

[20] I. Sutzkover, D. Hasson, R. Semiat, Simple technique for measuring the concentration polarization level in a reverse osmosis system, Desalination, 131 (2000) 117-127.

[21] L. Song, M. Elimelech, Theory of concentration polarization in crossflow filtration, Journal of the Chemical Society, Faraday Transactions, 91 (1995) 3389-3398.

[22] M. Mulder, Basic Principles of Membrane Technology, Dordrecht : Kluwer Academic, Boston 1996.

[23] J.M. Dickson, Fundamental aspects of reverse osmosis, in: B.S.Parekh (Ed.) reverse osmosis technology: Applications for high purity water production, Marcel Dekker Inc, New York, 1988, pp. 1-51.

[24] V. Gekas, B. Hallstrom, Mass transfer in the membrane concentration polarization layer under turbulent cross flow : I. Critical literature review and adaptation of existing sherwood correlations to membrane operations, Journal of Membrane Science, 30 (1987) 153-170.

[25] G.B. van den Berg, I.G. Rácz, C.A. Smolders, Mass transfer coefficients in cross-flow ultrafiltration, Journal of Membrane Science, 47 (1989) 25-51.

[26] L. Dresner, Boundary layer built-up in the demineralization of salt water by reverse osmosis., in: Oak Ridge National Laboratory Report, 1964.

[27] W. Zhou, L. Song, T.K. Guan, A numerical study on concentration polarization and system performance of spiral wound RO membrane modules, Journal of Membrane Science, 271 (2006) 38-46.

[28] L. Song, J.Y. Hu, S.L. Ong, W.J. Ng, M. Elimelech, M. Wilf, Emergence of thermodynamic restriction and its implications for full-scale reverse osmosis processes, Desalination, 155 (2003) 213-228.

[29] L. Song, J.Y. Hu, S.L. Ong, W.J. Ng, M. Elimelech, M. Wilf, Performance limitation of the full-scale reverse osmosis process, Journal of Membrane Science, 214 (2003) 239-244.

[30] L. Song, K.G. Tay, Performance prediction of a long crossflow reverse osmosis membrane channel, Journal of Membrane Science, 281 (2006) 163-169.

[31] L. Song, Concentration polarization in a narrow reverse osmosis membrane channel, AIChE Journal, 56 (2010) 143-149.

[32] E.M.V. Hoek, J. Allred, T. Knoell, B.-H. Jeong, Modeling the effects of fouling on full-scale reverse osmosis processes, Journal of Membrane Science, 314 (2008) 33-49.

[33] N. Epstein, Thinking about Heat Transfer Fouling: A 5 X 5 Matrix, Heat Transfer Engineering, 4 (1981) 43-56.

[34] A.P. Watkinson, Water quality effects on fouling from hard waters in heat exchangers– theory and practice, in: J. Taborek, G.F. Hewitt, N. Afgan (Eds.) Heat Exchanger Sourcebook, Hemispherc Publishing Corp., New York, 1983, pp. 853–861.

[35] J. Taborek, T. Aoki, R.B. Ritter, J.W. Palen, J.G. Knudsen, Fouling: the major unresolved problem in heat transfer, Chemical Engineering Progress, 68 (1972) 59-67.

[36] J. Taborek, T. Aoki, R.B. Ritter, J.W. Palen, J.G. Knudsen, Predictive methods for fouling behaviour, Chemical Engineering Progress, 68 (1972) 69–78.

[37] R. Sheikholeslami, Composite fouling - inorganic and biological: A review, Environmental Progress, 18 (1999) 113-122.

[38] R. Sheikholeslami, S. Tan, Effects of water quality on silica fouling of desalination plants, Desalination, 126 (1999) 267-280.

[39] R. Sheikholeslami, A. Jaljuli, Study of the interactive effects of inorganic and biological fouling in RO Desalination Phase-A in: P.M. Williams (Ed.), 2007, pp. 132.

[40] T.R. Bott, Fouling due to corrosion, in: Fouling of Heat Exchangers, Elsevier Science B.V., Amsterdam, 1995, pp. 149-183.

[41] S. Krause, Fouling of heat-transfer surfaces by crystallization and sedimentation, International Chemical Engineering Journal, 33 (1993) 355-401.

[42] A.I. Rushdi, J. McManus, R.W. Collier, Marine barite and celestite saturation in seawater, Marine Chemistry, 69 (2000) 19-31.

[43] E. Alhseinat, R. Sheikholeslami, D. Glass, Effect of co-existing scaling salts and process pressure on the prediction of scaling propensity during full scale reverse osmosis treatment, in: 11th World Filtration Congress & Exhibition, Graz-Austria, 2012.

[44] K.S. Pitzer, G. Mayorga, Thermodynamics of electrolytes. II. Activity and osmotic coefficients for strong electrolytes with one or both ions univalent, The Journal of Physical Chemistry, 77 (1973) 2300-2308.

[45] E. Alhseinat, R. Sheikholeslami, A completely theoretical approach for assessing fouling propensity along a full-scale reverse osmosis process, Desalination, 301 (2012) 1-9.

[46] D. Hasson, R. Semiat, Scale Control in Saline and Wastewater Desalination, Israel Journal of Chemistry, 46 (2006) 97-104.

[47] R. Sheikholeslami, Y. Wang, H. Yu, Application of theoretical scaling potential index to predict onset of composite calcium carbonate and calcium sulfate fouling and crystal types and phases in seawater reverse osmosis treatment, in: B. Antizar-Ladislao, R. Sheikholeslami (Eds.) Water Production and Wastewater Treatment, Nova Publisher, 2011, pp. 269–284.

[48] R. Sheikholeslami, Composite scale formation and assessment by the theoretical Scaling Potential Index (SPI) proposed previously for a single salt, Desalination, 278 (2011) 259-267.

[49] J.W. Mullin, Crystallization, Elsevier Butterworth-Heinemann, 2001.

[50] S. He, J.E. Oddo, M.B. Tomson, The Nucleation Kinetics of Calcium Sulfate Dihydrate in NaCl Solutions up to 6 m and 90Â°C, Journal of Colloid And Interface Science, 162 (1994) 297-303.

[51] A.E. Nielsen, O. Sohnel, Interfacial tensions electrolyte crystal-aqueous solution, from nucleation data, Journal of Crystal Growth, 11 (1971) 233-242.

[52] O. Sohnel, Electrolyte crystal-aqueous solution interfacial tensions from crystallization data, Journal of Crystal Growth, 57 (1982) 101-108.

[53] I.J. Reznik, I. Gavrieli, J. Ganor, Kinetics of gypsum nucleation and crystal growth from Dead Sea brine, Geochimica et Cosmochimica Acta, 73 (2009) 6218-6230.

[54] J. Zhang, G.H. Nancollas, Influence of calcium/sulfate molar ratio on the growth rate of calcium sulfate dihydrate at constant supersaturation, Journal of Crystal Growth, 118 (1992) 287-294.

[55] Bansal.B, Müller-Steinhagen.H, D. Chen.X, Effect of Suspended Particles on Crystallization Fouling in Plate Heat Exchangers, Transactions- American Society of Mechanical Engineers Journal of Heat transfer, 119 (1997) 568-574

[56] A.C. Todd, M.D. Yuan, Barium and Strontium Sulfate Solid-Solution Scale Formation at Elevated Temperatures, SPE Production Engineering, 7 (1992) 85-92.

[57] F. Torrades, J.G. Raurich, Study of the coprecipitation of calcium, potassium, sodium and chloride with barium sulfate using atomic spectrometry and visible spectrophotometry, Analyst, 118 (1993) 197-200.

[58] Y.-H. Li, S.D. Crane, J.R. Coleman, A Novel Approach to Predict the Co-Precipitation of $BaSO_4$ and $SrSO_4$, in: SPE Production Operations Symposium, 1995 Copyright 1995, Society of Petroleum Engineers, Inc., Oklahoma City, Oklahoma, 1995.

[59] E. Playa , L. Rosell, The celestite problem in gypsum Sr geochemistry: An evaluation of purifying methods of gypsiferous samples, Chemical Geology, 221 (2005) 102-116.

[60] M. Amiri, J. Moghadasi, M. Pordel, The Effect of Temperature, Pressure, and Mixing Ratio of the Injection Water With Formation Water on Strontium Sulfate Scale Formation in the Siri Oilfield, Petroleum Science and Technology, 30 635-645.

[61] M.S.H. Bader, Nanofiltration for oil-fields water injection operations: analysis of osmotic pressure and scale tendency, Desalination, 201 (2006) 114-120.

[62] R. Sheikholeslami, H.W.K. Ong, Kinetics and thermodynamics of calcium carbonate and calcium sulfate at salinities up to 1.5 M, Desalination, 157 (2003) 217-234.

[63] E.P. Partridge, A.H. White, The solubility of calcium sulfate from 0 to 200C°, Journal of the American Chemical Society, 51 (1929) 360-370.

[64] B. C.W., D. F.W., Gypsum anhydrite equilibria in systems $CaSO_4$-H_2O and $CaCO_3$-NaCl-H_2O, The American Mineralogist, 58 (1973) 323 -331.

[65] H. L.A., The gypsum-anhydrite equilibrium at one atmosphere pressure, The American Mineralogist, 52 (1967) 171 - 200.

[66] J. Gilron, D. Hasson, Calcium sulphate fouling of reverse osmosis membranes: Flux decline mechanism, Chemical Engineering Science, 42 (1987) 2351-2360.

[67] M. Brusilovsky, J. Borden, D. Hasson, Flux decline due to gypsum precipitation on RO membranes, Desalination, 86 (1992) 187-222.

[68] W.-Y. Shih, A. Rahardianto, R.-W. Lee, Y. Cohen, Morphometric characterization of calcium sulfate dihydrate (gypsum) scale on reverse osmosis membranes, Journal of Membrane Science, 252 (2005) 253-263.

[69] Y.D. Yeboah, M.R. Saeed, A.K.K. Lee, Kinetics of strontium sulfate precipitation from aqueous electrolyte solutions, Journal of Crystal Growth, 135 (1994) 323-330.

[70] I.X. Malollari, P.G. Klepetsanis, P.G. Koutsoukos, Precipitation of strontium sulfate in aqueous solutions at 25°C, Journal of Crystal Growth, 155 (1995) 240-246.

[71] J.R. Campbell, G.H. Nancollas, Crystallization and dissolution of strontium sulfate in aqueous solution, The Journal of Physical Chemistry, 73 (1969) 1735-1740.

[72] D.F. Jacques, B.I. Bourland, A Study of Solubility of Strontium Sulfate, Society of Petroleum Engineers Journal, 23 (1983) 292-300.

[73] A.C. Todd, M. Yuan, Barium and Strontium Sulfate Solid Solution Formation in Relation to North Sea Scaling Problems, SPE Production Engineering, 5 (1990) 279-285.

[74] A.B.B. Merdhah, A.A.M. Yassin, Scale formation due to water injection in berea sandstone cores, Journal of Applied Science 9(2009) 3298-3307.

[75] M. Amer Bin, Inhibition of Calcium Sulfate and Strontium Sulfate Scale in Waterflood, SPE Production & Operations, 25 (2010) pp. 545-552.

[76] Y. Wang, R.Sheikholeslami, The effects of SO_4^{2-}/HCO_3^- molar ratio on the composite fouling of calcium sulfate and calcium carbonate in a seawater RO desalination unit, in: Chemeca2005, Institute of Engineers Australia, Brisbane, 2005.

[77] Y. Wang, R.Sheikholeslami, Co-precipitation of calcium sulfate and calcium carbonate in a seawater RO system, in: IDA World Congress on Desalination and Water Reuse, International Desalination Association, Singapore, 2005.

[78] R. Sheikholeslami, Mixed salts--scaling limits and propensity, Desalination, 154 (2003) 117-127.

[79] R. Sheikholeslami, M. Ng, Calcium Sulfate Precipitation in the Presence of Nondominant Calcium Carbonate: Thermodynamics and Kinetics, Industrial & Engineering Chemistry Research, 40 (2001) 3570-3578.

[80] T.H. Chong, R. Sheikholeslami, Thermodynamics and kinetics for mixed calcium carbonate and calcium sulfate precipitation, Chemical Engineering Science, 56 (2001) 5391-5400.

[81] M. Sudmalis, R. Sheikholeslami, Coprecipitation of $CaCO_3$ and $CaSO_4$, The Canadian Journal of Chemical Engineering, 78 (2000) 21-31.

[82] M. Sudmalis, R. Sheikholeslami, Precipitation and co-precipitation of $CaCO_3$ and $CaSO_4$, in: N.Epstein's 75th Birthday Symposium, Vancouver, B.C., 1998.

[83] K.G. Tay, L. Song, A more effective method for fouling characterization in a full-scale reverse osmosis process, Desalination, 177 (2005) 95-107.

[84] A. Antony, J.H. Low, S. Gray, A.E. Childress, P. Le-Clech, G. Leslie, Scale formation and control in high pressure membrane water treatment systems: A review, Journal of Membrane Science, 383 (2011) 1-16.

[85] J.C. Schippers, J. Verdouw, The modified fouling index, a method of determining the fouling characteristics of water, Desalination, 32 (1980) 137-148.

[86] A. Alhadidi, A.J.B. Kemperman, B. Blankert, J.C. Schippers, M. Wessling, W.G.J. van der Meer, Silt Density Index and Modified Fouling Index relation, and effect of pressure, temperature and membrane resistance, Desalination, 273 (2011) 48-56.

[87] D.R. van der Vaart, E.P. Stahel, An investigation of the modified fouling index as a test for plugging potential of pretreated seawater, Desalination, 68 (1988) 45-56.

[88] ASTMstandard, Standard Test Method for Silt Density Index (SDI) of water, in: D19.08 on membrane and Ion Exchange Materials, 2007.

[89] P.R. Puckorius, J.M. Brooke, A New Practical Index for Calcium Carbonate Scale Prediction in Cooling Tower Systems, Corrosion, 47 (1991) 280-284.

[90] T. Larson, R. Skold, Laboratory Studies Relating Mineral Quality of Water to Corrosion of Steel and Cast Iron., in: Illinois State Water Survey:Champaign, 1958, pp. 43–46.

[91] J.E. Oddo, M.B. Tomson, Scale Control , Prediction and Treatment Or How Companies Evaluate A Scaling Problem and What They Do Wrong, NACE International, 34 (1992).

[92] X.Zhao, X.D. Chen, A critical review of basic crystallography to salt crystallization fouling in heat exchangers, in: M.R. Malayeri, H.Mulller-Steinhagen, A.P. Watkinson (Eds.) International Conference on Heat Exchanger Fouling and Cleaning, Crete Island, Greece, 2011.

[93] A. Drak, K. Glucina, M. Busch, D. Hasson, J.-M. Laîne, R. Semiat, Laboratory technique for predicting the scaling propensity of RO feed waters, Desalination, 132 (2000) 233-242.

[94] S.F.E. Boerlage, M.D. Kennedy, I. Bremere, G.J. Witkamp, J.P. Van der Hoek, J.C. Schippers, The scaling potential of barium sulphate in reverse osmosis systems, Journal of Membrane Science, 197 (2002) 251-268.

[95] A. Al-Amoudi, R.W. Lovitt, Fouling strategies and the cleaning system of NF membranes and factors affecting cleaning efficiency, Journal of Membrane Science, 303 (2007) 4-28.

[96] A. Jawor, E.M.V. Hoek, Effects of feed water temperature on inorganic fouling of brackish water RO membranes, Desalination, 235 (2009) 44-57.

[97] S. Lee, C.-H. Lee, Effect of operating conditions on $CaSO_4$ scale formation mechanism in nanofiltration for water softening, Water Research, 34 (2000) 3854-3866.

[98] G.M.J. Subir Bhattacharjee, A Model of Membrane Fouling by Salt Precipitation from Multicomponent Ionic Mixtures in Crossflow Nanofiltration, Environmental Engineering Science, 19 (2004) 399-412.

[99] P.P. Mane, P.-K. Park, H. Hyung, J.C. Brown, J.-H. Kim, Modeling boron rejection in pilot- and full-scale reverse osmosis desalination processes, Journal of Membrane Science, 338 (2009) 119-127.

[100] R.Sheikholeslami, Scaling of process equipment by saline streams - challenges ahead, Water Science & Technology, 49 (2004) 201–210.

[101] R. Feistel, Extended equation of state for seawater at elevated temperature and salinity, Desalination, 250 (2010) 14-18.

[102] J.H.G. van der Stegen, H. Weerdenburg, A.J. van der Veen, J.A. Hogendoorn, G.F. Versteeg, Application of the Pitzer model for the estimation of activity coefficients of electrolytes in ion selective membranes, Fluid Phase Equilibria, 157 (1999) 181-196.

[103] A. Anderko, P. Wang, M. Rafal, Electrolyte solutions: from thermodynamic and transport property models to the simulation of industrial processes, Fluid Phase Equilibria, 194-197 (2002) 123-142.

[104] J.R. Loehe, M.D. Donohue, Recent advances in modeling thermodynamic properties of aqueous strong electrolyte systems, AIChE Journal, 43 (1997) 180-195.

[105] P. K.S., Activity Coefficients in Electrolyte Solutions, 2 ed., Boston, 1991.

[106] K.S. Pitzer, L.F. Silvester, Thermodynamics of electrolytes. 11. Properties of 3:2, 4:2, and other high-valence types, The Journal of Physical Chemistry, 82 (1978) 1239-1245.

[107] K.S. Pitzer, Thermodynamics of electrolytes. V. effects of higher-order electrostatic terms, Journal of Solution Chemistry, 4 (1975) 249-265.

[108] K.S. Pitzer, J.J. Kim, Thermodynamics of electrolytes. IV. Activity and osmotic coefficients for mixed electrolytes, Journal of the American Chemical Society, 96 (1974) 5701-5707.

[109] B. Hamrouni, M. Dhahbi, Thermodynamic description of saline waters -- Prediction of scaling limits in desalination processes, Desalination, 137 (2001) 275-284.

[110] N. Møller, The prediction of mineral solubilities in natural waters: A chemical equilibrium model for the Na-Ca-Cl-SO_4-H_2O system, to high temperature and concentration, Geochimica et Cosmochimica Acta, 52 (1988) 821-837.

[111] L.N. Plummer, D.L. Parkhurst, G.W. Fleming, S.A. Dunkle, A computer program incorporating Pitzer's equations for calculation of geochemical reactions in brines, in: Water-Resources Investigations Report, 1988.

[112] C. Monnin, A thermodynamic model for the solubility of barite and celestite in electrolyte solutions and seawater to 200°C and to 1 kbar, Chemical Geology, 153 (1999) 187-209.

[113] J.P. Greenberg, N. Møller, The prediction of mineral solubilities in natural waters: A chemical equilibrium model for the Na-K-Ca-Cl-SO4-H2O system to high concentration from 0 to 250°C, Geochimica et Cosmochimica Acta, 53 (1989) 2503-2518.

[114] R.T. Pabalan, K.S. Pitzer, Thermodynamics of concentrated electrolyte mixtures and the prediction of mineral solubilities to high temperatures for mixtures in the system Na-K-Mg-Cl-SO4-OH-H2O, Geochimica et Cosmochimica Acta, 51 (1987) 2429-2443.

[115] R.C. Phutela, K.S. Pitzer, P.P.S. Saluja, Thermodynamics of aqueous magnesium chloride, calcium chloride, and strontium chloride at elevated temperatures, Journal of Chemical & Engineering Data, 32 (1987) 76-80.

[116] C. Monnin, Thermodynamic Properties of the Na-K-Ca-Ba-Cl-H_2O System to 473.15 K and Solubility of Barium-Chloride Hydrates, Journal of Chemical and Engineering Data, 40 (1995) 828-832.

[117] C. Christov, N. Moller, Chemical equilibrium model of solution behavior and solubility in the H-Na-K-OH-Cl-HSO4-SO_4-H_2O system to high concentration and temperature, Geochimica et Cosmochimica Acta, 68 (2004) 1309-1331.

[118] C. Christov, N. Moller, A chemical equilibrium model of solution behavior and solubility in the H-Na-K-Ca-OH-Cl-HSO_4-SO_4-H_2O system to high concentration and temperature, Geochimica et Cosmochimica Acta, 68 (2004) 3717-3739.

[119] E.J. Reardon, D.K. Armstrong, Celestite ($SrSO_4$(s)) solubility in water, seawater and NaCl solution, Geochimica et Cosmochimica Acta, 51 (1987) 63-72.

[120] T. Kwee Guan, S. Lianfa, S.L. Ong, W.J. Ng, Nonlinear Behavior of Permeate Flux in Full-Scale Reverse Osmosis Processes, Journal of Environmental Engineering, 131 (2005) 1481-1487.

[121] C.R. Bouchard, P.J. Carreau, T. Matsuura, S. Sourirajan, Modeling of ultrafiltration: Predictions of concentration polarization effects, Journal of Membrane Science, 97 (1994) 215-229.

[122] F. Millero, D.R. Schrieber, Use of the ion pairing model to estimate activity coefficients of the ionic components of natural waters, American Journal of Science, 282 (1982) 1508–1540.

[123] F. Hajbi, H. Hammi, R. Solimando, A. M'nif, Evaporation of a reverse osmosis discharge studied by Pitzer model and solubility phase diagrams, Fluid Phase Equilibria, 307 (2011) 126-134.

[124] W.J. Hamer, Y.-C. Wu, Osmotic Coefficients and Mean Activity Coefficients of Uni-univalent Electrolytes in Water at 25°C, Journal of Physical and Chemical Reference Data 1(1972) 54.

[125] P. Walker, R. Sheikholeslami, Preliminary numerical study of $CaSO_4$ precipitation in laminar flows in pipes and slits under isothermal conditions, in: 9th APCChE Congress and Chemeca, Christchurch, New Zealand, 2002.

[126] P. Walker, R. Sheikholeslami, Assessment of the effect of velocity and residence time in $CaSO_4$ precipitation flow reaction, Chemical Engineering Science, 58 (2003) 3807–3816.

[127] P. Walker, R. Sheikholeslami, A Novel Approach, Development and Validation of a Comprehensive Model for Prediction of Fouling from Saline Waters, in: IDA, World Congress on Desalination and water Reuse, Paradise Islands, Bahamas, 2003.

[128] P. Walker, R.Sheikholeslami, Development and validation of an unsteady state numerical model of fouling within a crystalline system, in: Chemeca, Sydbey, Australia, 2004.

[129] R. Sheikholeslami, Strategies and future directions for systematic characterization of feed water and determination of scaling limits and rates for

process assessment and optimization, in: International Desalination Association World Congress, Bahrain, 2001.

[130] R. Sheikholeslami, T.H. Chong, M. Ng, Calcium carbonate and calcium sulfate co-precipitation--thermodynamics and kinetics, in: Chemeca, Newcastle, Australia, 1999.

[131] H. Yu, R.Sheikholeslami, W.O.S. Doherty, Preliminary study of the mechanisms of composite fouling of amorphous silica and calcium oxalate in sugar mill evaporators, in: 6th World Congress of Chemical Engineering, Melbourne, Australia, 2001.

[132] M. Christophe, The influence of pressure on the activity coefficients of the solutes and on the solubility of minerals in the system Na-Ca-Cl-SO_4-H_2O to 200°C and 1 kbar and to high NaCl concentration, Geochimica et Cosmochimica Acta, 54 (1990) 3265-3282.

[133] F.J. Millero, The effect of pressure on the solubility of minerals in water and seawater, Geochimica et Cosmochimica Acta, 46 (1982) 11-22.

[134] T.M. Church, Marine Minerals, In: Burns, R.G. (Ed.), Mineralogical Society of America, 6 (1979) 175-209.

[135] R. Dehairs, R. Chesselet, J. Jedwab, Discrete suspended particles of barite and the barium cycle in the open ocean, Earth Planet. Sci. Lett, (1980) 529–550.

[136] N. Liu, L. Li, B. McPherson, R. Lee, Removal of organics from produced water by reverse osmosis using MFI-type zeolite membranes, Journal of Membrane Science, 325 (2008) 357-361.

[137] P.L. McGuire, J.R. Chatham, F.K. Paskvan, D.M. Sommer, F.H. Carini, Low Salinity Oil Recovery: An Exciting New EOR Opportunity for Alaska's North Slope, in: SPE Western Regional Meeting, 2005.

[138] E. Alhseinat, R. Sheikholeslami, An Application for New Reliable Approach to Predict the Onset of Barite, Celestite and Gypsum Scaling during Reverse Osmosis Treatment for Produced Water, International Journal of Environmental Science and Development (IJESD), 2 (2011) 454-459.

[139] S. Lee, J.-S. Choi, C.-H. Lee, Behaviors of dissolved organic matter in membrane desalination, Desalination, 238 (2009) 109-116.

[140] A.J.B. Hennessy, G.M. Graham, The effect of additives on the co-crystallisation of calcium with barium sulphate, Journal of Crystal Growth, 237-239, Part 3 (2002) 2153-2159.

[141] Fofonoff, Millard, Algorithms for computation of fundamental properties of seawater, UNESCO Technical papers in marine science (1983).

[142] N.P. Fofonoff, Physical Properties of Seawater: A New Salinity Scale and Equation of State of Seawater, Journal of Geophysical Research, 90 (1985) 3332-3342.

[143] R. Chapman, A Sea Water Equation of State Calculator, in, The Johns Hopkins University Applied Physics Laboratory 2006.

[144] E. Alhseinat, R. Sheikholeslami, A Reliable approach for Barite, Celestite and Gypsum scaling propensity prediction during reverse osmosis treatment for produced water, in: b.E.E. International Proceeding of Chemical (Ed.) 2011 International Conference on Oil, Gas and Environment, ICOGE 2011, International Proceeding of Chemical, biological & Environmental Engineering, Cairo, Egypt, 2011, pp. 52-57.

Appendix A: Journals and conferences published papers

Two journal papers and two conference papers [43, 45, 138, 144] have been published viewing the work that is described in this thesis. The Desalination Journal paper [45] highlighted the new approach that has been established in this work. The International Journal of Environmental Science and Development paper has been published [138] after the paper presented in the International Conference on Oil, Gas and Environment, ICOGE 2011 [144], which was awarded the ”Excellent Paper” prize in the conference. These two papers highlighted the power of the new approach in its application to complex systems such as RO desalination of Oil and Gas waste water (referred to as Produced Water). The fourth paper [43] was presented in the 11th World Filtration Congress & Exhibition, Graz-Austria, 2012. This paper highlighted the effect of co-existing scaling salts and process pressure on the prediction of scaling propensity during full scale reverse osmosis treatment. A new paper is under preparation to highlight the findings of the experimental work that has been carried out in this PhD work.

A.1 Desalination Journal paper

Desalination 301 (2012) 1–9

Contents lists available at SciVerse ScienceDirect

Desalination

journal homepage: www.elsevier.com/locate/desal

A completely theoretical approach for assessing fouling propensity along a full-scale reverse osmosis process

Emad Alhseinat, Roya Sheikholeslami *

The University of Edinburgh, Edinburgh, EH9 3JL, UK

ARTICLE INFO

Article history:
Received 24 May 2011
Received in revised form 15 November 2011
Accepted 15 December 2011
Available online 9 July 2012

Keywords:
Desalination
Reverse osmosis
Fouling
Scaling
SPI
Crystallization
Precipitation

ABSTRACT

This paper aims to develop a completely theoretical approach for assessing scaling (crystallization/precipitation fouling) propensity through the previously proposed and tested theoretical index of 2nd author (*SPI*) within a Reverse Osmosis (RO) module. This approach will incorporate the local varying foulants' properties along membrane filtration channel into fundamental transport and conservation equations to achieve a unified and scientific assessment of the scaling potential. Thus, a high accuracy simulation of the local fouling propensity along a full-scale RO module will be obtained. This paper has overcome the challenge of determining and incorporating the locally varying concentration of foulants (and factors affecting it) and effect of concentration polarization to predict the local fouling propensity along the membrane channel. Also it has incorporated the only available theoretical index without any need for empirical parameters and/or constant Therefore, a fundamental more realistic description of fouling propensity and onset of fouling next to membrane along feed channel is developed and explained. Moreover, the effects of initial applied pressure, initial cross flow velocity, initial feed water salinity, clean membrane resistance and feed water temperature on fouling propensity and onset of fouling along the channel are investigated and discussed. Our suggested model is a very powerful tool that could help in the specific design of RO process as well as in simulations of the operating variables for optimization of RO system.

1. Introduction

Water desalination has gained widespread use as a consequence of potable water shortage all over the world, especially in the arid regions such as gulf region and in most of Middle Eastern countries. Reverse osmosis (RO) process is considered as one of the most important technologies for water desalination due to its lower cost compared to other desalination processes such as thermal distillation [1]. However, the operation of RO is plagued by fouling; in particular, it increases operational costs by raising energy consumption, lowering the lifetime of membranes, and increasing cleaning costs. Moreover, fouling adds extra cost to the capital expenses for the need to have additional: (1) pre-treatment units to minimize its effect, and (2) energy, materials (membranes and equipment) and chemicals required to combat fouling and add to carbon footprint which make the process not environmentally friendly. For these reasons fouling is considered a fundamental limitation to economic viability of membrane in water treatment [2]. However, to predict and mitigate fouling one first needs to consider and understand fouling science.

1.1. Fouling science and fundamentals

Fouling is defined as the accumulation of unwanted materials at an interface or a transfer surface "at membrane surface in case of RO and other membrane processes". Fouling phenomena has been the subject interest since early 1970s by prominent scientists in the field such as Epstein [3], Watkinson [4] and Taborek [5,6] and in fact Taborek [5] highlighted its complexity and referred to fouling "science" or "art". In 1981, Epstein in his scientific pioneering 5×5 matrix of fouling "types" and "stages" paper [3] was the first to put a scientific basis for describing fouling. In 1999, Sheikholeslami after years of having worked in different types of fouling on both membranes and thermal units published her review paper [7] introducing a new type of fouling to the Epstein's categories. Later, Sheikholeslami greatly expanded Epstein's pioneering work and she scientifically divided fouling to a 6×6 matrix of fouling types and stages as described elsewhere in detail in her monograph which is on science of fouling in membrane and thermal units [8].

The first step in fouling mitigation is to determine the fouling propensity of feed water. Research studies usually consider a single foulant or a single fouling mechanism and they do not take into account the interactive and hydrodynamic effects. Majority of simulations mostly treat fouling only as a resistance and like a black-box and without considering its science and simply take flux decline as a measure of fouling. Tay and Song [9] in fact discusses that in some full-

* Corresponding author.
E-mail address: roya.sheikholeslami@gmail.com (R. Sheikholeslami).

0011-9164/$ – see front matter © 2011 Published by Elsevier B.V.
doi:10.1016/j.desal.2011.12.014

scale RO process it is shown that flux does not decline with fouling occurrence and hence they state that using permeate flux decline as a measure of fouling provides erroneous results for RO fouling assessment. The inaccuracy and inadequacy of simply using flux as a measure of fouling have been scientifically explained [7–9]. In fact, fouling build up could under certain conditions even temporarily increase flux as explained scientifically [8] and seen in practice [10]. As such the commonly used black-box approaches of considering fouling only as a resistance are generally inapplicable to real conditions. Moreover, the current practice for assessing the fouling propensity "irrespective" of the "membrane type" is inadequate and inappropriate as there are different mechanisms for passage in different membrane processes [11]. The proper measure, assessment, prediction and mitigation of fouling need considering, understanding and incorporating fouling science and membrane types as shown and discussed by the 2nd author elsewhere in detail [8].

In terms of crystallization fouling (commonly referred scaling) as discussed elsewhere [8,12–15] most of the fouling models that are proposed expand the black-box approach and do not consider the effect of varying hydrodynamics on fouling mechanisms and process within the equipment. Scaling propensity by sparingly soluble salts in any equipment could be more accurately simulated through incorporating the varying local flow, flux and fouling mechanism which would then allow assessment of fouling along a channel as shown using CFD modeling [8,12–15] for fouling by sparingly soluble salts.

1.2. Commonly used approaches

Fouling in membranes is not as historical as it is in other types of process equipment for the fact that membranes are relatively newer processes than others. Presumably for this reason majority, if not almost all, of models and simulations on membrane fouling treat fouling without any consideration to fouling science and purely as a resistance. Further within a module these approaches assume a uniform flow properties and fouling rate throughout the module and over the membrane surface while in a long a membrane channel system variables and parameters change substantially along the channel. Ignoring the science of fouling and making these further assumptions would render the existing models unrealistic in assessment of fouling in a full-scale RO process. Other papers consider flux decline as a "measure" of fouling which as discussed previously is not a "measure" but a "symptom" of fouling – flux decline could have other causes and also even fouling at times could temporarily increase flux.

Tay and Song [9] based on some operational reports criticized use of flux as a measure of fouling and suggested use of a filtration coefficient defined by a collective net pressure driving force describing the whole system with a single value. They suggested this approach for fouling characterization for two reasons: (1) for being a collective parameter and not changing as resistance along the channel, and (2) for resistance being considered practically impossible to measure. Their filtration coefficient was a collective parameter related to distribution of the membrane resistance to examine the effect of membrane fouling on full scale RO process. They obtained the filtration coefficient by the average permeate flux in a RO process. They interestingly initially criticized the use of flux for fouling characterization but then they proposed to use permeate flux to obtain collective filtration coefficient for fouling characterization. Also their filtration coefficient is a collective parameter and thus ignores very important details such as the fouling type and the interactive effect between the foulants which are very important on fouling mitigation. Their approach to flux decline concept is correct but the proposed filtration coefficient has the same inadequacy as other fouling measures and treats fouling as a black box ignoring its science and also incorrectly considers it as a uniform phenomenon along the membrane module. Their approach is actually based on an earlier work [16] for global performance limitation of RO in which Song et al. [16] showed the importance of thermodynamics and equilibrium in the performance of full scale RO. Tay and Song [9] thus very importantly highlighted the fact that flux decline is not a method to be used for characterization of fouling – as mentioned previously flux decline is a symptom and can have other causes.

For crystallization fouling the normal practice is to use empirical indices to assess the fouling potential of feed water by sparingly soluble salts – as shown and discussed [11] these empirical relationships are not suitable for membrane processes and also nanofiltration (NF) and RO membranes should not be treated identically. These empirical indices have been discussed in detail elsewhere [17] and most of which were developed in 1950s and 1960s and not for membrane processes. For example as discussed in detail [17] even the commonly used indices for calcium carbonate such as Langelier Saturation Index (LSI) [18], Stiff-Davis Stability Index (S & DSI) [19], Ryznar Stability Index [20], and Puckorius Scaling Index [21] are mostly empirically based. Even as discussed elsewhere [8,11] the LSI and S & DSI, which use the theoretical concept of saturation, include significant simplifications and empirical relationships in their derivation and do not reflect the high salinities, the interactive effects and the operational conditions within the membrane module. Therefore, it is inadequate to apply these indices to predict what may happen in the membrane desalination module train and their predictions are incorrect. In fact Mane et al. [22] have recently developed a mechanistic predictive model to simulate the rejection of boron by a spiral wound reverse osmosis (RO) membrane element under varying water quality and operating conditions. Their paper has no relevance to fouling. However, their paper highlights use of alkali at different stages for boron removal and therefore indirectly to the inadequacy of empirically based indices that do not have the capacity to assess varying conditions and water chemistry along the membrane module; thus, there is a further reason for having a theoretically based index such as Sheikholeslami's previously proposed theoretical index [11,17] that has the capability to incorporate water chemistry for assessing fouling by sparingly soluble salts at any location within the module with further capability of taking into account also membrane specific ion passages effects along the module.

1.3. Our approach

This paper is based on a completely theoretical approach for assessing the scaling propensity within a full-scale RO desalination module.

Our approach is to incorporate local concentrations and local flow properties into Sheikholeslami's previously proposed theoretical index [11,17] to assess local scaling potential of sparingly soluble salts within RO module.

Our approach considers science of fouling, chemistry, and thermodynamics and combines those with principles of osmosis, mass transport across the membrane and conservation of mass to assess the local scaling potential of the sparingly soluble salt of concern within the RO module and on the membrane surface. It results in a simulated model for scientifically and theoretically predicting onset of crystallization fouling within RO module.

Our suggested model is a very powerful tool that could help on the specific design of RO process as well as in simulations of the operating variables for optimization of RO system.

2. Content

The intent is to incorporate the effects of locally varying concentrations and that of the concentration polarization to predict the fouling propensity along the length of membrane channel for sparingly soluble salts. Since the local foulant concentration and the concentration polarization vary along a membrane channel, scaling propensity will not be uniform along the channel. These points are briefly

discussed in the previous section as more in-depth discussions are beyond the scope of this paper and readers are referred elsewhere [8] for full discussion of fouling. Thus, the fouling propensity at any location along the membrane channel can be predicted only by substituting the local values.

Also, the normal practice in modeling is to use concentrations; however, to take into account for high salinity effects in RO desalination, as initially suggested and used [11,23] the activities will be used and the specific ion interactive forces are taken into account.

The potential for onset of crystallization fouling will be determined using Sheikholeslami's theoretical index [11,17] which its accuracy was previously tested experimentally in membrane modules and reported elsewhere [24–27]. This theoretical index which she referred to as theoretical *SPI* is developed using thermodynamic principles including the use of Gibbs free energy concept and will be briefly discussed in Section 2.1.

The membrane transport and mass conservation principles, which were also used by Song et al. [9,28,29], will be used to predict the variations of local variables and parameters in a long membrane channel and will be briefly discussed in Section 2.2.

Sections 2.3 and 2.4 respectively include confidence of our model, and the model simulations of results and discussions.

2.1. Theoretical SPI

Sheikholeslami suggested and tested [11,17] her theoretical index based on a fundamental and unified approach for assessing the scaling potential of any salt by incorporating the ion activities and principles of thermodynamics including Gibbs free energies as introduced above and will be described below in Eqs. (1)–(8). In these equations the ions constituting the sparingly soluble salts (Y_cZ_a) are represented by "*Y*" and "*Z*", and "*c*" and "*a*" are respectively the number of cations and anions in one mole of electrolyte in the following equation showing the chemical reaction for precipitation/crystallization of the salt; $e+$ and $e-$ are the valences for cation and anion, respectively.

$$cY^{e+} + aZ^{e-} \underset{Ksp}{\leftrightarrow} Y_cZ_a(s) \tag{1}$$

Sheikholeslami [23,30–36] through experimental observations noticed that the thermodynamic solubility (*Ksp*) for the precipitation/crystallization reaction changes significantly based on presence of other components and the conditions. She then concluded that for any given sparingly soluble salt the *Ksp* of precipitation varies depending on the solution composition and that even presence of trace materials had significant effects. That leads to her hypothesis [30,37,38] that since the "structure" of precipitate is dependent on and varies in presence of trace materials and therefore its *Ksp* of the precipitate must vary based on the following thermodynamic principles and therefore the concept of "constant" solubility product even in the presence of trace compounds does not hold. As shown in Eq. (2) when the "product" changes even if the reactants are under the same conditions, the Gibbs free energy of the reaction $\{\Delta_{reac}G^{\Phi}\}$ shown in Eq. (3) will change and hence {*Ksp*} of reaction would change.

$$\Delta_{reac}G^{\Phi} = \left(\Delta_fG^{\Phi}\right)_{products} - \left(\Delta_fG^{\Phi}\right)_{reactants} \tag{2}$$

$$-RT\ln(Ksp) = \Delta_{reac}G^{\Phi} \tag{3}$$

Therefore, she concluded [23,30,33,35,37,38] that the onset of precipitation varies and then proposed her theoretical index represented by Eq. (4), tested it under controlled experimental conditions for calcium carbonate and reported its accuracy [17].

$$SPI = \log(IAP/Ksp) = \log\left(IAP/EXP\left(-\Delta_{reac}G^{\Phi}/RT\right)\right) \tag{4}$$

Gibbs free energy of reaction ($\Delta_{reac}G^{\Phi}$) according to Eq. (2) is related to the standard Gibbs free energies of formation (Δ_fG^{Φ}) and *IAP* is the ion activity products.

Sheikholeslami [11,17,23,33,35–37] then used thermodynamic principles and relationships and proposed the following for RO desalination: (1) Eq. (5) [17] to incorporate the effect of temperature on the Gibbs free energy; (2) Eq. (6) [11,23,33,35–37] to determine ion activity products; and (3) Eq. (7) [11,17,23] to incorporate high ionic strengths and salinity effects in RO desalination through the effects of ionic strength as well as the electrostatic effects and short and long range ion interaction forces and Pitzer relationships which is one of the most comprehensive ones.

$$-\mathrm{RT}\ln(Ksp) = \Delta_{reac}G^{T} = \frac{\mathrm{T}}{298.15}\Delta_{reac}G^{298} + \Delta_{reac}H^{298}\left(1-\frac{\mathrm{T}}{298.15}\right) \tag{5}$$

$$IAP = \left\{Y^{e+}\right\}^c\left\{Z^{e-}\right\}^a = \gamma_{Y^{e+}}\left[Y^{e+}\right]^c\gamma_{Z^{e-}}\left[Z^{e-}\right]^a \tag{6}$$

$$\gamma = \mathrm{f}(\text{salinity and concentration of species}) \tag{7}$$

In the above equations R is the gas constant (1.987×10^{-3} kcal/mol.K), and T is the temperature (*K*) which significantly affects temperature Gibbs free energy; standard Gibbs free energies are at 298 K, (ΔH_{reac}) is the enthalpy of reaction, the curly bracketed parameters are ion activities and related to concentrations by activity coefficients (γ) which are less or maximum unity.

Therefore, Sheikholeslami's theoretical index as shown in Eq. (4) could be used to assess potential for scale formation of a given salt such as that shown in Eq. (1). The *SPI* is related to the super saturation [11] which is defined by Eq. (8):

$$SS = \{IAP/Ksp\}^{\frac{1}{c+a}} = \left\{IAP/EXP\left(-\Delta_{reac}G^{\Phi}/RT\right)\right\}^{\frac{1}{c+a}}. \tag{8}$$

It is reported [11] that the above procedure is suitable, applicable and accurate also for very high salinities suitable for RO desalination. The Pitzer model which is used in calculation of activity coefficients is assessed to be valid for concentrated electrolyte mixtures of up to 6 M [39].

The challenge arises when mixed precipitates are formed and for which the Gibbs free energy is different from that of a pure compound [23,30–36] and as such the Gibbs free energy of reaction and the thermodynamic solubility product of the pure precipitate formation is different from that in presence of impurities and also in co-precipitating systems. A theoretical approach to calculate the thermodynamic solubility product in co-precipitating systems was proposed [8] and is under development through advances in computational chemistry.

In this project the Gibbs free energy of reaction and hence thermodynamic solubility product for precipitation of pure salt of $CaSO_4$ is used. Since the local concentration of foulants (ions of sparingly soluble salts in this case) and the concentration polarization vary along a membrane channel, fouling propensity will not be uniformly distributed along the channel. The work in this paper incorporates the locally varying foulants' concentration and concentration polarization on the *SPI* calculation to have accurate simulation and description for the onset of scaling propensity along the membrane channel. Thus, the scaling propensity at any location on membrane surface is calculated using the local values in Eqs. (9)–(15) and substituting our representative scaling ions (Ca^{2+} and SO_4^{2-}) in Eq. (4).

2.2. Modeling for variation of concentration along membrane channel

In order to calculate the change in local scaling propensity with position there is a need to have a correlation describing the variation of concentration of scaling salts as function of location along the membrane channel. The real RO feed membrane channel could be described as seen in Fig. 1 and it consists of two parallel membranes within which there is a feed spacer and the channel has a symmetric plane in the middle of it. For the ease of depiction, the feed spacer is not shown in Fig. 1. Thus, all the relevant transport and conservation equations for the RO feed channel, like any other symmetrical channel, are solved for half the channel where flux at the symmetrical boundary is zero. Some authors [28] use half of the channel and refer to it as a filtration channel with a permeate wall on one side and an impermeable wall on the other side which in our opinion causes problems for novices thinking that the real RO feed channel is like the small experiment flat sheet modules that in fact are half of the real RO feed channel. As such, we depict a simplified representation of a real RO feed channel. The aim of this paper as highlighted previously is to incorporate theoretical principles and thermodynamics of crystallization fouling with principles of membrane transport and conservation along the RO channel to predict the scaling propensity and onset of the scale formation along the module. Thus, this paper does not intend to include the effect of time and scale build-up with time within the RO channel. As such the steady state simulations are discussed in this paper. This prediction is very important for process optimization and design of both process and equipment predicting scaling propensity along the module so proper measures could be taken to minimize the onset of scale formation in the module. The information in this paper is required for preventative measures – it is a mitigation technique.

As fouling layer build-up is a transient process, the effect of time and the development of fouling layer will be through incorporation of temporal coordinate and that information is required for determining how long the piece of equipment can run under the fouled condition before it is cleaned or replaced or what factors slow down the fouling layer thickness. The temporal effects has been previously incorporated by our research team [8,12–15] by solving the partial differential equations for another fouling set up and system and can easily be incorporated in this model in the future.

The membrane transport and continuity equations were used in our model and also some of them were used by Song et al. [9,28,29] to obtain the variations of concentrations along the membrane feed channel are discussed below.

Concentration of any given species at location x along a membrane channel is obtained by Eq. (9) through applying mass conservation principle on that species.

$$c(x) = \frac{1}{u(x)H}\left[c_0 u_0 H - (1-r)\int_0^x c(\xi)v(\xi)d\xi\right] \tag{9}$$

In the above equation, $u(x)$ is the cross flow velocity at location x along the channel; H is the height of the membrane channel; u_0 is the feed flow velocity; c_0 is the species concentration at the feed channel entrance; v is permeate flux; r the fraction species rejected by and not passed through membrane; and ξ is the dummy integration variable. The two terms in the square brackets are respectively the total amounts of a given species entering the membrane feed channel and that passing through the membrane to the permeate channel.

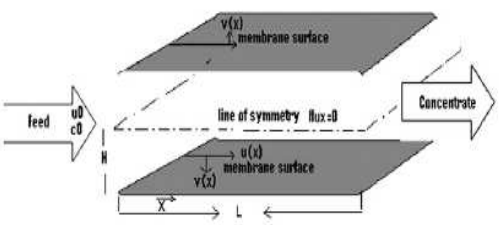

Fig. 1. Simplified schematics of real RO membrane channel.

It should be noted that the effect of concentration polarization is "implicitly" taken into account in Eqs. (13)–(14) by using the local species concentration at the membrane surface which is obtained through Eq. (10). With the small channel height and the spacers used a complete depolarization (uniform distribution across the feed channel height) prevails. However, for the purpose of completeness and accuracy Eq. (10) is used, where $c_w(x)$ is the concentration on membrane surface at location x, to check and confirm the value of concentration polarization within the system.

$$c_w(x) = c_0 + \exp(-v(x)H/D)\frac{rc_0}{uH}\int_0^x v(\xi)d\xi + \frac{rc_0 v(x)}{uD}\int_0^x v(\xi)d\xi \tag{10}$$

The relationship for local wall concentration (Eq. (10)) was also used elsewhere [40]. The effect of undisturbed concentration polarization in a channel filled with spacers is described as a combination of two extreme cases, namely the undisturbed concentration polarization and complete depolarization (uniform distribution across the channel height). With the introduction of a polarization factor for the degree of concentration polarization the wall concentration (Eq. (10)) is obtained.

In this paper the local salt concentration was calculated using both Eqs. (9) and (10) and results confirmed that within our system there was complete depolarization. All the concentration related values used in the following equations refer to the values at the wall.

Similarly, the application of mass conservation principle for water results in the following expression for cross flow velocity at any location along the membrane channel:

$$u(x) = u_0 - \frac{1}{H}\int_0^x v(\xi)d\xi. \tag{11}$$

The trans-membrane static pressure $(p_f - p_p)$ at any location is defined by Δp. The static pressure in the feed channel (p_f) changes substantially from that at entrance (p_{f0}) to that at any location along the feed channel $(p_f(x))$ due to frictional losses; but the changes in the static pressure in the permeate channel (p_p) is negligible and hence p_p is assumed constant along the channel. Therefore $(\Delta p_0) - (\Delta p(x))$ which is the change in the trans-membrane static pressure up to a point along the channel would have the same value as the frictional losses (Δp_{fric}) along the feed channel between the two points. Hence $\Delta p(x)$ is defined by Eq. (12) where the parameter in the bracket is (Δp_{fric}) up to location x along the feed channel due to friction by the membrane surfaces and spacers [41].

$$\Delta p(x) = \Delta p_0 - \left[\frac{12k_{spacer}\eta}{H^2}\int_0^x u(\xi)d\xi\right] \tag{12}$$

Finally, from the principles of membrane transport, the permeate flux at location x along the membrane feed channel is given by Eq. (13) where R_m is membrane resistance to water passage; $\Delta\pi$ is the osmotic pressure difference and is calculated by Eq. (14); α is relating the osmotic pressure to concentration through application of van't Hoff formula through Eq. (15); R is the universal gas constant; T is the absolute temperature; Mw is the molecular weight of the solute; and Θ is Pitzer osmotic coefficient.

$$v(x) = \frac{\Delta p(x) - \Delta\pi(x)}{R_m} \tag{13}$$

$$\Delta\pi(x) = \alpha\Delta c(x) \tag{14}$$

$$\alpha = \frac{\Theta RT}{Mw} \quad (15)$$

It should be noted that α is function of stream composition and the effect of the variation of feed composition should be taken into account. This has been included in this paper by using Pitzer equation and obtaining osmotic coefficient [42] as function of local stream concentration.

As discussed in the previous section, local scaling propensity is determined through solving Eqs. (9)–(15) for scaling species concentration next to membrane wall along the filtration channel. These equations will be solved initially considering salinity or total dissolved solid (TDS) as major parameter representing all dissolved species (scaling and non-scaling salts) which exist in the solution. Thus the calculated permeate velocity, cross flow velocity and transmembrane pressure as function of salinity will be used to find the change of each scaling salt species concentration along the filtration channel. Here in this paper as the aim is just to describe the distribution of scaling propensity along filtration channel immediately before the onset of scaling/precipitation reaction, the change of scaling salt species concentration due to actual formation of foulant does not need to be taken into account; however, in expanding the current model to transient condition and obtaining the build up of the fouling layer that change will be incorporated as well.

2.3. Confidence of the simulation

We used the following finite difference solution procedure to solve Eqs. (9)–(15). The membrane channel was divided into n segments of equal intervals represented by Δx. The start of the first segment and the end of the last segment are respectively denoted as 0 and $n+1$. Accordingly, the concentration, cross-flow velocity, driving force pressure and permeate velocity in segment i, where it ranges from 1 to n, are denoted as c_i, u_i, Δp_i and v_i respectively. The simulation parameters can be chosen for a given specific operating conditions and from the manufacturers' specifications for modules as shown in Table 1. In our simulations we used the channel RO parameters as those tested previously [9,28,29,40] to ensure we could compare our results for local permeate flux (Fig. 2) and local salinity (Fig. 3) with previous work [29]; our results shown here in Figs. 2 and 3 are identical to their simulations [29] shown in their Figs. 4 and 6 at the start (t = 0 time, day zero).

We conducted the convergence tests to find the optimum mesh size (the intervals and number of segments). The standard (default) local error control method in MATLAB® was used to monitor the error at each step; this method sets the relative tolerance as 0.1% (1e − 3) and if the local error at the end of each step is greater than the threshold acceptable error, then the solver reduces the step and reiterates. It should be noted that we have carefully tested the accuracy and rigor but rigor is of secondary importance in the current paper as the novelty of the paper and hence "primary" importance is to introduce our fundamental and realistic approach of using the *only* available theoretical index within the RO desalination module. When the rigor and accuracy of the simulations are of the "secondary" importance such as our case the confidence and convergence tests are not usually conducted as for example in the case Song et al. [16] when their main aim was to show the effect of thermodynamics on the performance limitation of the full-scale reverse osmosis process.

Table 1
Parameter values for model simulations.

Length of RO system, L (m)	6
Channel height, H (m)	7×10^{-4}
Applied (pump) pressure, p_0 (Pa)	5.516×10^{6}
Feed salinity (mg/l)	10000
Cross flow velocity at entrance,(m/s)	0.1
Membrane intrinsic resistance,(Pa s/m)	1.8×10^{11}
Number of elements along RO system	300
Temperature, °C	25
Water viscosity at 25 °C, Pa.s	0.89×10^{-3}
Friction coefficient due to spacers	5
Initial Ca^{2+} concentration, ppm	600
Initial SO_4^{2-}, ppm	1000

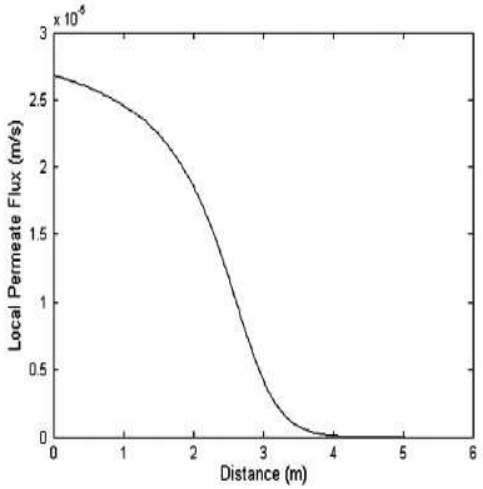

Fig. 2. Local permeate flux (m/s) change along the membrane filtration channel.

2.4. Simulation results and discussion

Numerical simulations have been conducted to investigate the onset scaling propensity along a full-scale RO process under various conditions. Table 1 shows the given conditions for the module and the feed water parameters used in our simulations; however, other parameters applicable to other cases could also be used.

2.4.1. Scaling propensity on a membrane along its channel

The theoretical index gives a conservative estimate for assessing onset of the scaling potential. If *SPI* is negative the scale will not form; when it is zero the system is at equilibrium but in certain circumstances may have the potential to form – behavior at equilibrium is discussed in detail elsewhere[8,11,17,37]. At the point where the *SPI* becomes positive the sparingly soluble salts certainly have

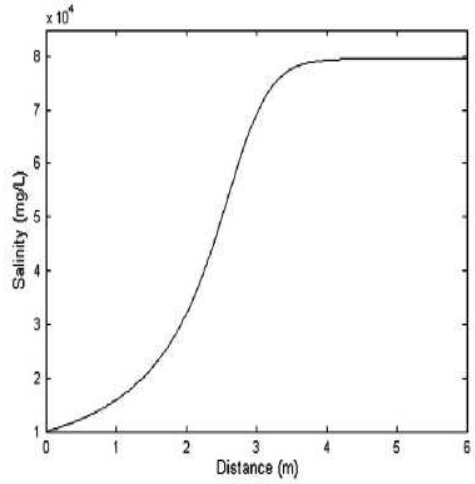

Fig. 3. Local salinity along 6 m membrane filtration channel.

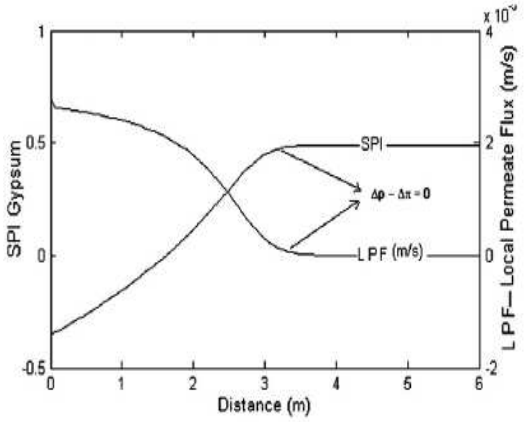

Fig. 4. Local *SPI* along 6 m membrane filtration channel and local permeate flux (LPF) (m/s) along the channel.

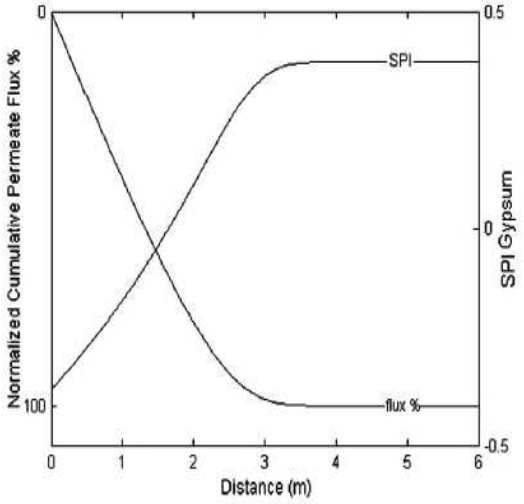

Fig. 5. Normalized cumulative permeate flux and local *SPI* along 6 m membrane filtration channel.

"potential" to form scale [11]. These results focus on the potential and the thermodynamic aspects. The matters related to scale thickness development and kinetics are the transient aspects which, as discussed previously, will be demonstrated later.

Fig. 4 shows the effects of local permeate flux (LPF) along the 6 m length of module on the local potential for scale formation (local *SPI*). Firstly as expected, it shows that the local flux declines due to concentration effects, and hence increases in the osmotic pressure, along the channel. At about 3.6 m point along the channel, pressure driving force ($\Delta P(x) - \Delta\pi(x)$) between the feed and permeate and hence LPF would approach zero where the desalination system reaches thermodynamic equilibrium. The local *SPI* rises as the LPF drops and reaches an asymptotic value of 0.5 at the point (about 3.6 m) where there will no longer be any permeation in the channel as the system is controlled thermodynamically which is what Song et al. reported [16] actually takes place in practice. The local *SPI* at the feed inlet has a value of −0.39 and rapidly increases but remains negative for another 1.65 m length within which length there is no potential for scale formation. From 1.65 m onwards the local *SPI* has positive value and there is potential for scale formation — in fact with the presence of spacers and with the magnitude of surface [8] in contact with the solution this potential is very strong. The increase in *SPI* is very rapid initially but slows a bit gradually till it reaches an asymptotic value of 0.5 at 3.6 m. Permeation affects the local *SPI* in two different ways: (1) by concentrating the sparingly soluble (scaling) species concentrations which increases the potential for fouling; and (2) by concentrating the non-scaling (NaCl, etc.) species that their concentration reduces the potential for scale formation [11,23]. The second effect is minor in comparison to the first one; however, it has taken into account in the simulations. We again stress that these results are to show the onset of local *SPI* and not the issues related to actual precipitation and "formation" of any fouling layer.

Fig. 5 shows the local *SPI* and the normalized "cumulative" flux, which is an important parameter for the overall performance of RO process, along the module. Fig. 5 shows that the cumulative permeate flux reached its maximum value within the first 3–4 m and the rest 2–3 m of the permeation channel will suffer a severe scaling since the *SPI* is at its highest value.

2.4.2. Effect of feed water salinity on scaling propensity

It is important to show the effect feed water salinity on local *SPI* as RO desalination is applied to lightly brackish to seawater and also industrial waters some of which are even much more saline than seawater. Also as briefly discussed previously and in detail elsewhere [11,17,23,37] presence of saline non-scaling (such as NaCl) species *reduces* the scaling potential of a given scaling species by increasing the solubility limits and also it affects nucleation and kinetics of precipitation.

Fig. 6 shows local *SPI* along the module for various feed salinities. As discussed in previous sections the theoretical index incorporates salinity effects on thermodynamics and hence the local *SPI* for various feed waters; its purpose is not to cover all the salinity ranges for RO desalination but to show the significance of salinity on local *SPI*.

It should be noted that in Fig. 6 the only variable between the curves is the concentration on "non-scaling" species; the concentration of scaling species and other parameters are the same in all the curves on the figure. It is shown as expected that at higher feed water salinities, the lower would be the local scaling propensity *at a given point* along the membrane feed channel. Also, the rate of increase in local *SPI* along the channel decreases with increasing the feed salinity.

In comparing these curves it should be noted that the feed salinity affects the onset of local *SPI* along the channel via two different routes: (1) through thermodynamics and kinetics of precipitation as discussed above; and (2) through changes in the driving force ($\Delta p(x) - \alpha c(x)$). Reduction in permeate flux for a given feed scaling salt concentration would reduce the "concentration factor" of the scaling ions along the length of feed channel and hence the scaling propensity (*SPI*) [24–27].

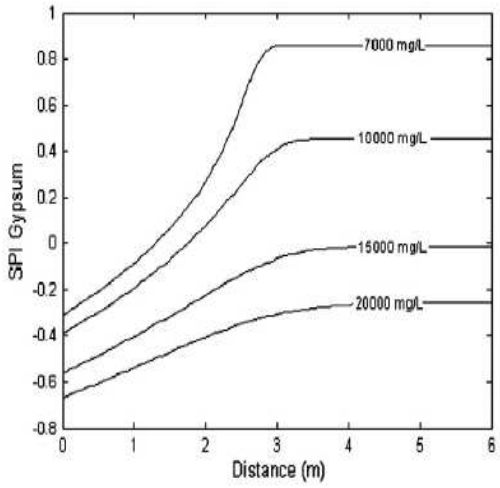

Fig. 6. Effect of feed water salinity on local *SPI* along 6 m membrane channel.

Fig. 6 is in accordance with theory and experimental observations showing that for a given concentration of scaling species and non-scaling species, the *SPI* will increase as the concentration of scaling ions increase along the channel in parallel with total salinity increase; this will continue until the osmotic pressure equals the applied pressure as explained before. However, the effect non-scaling species concentrations (salinity) for a given concentration of scaling species is governed by thermodynamics as discussed above.

2.4.3. Effect of membrane resistance on scaling propensity

Clean membrane resistance is a characteristic of the RO membranes and various ranges are available in the market. Fig. 7 depicts a comparison of two membranes and their different effects on local *SPI* along the membrane channel for otherwise identical conditions. One curve is for the membrane used in our simulations (with clean membrane resistance of 1.8×10^{11} Pa s/m which is one of the currently available in the market) and the other is a typical one used for RO process 10–20 years ago (8×10^{11} Pa s/m).

It can be seen from the figure that under otherwise identical conditions the scaling propensity is higher for the currently used membranes which have less specific resistance. This is due to higher local flux giving rise to a higher concentration factor for the more permeable membrane. As seen higher permeability values which are favored by industry and particularly are applicable in many brackish water systems that increase the potential for the onset of scaling.

2.4.4. Effect of initial cross flow velocity on scaling propensity

Fig. 8 shows the effect of various initial cross flow velocities (feed mass flow rates) on the local *SPI* along 6 m permeation channel. Cross flow velocity affects onset of fouling for several reasons [8] and, under otherwise identical conditions, the higher it is the lower becomes the potential for fouling. For example in our simulations, under otherwise identical conditions, when the feed water velocity is doubled from that of Table 1 (0.1 m/s) water could travel about 3.6 m, more than about twice the previous length (about 1.3 m), without having any potential for scale formation. This observation could be used as a reference to give the safe operational limit.

As mentioned above, the curves on the figure are for otherwise identical conditions.

2.4.5. Effect of applied pump pressure on scaling propensity

One of the operating parameters that affect the scaling potential and severity is the trans-membrane pressure and Fig. 9 shows simulated results for various pump pressures under otherwise identical conditions. As seen at highest applied pump pressure the membrane is more prone to scale formation. Also our simulations show that onset of local *SPI* along the module is moved downstream at lower pump pressures. Thus, theoretical assessment of the scaling potential

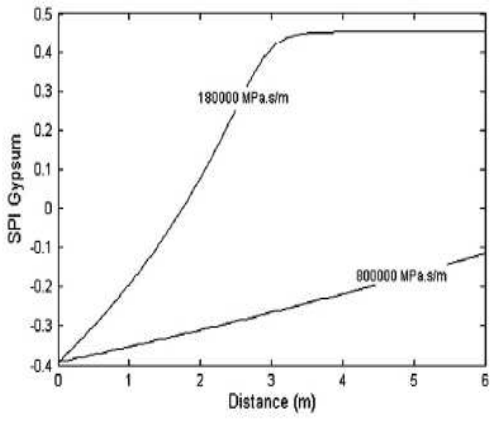

Fig. 7. Effect of clean membrane resistance on local *SPI*.

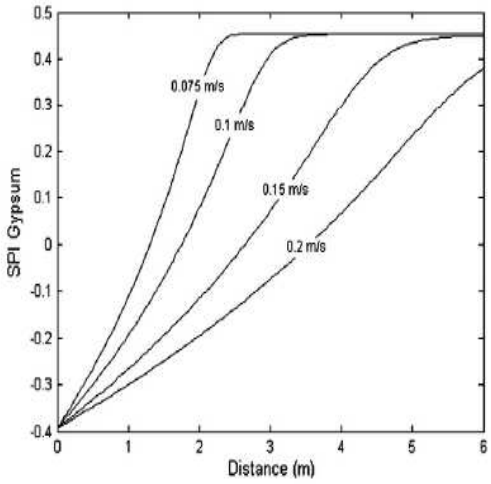

Fig. 8. Effect of initial cross flow velocity on local *SPI* along 6 m membrane feed channel.

enables one to assess and set operational parameters within safe limits.

2.4.6. Effect of feed water temperature on scaling propensity

Fig. 10 shows the effect of feed temperature on local *SPI* and along 6 m feed channel. The thermodynamic solubility (*Ksp*) was calculated using Eq. (5) for both temperatures; the effect of temperature on density and viscosity was also taken into account. Increasing temperature from 25 °C to 70 °C did not appreciably affect the scaling propensity. Gypsum is an inverse solubility salt and the figure shows that at any given point along the channel, the scaling propensity is slightly higher for the simulation at higher temperature. In these simulations a given membrane was used for all comparative assessments; therefore further attention should be given to the effect of high temperatures on the membrane structure and performance and also their interrelation with the scaling propensity.

3. Conclusion

This paper uses and incorporates the only available theoretical index (which was previously proposed and its accuracy tested) for fouling (scaling) by sparingly soluble salts with the fundamental equations of transport and continuity to reliably simulate and assess onset of scaling propensity locally on the membrane surface along a full-scale RO membrane. This reliable simulation is fundamentally based and does not

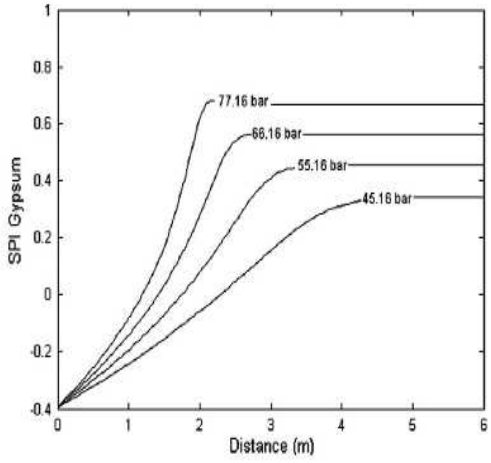

Fig. 9. Effect of initial applied pressure on local *SPI* along 6 m membrane channel.

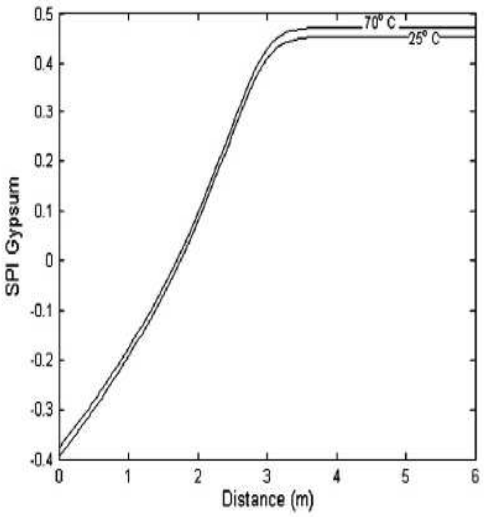

Fig. 10. Effect of feed water temperature on local *SPI* along 6 m filtration channel.

include any experimentally determined parameters or constants. This approach enables us to study locally on the membrane surface the effect of hydrodynamics and solution pH, salinity, temperature and concentration of the sparingly soluble salts on fouling potential along the feed module next to the membrane surface from the fundamental principles. Moreover, in view of the fact that different ions have specific passages, this approach would incorporate the effect of relative solution composition along a membrane module; this is even more significant for a nanofiltration module which has different passages for mono-valent and di-valent ions.

The suggested model is a very powerful tool that could help on design of the specifics of RO process as well as in the simulation and optimization of the operational variables. In this paper the effects of membrane resistance, pump feed pressure, feed mass flow rate, salinity and temperature the onset of fouling (scaling) propensity for a given sparingly salt next the membrane locally along the membrane module have been shown and discussed.

4. *Nomenclature*

c_0	initial feed salt concentration (mg/l)
$c(x)$	localized feed salt concentration (mg/l)
$c_w(x)$	localized salt concentration on membrane surface (mg/l)
D	diffusion coefficient of foulants (m^2/s)
G	standard Gibbs free energy
H	height of membrane channel (m)
IAP	ion activity products
k_{spacer}	coefficient to account for transmembrane pressure drop due to existence of spacers in membrane channel
Ksp	thermodynamic solubility product
L	length of RO system (m)
Mw	molecular weight of the solute
n	number of segments
r	salt rejection of membrane
p_f	the static pressure in the feed (Pa)
p_p	the static pressure in the permeate (Pa)
R	the universal gas constant
R_m	membrane resistance (Pa s/m)
SPI	scaling potential index
T	temperature (K)
u_0	initial feed flow velocity (m/s)
$u(x)$	localized cross flow velocity (m/s)
v	permeate velocity (m/s)
$v(x)$	localized permeate flux (m/s)
x	location along membrane channel (m)

Greek letters

α	osmotic coefficient (Pa l/mg)
Δ	denote the difference between two values
$\Delta c(x)$	localized difference between feed salt concentration and permeate salt concentration
$\Delta c_w(x)$	localized difference between feed salt concentration on membrane surface and permeate salt concentration
$\Delta\pi(x)$	localized osmotic pressure across the membrane (Pa)
$\Delta_f G^{\Phi}$	standard Gibbs free energy of formation
$\Delta_{reac} G^{\Phi}$	standard molar Gibbs free energy of reaction
ΔH_{reac}	enthalpy of reaction
Δp	the trans-membrane static pressure (Pa)
$\Delta p(x)$	localized trans-membrane static pressure (Pa)
Δp_0	initial transmembrane pressure (Pa)
Δp_{fric}	frictional losses due to friction by the membrane surfaces and spacers (Pa)
γ	activity coefficient
γ_{ZY}	mean activity coefficient
η	water viscosity (Pa.s)
Θ	Pitzer osmotic coefficient
ξ	dummy integration variable

Subscripts

0	reference or initial value
i	segment number
w	denote the variable at membrane wall

Superscripts

Φ	reference temperature value

References

[1] A.D. Khawaji, I.K. Kutubkhanah, J.-M. Wie, Advances in seawater desalination technologies, Desalination 221 (2008) 47–69.
[2] A. Fakhru'l-Razi, A. Pendashteh, L.C. Abdullah, D.R.A. Biak, S.S. Madaeni, Z.Z. Abidin, Review of technologies for oil and gas produced water treatment, J. Hazard. Mater. 170 (2009) 530–551.
[3] N. Epstein, Thinking about heat transfer fouling: a 5×5 matrix, Heat Transfer Eng. 4 (1981) 43–56.
[4] A.P. Watkinson, Water quality effects on fouling from hard waters in heat exchangers – theory and practice, in: J. Taborek, G.F. Hewitt, N. Afgan (Eds.), Heat Exchanger Sourcebook, Hemispherc Publishing Corp, New York, 1983, pp. 853–861.
[5] J. Taborek, T. Aoki, R.B. Ritter, J.W. Palen, J.G. Knudsen, Fouling: the major unresolved problem in heat transfer, Chem. Eng. Prog. 68 (1972) 59–67.
[6] J. Taborek, T. Aoki, R.B. Ritter, J.W. Palen, J.G. Knudsen, Predictive methods for fouling behaviour, Chem. Eng. Prog. 68 (1972) 69–78.
[7] R. Sheikholeslami, Composite fouling – inorganic and biological: a review, Environ. Prog. 18 (1999) 113–122.
[8] R. Sheikholeslami, Fouling in Membranes and Thermal Units: A Unified Approach – its Principles Assessment, Control and Mitigation, Balaban Desalination publications, L'Aquila, Italy, 2007.
[9] K.G. Tay, L. Song, A more effective method for fouling characterization in a full-scale reverse osmosis process, Desalination 177 (2005) 95–107.
[10] F. Fahiminia, Initial fouling rate and delay times studies of aqueous calcium sulphate scaling under sensible heating conditions, Chemical and Biological Engineering, The University of British Columbia, 2007, p. 230.
[11] R. Sheikholeslami, Assessment of the scaling potential for sparingly soluble salts in RO and NF units, Desalination 167 (2004) 247–256.
[12] P. Walker, R. Sheikholeslami, Preliminary numerical study of $CaSO_4$ precipitation in laminar flows in pipes and slits under isothermal conditions, 9th APCChE Congress and Chemeca, Christchurch, New Zealand, 2002.
[13] P. Walker, R. Sheikholeslami, Assessment of the effect of velocity and residence time in $CaSO_4$ precipitation flow reaction, Chem. Eng. Sci. 58 (2003) 3807–3816.
[14] P. Walker, R. Sheikholeslami, A novel approach, development and validation of a comprehensive model for prediction of fouling from saline waters, IDA, World Congress on Desalination and Water Reuse, Paradise Islands, Bahamas, 2003.
[15] P. Walker, R. Sheikholeslami, Development and Validation of an Unsteady State Numerical Model of Fouling Within a Crystalline System, Chemeca, Sydbey, Australia, 2004.
[16] L. Song, J.Y. Hu, S.L. Ong, W.J. Ng, M. Elimelech, M. Wilf, Performance limitation of the full-scale reverse osmosis process, J. Membr. Sci. 214 (2003) 239–244.
[17] R. Sheikholeslami, Scaling potential index (SPI) for $CaCO_3$ based on Gibbs free energies, AICHE J. 51 (2005) 1782–1789.

[18] W.E. Langelier, Chemical equilibria in water treatment, J. AWWA 38 (1946) 169.
[19] J.H.A. Stiff, L.E. Davis, A method for predicting the tendency of oil field water to deposit calcium carbonate, Pet. Trans. AIME 195 (1952) 213.
[20] J.W. Ryznar, A new index for determining amount of calcium carbonate scale formed by a water, J. AWWA 36 (1944) 472.
[21] P.R. Puckorius, J.M. Brooke, A new practical index for calcium carbonate scale producing in cooling tower systems, Corrosion 74 (1991) 280–284.
[22] P.P. Mane, P.-K. Park, H. Hyung, J.C. Brown, J.-H. Kim, Modeling boron rejection in pilot- and full-scale reverse osmosis desalination processes, J. Membr. Sci. 338 (2009) 119–127.
[23] R. Sheikholeslami, H.W.K. Ong, Kinetics and thermodynamics of calcium carbonate and calcium sulfate at salinities up to 1.5 M, Desalination 157 (2003) 217–234.
[24] R. Sheikholeslami, Y. Wang, H. Yu, Application of theoretical scaling potential index to predict onset of composite calcium carbonate and calcium sulfate fouling and crystal types and phases in seawater reverse osmosis treatment, in: B. Antizar-Ladislao, R. Sheikholeslami (Eds.), Water Production and Wastewater Treatment, Nova Publisher, 2011, pp. 269–284.
[25] R. Sheikholeslami, Composite scale formation and assessment by the theoretical Scaling Potential Index (SPI) proposed previously for a single salt, Desalination 278 (2011) 259–267.
[26] Y. Wang, R. Sheikholeslami, Co-precipitation of calcium sulfate and calcium carbonate in a seawater RO system, IDA World Congress on Desalination and Water Reuse, International Desalination Association, Singapore, 2005.
[27] Y. Wang, R. Sheikholeslami, The effects of SO4 2−/HCO3− molar ratio on the composite fouling of calcium sulfate and calcium carbonate in a seawater RO desalination unit, Chemeca 2005, Institute of Engineers Australia, Brisbane, 2005.
[28] L. Song, S. Hong, J. Hu, S. Ong, W. Ng, Simulations of full-scale reverse osmosis membrane process, J. Environ. Eng. 128 (2002) 960–966.
[29] K.L. Chen, L. Song, S.L. Ong, W.J. Ng, The development of membrane fouling in full-scale RO processes, J. Membr. Sci. 232 (2004) 63–72.
[30] R. Sheikholeslami, Strategies and future directions for systematic characterization of feed water and determination of scaling limits and rates for process assessment and optimization, International Desalination Association World Congress, Bahrain, 2001.
[31] M. Sudmalis, R. Sheikholeslami, Coprecipitation of $CaCO_3$ and $CaSO_4$, Can. J. Chem. Eng. 78 (2000) 21–31.
[32] M. Sudmalis, R. Sheikholeslami, Precipitation and co-precipitation of $CaCO_3$ and $CaSO_4$, N.Epstein's 75th Birthday Symposium, Vancouver, B.C., 1998.
[33] R. Sheikholeslami, T.H. Chong, M. Ng, Calcium Carbonate and Calcium Sulfate Co-precipitation–Thermodynamics and Kinetics, Chemeca, Newcastle, Australia, 1999.
[34] H. Yu, R. Sheikholeslami, W.O.S. Doherty, Preliminary study of the mechanisms of composite fouling of amorphous silica and calcium oxalate in sugar mill evaporators, 6th World Congress of Chemical Engineering, Melbourne, Australia, 2001.
[35] R. Sheikholeslami, M. Ng, Calcium sulfate precipitation in the presence of nondominant calcium carbonate: thermodynamics and kinetics, Ind. Eng. Chem. Res. 40 (2001) 3570–3578.
[36] T.H. Chong, R. Sheikholeslami, Thermodynamics and kinetics for mixed calcium carbonate and calcium sulfate precipitation, Chem. Eng. Sci. 56 (2001) 5391–5400.
[37] R. Sheikholeslami, Mixed salts–scaling limits and propensity, Desalination 154 (2003) 117–127.
[38] R. Sheikholeslami, Scaling of process equipment by saline streams – challenges ahead, Water Sci. Technol. 49 (2004) 201–210.
[39] R.T. Pabalan, K.S. Pitzer, Thermodynamics of concentrated electrolyte mixtures and the prediction of mineral solubilities to high temperatures for mixtures in the system $Na–K–Mg–Cl–SO_4–OH–H_2O$, Geochim. Cosmochim. Acta 51 (1987) 2429–2443.
[40] W. Zhou, L. Song, T.K. Guan, A numerical study on concentration polarization and system performance of spiral wound RO membrane modules, J. Membr. Sci. 271 (2006) 38–46.
[41] C.R. Bouchard, P.J. Carreau, T. Matsuura, S. Sourirajan, Modeling of ultrafiltration: predictions of concentration polarization effects, J. Membr. Sci. 97 (1994) 215–229.
[42] J.H.G. van der Stegen, H. Weerdenburg, A.J. van der Veen, J.A. Hogendoorn, G.F. Versteeg, Application of the Pitzer model for the estimation of activity coefficients of electrolytes in ion selective membranes, Fluid Phase Equilib. 157 (1999) 181–196.

A.2 International Journal of Environmental Science and Development paper

International Journal of Environmental Science and Development, Vol. 2, No. 6, December 2011

An Application for New Reliable Approach to Predict the Onset of Barite, Celestite and Gypsum Scaling during Reverse Osmosis Treatment for Produced Water

Emad Alhseinat and Roya Sheikholeslami

Abstract— **Reverse osmosis (RO) desalination is considered a promising solution for Produced Water treatment and reuse in the oil and gas industry. However, scaling problem is one of the main challenges that face Produced Water RO desalination. In this paper, the use of new completely theoretical approach for assessing fouling propensity along a full scale reverse osmosis process is introduced to predict the onset of barite, celestite and gypsum scaling, as major scaling salts facing the RO desalination of Produced Water. Thus, the scaling propensity of barite, celestite and gypsum have been assessed and discussed. Moreover, the effect of applied pressure, initial cross flow velocity, feed salinity and feed temperature on scaling propensity of barite, celestite and gypsum have been examined and discussed. This procedure could be considered as a very important guideline, for any attempt to use RO in Produced Water treatment. It could provide help on the specific design of RO process as well as in simulation of the operating variables for optimization of RO system.**

Index Terms—**Barite, celestite, produced water desalination, reverse osmosis, scaling, scaling propensity.**

I. Introduction

Produced Water is the wastewater produced during hydrocarbon (such as oil, gas and tar sand) processing. Desalination of Produced Water is attractive for the oil and gas industry for four reasons: Firstly, the substantial amount of globally Produced Water is estimated at around 250 million barrels/day compared with around 80 million barrels/day of oil [1]. The amount of Produced Water makes it the largest waste stream by volume associated with the oil and gas industry and makes the disposal of it a grave problem and burdens the operations of oil and gas industry. Secondly, the high overall cost of the Produced Water disposal as a result of increasing regulatory constraints for environmental concerns makes the economics unpalatable. Thirdly, the fresh water shortage especially in the arid regions like gulf region, where most oil and gas produced countries are located, makes the desalination of Produced Water beneficial, which could potentially help to reduce the problem of fresh water scarcity. Finally, the results of recent research studies by BP [2] show that injection of desalted water to the oil well has a significant positive impact on the oil recovery.

Scale formation seems to be a limiting factor in the desalination of Produced Water. Scaling limits the economic viability of Produced Water desalination by increasing the energy consumption and decreasing the efficiency of the process. Therefore, scaling mitigation is crucial for viably applying the desalination technology to the Produced Water. The first step on scaling mitigation is the prediction of the scaling propensity for specific feed water within the RO unit. As detailed elsewhere [3] the current practices for assessing the scaling propensity are based on empirical relationships that are not suitable for membrane processes; the empirical indices used for assessment the potential of precipitation fouling which is commonly referred to as scaling have been discussed in detail elsewhere [4]. In fact the complex characteristics of Produced Water exacerbate the problem of scaling because of the high probability of scaling when salts such as CaCO3, CaSO4, BaSO4 and SrSO4 co-exist. Since, the mechanism of fouling is expected to be different for different salts as it was demonstrated [5] for CaCO3 and CaSO4. Sheikholeslami [6] and her research group show that the co-existence of precipitating salt affects the mechanism of fouling, the thermodynamic, and kinetic behavior of each salt; hence, the single salt data is not applicable to the situation where salts co-exist. Thus, the application of the current industrial practice for assessing scaling propensity in desalination plant is limited and may only be able to crudely approximate the scaling propensity for simple feed water at the entrance to the RO desalination unit. Any effort for scaling propensity prediction must consider the substantial change on system variables and parameters throughout full scale RO desalination process and module. Indeed, the current practices make their prediction unrealistic for describing full-scale RO process by assuming homogeneity along the membrane channel, where system variable and parameters change substantially along the long channel [7].

Therefore, In this paper, the application of a newly developed reliable approach [8] is introduced for assisting and predicting the onset of scaling propensity during full scale RO treatment of Produced Water. This new approach is discussed in detail elsewhere [8] and is based on combining Sheikholeslami's Scaling Potential Index (SPI) [4] with a simulation for the behavior of salts' concentration and process parameters within a long membrane filtration channel. This reliable approach has been used to study the effect of operation variables, such as applied pressure and feed salinity, on onset of scaling propensity for the major scaling salts that could be faced during Produced Water

Manuscript received November 28, 2011; revised December 8, 2011. This work was supported in part by the University of Edinburgh.

Emad Alhseinat is PhD student with the Institute of Materials and Processes, School of Engineering, The University of Edinburgh, UK EH9 3JL (e-mail: e.alhseinat@ ed.ac.uk).

Professor Roya Sheikholeslami is Chair of Chemical Process Engineering at The University of Edinburgh, UK EH9 3JL (e-mail: Roya.Sheikholeslami@ed.ac.uk).

desalination. The results of this paper could be used as a guideline in the process design and operation of a full scale RO for Produced Water treatment.

II. Approach Development

To accurately predict the onset of scaling along a membrane channel there is a need to understand and include the thermodynamics of precipitation, which signify the effect of temperature, pressure, co-precipitation, high ionic strength and salinity on the solubility product. Then combining this solubility product with a simulation for the behavior of ions concentration along the membrane channel, which could be reached through using the principles of membrane transport and mass conservation used by [8], [9] to predict the variations of parameters in a long membrane channel. Thus, using this fundamental principle; the effect of operating parameters such as feed flow rate and the applied pressure on the onset of scaling propensity could be examined and verified.

A. Thermodynamic Analyses

Barite, celestite and gypsum are the common forms of barium sulphate, strontium sulphate and calcium sulphate that could be formed in Produced Water desalination. Equations (1)-(4) represent a general precipitation reaction for (*MX*) salt and the precipitation reactions of barium sulphate, calcium sulphate and strontium sulphate, respectively. Scaling potential of any salt could be assessed using the Scaling Potential Index (*SPI*) as described in (5)-(8). *SPI* was suggested and tested by Sheikholeslami [3],[4]; in fact, Sheikholeslami with introducing the *SPI* has opened the way for a completely theoretical assessment of the scaling propensity of any precipitation salt, through a fundamental and unified approach and by hypothesizing [10],[11],[12] the effect of product structure on Gibbs Free Energy of precipitation reaction and hence the thermodynamic solubility product (*Ksp*) not being a constant and by incorporating the principles of thermodynamics including Gibbs free energies as described below in (9)-(12) and the ion activities.

$$M^{e+} + X^{e-} \xleftrightarrow[Ksp]{} MX(s) \tag{1}$$

$$Ba^{2+} + SO_4^{2-} \xleftrightarrow[Ksp]{} BaSO_4 \tag{2}$$

$$Ca^{2+} + SO_4^{2-} \xleftrightarrow[Ksp]{} CaSO_4 \tag{3}$$

$$Sr^{2+} + SO_4^{2-} \xleftrightarrow[Ksp]{} SrSO_4 \tag{4}$$

$$SPI = \log\left(\frac{IAP}{Ksp}\right) \tag{5}$$

$$SPI_{barite} = \log\left(\frac{\{Ca^{2+}\}.\{SO_4^{2-}\}}{Ksp_{barite}}\right) \tag{6}$$

$$SPI_{gypsum} = \log\left(\frac{\{Ca^{2+}\}.\{SO_4^{2-}\}}{Ksp_{gypsum}}\right) \tag{7}$$

$$SPI_{celestite} = \log\left(\frac{\{Sr^{2+}\}.\{SO_4^{2-}\}}{Ksp_{celestite}}\right) \tag{8}$$

As seen in (5)-(8), *SPI* calculation for a targeted scaling salt required the calculation of Ion Activity Product (*IAP*) as well as the thermodynamic solubility constant (*Ksp*) for that salt as discussed before based on Sheikholeslami's approach using Gibbs Free Energies of reaction as described below in (9)-(12); where $\Delta_r G$ is Gibbs free energy of reaction, a is the activity, T is the absolute temperature (K) and R is the universal gas constant.

$$\Delta_r G = \Delta_r G^{\phi} + RT \ln\left(\frac{a_{M^{e+}}.a_{X^{e-}}}{a_{MX}}\right) \tag{9}$$

At equilibrium, the Gibbs free energy of reaction ($\Delta_r G$) is zero. Thus,

$$-RT \ln\left(\frac{a_{M^{e+}_{equ.}}.a_{X^{e-}_{equ.}}}{a_{MX_{equ.}}}\right) = \Delta_r G^{\phi} \tag{10}$$

$$\text{By definition } \left(\frac{a_{M^{e+}_{equ.}}.a_{X^{e-}_{equ.}}}{a_{MX_{equ.}}}\right) = Ksp \tag{11}$$

For pure *MX* precipitation, the activity of *MX* ($a_{MX_{equ.}}$) is by convention unity and the standard Gibbs Free Energy of reaction ($\Delta_r G^{\phi}$) is the difference between the total standard Gibbs free energy of formation of products and the reactants [4] and a function of precipitate structure [10],[11],[12].

$$\Delta_r G^{\phi} = (\Delta_f G^{\phi})_{products} - (\Delta_f G^{\phi})_{reactants} \tag{12}$$

For accurate calculation of the *SPI* along RO filtration channel, the effect of temperature and high ionic strength and salinity should be considered and also combined with a simulation for the change on concentrations and operational variables along the filtration channel.

1) Effect of temperature:

Effect of temperature is incorporated as discussed elsewhere [4] through the following equation for RO processes.

$$-RT \ln(Ksp) = \Delta_r G^T = \frac{T}{298.15}\Delta_r G^{298} + \Delta_r H^{298}\left(1 - \frac{T}{298.15}\right) \tag{13}$$

where R is the gas constant (1.987×10^{-3} kcal/mol.K), and T is the temperature (K); standard Gibbs free energies are at 298K, ($\Delta_r H$) is the enthalpy of reaction.

2) Effect of high ionic strengths and salinity:

As the second author originally introduced for RO desalination and discussed elsewhere [3],[4],[13] Pitzer model [14] was used to incorporate the high ionic strengths and salinity effects through the effects of ionic strength as well as the electrostatic effects and short and long range ion interaction forces. The *IAP* is calculated by using (14) and the activity coefficients (γ) are calculated by using (15).

$$IAP = a_{M^{e+}}.a_{X^{e-}} = \gamma_{M^{e+}}[M^{e+}]\gamma_{X^{e-}}[Z^{e-}] \tag{14}$$

$$\gamma = f(\text{salinity and concentration of species}) \tag{15}$$

B. Modeling for Variation of Concentration Along Membrane Channel.

The variation of ions concentrations and the operational variables in full scale RO is simulated by using finite differences for solution of differential equations of transport and continuity along the module. The details of the mathematical model are discussed elsewhere [8],[9].

In order to simulate the effect of operating parameters on onset of scaling propensity inside practical RO systems; the effects of temperature, pressure, high ionic strength and salinity on *SPI* were examined. The parameter values used in these simulations were either chosen from the manufacturers' specifications or from practical operating conditions as also used by others [9], [7],[15]. This simulation is capable to predict the effects of the variations of operational parameters along membrane channel on the onset of scaling tendency. Our procedure could be used as a very important guideline, for assessment of RO scaling in Produced Water treatment. It could guide on the specific design of RO process as well as in simulation of the operating variables for optimization of RO system.

III. Simulations for the Onset of Scaling

Numerical simulations have been conducted to investigate the effect of operating parameters on onset of scaling propensity prediction along a full-scale RO process. The confidence of the simulation has been discussed and shown elsewhere [8]. Unless otherwise specified, Table 1 shows the values of the parameters that have been used in these simulations - these values were also used by others [9]. The simulation parameters can be adapted to specific operating conditions and manufacture's design to suit any full scale RO process.

TABLE I: Parameter Values for Model Simulations

Length of RO system, L (m)	6
Channel height, H (m)	7×10^{-4}
Applied (pump) pressure, p_0 (Pa)	5.516×10^6
Feed Salinity (mg/l)	30000
Cross flow velocity at entrance (m/s)	0.1
Membrane intrinsic resistance, (Pa.s/m)	1.8×10^{11}
Number of elements along RO system	400
Temperature, °C	25
pH	7.1
Friction coefficient due to spacers	5
Initial Ca^{2+} concentration, ppm	1500
Initial SO_4^{2-}, ppm	2000
Initial Ba^{2+}, ppm	0.02
Initial Sr^{2+}, ppm	30

A. Scaling Propensity of $BaSO_4$, $SrSO_4$ and $CaSO_4$ along 6 m Membrane Modules.

The *SPI* gives a conservative estimate for assessing scaling potential; when *SPI* is negative, certainly no scale will form; when zero the system is at equilibrium; when the *SPI* is positive, the salt has a "potential" to form scales [4]. Fig. 1 shows the onset of scaling propensity for barite, celestite and gypsum in terms of *SPI*. The figure shows that at these particular simulation conditions the *SPI* for barite, celestite and gypsum were negative for the first meter of the module and this means that onset of scale formation will not be in the first meter. However, due to permeation and concentration factor, scaling propensities of barite, gypsum, and celestite increases afterwards and SPIs becomes positive after about 1.5m and increases further along the channel.

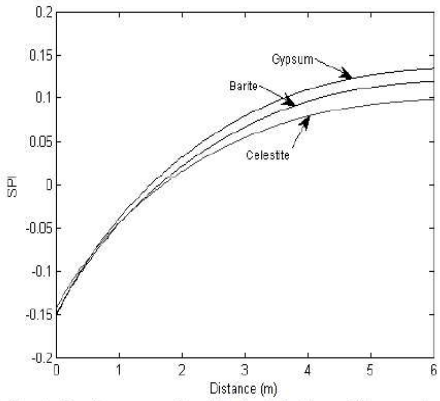

Fig.1. Onset of scaling propensity of Barite, Celestite and Gypsum along 6m membrane channel.

These observations demonstrate that scaling is expected to take place after 1.5m of the membrane channel.

B. Effect of Initial Cross Flow Velocity on Onset of Scaling Propensity for Barite, Celestite and Gypsum.

Fig. 2 shows the effect of various initial cross flow velocities on local *SPI* values for celestite along 6m RO permeation channel. It is shown that cross flow velocity has very important impact on localized scaling propensity. The same trends are observed for the barite, celestite and gypsum scales, confirming that the lowest cross flow velocity results in the highest scaling propensity. Thus, cross flow velocity should be optimized to reduce scaling propensity for all scaling salts. An optimum cross flow velocity can be obtained from our proposed approach. As seen in Fig. 3, under our simulation conditions, operating the RO at 0.2 m/s cross flow velocity will help to minimize barite, celestite and gypsum scaling. This observation could be used as a reference to set the best possible operational limit.

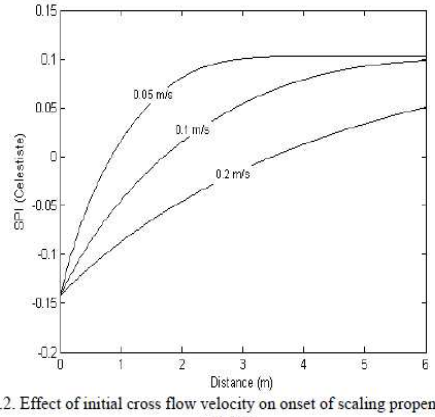

Fig.2. Effect of initial cross flow velocity on onset of scaling propensity for Celestite.

International Journal of Environmental Science and Development, Vol. 2, No. 6, December 2011

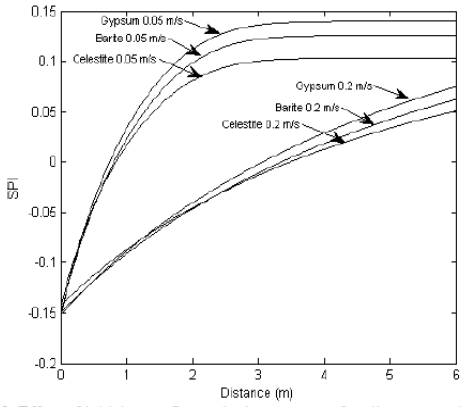

Fig.3. Effect of initial cross flow velocity on onset of scaling propensity for Gypsum, Barite and Celestite.

C. *Effect of Applied Pump Pressure on Onset of Scaling Propensity for Barite, Celestite and Gypsum*

The applied pressure is one of the operating variables that affect the onset of scaling propensity as shown for gypsum in Fig. 4 for different values of applied pressure. It is shown that increasing applied pressure increases the potential for onset of scaling propensity. At the highest applied pressure, the membrane is most prone to scale formation under otherwise identical feed Produced Water conditions. Thus, theoretical assessment of the scaling potential enables one to operate within the safe operational limit. For example Fig. 5 shows operating the RO at 45 bar will certainly minimize the potential barite, celestite and gypsum scaling.

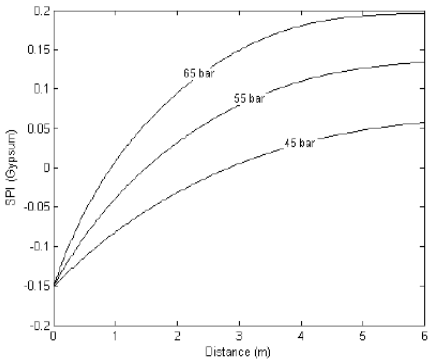

Fig. 4. Effect initial applied pump pressure on onset of scaling propensity for Gypsum.

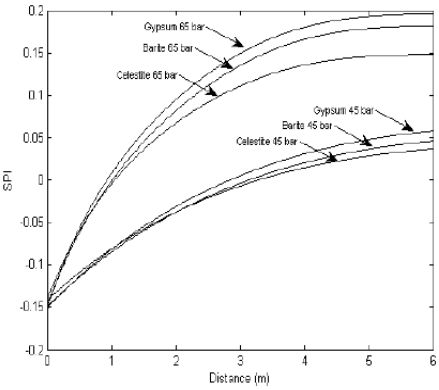

Fig. 5. Effect initial applied pump pressure on onset of scaling propensity for Gypsum, Barite and Celestite.

D. *Effect of Initial Feed Water Salinity on Onset of Scaling Propensity for Barite, Celestite and Gypsum.*

Salinity of feed water to RO process varies from location to location and may also vary with time at a given location. Therefore, Fig. 6 has been plotted to show the effect of salinity variation on scaling propensity of barite in term of *SPI*. It shows that at higher feed water salinities, with other parameters constant, the lower would be onset of barite scaling propensity along the membrane channel. Fig. 7 shows that at salinity of 40000 ppm no scales form along the channel, since the *SPI* curves for these three salts (barite, celestite and gypsum) are negative along the whole channel. The decrease in the potential for onset of scaling propensity along the permeation channel, as the feed water salinity increases is due to the salinity effects on the permeation driving force as well on the ion activity. As the salinity increases the net driving force decreases and the permeate flux will decrease leading to decrease in concentration factor and potential for scaling. Another reason for the decrease in scaling propensity as a result of an increase in feed salinity is the increase in solubility limit, due to the increase of non-scaling salt (NaCl) concentration [3],[4] , [11], [13].

It should be noted that in Fig. 6 and Fig. 7 the only variable between the curves are the concentration on "non-scaling" species; the concentration of scaling species and other parameters are the same in all the curves on the figures.

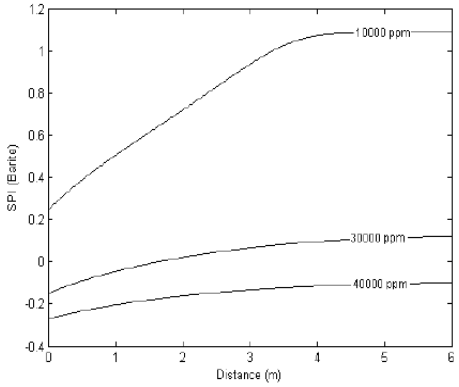

Fig.6. Effect of feed salinity on onset of scaling propensity for Barite.

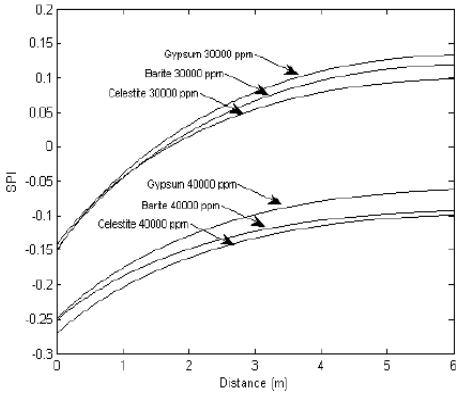

Fig.7. Effect of feed salinity on onset of scaling propensity for Barite, Celestite and Gypsum.

International Journal of Environmental Science and Development, Vol. 2, No. 6, December 2011

E. Effect of Feed Water Temperature on Onset of Scaling Propensity for Barite, Celestite and Gypsum

Figs. 8-10 show the scaling propensity (*SPI*) for barite, celestite and gypsum along a 6m permeation channel at different feed water temperatures. The thermodynamic solubility constant (*Ksp*) was calculated by using (13) at the simulated temperatures; the effect of temperature on density and viscosity was also taken into account. As seen in Fig. 8, increasing temperature from 15°C to 70°C appears to reduce the possibility of barite scale formation. By operating at 40°C, barite scaling can be avoided. Fig. 9 shows that increasing the temperature will increase the probability of celestite precipitation, as seen in Fig. 9 at 70°C the *SPI* curve of celestite will be positive along the whole 6 m filtration channel. As seen in Fig. 10, increasing temperature did not appreciably effect the scaling propensity of gypsum though gypsum is an inverse solubility salt. The effect of temperature on membrane properties should be considered and further attention should be given for the effect of high temperatures on the membrane structure and performance as it could be one of the main drawbacks of operating at high temperatures.

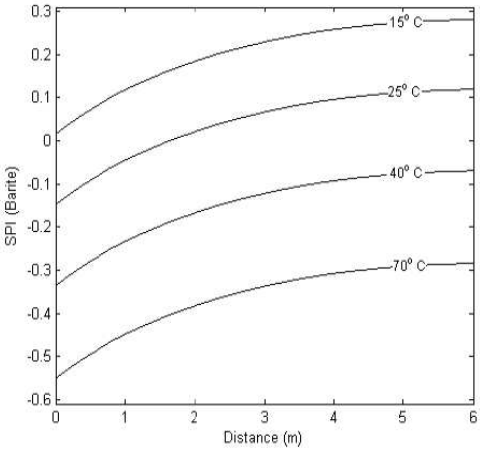

Fig. 8. Effect of feed temperature on onset of scaling propensity for Barite.

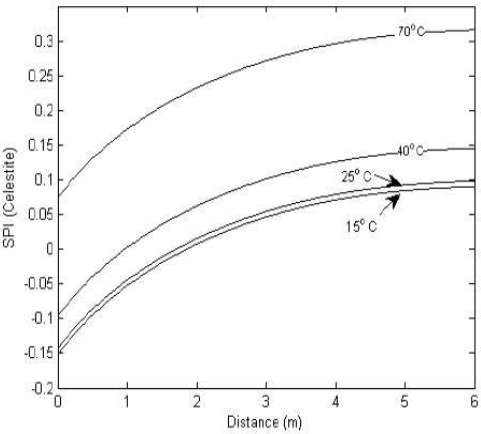

Fig. 9. Effect of feed temperature on onset of scaling propensity for Celestite.

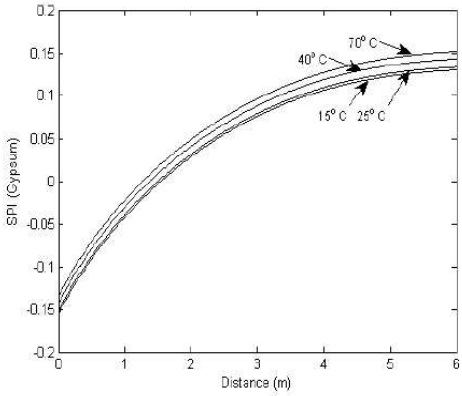

Fig. 10. Effect of feed temperature on onset of scaling propensity for Gypsum.

IV. Conclusion

In this paper fundamental relationships were used to reliably simulate and assess scaling propensity of barite, celestite and gypsum, along full-scale RO membrane. This reliable simulation has been reached through incorporation of the localized parameters along the membrane filtration channel in a fundamental and unified approach for assessing the scaling potential. This approach allows studying the effect of hydrodynamic and interactive effects on scaling potential from the fundamental principles. The effects of initial applied pressure, initial cross flow velocity, initial feed water salinity and feed water temperature on scaling propensity development of barite, celestite and gypsum were investigated. The ability to simulate the operational conditions and performance is important for process design and for operating the RO unit within the most suitable operational limit to avoid scaling.

V. Nomenclature

G	standard Gibbs free energy
IAP	ion activity products
Ksp	thermodynamic solubility product
R	the universal gas constant
SPI	scaling potential index
T	temperature (K)

Greek letters

α	activity
Δ	denote the difference between two values
$\Delta_f G^{\Phi}$	standard Gibbs free energy of formation
$\Delta_r G^{\Phi}$	standard molar Gibbs free energy of reaction
$\Delta_r H$	enthalpy of reaction
γ	activity coefficient

Subscripts

equ.	equilibrium
f	formation
r	reaction

Superscripts

0	reference value
Φ	reference temperature value

REFERENCES

[1] A. Fakhru'l-Razi, A. Pendashteh, L. C. Abdullah, D. R. A. Biak, S. S. Madaeni, and Z. Z. Abidin, "Review of technologies for oil and gas produced water treatment," *Journal of Hazardous Materials,* vol. 170, pp. 530-551, 2009.

[2] P. L. McGuire, J. R. Chatham, F. K. Paskvan, D. M. Sommer, and F. H. Carini, "Low Salinity Oil Recovery: An Exciting New EOR Opportunity for Alaska's North Slope," in *SPE Western Regional Meeting*, 2005.

[3] R. Sheikholeslami, "Assessment of the scaling potential for sparingly soluble salts in RO and NF units," *Desalination,* vol. 167, pp. 247-256, 2004.

[4] R. Sheikholeslami, "Scaling potential index (SPI) for CaCO3 based on Gibbs free energies," *AIChE Journal,* vol. 51, pp. 1782-1789, 2005.

[5] Bansal.B, Müller-Steinhagen.H, and D. Chen.X, "Effect of Suspended Particles on Crystallization Fouling in Plate Heat Exchangers," *TRANSACTIONS- AMERICAN SOCIETY OF MECHANICAL ENGINEERS JOURNAL OF HEAT TRANSFER,* vol. 119, pp. 568-574, 1997.

[6] R. Sheikholeslami, *Fouling in Membranes and Thermal Units: A Unified Approach- its Principles Assessment, Control and Mitigation*. L'Aquila, Italy: Balaban Desalination publications, pp. 88-102, 2007.

[7] K. L. Chen, L. Song, S. L. Ong, and W. J. Ng, "The development of membrane fouling in full-scale RO processes," *Journal of Membrane Science,* vol. 232, pp. 63-72, 2004.

[8] E. Alhseinat and R. Sheikholeslami, "A completely theoretical approach for assessing fouling propensity along full-scale RO process," *Desalination*.

[9] L. Song, S. Hong, J. Hu, S. Ong, and W. Ng, "Simulations of Full-Scale Reverse Osmosis Membrane Process " *Journal of Environmental Engineering* vol. 128, pp. 960-966, Oct 2002 2002.

[10] R. Sheikholeslami, "Strategies and future directions for systematic characterization of feed water and determination of scaling limits and rates for process assessment and optimization," presented at the International Desalination Association World Congress, Bahrain, 2001.

[11] R. Sheikholeslami, "Mixed salts--scaling limits and propensity," *Desalination,* vol. 154, pp. 117-127, 2003.

[12] R.Sheikholeslami, "Scaling of process equipment by saline streams - challenges ahead," *Water Science & Technology,* vol. 49, pp. 201–210, 2004.

[13] R. Sheikholeslami and H. W. K. Ong, "Kinetics and thermodynamics of calcium carbonate and calcium sulfate at salinities up to 1.5 M," *Desalination,* vol. 157, pp. 217-234, 2003.

[14] R. T. Pabalan and K. S. Pitzer, "Thermodynamics of concentrated electrolyte mixtures and the prediction of mineral solubilities to high temperatures for mixtures in the system Na-K-Mg-Cl-SO4-OH-H2O," *Geochimica et Cosmochimica Acta,* vol. 51, pp. 2429-2443, 1987.

[15] K. G. Tay and L. Song, "A more effective method for fouling characterization in a full-scale reverse osmosis process," *Desalination,* vol. 177, pp. 95-107, 2005.

A.3 ICOGE 2011 paper

2011 International Conference on Environment and BioScience
IPCBEE vol.21 (2011) © (2011) IACSIT Press, Singapore

A Reliable approach for Barite, Celestite and Gypsum scaling propensity prediction during reverse osmosis treatment for produced water

Emad Alhseinat[1+], Roya Sheikholeslami[1]

[1] The University of Edinburgh, EH9 3JL

Abstract. Reverse osmosis desalination is considered a promising solution for Produced Water problem in oil and gas industry. In fact, desalination of Produced Water may transfer Produced Water from a grave problem that burdens the oil and gas industry to a useful commodity used as part of a solution to the problem of fresh water shortage. However, Scaling problem is one of the main challenges that face Produced Water desalination. Actually, Scaling limits the economic viability of Produced Water desalination. Thus, scaling mitigation is very crucial and must be considered in any attempt for Produced Water desalination. The first step in scaling mitigation is to predict the scaling propensity of the feed water. Unfortunately, there is an immense shortage in the current industrial practice for determination of scaling propensity. This shortage comes from using old and inapplicable approaches where crucial assumptions are made to simplify these predictions; these old approaches were suitable for the era that the computer access was limited and also not generally applied in water industry. This paper uses the theoretical Scaling Potential Index (SPI) proposed by (Sheikholeslami 2005) and previously used in reverse osmosis set up (R.Sheikholeslami, Y.Wang et al. 2011; Sheikholeslami 2011) incorporates the use of Pitzer ion interactive forces previous proposed for seawater desalination (Sheikholeslami and Ong 2003) and combining them with the principles of mass transfer and membrane transport used by (Song, Hong et al. 2002) along the membrane module to predict the scaling propensity along the membrane module. This approach considers the interactive effect resulted from precipitation salts and non precipitation salts co-existence as recommended previously (Sheikholeslami and Ong 2003). And moreover it considers the substantial change in salts concentrations and system variables and parameters within a full-scale RO. As a result, a reliable prediction of the scaling propensity in full scale reveres osmosis process is made. In this paper scaling propensity of barite, celestite and gypsum, as a major scaling salts in Produced Water, have been assessed and discussed. Moreover, the effect of applied pressure, initial cross flow velocity and feed salinity on scaling propensity of barite, celestite and gypsum have been examined and discussed.

Keywords: Reverse Osmosis, Produced Water Desalination, Scaling, Scaling Propensity, Barite, Celestite.

1. Introduction

Produced Water is the wastewater produced during hydrocarbon (such as oil, gas and tar sand) processing. The following four reasons make the desalination of Produced Water attractive for the oil and gas industry: Firstly, the huge amount of globally Produce Water is estimated at around 250 million barrels/day compared with around 80 million barrels/day of oil (Fakhru'l-Razi, Pendashteh et al. 2009). The amount of Produced Water makes it the largest waste stream by volume associated with the oil and gas industry and makes the disposal of it a grave problem and burdens the oil and gas industry. Secondly, the high overall cost of the Produced Water disposal as a result of increasing in disposal regulatory constraints for environmental concerns makes the economics unpalatable. Thirdly, the fresh water shortage especially in the region, like gulf reign, where most oil and gas produced countries are located makes the desalination of Produced Water beneficial which could potentially help to reduce the problem of fresh water scarcity.

+ Corresponding author. Tel.: + (441316508564);
E-mail address: (e.alhseinat@ed.ac.uk).

Fourthly, the results of recent research studies by BP show that injection of desalted water to the oil well has a significant positive impact on the oil recovery (McGuire, Chatham et al. 2005).

However, scale formation seems to be a limiting factor in the desalination of Produced Water. Scaling limits the economic viability of Produced Water desalination by increasing the energy consumption and decreasing the efficiency of the process. Therefore, scaling mitigation is crucial for applying the desalination technology to the Produced Water. The first step on scaling mitigation is the prediction of the scaling propensity for specific feed water. The current practice for assessing the scaling propensity are based on empirical relationships that are not suitable for membrane processes (Sheikholeslami 2004), the empirical indices used for assessment the potential of precipitation fouling which is commonly referred to as scaling have been discussed in detail elsewhere (Sheikholeslami 2005). In fact the complex characteristics of Produced Water exacerbate the problem of scaling because of the high probability of scaling when salts such as $CaCO_3$, $CaSO_4$, $BaSO_4$ and $SrSO_4$ co-exist. Since, the mechanism of fouling is expected to be different for different salts as it was demonstrated for $CaCO_3$ and $CaSO_4$ (Bansal.B, Müller-Steinhagen.H et al. 1997). And moreover, (Sheikholeslami 2007) and her research group show that the co-existence of precipitating salt affects the mechanism of fouling, the thermodynamic, and kinetic behavior of each salt; hence, the single salt data is not applicable to the situation where salts co-exist. So the application of the current industrial practice for assessing the scaling propensity in desalination plant is limited and only maybe able to approximate the scaling propensity for simple feed water at the entrance to the RO desalination unit. Moreover, any effort for scaling propensity prediction must consider the substantial change on system variables and parameters during full scale desalination process. So the current practice make their prediction unrealistic for describing full-scale RO process that along membrane channel, where system variable and parameters change substantially along the long membrane channel (Chen, Song et al. 2004).

Therefore, this paper comes to apply a new reliable approach based on combining Sheikholeslami's SPI (Sheikholeslami 2005) to predict the scaling propensity of Produced Water in full scale RO desalination. This reliable approach has been used to study the effect of operation variables such as applied pressure and feed salinity on scaling propensity development for the major scaling salts that could be faced during Produced Water desalination

2. Model Development

To predict scaling development along a membrane channel there is need firstly to describe the change on scaling ions and non-scaling ions concentration along the membrane filtration channel. Simulating the ions behavior and interactive forces of Pitzer as previously used (Sheikholeslami and Ong 2003) concentrating along the membrane channel could be used to determine the interactive effects for the long and short interactive forces. Simulating the behavior of the ions concentration along the membrane channel could be reached through using the principles of membrane transport and mass conservation used by (Song, Hong et al. 2002) to predict the variations of variables and parameters in a long membrane channel. Moreover, using this fundamental principle; the effect of operating parameters such as feed flow rate and the applied pressure on scaling propensity development could be examined and verified. And furthermore, in case of scaling it could extend the theoretical Scaling Potential Index (SPI) developed by (Sheikholeslami 2005; R.Sheikholeslami, Y.Wang et al. 2011; Sheikholeslami 2011) which depends on Gibbes free Energy to find the scaling propensity of all the scaling salt along the membrane filtration channel.

3. Simulation for scaling propensity in full-scale RO

Numerical simulations have been conducted to investigate the effect of operating variables on scaling propensity development along a full-scale RO process. In order to clarify scaling propensity development inside practical RO systems, the parameter values used in these simulations were either chosen from the manufacturers' specifications or practical operating conditions as followed by (Song, Hong et al. 2002). This simulation is capable to predict the effects of the variations of operation variables and parameters along membrane channel on the development of scaling tendency. Unless otherwise specified, Table 1 shows the values of the parameters that have been used in this simulation as well as that of (Song, Hong et al. 2002).

Table1. Parameter values for model Simulations

Length of RO system, L (m)	6
Channel height, H (m)	7×10^{-4}
Applied (pump) pressure, p_0 (Pa)	5.516×10^6
Feed Salinity (mg/l)	30000
Cross flow velocity at entrance,(m/s)	0.1
Membrane intrinsic resistance,(Pa s/m)	1.8×10^{11}
Number of elements along RO system	400
Temperature, °C	25
Initial Ca^{2+} concentration, ppm	1500
Initial SO_4^{2-}, ppm	2000
Initial Ba^{2+}, ppm	0.02
Initial Sr^{2+}, ppm	20

3.1. Scaling propensity for $BaSO_4$, $SrSO_4$ and $CaSO_4$ along 6 m membrane channel.

Scaling potential index gives a conservative estimate for assessing scaling potential; when *SPI* is negative, certainly no scale will form; when zero the system is at equilibrium; when the *SPI* is positive, the salt has a "potential" to form scale (Sheikholeslami, 2005). Figure 1 shows the development of scaling propensity for barite, celestite and gypsum in terms of *SPI*, it is seen that at this particular simulation conditions the *SPI* for barite, celestite and gypsum were below zero for the first meter along the permeation channel which means that in this section of the membrane there will not be any scale formation. However, an increase in scaling propensity of barite and gypsum develops afterwards which reaches the maximum approximately at about 3m along the channel. Moreover, it is seen that the celestite precipitation could start to occur towards the last half of the membrane channel, where it is expected to have barite and gypsum scales as well.

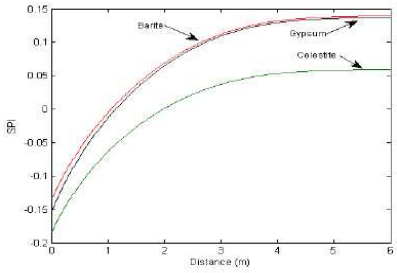

Fig.1. Scaling propensity development for Barite, Celestite and Gypsum precipitation.

These observations demonstrate that it is expected to have severe scaling after 3m of the membrane channel - *SPI* for all the species increases along the length as a result of increases in the concentration of the scaling salts along the concentrate channel.

3.2. Effect of initial cross flow velocity on scaling propensity development for Barite, Celestite and Gypsum.

Figure 2 shows the effect of various initial cross flow velocities on scaling propensity of barite, celestite and gypsum precipitation development along 6m RO channel. It is shown that cross flow velocity has very important impact on scaling propensity development. The same trends are observed for the three scales (barite, celestite and gypsum) confirming that the lowest cross flow velocity results in the highest scaling propensity. Thus, cross flow velocity should be optimized to reduce scaling propensity for all scaling salts. Therefore, this simulation could be used to have optimum cross flow velocity.

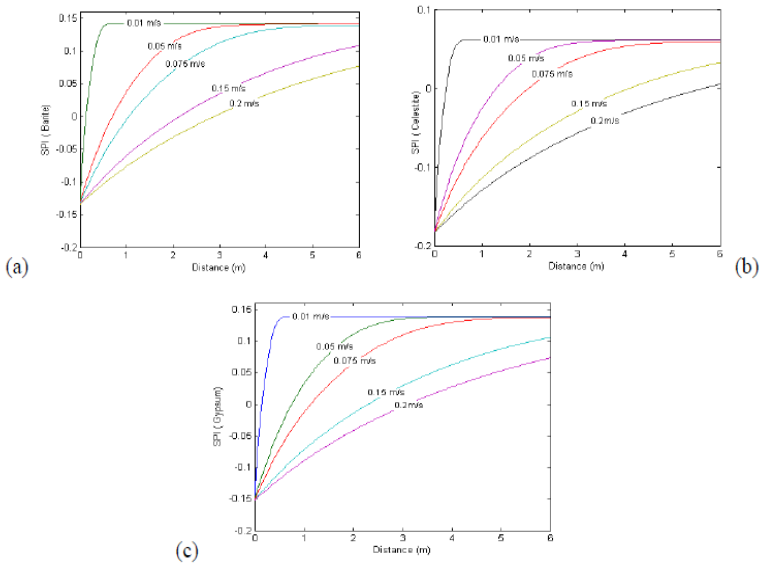

Fig.2. Effect of initial cross flow velocity on scaling propensity development for (a) Barite precipitation (b) Celestite precipitation (c) Gypsum precipitation.

As seen from the above figure operating the RO at 0.2 m/s cross flow velocity will help to avoid celestite scaling and minimize barite and gypsum scaling.

3.3. Effect of applied pump pressure on scaling propensity development for Barite, Celestite and Gypsum

The applied pressure is one of the operating variables that affect the scaling propensity. Figure 3 shows the development of scaling propensity of barite, celestite and gypsum for different values of applied pressure. It is shown that increasing applied pressure leads to change in the development of scaling propensity. As seen at highest applied pressure the membrane is more prone to scale formation. Thus, the theoretical *SPI* enables one to operate within the safe operational limit. For example according to figure 3 operating the RO at 45 bar will certainly avoid precipitating of celestite and minimize the barite and gypsum scaling.

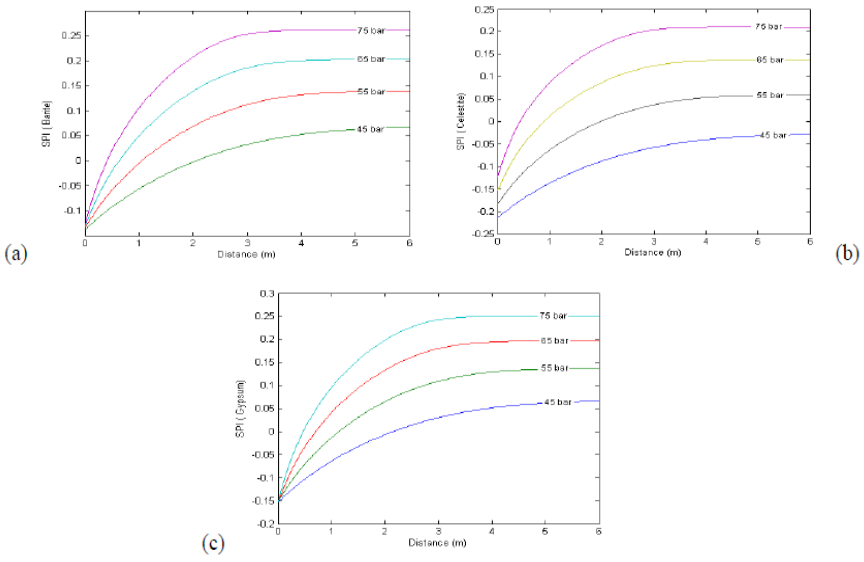

Fig. 3. Effect initial applied pressure on scaling propensity prediction for (a) Barite precipitation (b) Celestite precipitation (c) Gypsum precipitation.

3.4. Effect of initial feed water salinity on Scaling propensity development for Barite, Celestite and Gypsum.

Salinity of feed water to RO process varies from location to location and may vary with time at a given location as well. Therefore, Figure 4 has been plotted to show the effect of salinity variation on scaling propensity of barite, celestite and gypsum in term of *SPI*. It is noted from Figure 4 that at higher feed water salinities, with other parameters constant, the lower would be for scaling propensity along the membrane channel. Also it seen from figure 4(b) that at salinity 30000ppm will be no celestite scaling since the *SPI* curve is negative along the channel. The decrease in scaling propensity development along the permeation channel as the salinity of feed water increase is due to the effect of salinity on the driving force (ΔP-αCi) for the permeate flux as well on the ion activity. Therefore, as the salinity increases the net driving force decreases and the permeate flux will decrease leading to decrease in ions concentration and scaling development.

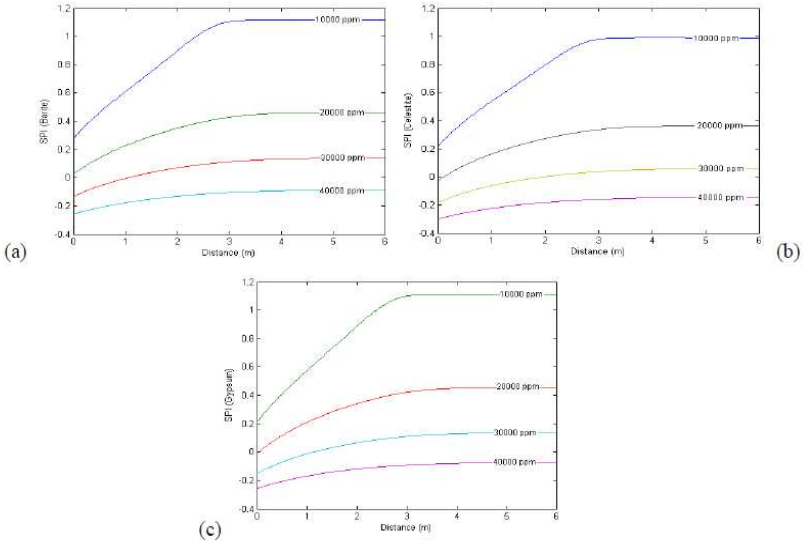

Fig.4. Effect of feed salinity on scaling propensity prediction for (a) Barite precipitation (b) Celestite precipitation (c) Gypsum precipitation.

Another reason for the decrease in scaling propensity as a result of increase in feed salinity is the increase in solubility limit due to the increase of non-precipitating salt (NaCl) concentration which increases the ionic strength of the solution thus increasing the interaction between the two precipitating species that elevate the solubility limit (Sheikholeslami and Ong 2003).

4. CONCLUSION

This paper uses fundamental relationships to reliably simulate and assess scaling propensity of barite, celestite and gypsum, as a major scaling salts face in produced water desalination, along full-scale RO membrane. This reliable simulation has been reached through incorporation of the localized parameters along the membrane filtration channel in a fundamental and unified approach for assessing the scaling potential. This approach enables us to study the effect of hydrodynamic and interactive effects on scaling potential from the fundamental principles. The effects of initial applied pressure, initial cross flow velocity, initial feed water salinity and feed water temperature on scaling propensity development of barite, celestite and gypsum were investigated and discussed. The ability to simulate the operational conditions and performance is important for operating the RO unit within the most suitable operational limit to avoid scaling.

5. RFERENCES

[1] Bansal.B, Müller-Steinhagen.H, et al. (1997). "Effect of Suspended Particles on Crystallization Fouling in Plate Heat Exchangers." TRANSACTIONS- AMERICAN SOCIETY OF MECHANICAL ENGINEERS JOURNAL

OF HEAT TRANSFER **119**(3): 568-574

[2] Chen, K. L., L. Song, et al. (2004). "The development of membrane fouling in full-scale RO processes." Journal of Membrane Science **232**(1-2): 63-72.

[3] Fakhru'l-Razi, A., A. Pendashteh, et al. (2009). "Review of technologies for oil and gas produced water treatment." Journal of Hazardous Materials **170**(2-3): 530-551.

[4] McGuire, P. L., J. R. Chatham, et al. (2005). Low Salinity Oil Recovery: An Exciting New EOR Opportunity for Alaska's North Slope. SPE Western Regional Meeting.

[5] R.Sheikholeslami, Y.Wang, et al. (2011). Application of Theoretical Scaling Potential Index to Predict Onset of Composite Calcium Carbonate and Calcium Sulfate Fouling and Crystal Types and Phases in Seawater Revese Osmosis Treatment. Water Production and Wastwater Treatment. B.Antizar-Ladislao and R.Sheikholeslami, Nova Publsher**:** 269-284.

[6] Sheikholeslami, R. (2004). "Assessment of the scaling potential for sparingly soluble salts in RO and NF units." Desalination **167**: 247-256.

[7] Sheikholeslami, R. (2005). "Scaling potential index (SPI) for CaCO3 based on Gibbs free energies." AIChE Journal **51**(6): 1782-1789.

[8] Sheikholeslami, R. (2007). Fouling in Membranes and thermal Units: A Unified Approach- Its Principles, Assessment, Control and Mitigation. Balaban Desalination Publications.

[9] Sheikholeslami, R. (2011). "Composite scale formation and assessment by the theoretical Scaling Potential Index (SPI) proposed previously for a single salt." Desalination **In Press, Corrected Proof**.

[10] Sheikholeslami, R. and H. W. K. Ong (2003). "Kinetics and thermodynamics of calcium carbonate and calcium sulfate at salinities up to 1.5 M." Desalination **157**(1-3): 217-234.

[11] Song, L., S. Hong, et al. (2002). "Simulations of Full-Scale Reverse Osmosis Membrane Process " Journal of Environmental Engineering **128**(10): 960-966.

A.4 11th World Filtration Congress & Exhibition Graz-Austria paper

11th World Filtration Congress - Session M15 - Membrane Fouling II

EFFECT OF CO-EXISTING SCALING SALTS AND PROCESS PRESSURE ON THE PREDICTION OF SCALING PROPENSITY DURING FULL SCALE REVERSE OSMOSIS TREATMENT

Emad Alhseinat [a], Roya Sheikholeslami, Donald Glass [a]
[a] The University of Edinburgh, Edinburgh, U.K, EH9 3JL

ABSTRACT

Reverse osmosis (RO) desalination is considered a promising solution for the water scarcity problem in arid regions. However, scaling is a major challenge facing RO desalination. Scaling limits its economic viability and is a very crucial factor in RO desalination. The first step in scaling mitigation is to predict the onset of scaling as a function of the feed water composition. Unfortunately, there are immense limitations in the current industrial practises for scaling propensity prediction. These limitations come from using old and inapplicable approaches, in which crucial assumptions are made. One of the major simplifications is the use of pure scaling salt data to predict the propensity of scaling when, in reality, co-precipitation is present. This paper proposes a novel procedure for including the effect of co-precipitation on scaling propensity prediction; and secondly theoretically includes the effect of process pressure on solubility products at the onset of scaling during the full scale RO process. It has been shown that process pressure has a significant effect on scaling propensity prediction; and the effect of co-precipitation must be considered during scaling propensity prediction. Thus, this paper helps to produce more reliable and accurate prediction of the onset of scaling which will help to mitigate scaling and increase the overall efficiency of RO desalination.

KEYWORDS

Reverse osmosis, scaling, co-precipitation, scaling propensity

1. Introduction

Water desalination has gained widespread use as a consequence of potable water shortages all over the world, especially in arid regions such as the Gulf region and in most Middle Eastern countries. The reverse osmosis (RO) process is considered to be one of the most important technologies for water desalination due to its lower cost compared to other desalination processes such as thermal distillation [1]. However, the operation of RO is plagued by fouling. In particular, fouling increases operational costs by lowering the lifetime of membranes and raising their energy consumption. Moreover, fouling adds extra cost to the capital expenses since the process needs further pre-treatment units to minimize its effect. For these reasons fouling is

considered a fundamental limitation to the economic viability of membranes in water treatment [2]. Needless to say, that additional energy, materials (membranes and equipment) and chemicals required to combat fouling add to the carbon footprint of the process and render it environmentally unfriendly.

The first step in fouling mitigation is to determine the fouling propensity of the feed water. Research studies usually consider a single foulant or a single fouling mechanism and they do not take into account the interactive and hydrodynamic effects. As such they are generally inapplicable to industrial conditions where, in reality, interactive effects and numerous simultaneous mechanisms are present and must be considered during any comprehensive assessment of fouling as discussed in detail by Sheikholeslami [3].

Moreover, the current practices for assessing fouling propensity are based on empirical relationships and are thus not suitable for membrane processes [4]. The empirical indices used for assessment of the potential of precipitation fouling, which is commonly referred to as scaling, have been discussed in detail elsewhere [5] Most of them were developed in the 1950's and 1960's and not originally for membrane processes. Even the commonly used indices for calcium carbonate, such as the Langelier Saturation Index (LSI) [6], Stiff-Davis Stability Index (S&DSI)[7], Ryznar Stability Index [8], and Puckorius Scaling Index [9] are mostly empirically based; and the LSI and S & DSI, which are based on the theoretical concept of saturation, include significant simplifications and empirical relationships in their derivation and do not reflect the high salinities, the interactive effects and the operational conditions within the membrane module [3],[4] . Therefore, the application of theses indices for membrane desalination is limited. Furthermore, most of the fouling models that attempt to describe fouling in the RO process have been developed for homogenous membrane systems, which assume uniform flow properties and fouling rate all over the membrane surface. This assumption renders the existing models unrealistic for describing the full-scale RO process. in which there is a long membrane channel, where system variables and parameters change substantially along the membrane [10-12]. Therefore, the fouling propensity in a full-scale RO process can be more accurately simulated through incorporating the varying local fouling, flux, and flow properties into a completely theoretical approach for assessing the scaling propensity.

To over come this massive shortage, Alhseinat and Sheikholeslami [13] have recently introduced a new and reliable approach for assisting and predicting the scaling propensity of any scaling salt during full scale RO desalination. This new approach is based on combining Sheikholeslami's Scaling Potential Index (*SPI*) [5] with a simulation of the behaviour of salts' concentrations and process parameters within a long membrane filtration channel. An application of this new approach to assess the scaling propensity of the major scaling salts during RO treatment for Produced Water has been discussed in details in [14]. The Alhseinat and Sheikholeslami approach opens the way to theoretically incorporating the effect of RO process pressure into the scaling salts' solubility product as a way to predicting the scaling propensity. Moreover, this new approach enables us for the first time to include the effect of co-precipitation in salt scaling propensity prediction. Thus, this paper

includes and discusses for the first time the effect of RO process pressure and co-precipitation on scaling propensity prediction.

2. Scaling Propensity Prediction

To predict accurately the onset of scaling along a membrane channel there is a need to understand and include the thermodynamics of precipitation, which signify the effect of temperature, pressure, co-precipitation, high ionic strength and salinity on the solubility product [14]. Subsequently, combining this solubility product with a simulation of the behaviour of ionic concentrations along the membrane channel, reached through use of the principles of membrane transport and mass conservation as in [10, 13], the variations of variables and parameters in a long membrane channel are predicted. Thus, using this fundamental principle, the effect of scaling salt co-existence and pressure on scaling propensity prediction has been examined and verified.

2.1. Effect of co-precipitation:

The coexistence of precipitating salts (co-precipitation) produces a product differing from that of a single salt precipitation [15]. Sheikholeslami [15] has concluded that the thermodynamic equilibrium constant of the co-precipitation is different from that of single salt precipitation. Until a completely theoretical approach is developed to calculate the solubility product of co-precipitation, the following semi-theoretical approach can be followed.

Equations 2 and 3 represent the theoretical solubility product for MX salt, which precipitates according to Eq. 1, in pure precipitation and co-precipitation systems respectively. For pure precipitation the convection is to assume the activity $a_{MX_{sp.(pure)}}$ of the solid to be unity; however, in the co-precipitation scenario the activity $a_{MX_{sp.(mix)}}$ of solid can not be assumed to be unity [16].

$$M^{z+} + X^{z-} \underset{Ksp}{\longleftrightarrow} MX(s) \qquad (1)$$

$$Ksp_{theo} = \left(\frac{a_{M^{z+}_{sp}} \, a_{X^{z-}_{sp}}}{a_{MX_{sp.(pure)}}} \right) = a_{M^{z+}_{sp}} \, a_{X^{z-}_{sp}} = Exp\left(-\frac{\Delta_r G^{\circ}}{RT}\right) \qquad (2)$$

$$Ksp_{real(sp.)} = \left(\frac{a_{M^{z+}_{sp}} \, a_{X^{z-}_{sp}}}{a_{MX_{sp.(mix)}}} \right) \qquad (3)$$

By dividing equation (3) by equation (2)

$$\frac{Ksp_{real(sp.)}}{Ksp_{theo}} = \frac{1}{a_{MX_{sp.(mix)}}} \qquad (4)$$

By defining the Co-precipitation Correction Factor (*Cf*) as $Cf = \frac{1}{a_{MX_{sp.(mix)}}}$

$$Ksp_{real(sp.)} = Cf \, . Exp\left(-\frac{\Delta_r G^{\circ}}{RT}\right) \qquad (6)$$

where T is the temperature in (*K*) and R is the Universal gas constant. $Ksp_{(exp)}$ is the experimental solubility product for the impure solid scaling salt resulting

from co-precipitation and $Ksp_{(aq)}$ is the solubility product for pure solid scaling salt calculated from the Gibbs free energy $\Delta_r G^\phi$ as seen in Eq. 2 and discussed in details elsewhere [4, 5, 13]. Therefore the scaling potential index (*SPI*) can be calculated for co-precipitation salts using Eq. 7.

$$SPI = \log(IAP / Ksp) = \log(IAP / Cf.EXP(-\Delta_r G^\phi / RT)) \quad (7)$$

where *IAP* represents the ion activity product. $Ksp_{(aq)}$ could be calculated for a specific feed water scenario using the experimental procedure followed by [17].

Thus, by using the Co-precipitation Correction Factor (*Cf*) a reliable prediction for scaling propensity for any scaling salt can be reached; and moreover the effect of temperature, pressure and salinity can be still included as described in details for pure scaling salts at [13, 14].

2.2. Effect of pressure:

The effect of pressure on the solubility product can be introduced by integrating the following Eqs (7-8),

$$\left(\frac{\partial \ln Ksp(T,P)}{\partial P}\right)_T = -\frac{\Delta V_r^\circ(T,P)}{RT} \quad (7)$$

and

$$\left(\frac{\partial \Delta V_r^\circ(T,P)}{\partial P}\right)_T = -\Delta K_r^\circ(T,P) \quad (8)$$

where ΔV_r° and ΔK_r° stand for the standard volume and compressibility changes of the precipitation reaction of the considered salt (MX) [18].

The integration of (7) and (8) leads to the following expression [16],[18, 19],.

$$\ln Ksp(T,P) = \ln Ksp(T,P_o) - \frac{\overline{\Delta V_r^\circ}}{RT}(P-P_o) + \frac{\overline{\Delta K_r^\circ}}{2RT}(P-P_o)^2 \quad (9)$$

where $\overline{\Delta V_r^\circ}$ is the standard molal volume change of the precipitation reaction and $\overline{\Delta K_r^\circ}$ is the standard molal compressibility change of the precipitation reaction. The effect of $\overline{\Delta K_r^\circ}$ can be neglected at RO pressures as it is reported [19] to be negligible at moderate pressures, which include the RO pressure. $\overline{\Delta V_r^\circ}$ is expressed for any scaling salt (MX) as:

$$\overline{\Delta V_r^\circ} = V^\circ(MX,s) - \overline{V^\circ}(MX,aq) \quad (10)$$

The values of $V^\circ(MX,s)$ for the most common scaling salts encountered in RO are tabulated in Table 1, and the value of $\overline{V^\circ}(MX,aq)$, the standard molal

volume of aqueous MX is calculated at T and P_o from those of sodium sulphate and sodium chloride [18] and of M-chloride at the same temperature and pressure using the additivity rule which is expresses by:

$$\overline{V^o}(MX,aq) = \overline{V^o}(MCl_2,aq) + \overline{V^o}(Na_2X,aq) - 2\overline{V^o}(NaClaq) \qquad (11)$$

where the value of ($\overline{V^*}$), the standard molal volume of designated aqueous electrolyte is calculated at 25°C using the algebraic transformation of [19] and tabulated on Table 1.

Table 1: The Standard Molal Volume change of the Precipitation Reaction for Common Scaling Salts

Scaling Salt	$*V^o(MX,s)$ cm^3/mol at 25°C and 1 bar	$**\overline{V^o}(MX,aq)$ cm^3/mol at 25°C	$\Delta\overline{V_r^o}$ cm^3/mol
Gypsum	74.94 [18]	2.14E+03	2.06E+03
Barite	52.1 [19],[20]	5.32E+02	4.80E+02
Celestite	46.25 [19],[20]	2.03E+03	1.98E+03

$*V^o(MX,s)$ is considered to be constant over the temperature and pressure ranges of RO desalination as it was considered constant by [19] for the range including the RO pressure range.

$**\overline{V^o}(MX,aq)$ may be calculated at any temperature up to 250°C see [19].

The solubility product, *Ksp* (T,P_o) at temperature T and reference pressure P_o (1 bar) can be calculated either from Gibbs free energies of reaction as described elsewhere [4, 5, 13] or by using Eqs (12-15) as described by [19]. Assuming the heat capacity is constant over the investigated temperature range, which is the case in the RO process, *Ksp* (T, P_o) is given by:

$$\ln Ksp\,(T,P_o) = A + B\ln T + \frac{C}{T} \qquad (12)$$

with

$$A = \frac{\Delta_r S^o}{R} - \frac{\Delta_r C_p^{\,o}}{R}[1+\ln T_o] \qquad (13)$$

$$B = \frac{\Delta_r C_p^{\,o}}{R} \qquad (14)$$

$$C = \frac{\Delta_r H^o}{R} - \frac{T_o \Delta_r C_p^{\,o}}{R} \qquad (15)$$

where $\Delta_r S^o$, $\Delta_r H^o$ and $\Delta_r C_p^o$ respectively refer to standard entropy, enthalpy and heat capacity of the dissolution reaction. R is the gas constant and T_o the reference temperature (298.15) [19].

2.3. Mathematical modeling for variation of scaling and non-scaling ion concentrations along full-scale RO membrane units.

The variation of ionic concentrations and operational variables for full scale RO can be simulated using a finite difference solution to a series of axial

pressure, concentration, and flow balance equations. The details of the mathematical model are discussed elsewhere [10, 13].

In order to predict the onset of scaling propensity inside practical RO systems, the effects of temperature, pressure, co-precipitation, high ionic strength and salinity on *SPI* were coupled with a simulation for the behaviour of ionic concentrations and operational variables. The parameter values used in these simulations were either chosen from the manufacturers' specifications or practical operating conditions as also used by others [10-12]. This simulation is capable of predicting the effects of the of operational variable variations and parameters along the membrane channel on the development of the scaling tendency, as explained and discussed in [13, 14].

3. Simulation for scaling propensity in full-scale RO

Numerical simulations have been conducted to investigate the effect of co-precipitation and RO process pressure on scaling propensity prediction along a full-scale RO unit. The confidence of the simulation has been discussed and proved elsewhere [13]. Unless otherwise specified, Table 2 shows the values of the parameters that have been used in this simulation. The simulation parameters can be adapted to specific operating conditions and unit design to suit any full scale RO process.

Table2. Parameter values for model Simulations

Length of RO system, L (m)	6
Channel height, H (m)	7×10^{-4}
Applied (pump) pressure, P_o (Pa)	5.516×10^6
Feed Salinity (mg/l)	30000
Cross flow velocity at entrance,(m/s)	0.1
Membrane intrinsic resistance,(Pa s/m)	1.8×10^{11}
Number of elements along RO system	400
Temperature, °C	25
pH	7.1
Friction coefficient due to spacers	5
Initial Na^+ concentration, ppm	9850
Initial Ca^{2+} concentration, ppm	1500
Initial Ba^{2+}, ppm	0.02
Initial Sr^{2+}, ppm	30
Initial Cl^-, ppm	15800
Initial SO_4^{2-}, ppm	2000

3.1. Scaling propensity for pure $BaSO_4$, pure $SrSO_4$ and pure $CaSO_4$ along 6 m membrane channel.

Scaling potential index gives a conservative estimate for assessing scaling potential; when *SPI* is negative, certainly no scale will form; when zero the system is at equilibrium; when the *SPI* is positive, the salt has a "potential" to form scale [4].

Figure 1 shows the development of scaling propensity in terms of *SPI* and the local permeate velocity profile along a 6m filtration channel. It is seen that the

SPI was below zero for the first meter along the permeation channel which means that in this section there would be no scale formation. However, a dramatic increase in fouling propensity develops afterwards which reaches a maximum approximately 3m along the channel.

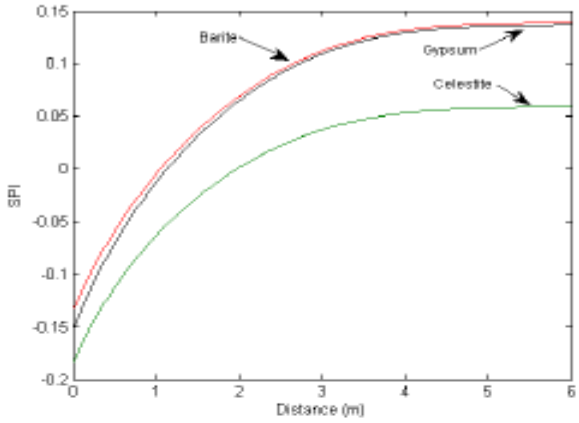

Fig.1. Scaling propensity for pure Barite, Celestite and Gypsum along a 6m membrane channel

3.2 Effect of incorporating process pressure in scaling propensity prediction

In this paper, the effect of pressure has been incorporated theoretically, for the first time, to predict the onset of scaling in a full scale RO process. The effect of pressure has usually been ignored and believed to be insignificant in RO process. However, this is not accurate as seen in Fig 2(a, b and c) for different scaling salts. It can be seen from Fig 2 (a, b and c) that neglect of the pressure effect can result in significant errors in the RO operation and design. Indeed, excluding the pressure effect will lead to a significant error in scaling propensity estimation. For celestite and gypsum, as seen in Fig. 2 (a) and Fig. 2 (c) respectively; ignoring the effect of pressure will lead to a positive *SPI* curve from the first meter downstream and further along the membrane channel, which indicates a high potential for scale formation. This prediction of high scale formation potential will require action such as installation of a pre-treatment process, decreasing of the system recovery, adding of antiscalant,…etc to mitigated the expected high scale formation, which mean additional cost will be added to the capital and production costs. In reality, after incorporating the pressure effect the *SPI* curve is negative, for both celestite and gypsum, along the whole membrane channel; indicating that no celestite and gypsum scales will form.

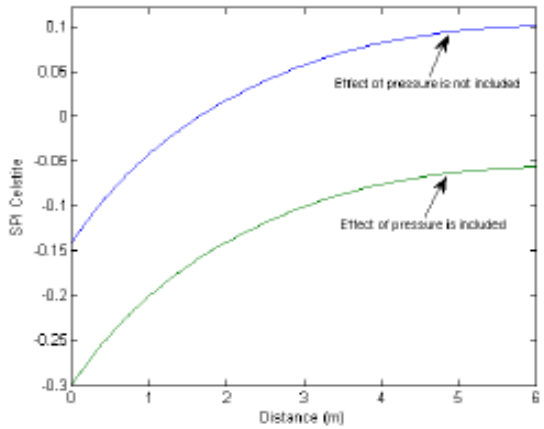

Fig.2.(a) Scaling propensity of celestite at 55 bar with and without inclusion of the pressure effect along a 6m membrane channel.

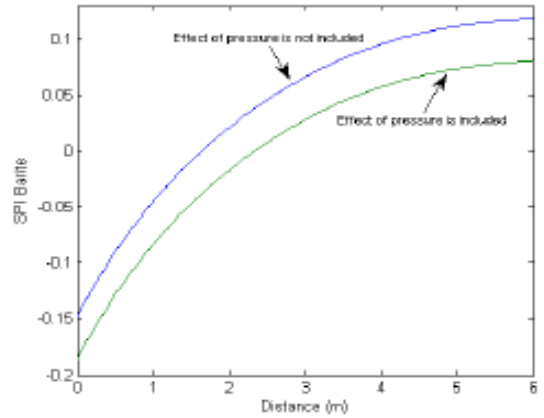

Fig.2.(b) Scaling propensity of barite at 55 bar with and without inclusion of the pressure effect along a 6m membrane channel.

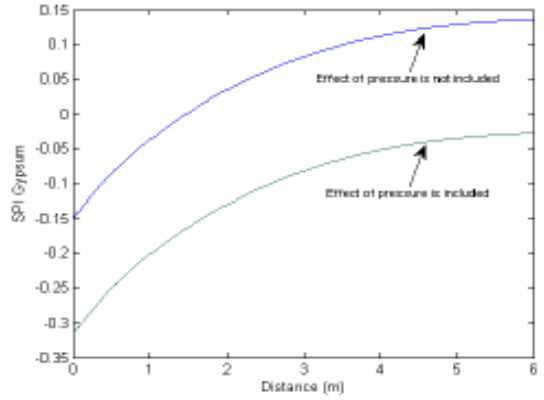

Fig.2.(c) Scaling propensity of gypsum at 55 bar with and without inclusion of the pressure effect along a 6m membrane channel.

3.3. Effect of salt co-existence in scaling propensity prediction

AS an example of the effect of co-precipitation; Rushdi et al. [16] found that the estimated barite activities at equilibrium with seawater at 20°C and 25°C is respectively 1.25 and 1.36 and that for celestite, it is 1.001. For Barite, involvement of other cations, such as Ca and K, in the crystal structure could affect its activity, but it has been reported that Sr is likely to be the primary contaminant [21, 22]. Rushdi et al. [16] Barite and Celestite activity values have been used to calculate the Co-precipitation correction factor (*Cf*) as explained in section 2.1.

Fig. 3a shows the scaling propensity prediction of Barite with and without taking into account the effect of Celestite- Barite co-precipitation. As seen in Fig. 3a the effect of co-precipitation on the Barite scaling propensity is a crucial factor and should not be ignored; as can be observed, ignoring the effect of co-precipitation gives a serious underestimate of the onset of Barite scaling. However, in case of Celestite precipitation it seems, as seen in Fig.3b, that there is no effect of Barite co-precipitation on the onset of Celestite scaling.

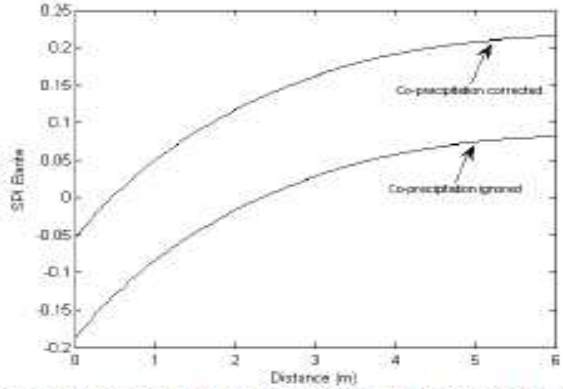

Fig. 3 (a) Scaling propensity prediction of Barite with and without taking into account the effect of Celestite- Barite co-precipitation

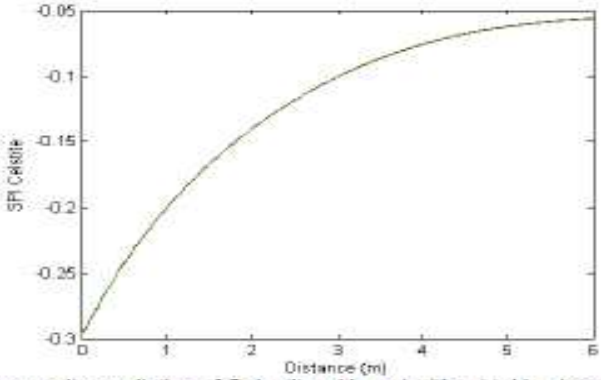

Fig. 3 (b) Scaling propensity prediction of Celestite with and without taking into account the effect of Celestite- Barite co-precipitation

4. CONCLUSION

In this paper a new procedure for incorporating the effect of co-precipitation of the scaling salts on scaling propensity prediction was introduced and discussed. The consequence of ignoring the effect of RO process pressure on solubility product and scaling propensity prediction during RO processes was highlighted and discussed. Taking into account the effect of co-precipitation and the pressure effect are essential to a reliable predication of the scaling propensity. The current industrial practice of using solubility data for single salt precipitation, where co-precipitation can exist, and ignoring the effect of pressure within the RO system in predicting the onset of scaling leads to a significant error in scaling propensity prediction, which adds extra costs to the RO process in pre-treatment and scheduled shutoffs.

NOMENCLATURE

aq	aqueous phase
G	standard Gibbs free energy
IAP	ion activity products
Ksp	thermodynamic solubility product
P	pressure (bar)
P_o	reference pressure (1 bar)
R	the universal gas constant
s	solid phase
SPI	scaling potential index
T	temperature (K)
V	volume of the dissolution reaction
$\bar{V}$	molal volume of the dissolution reaction

Greek letters

α	activity
Δ	denote the difference between two values
$\Delta_f G^{\Phi}$	standard Gibbs free energy of formation
ΔK_r°	standard compressibility of the dissolution reaction
$\Delta \overline{K_r^{\circ}}$	standard molal compressibility of the dissolution reaction
$\Delta_r C_p^{\circ}$	standard heat capacity
$\Delta_r G^{\Phi}$	standard molar Gibbs free energy of reaction
$\Delta_r H$	enthalpy of reaction
$\Delta_r S^{\circ}$	standard entropy
ΔV_r°	standard volume of the dissolution reaction
$\Delta \overline{V_r^{\circ}}$	standard molal volume of the dissolution reaction
γ	activity coefficient

Subscripts

0	reference value

Superscripts

Φ	reference temperature value
0	reference value
f	formation
r	reaction

References

[1] A.D. Khawaji, I.K. Kutubkhanah, J.-M. Wie, Advances in seawater desalination technologies, Desalination, 221 (2008) 47-69.

[2] A. Fakhru'l-Razi, A. Pendashteh, L.C. Abdullah, D.R.A. Biak, S.S. Madaeni, Z.Z. Abidin, Review of technologies for oil and gas produced water treatment, Journal of Hazardous Materials, 170 (2009) 530-551.

[3] R. Sheikholeslami, Fouling in Membranes and thermal Units: A Unified Approach- Its Principles, Assessment, Control and Mitigation, Balaban Desalination Publications, 2007.

[4] R. Sheikholeslami, Assessment of the scaling potential for sparingly soluble salts in RO and NF units, Desalination, 167 (2004) 247-256.

[5] R. Sheikholeslami, Scaling potential index (SPI) for CaCO3 based on Gibbs free energies, AIChE Journal, 51 (2005) 1782-1789.

[6] W.E. Langelier, Chemical equilibria in water treatment, J. AWWA, 38 (1946) 169.

[7] J.H.A. Stiff, L.E. Davis, a method for predicting the tendency of oil field water to deposit calcium carbonate, Pet. Trans. AIME, 195 (1952) 213.

[8] J.W. Ryznar, A new index for determining amount of calcium carbonate scale formed by a water, J. AWWA, 36 (1944) 472.

[9] P.R. Puckorius, J.M. Brooke, A new practical index for calcium carbonate scale producing in cooling tower systems, Corrosion, 74 (1991) 280-284.

[10] L. Song, S. Hong, J. Hu, S. Ong, W. Ng, Simulations of Full-Scale Reverse Osmosis Membrane Process Journal of Environmental Engineering 128 (2002) 960-966.

[11] K.L. Chen, L. Song, S.L. Ong, W.J. Ng, The development of membrane fouling in full-scale RO processes, Journal of Membrane Science, 232 (2004) 63-72.

[12] K.G. Tay, L. Song, A more effective method for fouling characterization in a full-scale reverse osmosis process, Desalination, 177 (2005) 95-107.

[13] E. Alhseinat, R. Sheikholeslami, A Completely Theoretical Approach for Assessing Fouling Propensity along Full-Scale RO Process Desalination, (in Press).

[14] E. Alhseinat, R. Sheikholeslami, An Application for New Reliable Approach to Predict the Onset of Barite, Celestite and Gypsum Scaling during Reverse Osmosis Treatment for Produced Water, International Journal of Environmental Science and Development (IJESD), 2 (2011) 454-459.

[15] R. Sheikholeslami, Fouling in Membranes and Thermal Units: A Unified Approach- its Principles Assessment, Control and Mitigation, Balaban Desalination publications, L'Aquila, Italy, 2007.

[16] A.I. Rushdi, J. McManus, R.W. Collier, Marine barite and celestite saturation in seawater, Marine Chemistry, 69 (2000) 19-31.

[17] R. Sheikholeslami, H.W.K. Ong, Kinetics and thermodynamics of calcium carbonate and calcium sulfate at salinities up to 1.5 M, Desalination, 157 (2003) 217-234.

[18] M. Christophe, The influence of pressure on the activity coefficients of the solutes and on the solubility of minerals in the system Na-Ca-Cl-SO4-H2O to 200°C and 1 kbar and to high NaCl concentration, Geochimica et Cosmochimica Acta, 54 (1990) 3265-3282.

[19] C. Monnin, A thermodynamic model for the solubility of barite and celestite in electrolyte solutions and seawater to 200°C and to 1 kbar, Chemical Geology, 153 (1999) 187-209.

[20] F.J. Millero, The effect of pressure on the solubility of minerals in water and seawater, Geochimica et Cosmochimica Acta, 46 (1982) 11-22.

[21] T.M. Church, Marine Minerals, In: Burns, R.G. (Ed.), Mineralogical Society of America, 6 (1979) 175-209.

[22] R. Dehairs, R. Chesselet, J. Jedwab, Discrete suspended particles of barite and the barium cycle in the open ocean, Earth Planet. Sci. Lett, (1980) 529–550.

Appendix B: Matlab programs

B.1 Anion activity coefficient

Here is below the main Matlab code that have been written and used with other Matlab programs to calculate the anion activity coefficient.

Matlab anion activity coefficient program:

```
function[gammaa] = gamma_anion(ioi, no_anions, no_cations, molality_i, z_mat, b, A_phi,
alpha_1, alpha_2, beta_0_mat, beta_1_mat, beta_2_mat, phi_cc_mat, phi_aa_mat,
C_phi_mat, Psi_ccA_mat, Psi_aaC_mat, identifier_mat, phi_cc_prime_mat,
phi_aa_prime_mat)


total_no_ions = no_cations + no_anions; % defines the total number of ions to be
analysed.


%% Part 1 %%

% Calculate F %

% Part 1 of F %
I_sum_mat = zeros(1,total_no_ions);
for ii = 1:1:total_no_ions
    I_sum_mat(1,ii) = molality_i(1,ii) * (z_mat(1,ii)^2);
end
I = 0.5 * sum(I_sum_mat); % calculates I

f_gamma = (-1 * A_phi) * ( ((I^0.5)/(1 + (b*(I^0.5)))) + ((2/b)*log(1+b*(I^0.5))) ); %
calculates f_gamma

% Part 2 of F %
g_prime_alpha_1 = (-2 * (1 - ((1 + (alpha_1*(I^0.5)) + (0.5*((alpha_1*(I^0.5))^2)))*exp
(-(alpha_1*(I^0.5)))))) / ((alpha_1*(I^0.5))^2);
g_prime_alpha_2 = (-2 * (1 - ((1 + (alpha_2*(I^0.5)) + (0.5*((alpha_2*(I^0.5))^2)))*exp
(-(alpha_2*(I^0.5)))))) / ((alpha_2*(I^0.5))^2);
g_prime_alpha_3 = (-2 * (1 - ((1 + (2*(I^0.5)) + (0.5*((2*(I^0.5))^2)))*exp(-(2*(I^0.
5)))))) / ((2*(I^0.5))^2);
g_prime_alpha_4 =0;
B_prime_mat = zeros(no_cations,no_anions);
for ii = 1:1:no_cations
    for jj = 1:1:no_anions
        ioi_c = identifier_mat(1,ii);
        ioi_a = identifier_mat(1,jj);
        if z_mat(1,ioi_c)==2 && z_mat(1,ioi_a)==2
            B_prime_mat(ii,jj) = (beta_1_mat(ii,jj)/I * g_prime_alpha_1) + (beta_2_mat
(ii,jj)/I * g_prime_alpha_2);
        else
            B_prime_mat(ii,jj) = (beta_1_mat(ii,jj)/I * g_prime_alpha_3);
       end
    end
end

sum_2 = 0;
for ii = 1:1:no_cations
    for jj = no_cations+1:1:total_no_ions
        sum_2 = sum_2 + (molality_i(1,ii) * molality_i(1,jj)*B_prime_mat(ii,jj-
no_cations));
    end
end

% Part 3 of F %
sum_3 = 0;
```

```
for ii = 1:1:no_cations
    for jj = ii+1:1:no_cations
        sum_3 = sum_3 + (molality_i(1,ii)*molality_i(1,jj)*phi_cc_prime_mat(ii,jj));
    end
end

% Part 4 of F %
sum_4 = 0;
for ii = 1:1:no_anions
    for jj = ii+1:1:no_anions
        sum_4 = sum_4 + (molality_i(1,ii+no_cations)*molality_i(1,jj+no_cations)↙
*phi_aa_prime_mat(ii,jj));
    end
end

F = f_gamma + sum_2 + sum_3 + sum_4; % calculates F

part_1 = 0.85*(z_mat(1,ioi)^2) * F; % calculates part 1 of Gamma equation


%% Part 2 %%

Z_sum_mat = zeros(1,total_no_ions);
for ii = 1:1:total_no_ions
    Z_sum_mat(1,ii) = molality_i(1,ii) * (sqrt(z_mat(1,ii)^2));
end
Z = sum(Z_sum_mat); % calculates Z

g_alpha_1 = (2 * (1 - ((1 + (alpha_1*(I^0.5)))*exp(-(alpha_1*(I^0.5)))))) / ((alpha_1*↙
(I^0.5))^2);
g_alpha_2 = (2 * (1 - ((1 + (alpha_2*(I^0.5)))*exp(-(alpha_2*(I^0.5)))))) / ((alpha_2*↙
(I^0.5))^2);
g_alpha_3 = (2 * (1 - ((1 + (2*(I^0.5)))*exp(-(2*(I^0.5)))))) / ((2*(I^0.5))^2);
g_alpha_4 = 0;
B_mat = zeros(no_cations, no_anions);
for ii = 1:1:no_cations
    for jj = 1:1:no_anions
        ioi_c = identifier_mat(1,ii);
        ioi_a = identifier_mat(1,jj);
        if z_mat(1,ioi_c)==2 && z_mat(1,ioi_a)==2
        B_mat(ii,jj) = beta_0_mat(ii,jj) + (beta_1_mat(ii,jj) * g_alpha_1) +↙
(beta_2_mat(ii,jj) * g_alpha_2);
        else
        B_mat(ii,jj) = beta_0_mat(ii,jj) + (beta_1_mat(ii,jj) * g_alpha_3) +↙
(beta_2_mat(ii,jj) * g_alpha_4);
        end
    end
end

C_mat = zeros(no_cations, no_anions);
for ii = 1:1:no_cations
    for jj = 1:1:no_anions
        ioi_c = identifier_mat(1,ii);
        ioi_a = identifier_mat(1,jj);
        C_mat(ii,jj) = C_phi_mat(ii,jj) / ((2*(sqrt((sqrt((z_mat(1,ioi_c)*z_mat(1,↙
ioi_a))^2))))));
```

```
    end
end

part_2 = 0;
for ii = 1:1:no_cations
    part_2 = part_2 + (molality_i(1,no_cations)*((2*B_mat(ii,ioi))+(Z*C_mat(ii,ioi))));
end


%% Part 3 %%

part_3 = 0;
for ii = 1:1:no_anions
    sub_sum_3 = 0;
    for jj = 1:1:no_cations
        sub_sum_3 = sub_sum_3 + (molality_i(1,jj) * Psi_aaC_mat(ii,ioi,jj));
    end
    part_3 = part_3 + (molality_i(1,ii+no_cations) * ((2*phi_aa_mat(ioi,ii)) +↙
sub_sum_3));
end

%% Part 4 %%

part_4 = 0;
for ii = 1:1:no_cations
    for jj = ii+1:1:no_cations
        part_4 = part_4 + (molality_i(1,ii) * molality_i(1,jj) * Psi_ccA_mat(ii,jj,↙
ioi));
    end
end


%% Part 5 %%

part_5 = 0;
for ii = 1:1:no_cations
    for jj = 1:1:no_anions
        part_5 = part_5 + z_mat(1,ioi)* (molality_i(1,ii) * molality_i(1,jj+no_cations)↙
* C_mat(ii,jj));
    end
end


%% Final %%

ln_gamma_a = part_1 + part_2 + part_3 + part_4 + part_5;

gammaa = exp(ln_gamma_a);
```

B.2 Cation activity coefficient

Here is below the main Matlab code that have been written and used with other Matlab programs to calculate the cation activity coefficient.

Cation Matlab program:

```
function[gammac] = gamma_cation(ioi, no_anions, no_cations, molality_i, z_mat, b,
A_phi, alpha_1, alpha_2, beta_0_mat, beta_1_mat, beta_2_mat, phi_cc_mat, phi_aa_mat,
C_phi_mat, Psi_ccA_mat, Psi_aaC_mat, identifier_mat, phi_cc_prime_mat,
phi_aa_prime_mat)


total_no_ions = no_cations + no_anions; % defines the total number of ions to be
analysed


%% Part 1 %%

% Calculate F %

% Part 1 of F %
I_sum_mat = zeros(1,total_no_ions);
for ii = 1:1:total_no_ions
    I_sum_mat(1,ii) = molality_i(1,ii) * (z_mat(1,ii)^2);
end
I = 0.5 * sum(I_sum_mat); % calculates I

f_gamma = (-1 * A_phi) * ( ((I^0.5)/(1 + (b*(I^0.5)))) + ((2/b)*log(1+b*(I^0.5))) ); %
calculates f_gamma

% Part 2 of F %
g_prime_alpha_1 = (-2 * (1 - ((1 + (alpha_1*(I^0.5)) + (0.5*((alpha_1*(I^0.5))^2)))*exp
(-(alpha_1*(I^0.5)))))) / ((alpha_1*(I^0.5))^2);
g_prime_alpha_2 = (-2 * (1 - ((1 + (alpha_2*(I^0.5)) + (0.5*((alpha_2*(I^0.5))^2)))*exp
(-(alpha_2*(I^0.5)))))) / ((alpha_2*(I^0.5))^2);
g_prime_alpha_3 = (-2 * (1 - ((1 + (2*(I^0.5)) + (0.5*((2*(I^0.5))^2)))*exp(-(2*(I^0.
5)))))) / ((2*(I^0.5))^2);
g_prime_alpha_4 =0;
B_prime_mat = zeros(no_cations,no_anions);
for ii = 1:1:no_cations
    for jj = 1:1:no_anions
        ioi_c = identifier_mat(1,ii);
        ioi_a = identifier_mat(1,jj);
        if z_mat(1,ioi_c)==2 && z_mat(1,ioi_a)==2
            B_prime_mat(ii,jj) = (beta_1_mat(ii,jj)/I * g_prime_alpha_1) + (beta_2_mat
(ii,jj)/I * g_prime_alpha_2);
        else
            B_prime_mat(ii,jj) = (beta_1_mat(ii,jj)/I * g_prime_alpha_3);
       end
    end
end

sum_2 = 0;
for ii = 1:1:no_cations
    for jj = no_cations+1:1:total_no_ions
        sum_2 = sum_2 + (molality_i(1,ii) * molality_i(1,jj)*B_prime_mat(ii,jj-
no_cations));
    end
end

% Part 3 of F %
```

```
sum_3 = 0;
for ii = 1:1:no_cations
    for jj = ii+1:1:no_cations
        sum_3 = sum_3 + (molality_i(1,ii)*molality_i(1,jj)*phi_cc_prime_mat(ii,jj));
    end
end

% Part 4 of F %
sum_4 = 0;
for ii = 1:1:no_anions
    for jj = ii+1:1:no_anions
        sum_4 = sum_4 + (molality_i(1,ii+no_cations)*molality_i(1,jj+no_cations)↙
*phi_aa_prime_mat(ii,jj));
    end
end

F = f_gamma + sum_2 + sum_3 + sum_4; % calculates F

part_1 = (z_mat(1,ioi)^2) * F; % calculates part 1 of Gamma equation


%% Part 2 %%

Z_sum_mat = zeros(1,total_no_ions);
for ii = 1:1:total_no_ions
    Z_sum_mat(1,ii) = molality_i(1,ii) * (sqrt(z_mat(1,ii)^2));
end
Z = sum(Z_sum_mat); % calculates Z

g_alpha_1 = (2 * (1 - ((1 + (alpha_1*(I^0.5)))*exp(-(alpha_1*(I^0.5)))))) / ((alpha_1*↙
(I^0.5))^2);
g_alpha_2 = (2 * (1 - ((1 + (alpha_2*(I^0.5)))*exp(-(alpha_2*(I^0.5)))))) / ((alpha_2*↙
(I^0.5))^2);
g_alpha_3 = (2 * (1 - ((1 + (2*(I^0.5)))*exp(-(2*(I^0.5)))))) / ((2*(I^0.5))^2);
g_alpha_4 = 0;
B_mat = zeros(no_cations, no_anions);
for ii = 1:1:no_cations
    for jj = 1:1:no_anions
        ioi_c = identifier_mat(1,ii);
        ioi_a = identifier_mat(1,jj);
        if z_mat(1,ioi_c)==2 && z_mat(1,ioi_a)==2
        B_mat(ii,jj) = beta_0_mat(ii,jj) + (beta_1_mat(ii,jj) * g_alpha_1) +↙
(beta_2_mat(ii,jj) * g_alpha_2);
        else
        B_mat(ii,jj) = beta_0_mat(ii,jj) + (beta_1_mat(ii,jj) * g_alpha_3) +↙
(beta_2_mat(ii,jj) * g_alpha_4);
        end
    end
end

C_mat = zeros(no_cations, no_anions);
for ii = 1:1:no_cations
    for jj = 1:1:no_anions
        ioi_c = identifier_mat(1,ii);
        ioi_a = identifier_mat(1,jj);
        C_mat(ii,jj) = C_phi_mat(ii,jj) / ((2*(sqrt((sqrt((z_mat(1,ioi_c)*z_mat(1,↙
```

```
ioi_a))^2))))));
    end
end

part_2 = 0;
for ii = 1:1:no_anions
    part_2 = part_2 + (molality_i(1,ii+no_cations)*((2*B_mat(ioi,ii))+(Z*C_mat(ioi,↙
ii))));
end


%% Part 3 %%

part_3 = 0;
for ii = 1:1:no_cations
    sub_sum_3 = 0;
    for jj = 1:1:no_anions
        sub_sum_3 = sub_sum_3 + (molality_i(1,jj+no_cations) * Psi_ccA_mat(ioi,ii,jj));
    end
    part_3 = part_3 + (molality_i(1,ii) * ((2*phi_cc_mat(ioi,ii)) + sub_sum_3));

end

%% Part 4 %%

part_4 = 0;
for ii = 1:1:no_anions
    for jj = ii+1:1:no_anions
        part_4 = part_4 + (molality_i(1,ii+no_cations) * molality_i(1,jj+no_cations) *↙
Psi_aaC_mat(ii,jj,ioi));
    end
end

%% Part 5 %%

part_5 = 0;
for ii = 1:1:no_cations
    for jj = 1:1:no_anions
        part_5 = part_5 + (z_mat(1,ioi) * (molality_i(1,ii) * molality_i(1,↙
jj+no_cations) * C_mat(ii,jj)));
    end
end


%% Final %%

ln_gamma_c = part_1 + part_2 + part_3 + part_4 + part_5;

gammac = exp(ln_gamma_c);
```

B.3 Osmotic coefficient

```
function[alpha_os] = alphaosmo(A_phi, molality_i, no_anions, no_cations, C_phi_mat,
z_mat, b, alpha_1, alpha_2, beta_0_mat, beta_1_mat, beta_2_mat, phi_cc_mat, phi_aa_mat,
phi_cc_prime_mat, phi_aa_prime_mat, Psi_ccA_mat, Psi_aaC_mat, identifier_mat)

%% background calcs %%
total_no_ions = no_anions + no_cations;


%% part 1 %%

I_sum_mat = zeros(1,total_no_ions);
for ii = 1:1:total_no_ions
    I_sum_mat(1,ii) = molality_i(1,ii) * (z_mat(1,ii)^2);
end
I = 0.5 * sum(I_sum_mat);

part_1 = ((-1*A_phi)*(I^(3/2))) / (1 + (b*(I^(1/2))));

%% part 2 %%

B_phi_mat = zeros(no_cations,no_anions);
for ii = 1:1:no_cations
    for jj = 1:1:no_anions
        ioi_c = identifier_mat(1,ii);
        ioi_a = identifier_mat(1,jj);
        if z_mat(1,ioi_c)==2 && z_mat(1,ioi_a)==2
        B_phi_mat(ii,jj) = beta_0_mat(ii,jj) + (beta_1_mat(ii,jj) * (exp((-1*alpha_1)*
(I^0.5)))) + (beta_2_mat(ii,jj) * (exp((-1*alpha_2)*(I^0.5))));
        else
        B_phi_mat(ii,jj) = beta_0_mat(ii,jj) + (beta_1_mat(ii,jj) * (exp((-1*2)*(I^0.
5)))) + (beta_2_mat(ii,jj) * (exp((-1*0)*(I^0.5))));
        end
    end
end

C_mat = zeros(no_cations, no_anions);
for ii = 1:1:no_cations
    for jj = 1:1:no_anions
        ioi_c = identifier_mat(1,ii);
        ioi_a = identifier_mat(1,jj);
        C_mat(ii,jj) = C_phi_mat(ii,jj) / ((2*((sqrt((z_mat(1,ioi_c)*z_mat(1,ioi_a))
^2))^0.5)));
    end
end

Z_sum_mat = zeros(1,total_no_ions);
for ii = 1:1:total_no_ions
    Z_sum_mat(1,ii) = molality_i(1,ii) * (sqrt(z_mat(1,ii)^2));
end
Z =0.5 * sum(Z_sum_mat);


part_2 = 0;
for ii = 1:1:no_cations
    for jj = 1:1:no_anions
        part_2 = part_2 + (molality_i(1,ii) * molality_i(1,no_cations+jj)*(B_phi_mat
(ii,jj) + (Z * C_mat(ii,jj))));
```

```
    end
end

%% part 3 %%

phi_phi_cc_mat = zeros(no_cations,no_cations);
for ii = 1:1:no_cations
    for jj = 1:1:no_cations
        phi_phi_cc_mat(ii,jj) = phi_cc_mat(ii,jj) + (I * phi_cc_prime_mat(ii,jj));
    end
end

part_3 = 0;
for ii = 1:1:no_cations
    for jj = ii+1:1:no_cations

        sub_sum = 0;
        for kk = 1:1:no_anions
            sub_sum = sub_sum + (molality_i(1,kk+no_cations) * Psi_ccA_mat(ii,jj,kk));
        end

        part_3 = part_3 + molality_i(1,ii) * molality_i(1,jj) * (phi_phi_cc_mat(ii,jj)↙
+ sub_sum);

    end
end

%% part 4 %%
phi_phi_aa_mat = zeros(no_anions,no_anions);
for ii = 1:1:no_anions
    for jj = 1:1:no_anions
        phi_phi_aa_mat(ii,jj) = phi_aa_mat(ii,jj) + (I * phi_aa_prime_mat(ii,jj));
    end
end

part_4 = 0;
for ii = 1:1:no_anions
    for jj = ii+1:1:no_anions

        sub_sum = 0;
        for kk = 1:1:no_cations
            sub_sum = sub_sum + (molality_i(1,kk) * Psi_aaC_mat(ii,jj,kk));
        end

        part_4 = part_4 + molality_i(1,ii+no_cations) * molality_i(1,jj+no_cations) *↙
(phi_phi_aa_mat(ii,jj) + sub_sum);

    end
end


%% final summation %%
sum_mol = sum(molality_i);

alpha_os = ((2/sum_mol)*(part_1 + part_2 + part_3 + part_4)) + 1;
```

B.4 Full scale membrane process

```
clear all
close all
clc

%% Read In from XL Sheets - to be set prior to running %%

charge_identity_c = xlsread('Constants_Tables.xls', 'Cation', 'D10:J10');
charge_identity_a = xlsread('Constants_Tables.xls', 'Anion', 'D10:I10');
charge_identity = [charge_identity_c charge_identity_a];
beta_values = xlsread('Constants_Tables.xls', 'Beta_Values', 'E5:J46');
phi_cc_vals = xlsread('Constants_Tables.xls', 'Phi_Values', 'F6:I54');
phi_aa_vals = xlsread('Constants_Tables.xls', 'Phi_Values', 'L6:O41');
Psi_ccA_vals = xlsread('Constants_Tables.xls', 'Psi_Values', 'F6:M54');
Psi_aaC_vals = xlsread('Constants_Tables.xls', 'Psi_Values', 'Q6:Y41');
```

```
%% Input of Initial Parameters by User %%

L =input('input Length of RO system (m) - ');
H = input('input channel height (m) - ');
Kspcer = input('input Kspacer - ');
no_cations = input('input number of cations - ');
no_anions = input('input number of aniaons - ');
T = input('input system Temperature(K) -');
R=8.314*10^-3;
delta_gibbsCa=-553.5;%kj/mol
delta_gibbsSO4=-744.5;
delta_gibbsCO3=-527.9;
delta_gibbsCalcite=-1128.8;
delta_gibbsGypsum=-1798.2;
delta_gibbsArgonite=-1127.8;
delta_gibbsH2O= -237.1;
delta_enthalpy_Ca=-542.83;
delta_enthalpy_SO4=-909.2;
delta_enthalpy_CO3=-677.1;
delta_enthalpy_CaSO4=-2022.6;
delta_enthalpy_Calicite=-1207.4;
delta_enthalpy_argonate=-1207.4;
delta_enthalpy_H2O=-285.83;
Ksp_Calcite=exp(-1*((delta_gibbsCa+delta_gibbsCO3-delta_gibbsCalcite)/(R*298.15)));
delta_gibbs_calcite=(delta_gibbsCa+delta_gibbsCO3-delta_gibbsCalcite);
Ksp_T_Calcite=exp(-1*((((T/298.15)*delta_gibbs_calcite)+↙
((delta_enthalpy_Ca+delta_enthalpy_CO3-delta_enthalpy_Calicite)*(1-(T/298.15))))/↙
(R*T)));
Ksp_Argonate=exp(-1*((delta_gibbsCa+delta_gibbsCO3-delta_gibbsArgonite)/(R*298.15)));
delta_gibbs_argonate=(delta_gibbsCa+delta_gibbsCO3-delta_gibbsArgonite);
Ksp_T_Argonate=exp(-1*((((T/298.15)*delta_gibbs_argonate)+↙
((delta_enthalpy_Ca+delta_enthalpy_CO3-delta_enthalpy_argonate)*(1-(T/298.15))))/↙
(R*T)));
Ksp_Gypsum=exp(-1*((delta_gibbsCa+delta_gibbsSO4+2*delta_gibbsH2O-(delta_gibbsGypsum))/↙
(R*298.15)));
delta_gibbs_gypsum=(delta_gibbsCa+delta_gibbsSO4+2*delta_gibbsH2O-delta_gibbsGypsum);
Ksp_T_Gypsum=exp(-1*((((T/298.15)*delta_gibbs_gypsum)+↙
(delta_enthalpy_Ca+delta_enthalpy_SO4+2*delta_enthalpy_H2O-delta_enthalpy_CaSO4)*(1-↙
(T/298.15))))/(R*T));

total_no_ions = no_cations + no_anions; % defines the total number of ions to be↙


analysed
importance_mat = zeros(1,total_no_ions);
identifier_mat = zeros(1,total_no_ions);
for i = 1:1:no_cations
    identifier_mat(1,i) = input(['input identifier for cation ', num2str(i), ' where↙
Na=1, Ca=2, Mg=3, MgOH=4, H=5, K=6, Sr=7 - ']);
    importance_mat(1,i) = input('Is this an ion of interest? yes = 1, no = 0 ');
end
for i = 1:1:no_anions
    identifier_mat(1,(no_cations+i)) = input(['input identifier for anion ', num2str↙
(i), ' where Cl=1, SO4=2, HSO4=3, OH=4, HCO3=5, CO3=6 - ']);
    importance_mat(1,(no_cations+i)) = input('Is this an ion of interest? yes = 1, no =↙
0 ');
end
```

```
zeta = input('input water visvosity - ');
Rm =input('input membrane intrinsic resistance (Pa.s/m) - ');
n = input('input number of elements along RO system - ');
dx = L / n; % defines the increment
r = input('enter the rejection of Na(%) '); % 0.995
Water_density = input(['enter water Dinsity  (g/L) ', num2str(i), ' - ']);
Salinity = zeros(n+1,1); % one value per loop
S=zeros(n+1,1);
Salinity(1,1) = input(['enter water Salinity  (mg/L) ', num2str(i), ' - ']);
Mass_solvent = zeros(n+1,1); % one value per loop
Mass_solvent_n=zeros(n+1,1);
Mass_solvent_w=zeros(n+1,1);
Salinity_w=zeros(n+1,1);
Salinity_w(1,1)=Salinity(1,1);
S_w=zeros(n+1,1);
%% Values for the Gamma Calculation

b = 1.2;% input('Input value of interaction parameter b ');
A_phi =0.3915;% input('Input value of interaction parameter A (phi) ');
alpha_1 = 1.4;%input('Input value of interaction parameter alpha 1 ');
alpha_2 = 12;%input('Input value of interaction parameter alpha 2 ');

% create z matricies %
z_mat = zeros(1,total_no_ions);
for i = 1:1:no_cations
    locator = identifier_mat(1,i);
    z_mat(1,i) = charge_identity(1,locator);
end
for i = 1:1:no_anions
    locator = identifier_mat(1,(no_cations+i));
    z_mat(1,(no_cations+i)) = charge_identity(1,locator);
end

% create beta and C_phi matricies %
[r_beta_values,c_beta_values] = size(beta_values);
beta_0_mat = zeros(no_cations,no_anions);
beta_1_mat = zeros(no_cations,no_anions);
beta_2_mat = zeros(no_cations,no_anions);
C_phi_mat = zeros(no_cations,no_anions);
for i = 1:1:no_cations
    for j = 1:1:no_anions

        ioi_c = identifier_mat(1,i);
        ioi_a = identifier_mat(1,(no_cations+j));
        for ii = 1:1:r_beta_values
            if beta_values(ii,1) == ioi_c && beta_values(ii,2) == ioi_a
                beta_0_mat(i,j) = beta_values(ii,3);
                beta_1_mat(i,j) = beta_values(ii,4);
                beta_2_mat(i,j) = beta_values(ii,5);
                C_phi_mat(i,j) = beta_values(ii,6);
                break
            end
        end

    end
end
```

```
        ioi_c = identifier_mat(1,i);
        ioi_a = identifier_mat(1,(no_cations+j));
        for ii = 1:1:r_beta_values
            if beta_values(ii,1) == ioi_c && beta_values(ii,2) == ioi_a
                beta_0_mat(i,j) = beta_values(ii,3);
                beta_1_mat(i,j) = beta_values(ii,4);
                beta_2_mat(i,j) = beta_values(ii,5);
                C_phi_mat(i,j) = beta_values(ii,6);
                break
            end
        end

    end
end

% create Phi Matricies
[r_Phi_cc, c_Phi_cc] = size(phi_cc_vals);
phi_cc_mat = zeros(no_cations,no_cations);
phi_cc_prime_mat = zeros(no_cations,no_cations);
for i = 1:1:no_cations
    for j = 1:1:no_cations
        ioi_c1 = identifier_mat(1,i);
        ioi_c2 = identifier_mat(1,j);
        for ii = 1:1:r_Phi_cc
            if phi_cc_vals(ii,1) == ioi_c1 && phi_cc_vals(ii,2) == ioi_c2
                phi_cc_mat(i,j) = phi_cc_vals(ii,3);
                phi_cc_prime_mat(i,j) = phi_cc_vals(ii,4);
                break
            end
        end
    end
end
[r_Phi_aa, c_Phi_aa] = size(phi_aa_vals);
phi_aa_mat = zeros(no_anions,no_anions);
phi_aa_prime_mat = zeros(no_anions,no_anions);
for i = 1:1:no_anions
    for j = 1:1:no_anions
        ioi_a1 = identifier_mat(1,i+no_cations);
        ioi_a2 = identifier_mat(1,j+no_cations);
        for ii = 1:1:r_Phi_aa
            if phi_aa_vals(ii,1) == ioi_a1 && phi_aa_vals(ii,2) == ioi_a2
                phi_aa_mat(i,j) = phi_aa_vals(ii,3);
                phi_aa_prime_mat(i,j) = phi_aa_vals(ii,4);
                break
            end
        end
    end
end

% create 3D Psi Matricies
[r_Psi_ccA,c_Psi_ccA] = size(Psi_ccA_vals);
Psi_ccA_mat = zeros(no_cations,no_cations,(no_anions+2));
for ia = 1:1:no_anions
    ioi_a = identifier_mat(1,ia);
    for ic = 1:1:no_cations
        for jc = 1:1:no_cations
```

```
            ioi_c1 = identifier_mat(1,ic);
            ioi_c2 = identifier_mat(1,jc);
            for ii = 1:1:r_Psi_ccA
                if Psi_ccA_vals(ii,1) == ioi_c1 && Psi_ccA_vals(ii,2) == ioi_c2
                    Psi_ccA_mat(ic,jc,ia) = Psi_ccA_vals(ii,(ia+2));
                    break
                end
            end
        end
    end
end
[r_Psi_aaC,c_Psi_aaC] = size(Psi_aaC_vals);
Psi_aaC_mat = zeros(no_anions,no_anions,(no_cations+2));
for ic = 1:1:no_cations
    ioi_c = identifier_mat(1,ic);
    for ia = 1:1:no_anions
        for ja = 1:1:no_anions
            ioi_a1 = identifier_mat(1,ia+no_cations);
            ioi_a2 = identifier_mat(1,ja+no_cations);
            for ii = 1:1:r_Psi_aaC
                if Psi_aaC_vals(ii,1) == ioi_a1 && Psi_aaC_vals(ii,2) == ioi_a2
                    Psi_aaC_mat(ia,ja,ic) = Psi_aaC_vals(ii,(ic+2));
                    break
                end
            end
        end
    end
end

dx_mat = zeros(n+1,1);
for dxdx = 1:1:n+1
    dx_mat(dxdx,1) = (dxdx-1) * dx;
end

% ion concentrations %

c_mat = zeros(n+1,total_no_ions); % concentration matrix
for j = 1:1:no_cations
    c_mat(1,j) = input(['enter the initial concentration of cation in ppm', num2str(j),↙
' - ']); % 10000
end

c_mat_w =zeros(n+1,total_no_ions);
for j = 1:1:no_cations
    c_mat_w(1,j) = c_mat(1,j);%input(['enter the initial concentration of cation ',↙
num2str(j), ' - ']); % 10000
end
r_ca = zeros(1,total_no_ions);
for i=1:1:no_cations
    r_ca(1,i) = input(['enter the rejection value of cation(%) ', num2str(i), ' - ']);
end
for j = no_cations+1:1:total_no_ions
    c_mat(1,j) = input(['enter the initial concentration of anion in ppm ', num2str(j-↙
no_cations), ' - ']);
end
```

```
for j = no_cations+1:1:total_no_ions
    c_mat_w(1,j) =c_mat(1,j); %input(['enter the initial concentration of anion ',↙
num2str(j-no_cations), ' - ']);
end
for i=no_cations+1:1:total_no_ions
    r_ca(1,i) = input(['enter the rejection value of anion(%) ', num2str(i), ' - ']);
end
D=zeros(1,total_no_ions);
for i=1:1:no_cations
    D(1,i) = input(['enter the diffusion coefficient(m^2/s) of cation ', num2str(i), '↙
- ']);
end
for i=no_cations+1:1:total_no_ions
    D(1,i) = input(['enter the diffusion coefficient(m^2/s) of anion ', num2str(i-↙
no_cations), ' - ']);
end
mw_ca = zeros(1,total_no_ions);
for i=1:1:no_cations
    mw_ca(1,i) = input(['enter the MW of cation(%) ', num2str(i), ' - ']);
end
for i=no_cations+1:1:total_no_ions
    mw_ca(1,i) = input(['enter the MW of anion(%) ', num2str(i-no_cations), ' - ']);
end
u_mat = zeros(n+1,1);
u_mat(1,1) = input('input initial cross flow velocity (m/s)- ');
Recovery = zeros(n+1,1);
Recovery (1,1)= 1-(u_mat(1,1)/u_mat(1,1));
V=zeros(n+1,1);
V(1,1)=((u_mat(1,1)-u_mat(1,1))*H)/L;
dp_mat = zeros(n+1,1);
dp_mat(1,1) = input('input initial applied pressure (Pa)- ');

S(1,1) = Salinity(1,1)/1000;
S_w(1,1)=Salinity_w(1,1)/1000;
t = T-273.15;

p=zeros(n+1,1);
p(1,1)=dp_mat(1,1)*0.000001;
Ksp_T_Celestite=zeros(n+1,1);
Ksp_T_Celestite_pre=zeros(n+1,1);
Ksp_T_Celestite_pre_mix=zeros(n+1,1);
Ksp_T_Celestite_p_con=zeros(n+1,1);
Ksp_T_Barite_p_con=zeros(n+1,1);
Ksp_T_Barite_pre=zeros(n+1,1);
Ksp_T_Barite_pre_mix=zeros(n+1,1);
Ksp_T_Gypsum_p=zeros(n+1,1);
Ksp_T_Gypsum_p_pre=zeros(n+1,1);
Ksp_T_Celestite(1,1) = exp(224.069-35.9422*log(T)-10302.32/T-((1.98*10^3/(82.05746*T))*↙
(p(1,1)-1)));
Ksp_T_Celestite_pre(1,1)=exp(224.069-35.9422*log(T)-10302.32/T-((-1.98*10^3/(82.05746↙
*T))*(p(1,1)-1)));
Ksp_T_Celestite_pre_mix(1,1)=exp(224.069-35.9422*log(T)-10302.32/T-((-1.98*10^3/↙
(82.05746*T))*(p(1,1)-1)))*(1/1.001);
Ksp_T_Celestite_p_con(1,1)=exp(224.069-35.9422*log(T)-10302.32/T-((1.98*10^3/(82.05746↙
*T))*(p(1,1)-p(1,1))));
Ksp_T_Barite=zeros(n+1,1);
```

```
Ksp_T_Barite(1,1) = exp(275.053-43.014*log(T)-15806.3/T-((4.79*10^2/(82.05746*T))*(p↙
(1,1)-1)));
Ksp_T_Barite_pre(1,1)=exp(275.053-43.014*log(T)-15806.3/T-((-4.79*10^2/(82.05746*T))*(p↙
(1,1)-1)));
Ksp_T_Barite_pre_mix(1,1)=exp(275.053-43.014*log(T)-15806.3/T-((-4.79*10^2/(82.05746↙
*T))*(p(1,1)-1)))*(1/1.36);
Ksp_T_Barite_p_con(1,1)=exp(275.053-43.014*log(T)-15806.3/T-((4.79*10^2/(82.05746*T))*↙
(p(1,1)-p(1,1))));
Ksp_Celestite=2.23*10^(-07);
Ksp_T_Gypsum_p(1,1)=exp(-1*((((T/298.15)*delta_gibbs_gypsum)+↙
(delta_enthalpy_Ca+delta_enthalpy_SO4+2*delta_enthalpy_H2O-delta_enthalpy_CaSO4)*(1-↙
(T/298.15))))/(R*T)-((2.06*10^3/(82.05746*T))*(p(1,1)-1)));
Ksp_T_Gypsum_p_pre(1,1)=exp(-1*((((T/298.15)*delta_gibbs_gypsum)+↙
(delta_enthalpy_Ca+delta_enthalpy_SO4+2*delta_enthalpy_H2O-delta_enthalpy_CaSO4)*(1-↙
(T/298.15))))/(R*T)-((-2.06*10^3/(82.05746*T))*(p(1,1)-1)));
density =zeros(n+1,1);
density(1,1)=(9.9920571*10^2+9.5390097*10^(-2)*t-7.6186636*10^(-3)*t^2+3.1305828*10^↙
(-5)*t^3-6.1737704*10^(-8)*t^4+4.3368858*10^(-1)*p(1,1)+2.5495667*10^(-5)*p(1,1)*t^2-↙
2.8988021*10^(-7)*p(1,1)*t^3+9.5784313*10^(-10)*p(1,1)*t^4+1.7627497*10^(-3)*p(1,1)^2-↙
1.2312703*10^(-4)*p(1,1)^2*t+1.3659381*10^(-6)*p(1,1)^2*t^2+4.0454583*10^(-9)*p(1,1)↙
^2*t^3-1.4673241*10^(-5)*p(1,1)^3+8.8391585*10^(-7)*p(1,1)^3*t-1.1021321*10^(-9)*p(1,1)↙
^3*t^2+4.24727611*10^(-11)*p(1,1)^3*t^3-3.9591772*10^(-14)*p(1,1)^3*t^4)-(-7.99992230↙
*10^(-1)*S(1,1)+2.40936500*10^(-3)*S(1,1)*t-2.58052775*10^(-5)*S(1,1)*t^2+6.↙
85608405*10^(-8)*S(1,1)*t^3+6.29761106*10^(-4)*p(1,1)*S(1,1)-9.36263713*10^(-7)*p(1,1)↙
^2*S(1,1));
density_w(1,1)=(9.9920571*10^2+9.5390097*10^(-2)*t-7.6186636*10^(-3)*t^2+3.1305828*10^↙
(-5)*t^3-6.1737704*10^(-8)*t^4+4.3368858*10^(-1)*p(1,1)+2.5495667*10^(-5)*p(1,1)*t^2-↙
2.8988021*10^(-7)*p(1,1)*t^3+9.5784313*10^(-10)*p(1,1)*t^4+1.7627497*10^(-3)*p(1,1)^2-↙
1.2312703*10^(-4)*p(1,1)^2*t+1.3659381*10^(-6)*p(1,1)^2*t^2+4.0454583*10^(-9)*p(1,1)↙
^2*t^3-1.4673241*10^(-5)*p(1,1)^3+8.8391585*10^(-7)*p(1,1)^3*t-1.1021321*10^(-9)*p(1,1)↙
^3*t^2+4.24727611*10^(-11)*p(1,1)^3*t^3-3.9591772*10^(-14)*p(1,1)^3*t^4)-(-7.99992230↙
*10^(-1)*S_w(1,1)+2.40936500*10^(-3)*S_w(1,1)*t-2.58052775*10^(-5)*S_w(1,1)*t^2+6.↙
85608405*10^(-8)*S_w(1,1)*t^3+6.29761106*10^(-4)*p(1,1)*S_w(1,1)-9.36263713*10^(-7)*p↙
(1,1)^2*S_w(1,1));
viscusity =zeros(n+1,1);
viscusity(1,1)=1.234*10^(-6)*exp(.00212*S_w(1,1)+1965/T);
Diffusivity=zeros(n+1,1);
Diffusivity(1,1)=6.725*10^(-6)*exp(0.1546*10^(-3)*S_w(1,1)-2513/T);

c_SiO2_molar = zeros(n+1,1);
c_SiO2_molar (1,1)=c_SiO2(1,1) /(1000 * 60.08 );

c_mat_molar = zeros(n+1,total_no_ions);
for k = 1:1:total_no_ions
    c_mat_molar(1,k) = c_mat_w(1,k) /(1000 * mw_ca(1,k) );
end
Mass_solvent(1,1) = density(1,1) - Salinity(1,1)/1000;
Mass_solvent_n(1,1) = density_n(1,1) - Salinity_n(1,1)/1000;
Mass_solvent_w(1,1) = density_w(1,1) - Salinity_w(1,1)/1000;

molality = zeros(n+1,total_no_ions); % one value per ion
for k = 1:1:total_no_ions
     molality(1,k) = c_mat_molar(1,k) / (Mass_solvent_w(1,1)/1000);
end

gamma_mat = zeros(n+1,total_no_ions);
```

```
for w = 1:1:no_cations
   gamma_mat(1,w) = gamma_cation(w,no_anions,no_cations,molality(1,:),z_mat,b,A_phi,
alpha_1,alpha_2,beta_0_mat,beta_1_mat,beta_2_mat,phi_cc_mat,phi_aa_mat,C_phi_mat,
Psi_ccA_mat,Psi_aaC_mat,identifier_mat, phi_cc_prime_mat, phi_aa_prime_mat); % change
molality terms according to requirements of
end
for w = no_cations+1:1:total_no_ions
   gamma_mat(1,w) = gamma_anion((w-no_cations),no_anions,no_cations,molality(1,:),
z_mat,b,A_phi,alpha_1,alpha_2,beta_0_mat,beta_1_mat,beta_2_mat,phi_cc_mat,phi_aa_mat,
C_phi_mat,Psi_ccA_mat,Psi_aaC_mat,identifier_mat, phi_cc_prime_mat, phi_aa_prime_mat);
% change molality terms to match above
end
alpha = zeros(n+1,1);
alpha(1,1) = alphaosmo(A_phi, molality(1,:), no_anions, no_cations, C_phi_mat, z_mat,
b, alpha_1, alpha_2, beta_0_mat, beta_1_mat, beta_2_mat, phi_cc_mat, phi_aa_mat,
phi_cc_prime_mat, phi_aa_prime_mat, Psi_ccA_mat, Psi_aaC_mat, identifier_mat);
fi = zeros(n+1,1);
fi (1,1) =2*alpha(1,1)*8.3145*298/58.44;
v_mat = zeros(n+1,1);
v_mat(1,1) = (dp_mat(1,1) - (fi (1,1) * Salinity_w(1,1))) / Rm;
%% Create results matricies with initial vaules on top line %%
IAP = zeros((n+1),total_no_ions);
SPI_Calcite = zeros((n+1),total_no_ions);
SPI_Argonite = zeros((n+1),total_no_ions);
SPI_Gypsum_mixed =zeros((n+1),total_no_ions);
SPI_Celestite=zeros((n+1),1);
SPI_Celestite_pre=zeros((n+1),1);
SPI_Celestite_pre_mix=zeros((n+1),1);
SPI_Barite=zeros((n+1),1);
SPI_Barite_pre=zeros((n+1),1);
SPI_Barite_pre_mix=zeros((n+1),1);
SPI_Celestite_constant_p=zeros((n+1),1);
SPI_Celestite_constant=zeros((n+1),1);
SPI_Gypsum_p=zeros((n+1),1);
SPI_Gypsum_p_pre=zeros((n+1),1);
SPI_Barite_con_p=zeros((n+1),1);
gamma_prod = 1;
    for kk = 1:1:total_no_ions
        if importance_mat(1,kk) == 1
           gamma_prod = gamma_prod * gamma_mat(1,kk);
        end
    end
    c_prod = 1;
    for kk = 1:1:total_no_ions
        if importance_mat(1,kk) == 1
           c_prod = c_prod * c_mat_molar(1,kk); % calculates the product of all
concentration values
        end
    end
v_sum=0;
v_sum_zeros=zeros(n+1,1);
v_sum_zeros(1,1)=0;
IAP(1,1) = gamma_prod*c_prod;
SPI_Gypsum(1,1) = log10(IAP(1,1)/Ksp_T_Gypsum);
SPI_Celestite(1,1)=log10(IAP(1,1)/Ksp_T_Celestite(1,1));
SPI_Celestite_pre(1,1)=log10(IAP(1,1)/Ksp_T_Celestite_pre(1,1));
```

```
SPI_Celestite_pre_mix(1,1)=log10(IAP(1,1)/Ksp_T_Celestite_pre_mix(1,1));
SPI_Barite(1,1)= log10(IAP(1,1)/Ksp_T_Barite(1,1));
SPI_Barite_pre(1,1)=log10(IAP(1,1)/Ksp_T_Barite_pre(1,1));
SPI_Barite_pre_mix(1,1)=log10(IAP(1,1)/Ksp_T_Barite_pre_mix(1,1));
SPI_Celestite_constant(1,1)=log10(IAP(1,1)/Ksp_Celestite);
SPI_Celestite_constant_p(1,1)=log10(IAP(1,1)/Ksp_T_Celestite_p_con(1,1));
SPI_Barite_con_p(1,1)= log10(IAP(1,1)/Ksp_T_Barite_p_con(1,1));
SPI_Gypsum_p(1,1)=log10(IAP(1,1)/Ksp_T_Gypsum_p(1,1));
SPI_Gypsum_p_pre(1,1)=log10(IAP(1,1)/Ksp_T_Gypsum_p_pre(1,1));

%% Main Loop %%

for i = 2:1:n+1

    v_mat(i,1) = (dp_mat((i-1),1) - (fi((i-1),1)*Salinity_w((i-1),1))) / Rm;
    u_mat(i,1) = u_mat((i-1),1) - ((v_mat((i-1),1)*dx)/H);
    Salinity(i,1) =  ((Salinity((i-1),1) * u_mat((i-1),1)) - (((1 - r)*v_mat(i,1)*dx)↙
/H))/u_mat(i,1);
    S(i,1) = Salinity(i,1)/1000;
    v_sum=v_sum+v_mat((i-1),1);
    v_sum_zeros(i,1)=v_sum_zeros((i-1),1)+v_mat((i-1),1);
    Salinity_w(i,1)= Salinity_w(1,1)*(1+ (((r*exp(-v_mat(i,1)*H/D(1,k)))/(u_mat((i-1),↙
1)*H))+((r*v_mat(i,1))/(u_mat((i-1),1)*D(1,k))))*v_sum*dx);
    S_w(i,1)=Salinity_w(i,1)/1000;
    viscusity(i,1)=1.234*10^(-6)*exp(.00212*S_w(i,1)+1965/T);
    Diffusivity(i,1)=6.725*10^(-6)*exp(0.1546*10^(-3)*S_w(i,1)-2513/T);
    dp_mat(i,1)= dp_mat((i-1),1) - ((12*Kspcer*viscusity(i,1)*u_mat((i-1),1)*dx)/↙
(H*H));
    p(i,1)=dp_mat(i,1)*0.000001;
    Recovery (i,1)= 1-(u_mat(i,1)/u_mat(1,1));
    V(i,1)=((u_mat(1,1)-u_mat(i,1))*H)/L;
    density_w(i,1)=(9.9920571*10^2+9.5390097*10^(-2)*t-7.6186636*10^(-3)*t^2+3.↙
1305828*10^(-5)*t^3-6.1737704*10^(-8)*t^4+4.3368858*10^(-1)*p(i,1)+2.5495667*10^(-5)*p↙
(i,1)*t^2-2.8988021*10^(-7)*p(i,1)*t^3+9.5784313*10^(-10)*p(i,1)*t^4+1.7627497*10^(-3)↙
*p(i,1)^2-1.2312703*10^(-4)*p(i,1)^2*t+1.3659381*10^(-6)*p(i,1)^2*t^2+4.0454583*10^(-9)↙
*p(i,1)^2*t^3-1.4673241*10^(-5)*p(i,1)^3+8.8391585*10^(-7)*p(i,1)^3*t(1,1)-1.1021321↙
*10^(-9)*p(i,1)^3*t^2+4.24727611*10^(-11)*p(i,1)^3*t^3-3.9591772*10^(-14)*p(i,1)^3*t^4)↙
-(-7.99992230*10^(-1)*S_w(i,1)+2.40936500*10^(-3)*S_w(i,1)*t-2.58052775*10^(-5)*S_w(i,↙
1)*t^2+6.85608405*10^(-8)*S_w(i,1)*t^3+6.29761106*10^(-4)*p(i,1)*S_w(i,1)-9.36263713↙
*10^(-7)*p(i,1)^2*S_w(i,1));
    Mass_solvent_w(i,1) = density_w(i,1) - Salinity_w(i,1)/1000;
    for k = 1:1:total_no_ions
        if c_mat((i-1),k)==0
            c_mat(i,k)=0;
        else
        c_mat(i,k) =  ((u_mat((i-1),1)*c_mat((i-1),k)) - (((1-r_ca(1,k))*v_mat(i,1)*dx)↙
/H)) / u_mat(i,1);
        c_mat_w(i,k)= c_mat_w(1,k)*(1+ (((r_ca(1,k)*exp(-v_mat(i,1)*H/(D(1,k))))/(u_mat↙
((i-1),1)*H))+((r_ca(1,k)*v_mat(i,1))/(u_mat((i-1),1)*D(1,k))))*v_sum*dx);
        c_mat_molar(i,k) = c_mat_w(i,k) /(1000 * mw_ca(1,k) );
        molality(i,k) = c_mat_molar(i,k) / (Mass_solvent_w(i,1)/1000);

        end
    end

    alpha(i,1) = alphaosmo(A_phi, molality(i,:), no_anions, no_cations, C_phi_mat,↙
```

```
z_mat, b, alpha_1, alpha_2, beta_0_mat, beta_1_mat, beta_2_mat, phi_cc_mat, phi_aa_mat,
phi_cc_prime_mat, phi_aa_prime_mat, Psi_ccA_mat, Psi_aaC_mat, identifier_mat);
    fi (i,1) =2*alpha(i,1)*8.3145*298.15/58.44;

    %% reference external %%
   for w = 1:1:no_cations
       gamma_mat(i,w) = gamma_cation(w,no_anions,no_cations,molality(i,:),z_mat,b,
A_phi,alpha_1,alpha_2,beta_0_mat,beta_1_mat,beta_2_mat,phi_cc_mat,phi_aa_mat,C_phi_mat,
Psi_ccA_mat,Psi_aaC_mat,identifier_mat, phi_cc_prime_mat, phi_aa_prime_mat); % change
molality terms according to requirements of
   end
   for w = no_cations+1:1:total_no_ions
       gamma_mat(i,w) = gamma_anion((w-no_cations),no_anions,no_cations,molality(i,:),
z_mat,b,A_phi,alpha_1,alpha_2,beta_0_mat,beta_1_mat,beta_2_mat,phi_cc_mat,phi_aa_mat,
C_phi_mat,Psi_ccA_mat,Psi_aaC_mat,identifier_mat, phi_cc_prime_mat, phi_aa_prime_mat);
% change molality terms to match above
   end

    %% calculate IAP and SPI %%
    gamma_prod = 1;
    for kk = 1:1:total_no_ions
        if importance_mat(1,kk) == 1
           gamma_prod = gamma_prod * gamma_mat(i,kk);
        end
    end
    c_prod = 1;
    for kk = 1:1:total_no_ions
        if importance_mat(1,kk) == 1
           c_prod = c_prod * c_mat_molar(i,kk); % calculates the product of all
concentration values
        end
    end
    IAP(i,1) = gamma_prod*c_prod;
    Ksp_T_Celestite(i,1)= exp(224.069-35.9422*log(T)-10302.32/T-((1.98*10^3/(82.05746
*T))*(p(i,1)-1)));
    Ksp_T_Celestite_pre(i,1)=exp(224.069-35.9422*log(T)-10302.32/T-((-1.98*10^3/
(82.05746*T))*(p(i,1)-1)));
    Ksp_T_Celestite_pre_mix(i,1)=exp(224.069-35.9422*log(T)-10302.32/T-((-1.98*10^3/
(82.05746*T))*(p(i,1)-1)))*(1/1.001);
    Ksp_T_Celestite_p_con(i,1)= exp(224.069-35.9422*log(T)-10302.32/T-((1.98*10^3/
(82.05746*T))*(p(i,1)-p(i,1))));
    Ksp_T_Barite(i,1) = exp(275.053-43.014*log(T)-15806.3/T-((4.79*10^2/(82.05746*T))*
(p(i,1)-1)));
    Ksp_T_Barite_pre(i,1)=exp(275.053-43.014*log(T)-15806.3/T-((-4.79*10^2/(82.05746
*T))*(p(i,1)-1)));
    Ksp_T_Barite_pre_mix(i,1)=exp(275.053-43.014*log(T)-15806.3/T-((-4.79*10^2/
(82.05746*T))*(p(i,1)-1)))*(1/1.36);
    Ksp_T_Barite_p_con(i,1) = exp(275.053-43.014*log(T)-15806.3/T-((4.79*10^2/(82.05746
*T))*(p(i,1)-p(i,1))));
    Ksp_T_Gypsum_p(i,1)=exp(-1*((((T/298.15)*delta_gibbs_gypsum)+
(delta_enthalpy_Ca+delta_enthalpy_SO4+2*delta_enthalpy_H2O-delta_enthalpy_CaSO4)*(1-
(T/298.15))))/(R*T)-((2.06*10^3/(82.05746*T))*(p(i,1)-1)));
    Ksp_T_Gypsum_p_pre(i,1)=exp(-1*((((T/298.15)*delta_gibbs_gypsum)+
(delta_enthalpy_Ca+delta_enthalpy_SO4+2*delta_enthalpy_H2O-delta_enthalpy_CaSO4)*(1-
(T/298.15))))/(R*T)-((-2.06*10^3/(82.05746*T))*(p(i,1)-1)));
    SPI_Gypsum(i,1) = log10(IAP(i,1)/Ksp_T_Gypsum);
```

```
    SPI_Gypsum_p(i,1)=log10(IAP(i,1)/Ksp_T_Gypsum_p(i,1));
    SPI_Gypsum_p_pre(i,1)=log10(IAP(i,1)/Ksp_T_Gypsum_p_pre(i,1));
    SPI_Celestite_constant_p(i,1)=log10(IAP(i,1)/Ksp_T_Celestite_p_con(i,1));
    SPI_Barite_con_p(i,1)= log10(IAP(i,1)/Ksp_T_Barite_p_con(i,1));
    SPI_Barite_pre(i,1)=log10(IAP(i,1)/Ksp_T_Barite_pre(i,1));
    SPI_Barite_pre_mix(i,1)=log10(IAP(i,1)/Ksp_T_Barite_pre_mix(i,1));
    SPI_Celestite(i,1) = log10(IAP(i,1)/Ksp_T_Celestite(i,1));
    SPI_Celestite_pre(i,1)=log10(IAP(i,1)/Ksp_T_Celestite_pre(i,1));
    SPI_Celestite_pre_mix(i,1)=log10(IAP(i,1)/Ksp_T_Celestite_pre_mix(i,1));
    SPI_Barite(i,1)= log10(IAP(i,1)/Ksp_T_Barite(i,1));
    SPI_Celestite_constant(i,1)=log10(IAP(i,1)/Ksp_Celestite);
end

%% Plot results %%

figure
plot(dx_mat(:,1), v_mat(:,1), 'xr');
legend('Permeate Flux (m/s) ')
xlabel('Distance (m)')
ylabel('Permeate Flux (m/s) ')

figure
plot(dx_mat(:,1), u_mat(:,1), 'xr');
legend('Cross flow velocity (m/s) ')
xlabel('Distance (m)')
ylabel('Cross flow velocity (m/s) ')

figure
plot(dx_mat(:,1), Salinity_w(:,1), 'xr');
legend('Salinity (mg/L)')
xlabel('Distance (m)')
ylabel('Salinity (mg/L)')

figure
plot(dx_mat(:,1), dp_mat(:,1), 'xr');
legend('dp ')
xlabel('Distance (m)')
ylabel('transmembrane pressure (Pa) ')

figure
plot(dx_mat(:,1), IAP(:,1), 'xr');
legend('IAP ')
xlabel('Distance (m)')
ylabel('IAP')

figure
plot(dx_mat(:,1),  v_sum_zeros(:,1), 'xr');
legend('V ')
xlabel('Distance (m)')
ylabel('Acummlated peremate flux')

figure
plot(dx_mat(:,1), Recovery (:,1), 'xr');
legend('Recovery ')
xlabel('Distance (m)')
ylabel('Recovery')
```

Appindix C: Full discribtion of the membrane rig

Here is below a full description of the installed and used laboratory membrane rig. This membrane rig consist of three streams; stream 1 (feed side) will be supplying water to the test cell and will be operating at temperatures typically no higher than 20-40 (^{o}C) with flows between 0.5 and 8.0 (L/min), stream 2 (permeate side) will consist of pure water passing from the test cell and will be operating at temperature of 20-30 (^{o}C) with flows between 1.0 and 15.0 (mL/min), and stream 3 (concentrate side) will re-circulate water from the test cell to the feed tank and will be operating at a temperature of 20-50 (^{o}C) with flows of between 0.5 and 8.0 (L/min).

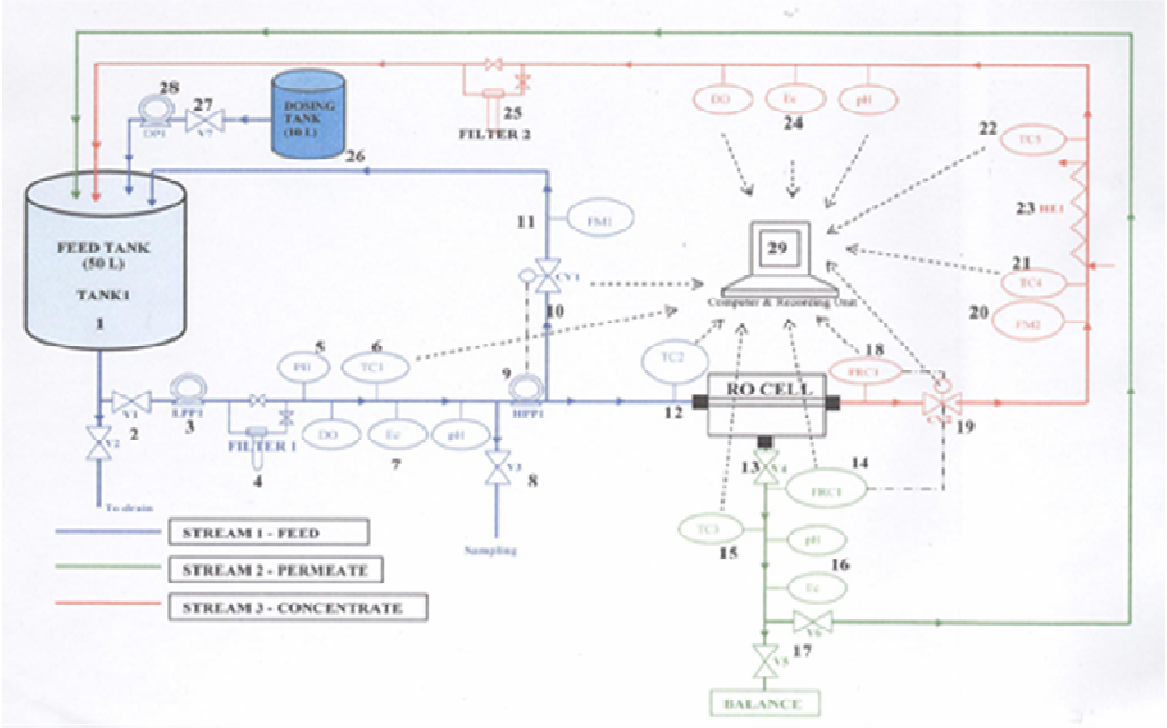

Figure 5.3: *Schematic diagram for the membrane rig*

Feed Side

1- 50L Feed tank

2- Solenoid Valve

3- Low pressure pump (up to 5bar)

4- Pre-treatment filter(1micro-5micro Meter)

5- Pressure sensor

6- Temperature sensor

7- Conductivity, Dissolved Oxygen and pH sensors

8- Solenoid valve

9- High pressure pump (up to 70 bar)

10- Control valve

11- Flow rate meter

12- Temperature sensor

Permeate side

13- Solenoid valve

14- Mass flow meter

15- Temperature sensor

16- Conductivity and pH sensors

17- Solenoid valve

Concentrate side

18- Pressure sensor

19- Control valve

20- Flow rate meter

21- Temperature sensor

22- Temperature sensor

23- Heat exchanger

24- Conductivity, Dissolved Oxygen and pH sensors

25- filter(1micro-5micro Meter)

26- Dosing (Additives) tank

27- Solenoid valve

28- Dosing pump

Appendix D: ESPA2 membrane data sheet

NITTO DENKO HYDRANAUTICS

	Membrane Element	ESPA2-8040
Performance:	Permeate Flow:	9,000 gpd (34.1 m^3/d)
	Salt Rejection:	99.6 % (99.5 % minimum)
Type	Configuration:	Spiral Wound
	Membrane Polymer:	Composite Polyamide
	Membrane Active Area:	400 ft^2 (37.1 m^2)
Application Data*	Maximum Applied Pressure:	600 psig (4.16 MPa)
	Maximum Chlorine Concentration:	< 0.1 PPM
	Maximum Operating Temperature:	113 °F (45 °C)
	pH Range, Continuous (Cleaning):	2-10.6 (1-12)*
	Maximum Feedwater Turbidity:	1.0 NTU
	Maximum Feedwater SDI (15 mins):	5.0
	Maximum Feed Flow:	75 GPM (17.0 m^3/h)
	Minimum Ratio of Concentrate to Permeate Flow for any Element:	5:1
	Maximum Pressure Drop for Each Element:	10 psi

* The limitations shown here are for general use. For specific projects, operating at more conservative values may ensure the best performance and longest life of the membrane. See Hydranautics Technical Bulletins for more detail on operation limits, cleaning pH, and cleaning temperatures.

Test Conditions

The stated performance is initial (data taken after 30 minutes of operation), based on the following conditions:

1500 PPM NaCl solution
150 psi (1.05 MPa) Applied Pressure
77 °F (25 °C) Operating Temperature
15% Permeate Recovery
6.5 - 7.0 pH Range

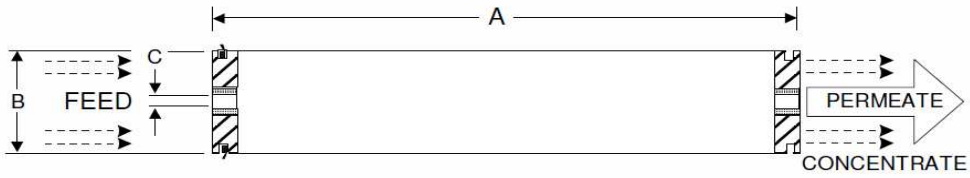

A, inches (mm)	B, inches (mm)	C, inches (mm)	Weight, lbs. (kg)
40.0 (1016)	7.89 (200)	1.125 (28.6)	36 (16.4)

Notice: Permeate flow for individual elements may vary + or - 15 percent. Membrane active area may vary +/-4%. All membrane elements are supplied with a brine seal, interconnector, and o-rings. Elements are enclosed in a sealed polyethylene bag containing less than 1.0% sodium meta-bisulfite solution, and then packaged in a cardboard box.

Hydranautics believes the information and data contained herein to be accurate and useful. The information and data are offered in good faith, but without guarantee, as conditions and methods of use of our products are beyond our control. Hydranautics assumes no liability for results obtained or damages incurred through the application of the presented information and data. It is the user's responsibility to determine the appropriateness of Hydranautics' products for the user's specific end uses. 8/12/09

For information contact: info@lenntech.com www.lenntech.com Tel. +31-15-26.10.900 Fax. +31-15-26.16.289

Appendix E: Data reproducibility

E.1 Batch experiments

A selected experiment from every set of batch experiments was duplicated to assure data reproducibility.

E.1.1 Experiments number 9 in Table 6.1

Experiments number 9 in Table 6.1. has been duplicated. Figure E.1 and Figure E.2 show the measured [Ca^{2+}] and [SO_4^{2-}] in both experiments.

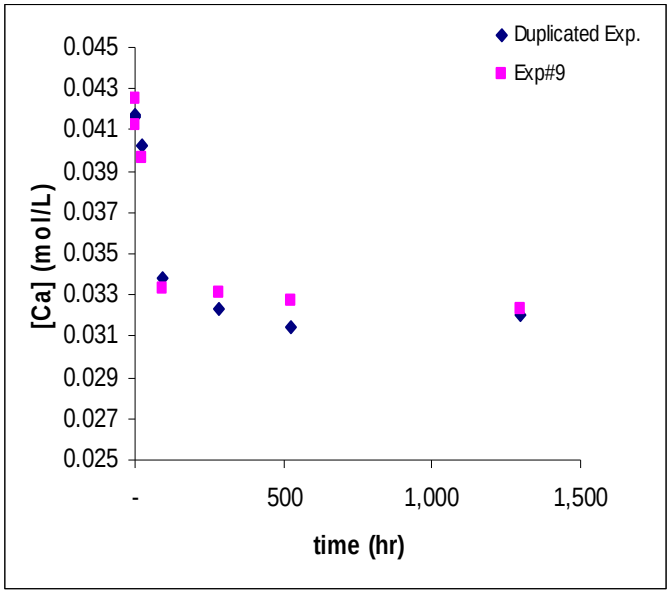

Figure E.1: *Measured [Ca^{2+}] in Experiment 9 and in the duplicated experiment.*

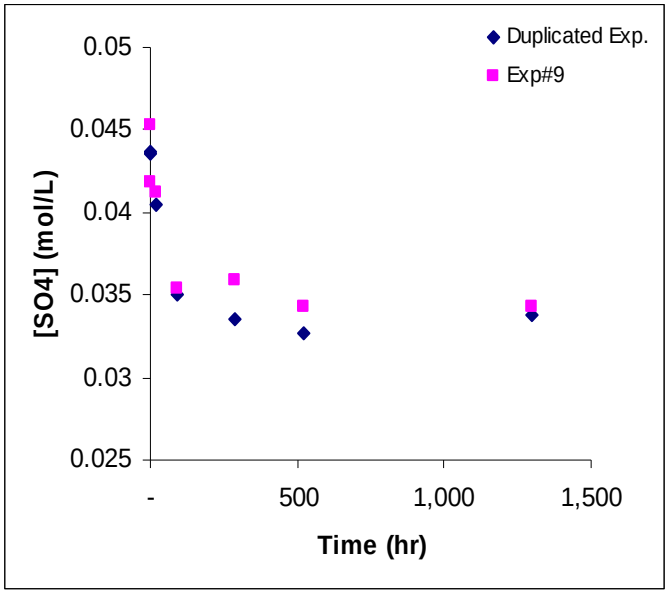

Figure E.2: *Measured* $[SO_4^{2-}]$ *in Experiment 9 and in the duplicated experiment.*

E.1.2 Experiments number 17 in Table 6.1

Experiments number 17 in Table 6.1. has been duplicated. Figures E.3, E.4 and E.5 show the measured $[Ca^{2+}]$, $[Sr^{2+}]$, and $[SO_4^{2-}]$ in both experiments.

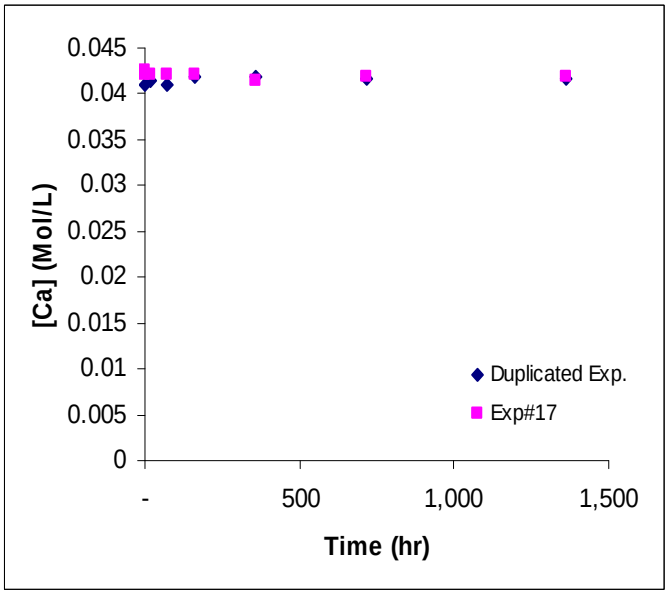

Figure E.3: *Measured* $[Ca^{2+}]$ *in Experiment 17 and in the duplicated experiment.*

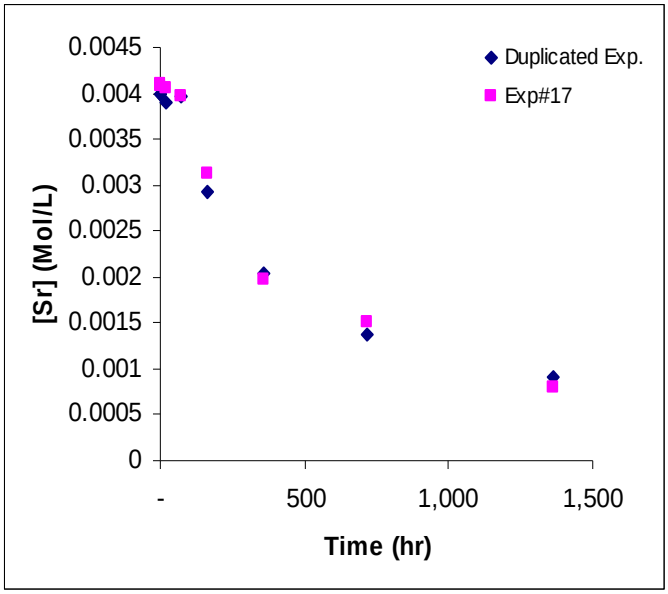

Figure E.4: *Measured [Sr^{2+}] in Experiment 17 and in the duplicated experiment.*

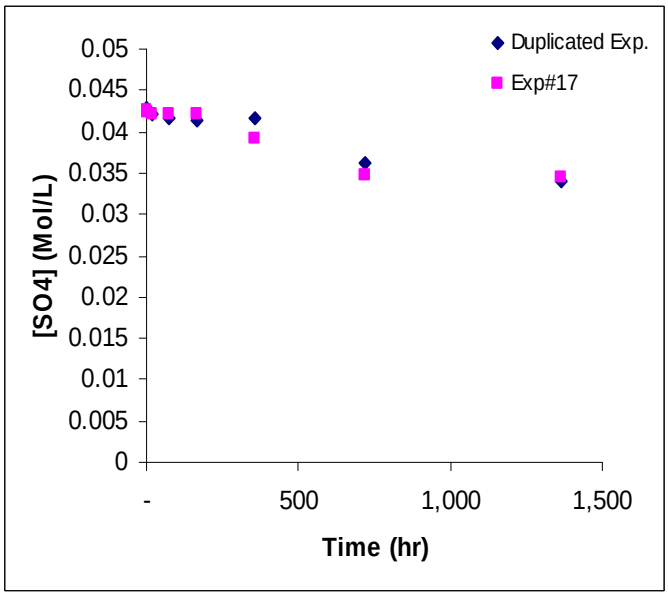

Figure E.5: *Measured [SO_4^{2-}] in Experiment 17 and in the duplicated experiment.*

E.2. Hydrodynamic experiments

In order to check the reproducibility of the hydrodynamic tests; two experiments have been carried out under the same operating conditions of Table 7.4. Figure E.6 shows the measured permeate flow rate for the main and the duplicate runs at different recovery percentage.

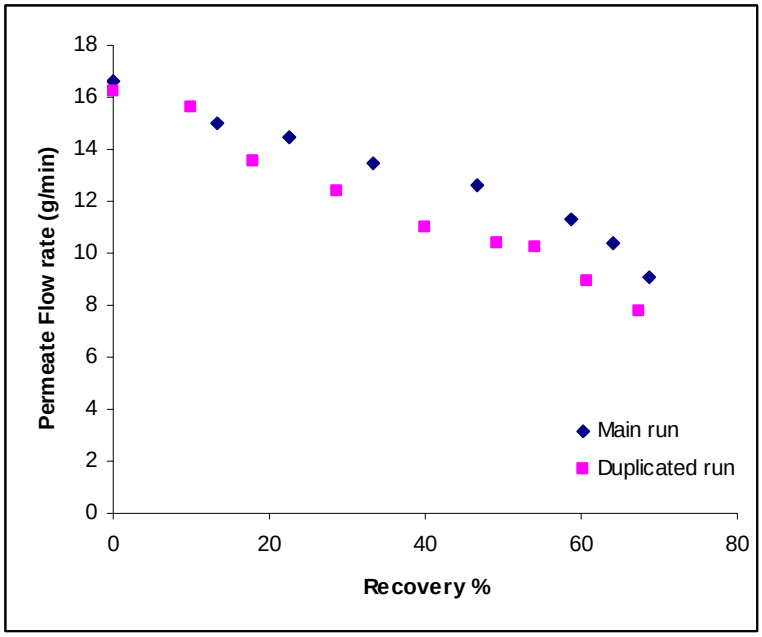

Figure E.6: *Measured permeate flow rate for the main and the duplicate runs at different recovery percentage.*

E.3. Simulation of full scale membrane process using laboratory rig

Reliable simulation of full scale membrane process using laboratory rig can reduce the overall cost of the membrane plant through facilitating the decision making to achieve more effective design for the process itself and the pre-treatment facilities and for choosing the best operating conditions. The laboratory rig is cheaper than the pilot plant currently required by a membrane plant designer [20, 93]. However, laboratory rigs are not realistic models of the full-scale plant, for example the membrane cell or unit is much smaller than the real full scale membrane unit (FSMU). Thus, simulation of the full scale membrane unit using a laboratory rig cannot be direct. Below is a description of a new simple technique that can be used to achieve reliable simulation of full scale membrane processes using the program developed in chapter 3 of this thesis and a new installed laboratory membrane rig similar to the one described here.

1) The laboratory membrane rig (LMR) should be designed to operate in either full recycle mode (recycle both the concentrate and permeate streams) or partial recycle mode (withdrawing the permeate stream).

2) The feed water of the LMR should be the same as the feed water of the FSMU or at least have the same ionic composition.

3) The LMR should be operated with the same expected operating parameters as the FSMU, using the same type of the membrane.

4) The Matlab simulation should be carried out using the same operating conditions and feed composition.

5) A predicted curve of Recovery levels vs the Distance along the membrane channel (R-D chart) can be produced from the Matlab program for the FSMU.

6) The LMR then should be operated according to the procedure described in section 7.2.4.

7) The recovery level indicated by the LMR experiments will then be used to specify the exact position within the simulated FSMU using the R-D chart.

8) Then the required study can be carried out on the LMR simulating the FSMU knowing what position along the FSMU corresponds to the laboratory rig conditions. For example, to simulate the concentration polarisation along a long feed channel, the permeate flux of pure water is recorded at the beginning of the run. Then the permeate flux of saline solution is measured at every recovery level. The composition of the feed and permeate are determined experimentally. The change of K_m and CP with recovery will be evaluated. The distance along the membrane channel will be calculated from the Recovery vs Distance (m) curve, R-D chart. At every recovery (R) the system is operated at full recycle mode for an hour then the permeate flux at that R% is checked.

E.4. General calculation

Below is a more detailed description of the calculations that have been carried out in this chapter.

(1) Superficial velocity (u) and Reynolds number calculation

The Superficial velocity (u) is calculated using Eq.7.5

$u = Q/(W.H)$ (7.5)

where Q is the feed flow rate, W is the width of the flow Channel (0.0975 m), H is the feed channel height (spacer height, 0.00085 m mid fouling spacer from the manufacturer's specification sheet).

Q= 4.6 L/min= 7.67×10^{-5} m^3/s

So u = 0.000076666/(0.0975*0.00085)= 0.925 m/s

$\mathrm{Re} = \frac{\rho . d_h . u}{\mu}$; where Re is Reynolds number, ρ is feed density, u is superficial velocity, μ is the feed viscosity and d_h is the hydraulic diameter.

For rectangular duct full of fluid d_h is giving by the below equation

$d_h = \frac{4(W.H)}{2(W+H)}$ = 4(0.0975*0.00085)/2(0.0975+0.00085) = 0.00168m

For 0.15 M NaCl solution at 20 ^{o}C and 25 bar (calculated using the Matlab programme).

ρ = 1006.66 Kg/m^3

μ = 0.00107 Pa.S

Thus Re = (1006.66*0.00168*0.925)/0.00107 = 1470 (laminar flow)

(2) R_m calculation using the Manufacturer data sheet data

R_m is calculated using Eq. 3.32. The osmotic pressure difference $\Delta\pi$ is calculated by Eq 3.33; where α relates the osmotic pressure to concentration through application of the van't Hoff formula through Eq. 3.34; R is the universal gas constant; T is the absolute temperature; Mw is the molecular weight of the solute; N is the number of ions in solution that result from one salt molecule (N is 2 for NaCl); and $\varphi_{osmotic}$ is the Pitzer osmotic coefficient (calculated using the Matlab program).

$$v = \frac{\Delta P - \Delta\pi}{R_m} \qquad (3.32)$$

$$\Delta\pi = \alpha \Delta c \qquad (3.33)$$

$$\alpha = \frac{N \varphi_{osmotic} RT}{Mw} \qquad (3.34)$$

R = 8.314 x10^3 Pa.L/(K.mol)

ΔP = 1050000 Pa

$\Delta\pi$ is calculated using Eqs 3.33 and 3.34

$$\Delta\pi(x) = \alpha \Delta c(x) \qquad (3.33)$$

$$\alpha = \frac{N \varphi_{osmotic} RT}{Mw} \qquad (3.34)$$

φ_{osmol}= 0.8895

MW_{NaCl}=58.44 g/mol

N = 2

T=25 ^{o}C = 298.15K

Initial ΔC=0.0257 mol/L = 1.5 g/L so at 15% recovery ΔC= 1.725 g/L

$\Delta\pi$ = (2*0.8895*8.314*10^3 * 298.15*1.725)/58.44 = 130166.66 Pa = 1.302 bar

v = 0.919 $m^3/(day.m^2)$ = 1.0638 *10^{-5} $m^3/(s.m^2)$

R_m = (1050000 -130166.66)/ (1.0638 *10^{-5}) = 8.64668x10^{10} Pa.s/m

(3) Permeate flux calculation

For 0.15 M NaCl solution the measured mass flow rate is J_{salt} = 17.27 g/L for 140 cm^2 membrane surface area.

v = 17.27/(998.99*60*1000*0.014) = 2.058x10^{-5} m/s

From the Matlab; v = 2.068x10^{-5} m/s.

(4) K_m and CP Calculations

1- Using Sutzkover technique

The measured permeate mass flow rate for pure water, $J_{H2O,}$ (before salts addition) found to be 26.50 g/min under test 2 operation conditions.

Thus the measured v_{H2O} = 4.43x10^{-7} (m^3/s.0.014m^2) = 3.176x10^{-5} ($m^3/s.m^2$)

After the addition of NaCl solution and under test 3 operating conditions the measured permeate mass flow rate J_{salt} was found to be 16.59g/min.

Thus the measured v_{salt}= 2.77*10^{-7} (m^3/s.0.014m^2) = 1.98x10^{-5} ($m^3/s.m^2$)

ΔP = 25 bar =2500000 Pa

$\Delta\pi$ is calculated using Eqs. 3.33 and 3.34

Δπ = 667324 Pa

Thus by substituting in Eq.2.12

K_m= 4.74x10^{-05} m/s

By substituting in Eq.2.13

CP = 1.517

2- Using Eqs 7.3 and 2.10

$$\pi_w - \pi_p = \Delta P.\left[1 - \frac{v_{salt}}{v_{H_2O}}\right] \qquad (7.3)$$

$$\frac{c_w - c_p}{c_b - c_p} = \exp\left(\frac{v}{k_m}\right) \qquad (2.10)$$

$\pi_w - \pi_p$ = 2500000*(1-(1.98*10^{-5} /3.176*10^{-5})) =1.01x10^{+06} Pa

The π_p was calculated using Eqs 3.33 and 3.34, the measured c_p is 0.0275 M

π_p = 2031.9214 Pa

Thus π_w is 1.01E+06 Pa and therefore c_w is 0.232 M

$$\frac{c_w - c_p}{c_b - c_p} = \frac{0.232 - 0.0275}{0.154 - 0.0275} = 1.62$$

And K_m = 4.10x10^{-05} m/s

3- Using Dresner model

The entrance region found to be 0.003-0.007 m through Eq.7.2

$$\frac{EL}{d_h} = \frac{1000\,to\,2500}{\mathrm{Re}^{0.875}} \qquad (7.2)$$

where Re = (1006.66*0.00168*0.925)/0.00107 = 1466.628, d_h = 0.00168m.

CP and K_m downstream in the filtration channel are calculated via Eqs 7.1 and 2.12

$$CP = 1 + \frac{v^3.H.L}{3.u.D^2} \qquad (7.1)$$

where H = 0.00085 m; L = 0.14 m, v = 1.98x10^{-5} (m^3/s.m^2); u =0.92 m/s;
D = 1.474x10^{-09} m^2/s. Thus CP = 1.23 and K_m = 9.56x10^{-05} m/s.